Vol 21 № 3/2019 ENERGY SECTOR PROBLEMS

C O N T E N T S

POWER ENGINEERING

MAKSIMOV V.I., NURPEIIS A.E. Mathematical modeling of heat transfer in a closed two-phase thermosyphon. 3

MUSTAFIN R.G., Inter turn fault detection by parameters of transition process in transformers. . . 14

KAZAKOV V.G., GROMOVA E.N. Closed cycle air-steam mixture in the drying section of paper machine.. 24

KISELEV V.G. Carnot's theorem and the efficiency of a reversible heat engine. 32

LYKIN A.V., UTKIN E.A. Power distribution networks 10/0.4 KV with the maximal nearby location of transforming substations to cons. 46

VESELOVSKAYA E.V, VOLOSHINA, E.N. LYSENKO S.E. Application of x-ray fluorescent spectrometry for assessing the ultra filtration membrane surface condition at water preparatory units of thermal power plants (TPP). 55

BOLSHANIN G.A., PLOTNIKOV M.P. The development of the wave method of calculation of operational parameters of a double circuit power transmission line with known values of output voltages and currents at the end of the line. 63

TARASOV V.A., TARASOVA V.V., AFANASYEV V.V., KOVALEV V.G., ORLOV V.N. Mathematical modeling of the forecast and standby heating modes. 73

SHARAPOV A.I, CHERNYKH A.A., PESHKOVA A.V. Supersonic flow of two-phase gas-droplet flows in nozzles 86

KHRUSTALEV V.A., GARIEVSKII M.V., ROSTUNTSOVA I.A., PORTYANKIN A.V. On the possibility of participation of NNPS with VVER in emergency frequency regulation in power systems . . . 99

TAYMAROV M.A., ILYIN V.K., CHIKLYAEV E.G., SUNGATULLIN R.G. Features of application of fraction as fuel for coppers of thermal power plant. 109

GENBACH A.A., BONDARTSEV D.YU. Odeling of thermal stresses destroying the porous coating of heat-exchange surfaces of power plants. 117

GAZIZOV F.N., AKHMETOVA I.G. Development of technique and program for analysis of options for transition to a closed hot-water supply scheme for heat supply systems. 126

ELECTRICAL ENGINEERING

KLIMASH V.S., TABAROV B.D. Method for control of the start-up regulating device for power transformers of the power supply system. 135

KASIMOV V.A. Distortion of location pulses in high-frequency paths of overhead power lines 146

INSTRUMENT MAKING, METROLOGY AND INFORMATION-MEASURING DEVICES AND SYSTEMS

GORYACHEV M.P., SADYKOV M.F., YAROSLAVSKIY D.A. Method of mechanical parameters of power lines based on improved in clinometric method. 160

Том 21 № 3/2019 **ПРОБЛЕМЫ ЭНЕРГЕТИКИ**

С О Д Е Р Ж А Н И Е

ЭНЕРГЕТИКА

МАКСИМОВ В.И., НУРПЕЙИС А.Е. Математическое моделирование теплопереноса в замкнутом двухфазном термосифоне в системах охлаждения энергонасыщенного оборудования. 3

МУСТАФИН Р.Г. Обнаружения витковых замыканий обмоток трансформаторов по параметрам переходного процесса. 14

КАЗАКОВ В.Г., ГРОМОВА Е.Н. Замкнутый цикл паровоздушной смеси в сушильной части бумагоделательной машины. 23

КИСЕЛЁВ В.Г. Об ограниченности области применения теоремы Карно. 33

ЛЫКИН А.В., УТКИН Е.А. Распределительные электрические сети 10/0,4 КВ с максимальным приближением трансформаторных подстанций к потребителям. 49

ВЕСЕЛОВСКАЯ Е.В., ВОЛОШИНА Е.Н., ЛЫСЕНКО С.Е. Применение рентгенофлуоресцентной спектрометрии для оценки состояния поверхности ультрафильтрационных мембран водоподготовительных установок ТЭС. 59

БОЛЬШАНИН Г.А., ПЛОТНИКОВ М.П. Определение токов и напряжений в двухцепной линии электропередачи на основе вычисления падающих и отраженных волн. 68

ТАРАСОВ В.А., ТАРАСОВА В.В., АФАНАСЬЕВ В.В., КОВАЛЕВ В.Г., ОРЛОВ В.Н. Математическое моделирование режимов прогнозного и дежурного отопления. 79

ШАРАПОВ А.И., ЧЕРНЫХ А.А., ПЕШКОВА А.В. Сверхзвуковое течение двухфазных газокапельных потоков в соплах. 91

ХРУСТАЛЕВ В.А., ГАРИЕВСКИЙ М.В., РОСТУНЦОВА И.А., ПОРТЯНКИН А.В.О возможности участия АЭС с ВВЭР в противоаварийном частотном регулировании в энергосистемах. . 105

ТАЙМАРОВ М.А., ИЛЬИН В.К., ЧИКЛЯЕВ Е.Г., СУНГАТУЛЛИН Р.Г. Особенности применения метано-водородной фракции в качестве топлива для котлов ТЭС 116

ГЕНБАЧ А.А., БОНДАРЦЕВ Д.Ю. Моделирование термических напряжений, разрушающих пористые покрытия теплообменных поверхностей энергоустановок. 123

ГАЗИЗОВ Ф.Н., АХМЕТОВА И.Г. Разработка методики и программы анализа вариантов перевода на закрытую схему ГВС систем теплоснабжения. 132

ЭЛЕКТРОТЕХНИКА

КЛИМАШ В.С., ТАБАРОВ Б.Д. Способ управления пускорегулирующим устройством для силовых трансформаторов системы электроснабжения. 142

КАСИМОВ В.А. Искажения локационных импульсов в высокочастотном тракте воздушной линии электропередачи. 153

ПРИБОРОСТРОЕНИЕ, МЕТРОЛОГИЯ И ИНФОРМАЦИОННО-ИЗМЕРИТЕЛЬНЫЕ ПРИБОРЫ И СИСТЕМЫ

ГОРЯЧЕВ М.П., САДЫКОВ М.Ф., Ярославский Д.А. Методика контроля механических параметров воздушных линий электропередачи на основе улучшенного инклинометрического метода. . . 168

POWER ENGINEERING

UDC 536.2 **DOI:10.30724/1998-9903-2019-21-3-3-13**

MATHEMATICAL MODELING OF HEAT TRANSFER IN A CLOSED TWO-PHASE THERMOSYPHON

V.I. Maksimov, A.E.Nurpeiis

Tomsk Polytechnic University, Tomsk, Russia
E-mail: nurpeiis_atlant@mail.ru

***Abstract**: We suggested a new approach for describing heat transfer in thermosyphons and determining the characteristic temperatures. The processes of thermogravitation convection in the coolant layer at the lower cap, phase transitions in the evaporation zone, heat transfer as a result of conduction in the lower cap are described at the problem statement. The main assumption, which was used during the problem formulation, is that the characteristic times of steam motion through the thermosyphon channel are much less than the characteristic times of thermal conductivity and free convection in the coolant layer at the lower cap of the thermosyphon. For this reason, the processes of steam motion in the thermosyphon channel, the condensate film on the upper cap and the vertical walls were not considered. The problem solution domain is a thermosyphon through which heat is removed from the energy-saturated equipment. The ranges of heat flow changes were chosen based on experimental data. The geometric parameters of thermosyphon and the fill factors were chosen the same as in the experiments (height is 161 mm, diameter is 42 mm, wall thickness is 1.5 mm, ε=4-16%) for subsequent comparison of numerical simulation results and experimental data. In the numerical analysis it was assumed that the thermophysical properties of thermosyphon and coolant caps do not depend on temperature; laminar flow regime was considered. The dimensionless equations of vortex, Poisson and energy transfer for the liquid coolant under natural convection and the equations of thermal conductivity for the lower cap wall are solved by the method of finite differences. Numerical simulation results showed the relationship between the characteristic temperatures and the heat flow supplied to the bottom cap of thermosyphon. The results of the theoretical analysis are in satisfactory agreement with the known experimental data.*

***Keywords**: two-phase thermosyphon, mathematical modeling, heat flow, heat transfer, evaporation, condensation, thermo-gravitational convection.*

***Acknowledgments:** The study was conducted in the framework of the program of increasing the competitiveness of National research Tomsk Polytechnic University among world's leading research and educational centers (state assignment "Science" 8.13264.2018/8.9, project VIU-ISHE-300/2018).*

For citation: Maksimov VI, Nurpeiis AE. Mathematical modeling of heat transfer in a closed two-phase thermosyphon. *Power engineering: research, equipment, technology*. 2019; 21(3):3-13. (In Russ). doi:10.30724/1998-9903-2019-21-3-3-13.

МАТЕМАТИЧЕСКОЕ МОДЕЛИРОВАНИЕ ТЕПЛОПЕРЕНОСА В ЗАМКНУТОМ ДВУХФАЗНОМ ТЕРМОСИФОНЕ

В.И. Максимов, А.Е. Нурпейис

Национальный исследовательский Томский политехнический университет, г. Томск, Россия
nurpeiis_atlant@mail.ru

Резюме: *Предложен новый подход к описанию процессов теплопереноса в термосифонах и определения характерных температур. При постановке задачи описываются процессы термогравитационной конвекции в слое теплоносителя на нижней крышке, фазовые превращения в зоне испарения, теплоперенос в результате кондукции в нижней крышке. Основное допущение, которое использовалось при постановке задачи, – это положение о том, что характерные времена движения паров по каналу термосифона много меньше характерных времен теплопроводности и свободной конвекции в слое хладагента на нижней крышке термосифона. По этой причине не рассматривались процессы движения пара в канале термосифона, пленке конденсата на верхней крышке и вертикальных стенках. Область решения задачи представляет собой термосифон, через который осуществляется отвод теплоты от энергонасыщенного оборудования. Диапазоны изменения тепловых потоков выбирались исходя из экспериментальных данных. Геометрические параметры термосифона и коэффициенты заполнения выбирались такими же, как и в экспериментах (высота – 161 мм, диметр – 42 мм, толщина стенок – 1,5 мм, ε=4–16%) для последующего сравнения результатов численного моделирования и экспериментальных данных. При проведении численного анализа предполагалось, что теплофизические свойства крышек термосифона и хладагента не зависят от температуры; рассматривался ламинарный режим течения. Безразмерные уравнения переноса вихря, Пуассона и энергии для жидкого теплоносителя в условиях естественной конвекции и уравнения теплопроводности для стенки нижней крышки решены методом конечных разностей. По результатам численного моделирования установлена зависимость характерных температур от величины теплового потока, подводимого к нижней крышке термосифона. Результаты теоретического анализа находятся в удовлетворительном соответствии с известными экспериментальными данными.*

Ключевые слова: *двухфазный термосифон, математическое моделирование, тепловой поток, теплоперенос, испарение, конденсация, термогравитационная конвекция.*

Благодарности: *Исследование проведено в рамках программы повышения конкурентоспособности Национального исследовательского Томского политехнического университета среди ведущих мировых научно-образовательных центров (проект ВИУ-ИШЭ-300/2018).*

Introduction

The prerequisite for successful operation of modern energy-saturated equipment (ESE) is the removal of heat from heat-generating parts and modules [1-3]. Utilization of traditional air cooling systems using various kinds of superchargers is not always possible. Failure of such auxiliary equipment leads to an emergency operation of energy-saturated equipment. For this reason, the use of heat transfer devices that are independent of power sources is relevant.

Closed two-phase thermosyphons (TS), which can be used for thermostating and thermoregulation of various technological processes are the autonomous (independent of energy sources) heat

exchangers [4, 5]. Evaporation and condensation in heat exchangers of this type are spatially separated, which makes it possible to transform heat flows by changing the ratio of evaporation and condensation surfaces. But at present, thermosyphons are almost not used in industry due to the fact that the physics of heat transfer processes and phase transformations in the steam channel, evaporation and condensation zones, and the condensate film flowing along the side walls in the thermosyphon case is not well understood. For a detailed analysis of these processes, information is needed on the temperature fields in the characteristic zones of the thermosyphon. But due to the difficulties of sealing such heat exchangers when installing temperature sensors, the majority of publications present the results of recording the temperatures of the external surfaces of the thermosyphon walls. Such measurements are insufficient for the analysis of heat transfer processes, because the heat flow through the TS case is intense both along the longitudinal and transverse coordinates. The few results of temperature determination in a closed two-phase thermosyphon [6–8] show its change only at individual points on the inner surface of the heat exchanger under consideration. To analyze the operation efficiency of thermosyphons, one needs information about the temperature distributions in the areas corresponding to the evaporation, transport, and steam condensation zones [7–9].

Analysis of the relevant literature shows that various heat transfer models are currently used for calculation of thermosyphons [10–14]: original researchers' codes [10–11] and commercial software packages [12–13]. Models and methods [10–14] have certain advantages (the completeness of description of hydrodynamic and thermophysical processes in all zones of the thermosyphon; the possibility of solving spatial problems in the conjugate formulation, the mathematical interpretation of various options for structural solutions, taking into account the temperature and steam dependences of the characteristics of steam and condensate, and some others). But the use of commercial packages and original codes for calculation of heat transfer processes in thermosyphons is associated with the solution of a number of complex problems. For example, working with packages of the ANSYS FLUENT type implies a highly-skilled user, which is almost impossible in many cases when such packages are used by heating engineers to solve specific problems. In addition, numerical simulation using such packages involves time-consuming computations even when the processes are described in two-dimensional statements. A well-proven and simple method for calculating heat transfer using balanced models [5, 9] does not allow determining the temperature in the characteristic sections of the thermosyphon. For this reason, it is necessary to develop a mathematical model less complicated than [10–14] and a method for calculating unsteady heat transfer in a two-phase thermosyphon in order to describe heat transfer processes taking into account phase transitions at media interfaces.

Analysis and generalization of the experimental results [15–16] made it possible to develop a new approach to the mathematical modeling of heat transfer processes in two-phase thermosyphons. An important difference between the mathematical model formulated in the article and the known ones [10–14] is that when setting the problem, only thermogravitational convection processes in the coolant layer on the lower cap, phase transformations in the evaporation zone, and heat transfer as a result of conduction in the lower cap are described. The main assumption that was used during the problem formulation is the provision that the characteristic times of steam motion through the thermosyphon channel are much shorter than the characteristic times of heat conduction and free convection in the coolant layer on the bottom cap of the thermosyphon. For this reason, the processes of steam motion in the TS channel, the condensate film on the top cap and the vertical walls of the thermosyphon were not considered. Further the problem statement is presented.

Problem statement and solution method

The problem solution domain is a thermosyphon, through which heat is removed from energy-saturated equipment. At the initial moment of time, the TS case and the coolant have a constant and uniform temperature at all points. The ranges of heat flows variation were selected based on experimental data [16]. Geometrical parameters of the thermosyphon and the filling

factors were chosen the same as in the experiments [15–16] (height is 161 mm, diameter is 42 mm, wall thickness is 1.5 mm, ε = 4–16%) for subsequent comparison of the results of numerical modeling and experimental data.

In this formulation, hydrodynamic processes (steam motion) in the steam channel were excluded from consideration, but the processes of conduction and convection in the coolant layer were considered, and the processes of thermal conductivity in the lower cap of the thermosyphon were taken into account. Based on the results of previous experiments [15–16], it was also assumed that in the range of heat flows up to q=1.8 kW/m^2, all water steam formed on the surface of the coolant layer rises very quickly, where it condenses on the lower surface of the top cap of the thermosyphon and manages to return to the evaporation zone when draining along vertical walls. The solution of the heat transfer problem in a thermosyphon in this formulation reduces to solving the system of equations of continuity, motion, and energy for the coolant layer on the bottom cap and thermal conductivity for the plate (Fig. 1) in an axisymmetric formulation.

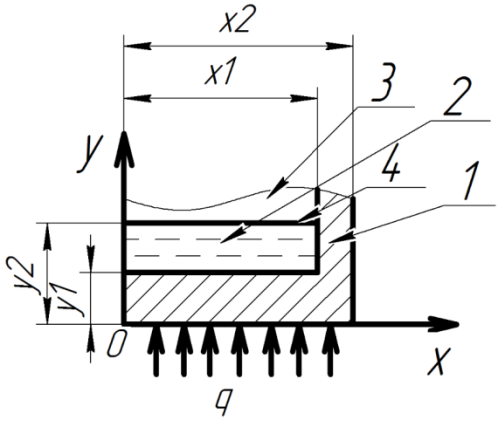

Fig. 1. The problem solution domain: 1 - metal case; 2 - layers of condensate; 3 - steam channel; 4 - evaporation surface

The dimensionless equations of vortex transfer, Poisson, and energy for the liquid coolant under conditions of natural convection and the heat transfer equation for the lower cap wall have the form [11]:

$$\frac{\partial \Omega_2}{\partial \tau}+U_2\frac{\partial \Omega_2}{\partial X}+V_2\frac{\partial \Omega_2}{\partial Y}=\sqrt{\frac{\mathrm{Pr}_2}{\mathrm{Ra}_2}}\left(\frac{\partial^2\Omega}{\partial X^2}+\frac{\partial^2\Omega}{\partial Y^2}\right)+\frac{\partial \Theta_2}{\partial X}, \tag{1}$$

$$\frac{\partial^2\Psi_2}{\partial X^2}+\frac{\partial^2\Psi_2}{\partial Y^2}=-\Omega_2, \tag{2}$$

$$\frac{\partial \Theta_2}{\partial \tau}+U_2\frac{\partial \Theta_2}{\partial X}+V_2\frac{\partial \Theta_2}{\partial Y}=\frac{1}{\sqrt{\mathrm{Ra}_2\,\mathrm{Pr}_2}}\cdot\left(\frac{\partial^2\Theta_2}{\partial X^2}+\frac{\partial^2\Theta_2}{\partial Y^2}\right), \tag{3}$$

$$\frac{1}{\mathrm{Fo}_1}\frac{\partial \Theta_1}{\partial \tau}=\frac{\partial^2\Theta_1}{\partial X^2}+\frac{\partial^2\Theta_1}{\partial Y^2}. \tag{4}$$

where $\mathrm{Pr}=\frac{\nu}{a}$ is the Prandtl number; $\mathrm{Ra}=\frac{g_y\beta(T_h-T_0)H^3}{\nu a}$ is the Rayleigh number; $\mathrm{Fo}=\frac{a_1 t_0}{H^2}$ is the Fourier number; X, Y are the dimensionless system coordinates corresponding to x, y; a is the thermal diffusivity, m^2/s; ν is the kinematic viscosity coefficient, m^2/s; β is the volume expansivity, 1/K; g is the gravitational acceleration, m/s^2; $H=y_2-y_1$ is the characteristic dimension, m; t_0 is the time scale, s; τ is the dimensionless time; u, v are the motion rates, m/s; U, V are the dimensionless rates corresponding to u, v; V_{in} is the rate scale, m/s; T_0 is the thermosyphon temperature at the initial time, K; T_h is the boiling temperature of coolant, K; Θ is

the dimensionless temperature; ψ is the flow function, m^2/s; ψ_0 is the flow function scale, m^2/s; Ψ is the dimensionless analog of ψ; ω is the vorticity vector, 1/c; ω_0 is the vorticity vector scale, 1/s; Ω is the dimensionless analog of ω.

The initial conditions for equations (1 – 4) are:

$$\Psi(X,Y,0)=\Omega(X,Y,0)=0,\ \Theta_1(X,Y,0)=\Theta_2(X,Y,0)=0, \tag{5}$$

Dimensionless boundary conditions for equations (1 – 4) are:

$$X=0,\quad 0<Y<Y_1:\ \frac{\partial\Theta_1}{\partial X}=0, \tag{6}$$

$$X=0,\quad Y_1<Y<Y_2:\ \frac{\partial\Theta_2}{\partial X}=0,\ \begin{cases}\dfrac{\partial^2\Psi_2}{\partial X^2}=0,\end{cases} \tag{7}$$

$$X=X_2,\quad 0<Y<Y_2:\ -\lambda\frac{\partial\Theta_1}{\partial X}=0, \tag{8}$$

$$Y=0,\quad 0<X<X_2:-\frac{\partial\Theta_1}{\partial Y}=Ki, \tag{9}$$

$$Y=Y_2,\quad 0<X<X_1:\frac{\partial\Theta_2}{\partial Y}=-\frac{Q_u W_u H}{\lambda(T_h-T_0)},\ \{\Psi_2=0, \tag{10}$$

$$Y=Y_2,\quad X_1<X<X_2:-\lambda\frac{\partial\Theta_1}{\partial Y}=0, \tag{11}$$

$$X=X_1,\quad Y_1<Y<Y_2:\ \begin{cases}\Theta_1=\Theta_2,\\ \dfrac{\partial\Theta_1}{\partial X}=\dfrac{\lambda_2}{\lambda_1}\dfrac{\partial\Theta_2}{\partial X},\end{cases}\ \begin{cases}\Psi_2=0,\\ \dfrac{\partial\Psi_2}{\partial X}=0,\end{cases} \tag{12}$$

$$Y=Y_1,\ 0<X<X_1:\ \begin{cases}\Theta_1=\Theta_2,\\ \dfrac{\partial\Theta_1}{\partial Y}=\dfrac{\lambda_2}{\lambda_1}\dfrac{\partial\Theta_2}{\partial Y},\end{cases}\ \begin{cases}\Psi_2=0,\\ \dfrac{\partial\Psi_2}{\partial Y}=0,\end{cases} \tag{13}$$

$$W_u=\frac{A(P_n-P_n)}{\sqrt{\dfrac{2\pi RT}{M}}} \tag{14}$$

where $\mathrm{Ki}=\dfrac{qH}{\lambda_1(T_h-T_0)}$ is the Kirpichev number; $\mathrm{Bi}=\dfrac{\alpha\cdot H}{\lambda_1}$ is the Biot number; Q_e is the evaporation heat; W_e is the evaporation rate; q is the heat flow; A is the accomodation coefficient; P_s is the saturated steam pressure; P_p is the partial steam pressure above the liquid surface; R = 8314 J/kmol·K is the universal gas constant; M is the molecular weight; 1 is for the cap material; 2 is for liquid.

For numerical analysis it was assumed that the thermophysical properties of the thermosyphon and coolant caps are independent of temperature; the laminar flow regime was considered. The fluid was assumed to be Newtonian, incompressible, and satisfying the Boussinesq approximation [11, 18].

The system of equations (1–4) with the corresponding initial and boundary conditions was solved by the finite difference method [18]. Mass rates of evaporation and condensation were calculated by the Hertz – Knudsen formula [19]. When solving the Poisson equation for the flow function, the implicit method of variable directions was used, similarly to [18–20]. In determining the boundary condition for the velocity vortex, the Woods formula was used.

Numerical studies of heat transfer in TS under conditions of energy removal from energy-saturated equipment were carried out in typical ranges of heat flow changes corresponding to

operating modes of energy-saturated equipment [21]. Heat flows to the bottom cap of the thermosyphon ranged from 0.3 kW/m^2 to 1.8 kW/m^2.

Results and discussion

Figures 2–3 show thermograms obtained from numerical simulation of heat transfer process and conducting experiments when filling the thermosyphon cavity with distilled water in the range of heat flows q=0.4–1.8 kW/m^2.

It can be seen from Fig. 2 that the time to reach the steady-state regime of characteristic temperatures obtained in numerical studies and experiments is quite large in the entire range of changes in heat flows. Temperatures grow rapidly in the first 5000 - 6000 s, and then slowly. This is due to the fact that within 2.5 hours the walls, the TS cap and the coolant itself are evenly heated.

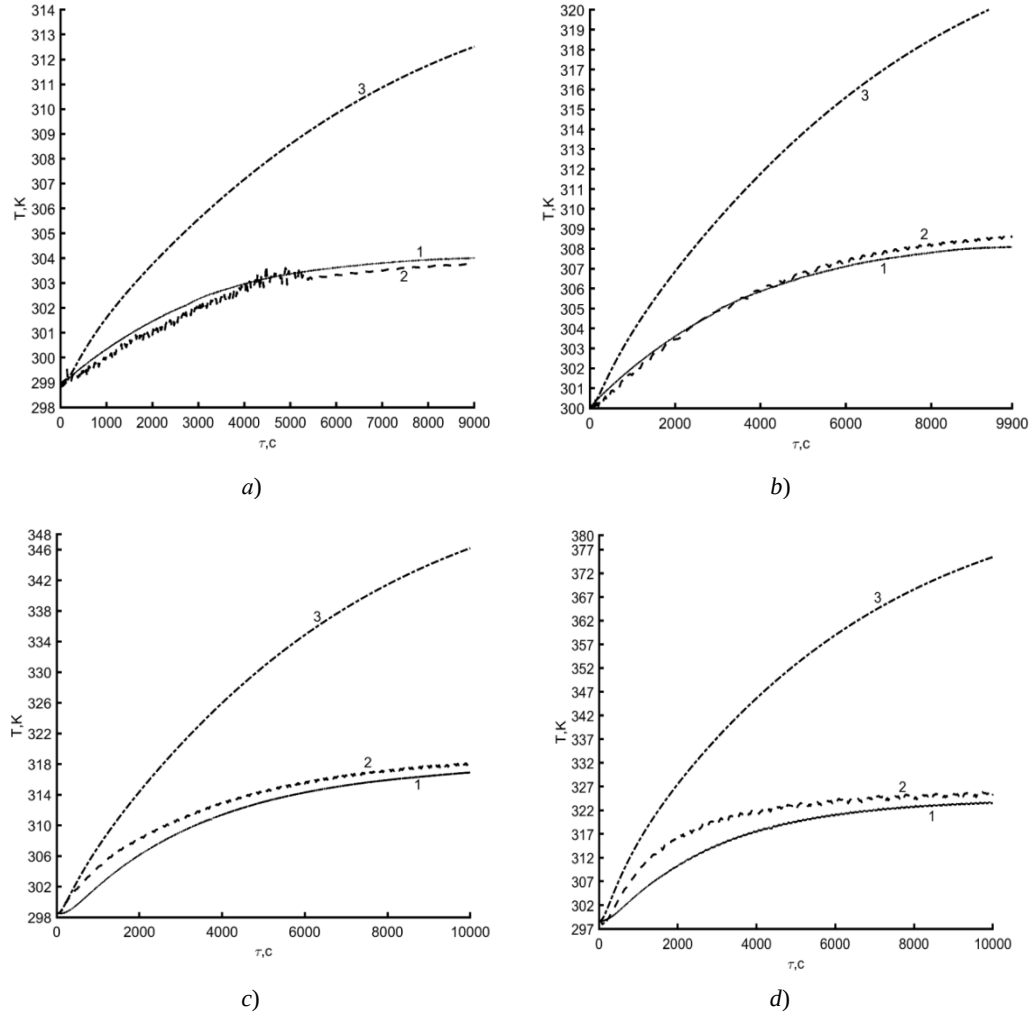

a) *b*)

c) *d*)

Fig. 2. Relationship between temperatures in the coolant layer on the bottom cap of the thermosyphon (x=0 mm, y=6 mm) and time for a thermosyphon fill factor of 8% and heat load q, kW/m^2: a) 0.3; b) 0.4; c) 0.9; d) 1.8. 1 - experiment (-); 2 - numerical modeling (model taking into account thermal conductivity and free convection) (- - -); 3 - numerical modeling (model taking into account only conduction) (-·-·-)

As the heat flow increases to 1.8 kW/m^2, the changes in T in the coolant layer on the bottom cap increase both in numerical simulation and in experiment. In the initial period of time (up to 500 s), the growth dynamics and temperatures are the same for two cases of numerical simulation (Fig. 2, curves 2, 3) and are in good agreement with experimental data (Fig. 2, curve 1). This is explained by the fact that during this period of time convective flows are just beginning to form, their intensity is minimal (Fig. 3, a), and they do not significantly affect the heat transfer in liquid (Fig. 3, b).

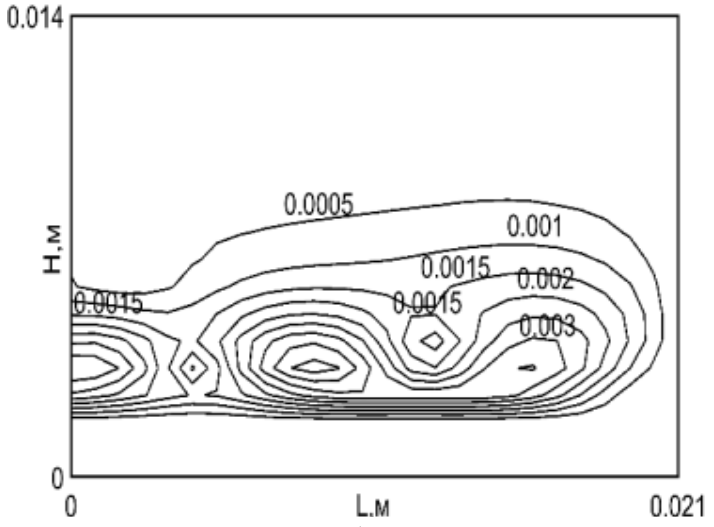

a)

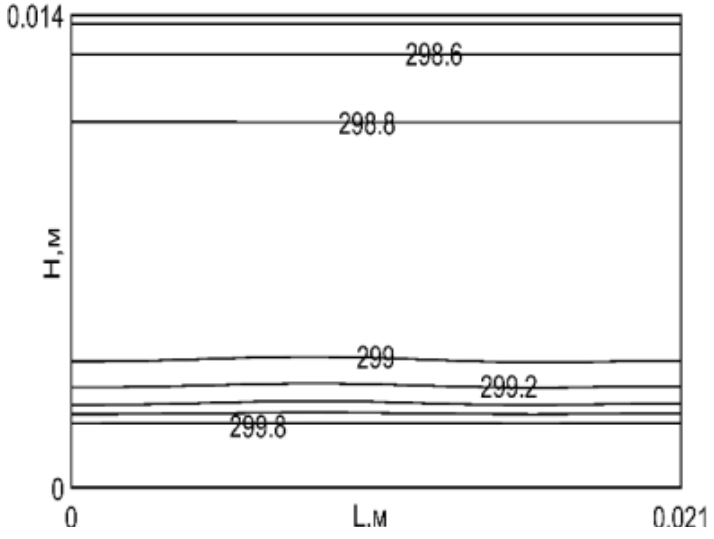

b)

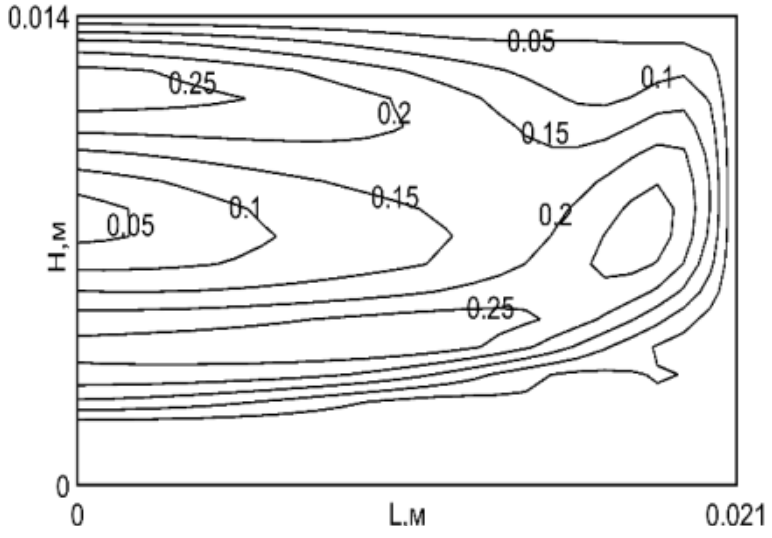

c)

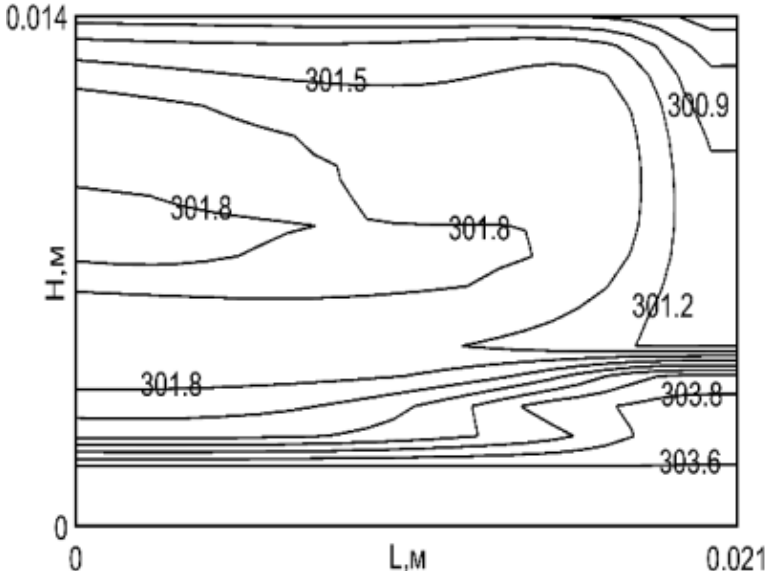

d)

Fig. 3. Isolines of velocities (isotaches) (a, c) and temperature fields (b, d) in the coolant layer on the bottom cap of the thermosyphon at q=300 W/m^2 and time: a, b - 100 s; c, d - 3000 s. Temperature, K; velocity, cm/s

The energy transfer in this case is predominantly conductive. Over time, the forces of thermogravitational convection increase, which leads to the formation of intense circulation flows in the studied area (Fig. 3, c). The heated liquid rises up to the free surface, where heat is removed due to evaporation (Fig. 3, d), the cold one drops down. The temperature difference (curves 2 and 3, Fig. 2) increases with time up to reaching the stationary mode. The temperatures (curve 2, Fig. 2) obtained from numerical simulation (using a model that takes into account thermogravitational convection) are in good agreement with experimental data (discrepancy of not more than 5%),

while the temperatures obtained taking into account only conduction in the bottom cap and the coolant layer differ from experimental ones up to 50%.

Conclusion

Modeling of heat transfer processes in TS can be performed with a fairly high reliability, without description of processes of steam motion in the steam channel, when solving the problem of heat transfer in the heat transfer layer on the bottom cap of the thermosyphon and heat conduction in this cap.

References

1. Fu W, Li X, Wu X, Zhang Z. Investigation of a long term passive cooling system using two-phase thermosyphon loops for the nuclear reactor spent fuel pool. *Annals of Nuclear Energy*. 2015. Vol. 85. P. 346–356.

2. Parida PR, Sridhar A, Vega A, Buyuktosunoglu A., Chainer T. Thermal model for embedded two-phase liquid cooled microprocessor: *Proceedings of the 16th InterSociety Conference on Thermal and Thermomechanical Phenomena in Electronic Systems, ITherm;*30May 2- Jun, 2017;Orlando, USA. 2017. pp. 441-449.

3. Fluder PF, Marzec P, Kos A. Compact model of microprocessor cooling system based on ambient circumstances. *Proceedings of the 24th International Conference on Mixed Design of Integrated Circuits and Systems, MIXDES* 2017. P. 341-344.

4. Karavaev IS, Shtern YI, Kozhevnikov YS., Shtern MY, Degtyarev AA. Thermostating Components for Control of Heat-Transfer Agent Flow. *Measurement Techniques*. 2016. Vol. 59(9). P. 964-970.

5. Vasilyev LL. Perspectives of application of heat pumps in the Republic of Belarus. *IFZh.* 2005; 78(1):23–34. (In Russ.).

6. Ibrahim E, Moawed M, Berbish NS. Heat transfer characteristics of rotating triangular thermosyphon. *Heat Mass Transfer*. 2012; 48:1539–1548. (In Russ).

7.Oh SH, Choi JW, Lee KJ, Cho HH, Kim SI. Experimental study on heat transfer performance of a two-phase single thermosyphon using HFE-7100. *Journal of Mechanical Science and Technology*. 2017; 31(10):4957-4964.

8. Zhang P, Wang B, Shi W, Li X, Experimental investigation on two-phase thermosyphon loop with partially liquid-filled downcomer. *Applied Energy.* 2015. Vol. 160. P. 10–17.

9. Bezrodnyy MK, *Transfer processes in the biphasic thermal siphon systems.* Bezrodnyy MK., Pioro IL, Kostyuk TO. Kiev: Fact, 2005. P. 704. (In Russ.).

10. Kuznetsov GV., Sitnikov AE. *Numerical analysis of basic regularities of heat and mass transfer in*

Литература

1. Fu W., Li X., Wu X., Zhang Z. Investigation of a long term passive cooling system using two-phase thermosyphon loops for the nuclear reactor spent fuel pool // Annals of Nuclear Energy. 2015. Vol. 85. P. 346–356.

2. Parida P.R., Sridhar A., Vega A., Buyuktosunoglu A., Chainer T. Thermal model for embedded two-phase liquid cooled microprocessor // Proceedings of the 16th InterSociety Conference on Thermal and Thermomechanical Phenomena in Electronic Systems, ITherm 2017. P. 441-449.

3. Fluder P.F., Marzec P., Kos A. Compact model of microprocessor cooling system based on ambient circumstances // Proceedings of the 24th International Conference on Mixed Design of Integrated Circuits and Systems, MIXDES 2017. P. 341-344.

4. Karavaev I.S., Shtern Y.I., Kozhevnikov Y.S., Shtern M.Y., Degtyarev A.A. Thermostating Components for Control of Heat-Transfer Agent Flow // Measurement Techniques. 2016. Vol. 59(9). P. 964-970.

5. Васильев Л.Л. Перспективы применения тепловых насосов в Республике Беларусь // ИФЖ. 2005. Т. 78, №1. С. 23–34.

6. Ibrahim E., Moawed M., Berbish N. S. Heat transfer characteristics of rotating triangular thermosyphon // Heat Mass Transfer. 2012. Vol. 48. pp. 1539 –1548.

7. Oh S.H., Choi J.W., Lee K.J., Cho H.H., Kim S.I. Experimental study on heat transfer performance of a two-phase single thermosyphon using HFE-7100 // Journal of Mechanical Science and Technology. 2017. Vol. 31(10), pp. 4957-4964.

8. P. Zhang, B. Wang, W. Shi, X. Li, Experimental investigation on two-phase thermosyphon loop with partially liquid-filled downcomer. // Applied Energy. 2015. Vol. 160. pp. 10–17.

9. Безродный М.К. Процессы переноса в двухфазных термосифонных системах / М.К. Безродный, И.Л. Пиоро, Т.О. Костюк. Киев: Факт, 2005. 704 с.

high-temperature heat pipe. TVT, 40:6 (2002), 964–970.

11. Kuznetsov GV, Al-Ani MA, Sheremet MA. Numerical analyses of convective heat transfer in a closed two-phase thermosiphon. *Journal of Engineering Thermophysics.* 2011; 20 (2): 201–210. (In Russ).

12. Fadhl B, Wrobel LC, Jouhara H. Numerical modelling of the temperature distribution in a two-phase closed thermosyphon. *Applied Thermal Engineering*. 2013. Vol. 60 P. 122–131.

13. Wang X, Zhu Y, Chen H, Wang Y, Fan H. CFD modeling of phase change heat transfer behaviors in thermosyphons. Zhongnan Daxue Xuebao (Ziran Kexue Ban). *Journal of Central South University (Science and Technology).* 2017. Vol. 48(5). P. 1391-1397.

14. Jafari D, Franco A, Filippeschi S, Di Marco P. Two–phase closed thermosyphons: A review of studies and solar applications. *Renewable and Sustainable Energy Reviews.* 2016. Vol. 53. P. 575–593.

15. Feoktistov EA, Vympin EA, Nurpeiis AE. *Experimental research of thermophysical processes in a closed two–phase thermosyphon. MATEC Web of Conf*. 2016.

16. Nurpeiis AE, Orlova EG, Ponomarev KO. *An experimental study of the influence of a thermosyphon filling ratio on a temperature distribution in characteristic points along the vapor channel height. MATEC Web of Conferences.* Les Ulis: EDP Sciences. 2017. Vol. 110: *Heat and Mass Transfer in the Thermal Control System of Technical and Technological Energy Equipment.*

17. Strakhov VL, Garaschenko AN, Kuznetsov GV, Rudzinskii VP. Mathematical simulation of thermophysical and thermos chemical processes during combustion of intumescent fire-protective coating. *Combustion, Explosion and Shock Waves*. 2001; 37:1178–186.(In Russ).

18. Samarskiy AA. *Numerical methods for solving convection – diffusion.* Samarskiy AA, Vabishchevich PN. URSS, 2009. pp 246. (In Russ.).

19. Kuznetsov GV, Strizhak PA. Evaporation of single droplets and dispersed liquid flow in motion through high-temperature combustion products. *High Temperature.* 2014; 52: 568–575. (In Russ).
doi: https://doi.org/10.7868/S0040364414030181.

20. Kuznetsov GV, Strizhak PA. Numerical investigation of the influence of convection in a mixture of combustion products on the integral

10. Kuznetsov G.V., Sitnikov A.E. Numerical analysis of basic regularities of heat and mass transfer in high-temperature heat pipe // TVT. 2002. Vol. 40(6).pp 964–970.

11. Kuznetsov G.V., Al-Ani M.A., Sheremet M.A. Numerical analyses of convective heat transfer in a closed two-phase thermosiphon // Journal of Engineering Thermophysics. 2011. Vol. 20 (2). pp. 201–210.

12. Fadhl B., Wrobel L.C., Jouhara H. Three-dimensional CFD simulation of geyser boiling in a two-phase closed thermosyphon // International Journal of Hydrogen Energy. 2019. Vol. 41(37), pp. 16463-16476.

13. Wang X., Zhu Y., Chen H., Wang Y., Fan H. CFD modeling of phase change heat transfer behaviors in thermosyphons // Zhongnan Daxue Xuebao (Ziran Kexue Ban)/Journal of Central South University (Science and Technology). 2017. Vol. 48(5). pp. 1391-1397.

14. Jafari D., Franco A., Filippeschi S., Di Marco P. Two–phase closed thermosyphons: A review of studies and solar applications // Renewable and Sustainable Energy Reviews. 2016. Vol. 53. P. 575–593.

15. Feoktistov E.A., Vympin E.A., Nurpeiis A.E. Experimental research of thermophysical processes in a closed two–phase thermosyphon // MATEC Web of Conf. 2016. Vol. 72.

16. Nurpeiis A.E., Orlova E.G., Ponomarev K.O. An experimental study of the influence of a thermosyphon filling ratio on a temperature distribution in characteristic points along the vapor channel height // MATEC Web of Conferences. Les Ulis: EDP Sciences. 2017. Vol. 110: Heat and Mass Transfer in the Thermal Control System of Technical and Technological Energy Equipment.

17. Strakhov V.L., Garaschenko A.N., Kuznetsov G.V., et al. Mathematical simulation of thermophysical and thermos chemical processes during combustion of intumescent fire-protective coating // Combustion, Explosion and Shock Waves. 2001.Vol. 37. pp 1178–186.

18. Самарский А.А. Численные методы решения задач конвекции – диффузии / А.А. Самарский, П.Н. Вабищевич. URSS, 2009. 246 с.

19. Kuznetsov G.V., Strizhak P.A. Evaporation of single droplets and dispersed liquid flow in motionthrough high-temperature combustion products // High Temperature. 2014. Vol. 52: pp. 568–575.

characteristics of the evaporation of a finely atomized water drop. *Journal of Engineering Physics and Thermophysics.* 2014; 87:103–111. (In Russ) doi.org/10.1007/s10891-014-0990-8.

21. Nurpeiis A, Nemova T. *The Opportunity Analyses of Using Thermosyphons in Cooling Systems of Power Transformers on Thermal Stations. MATEC Web of Conferences* 72, 01077 (2016).

20. Kuznetsov G.V., Strizhak P.A. Numerical investigation of the influence of convection in a mixture of combustion products on the integral characteristics of the evaporation of a finely atomized water drop // Journal of Engineering Physics and Thermophysics. 2014. Vol. 87.pp 103–111.

21. Nurpeiis A., Nemova T. The Opportunity Analyses of Using Thermosyphons in Cooling Systems of Power Transformers on Thermal Stations // MATEC Web of Conferences 72, 01077 (2016).

Authors of the publication

Vyacheslav I. Maksimov – Tomsk Polytechnic University, School of Energy & Power Engineering.

Atlant E. Nurpeiis –Tomsk Polytechnic University, School of Energy & Power Engineering.

Received ***December 3, 2018***

UDC 620.9 **DOI:10.30724/1998-9903-2019-21-3-14-23**

DETECTION OF INTER TURN FAULT IN TRANSFORMER WINDINGS BY PARAMETERS OF THEIR TRANSITION PROCESSES

R.G. Mustafin

Kazan State Power Engineering University, Kazan, Russia

ramil.mustafin@gmail.com

Abstract: *The proposed method of detection the inter turn fault of transformer windings relates to the area of defectoscopy and allows detecting inter turn faults in a wide range of damaged (closed) turns. Power and instrument transformers with iron-core are widely used in power networks. As the insulation ages or is damaged, the wires between various transformer sections short circuits occur, which inevitably leads to a complete damage of the transformer. Short-circuited part of the transformer forms an additional winding, the outputs of which are short-circuited. The transition process of current increasing when DC voltage is connected to the transformer outputs occurs in diverse ways in undamaged (cut-off) winding section and in the damaged (short-circuited) section. The current growth rate in the undamaged section of the winding is determined by high magnetization inductance. The inductance of the short-circuited part of the winding is much less, so, the current growth rate in the short-circuited part is significantly greater than the current growth rate in the undamaged part of the winding. The article presents observations from computer models and real measurements of the substation auxiliary power transformer, which show the possibility of determining the presence of a turn fault in regards to the transition process parameters, the rate of current increase and decay in the transformer winding. The device aimed to find the inter turn faults in the transformer windings, working according to the proposed method will be quite simple and have a high sensitivity*.

Keywords: *transformer, ferromagnetic core, inter turn fault, transition process.*

For citation: Mustafin RG. Detection of inter turn fault in transformer windings by parameters of their transition processes. *Power engineering: research, equipment, technology*. 2019; 21(3):14-23. (In Russ). doi:10.30724/1998-9903-2019-21-3-14-23.

ОБНАРУЖЕНИЯ ВИТКОВЫХ ЗАМЫКАНИЙ ОБМОТОК ТРАНСФОРМАТОРОВ ПО ПАРАМЕТРАМ ПЕРЕХОДНОГО ПРОЦЕССА

Р.Г. Мустафин

Казанский государственный энергетический университет, г. Казань, Россия
ramil.mustafin@gmail.com

Резюме: *Предлагаемая методика обнаружения витковых замыканий обмоток трансформаторов относится к области дефектоскопии и позволяет обнаруживать витковые замыкания в обмотках трансформатора в широком диапазоне поврежденных (замкнутых) витков. Силовые и измерительные трансформаторы с железным сердечником широко применяются в электроэнергетических сетях. При старении изоляции, при повреждении изоляции, в трансформаторах возникают замыкания между*

витками из разных частей обмотки, что неизбежно приводит к полному повреждению трансформатора. Короткозамкнутая часть обмотки трансформатора образует дополнительную обмотку, выводы которой замкнуты накоротко. Переходный процесс роста тока при подключении постоянного напряжения к выводам трансформатора по-разному происходит в неповрежденной (разомкнутой) части обмотки, и в поврежденной (короткозамкнутой) части. Скорость роста тока в неповрежденной части обмотки определяется большой величиной индуктивности намагничения. Индуктивность короткозамкнутой части обмотки значительно меньше, соответственно скорость роста тока в короткозамкнутой части существенно больше скорости роста тока в неповрежденной части обмотки. В статье приводятся наблюдения в компьютерной модели и в реальных измерениях на трансформаторе собственных нужд подстанции возможность определения наличия витковых замыканий по параметрам переходного процесса, по скорости нарастания и спада тока в обмотке трансформатора. Прибор, предназначенный для поиска витковых замыканий в обмотках трансформатора, работающий по предлагаемой методике будет достаточно простым и иметь высокую чувствительность.

Ключевые слова: *трансформатор, ферромагнитный сердечник, витковые замыкания, переходный процесс.*

Introduction

One of the most frequently-occurring transformer defects is the inter turn fault, when some of the transformer winding turns is short-circuited [1]. Usually, the presence of inter turn faults is detected from the parameters of the transformer normal operation at industrial frequency of 50 Hz [2-6]. Increasing the frequency range during measurements of transformer parameters can increase the sensitivity of detection methods of inter turn faults [7, 8].

In case of inter turn faults, two parts of a winding are formed: the undamaged part (A in Fig. 1), which plays the role of the primary transformer winding, and short-circuited one (B in Fig. 1), which works as a secondary transformer winding.

To analyze the operation of the transformer winding with an inter turn fault, consider the T-shaped model [9] (Fig. 1), where the active resistance of the A turns is *Ra*; scattering inductance of the A turns is *La*; active resistance of B turns is *Rb*; scattering inductance of the B turns is *Lb*; inductance of saturation is *L'o* (which is less than the initial inductance *Lo* due to short-circuiting of B turns); E is the EMF connected to the winding. (All values are given for side A).

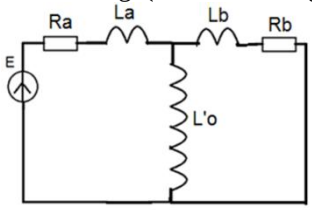

Fig. 1. T-shaped model of winding with inter turn fault (B turns)

Note that the scattering inductances of turns *La* and *Lb* are significantly less than the saturation inductance of *L'o*, so the time constant *Tab* (of the *Ra-La-Lb-Rb* circuit), equal to, $T_{ab} = (L_a + L_b)/(R_a + R_b)$, is significantly less than the time constant *T'o* (of the *Ra-La-L'o* chain), which is equal to. $T_o^{'} = (L_a + L_o^{'})/R_a$. Thus, the time constant *Tab* of the winding with inter turn fault is significantly less than the time constant of the saturation circui *T'o*: $T_{ab} \ll T_o^{'}$ This difference governs the principle of detection the inter turn faults of transformer windings: the

time constant is measured in wide range, and the presence of transients with a small transition time clearly indicates the winding short circuits in the transformer winding.

Materials and methods

To illustrate the operating principle of method for detection the inter turn fault of transformed windings, the Matlab/Simulink software was used to build the model (Figure 2).

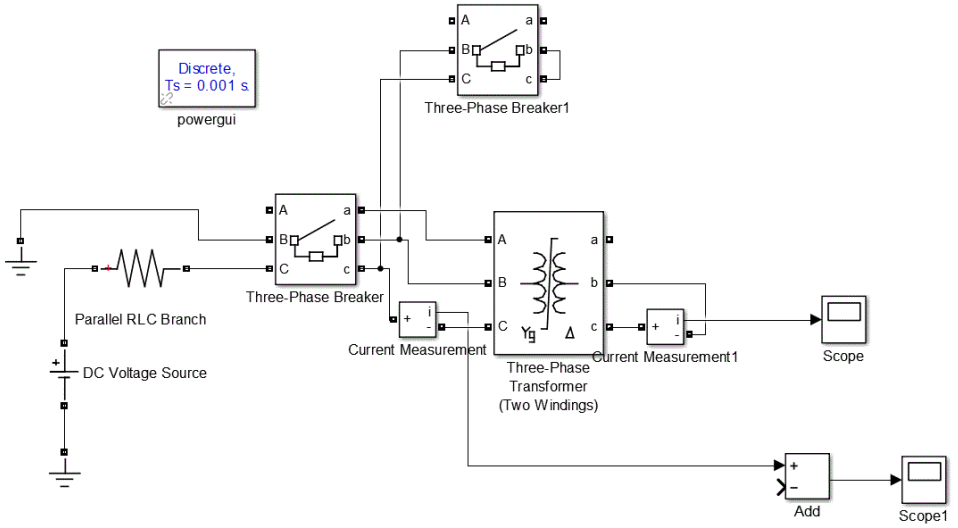

Fig. 2. The model of a transformer with a inter turn short-circuit, which is presented in the form of a short-circuited secondary transformer winding

Fig 3 presents the parameters of the three-phase transformer model.

A short-term DC voltage of 100 V (from *DC Voltage Source* in Fig. 2), is supplied to the primary winding of transformer (*Three-Phase Transformer*) through the current limiting resistance (*Parallel RLC Branch*) of 60 Ohms active resistance. Three-phase breaker (*Three-Phase Breaker*) connects DC voltage to the primary winding of the transformer (to the BC winding) in 0.02 seconds after the model start-up. The second three-phase switch (*Three-Phase Breaker1*) closes the primary winding of the transformer (BC winding) in 0.5 seconds after the model start-up. Thus, magnetization of the transformer core occurs in the range of 0.02 – 0.5 seconds (current increase in the primary winding), after 0.5 seconds, the demagnetization of the transformer core occurs (current drop in the primary winding).

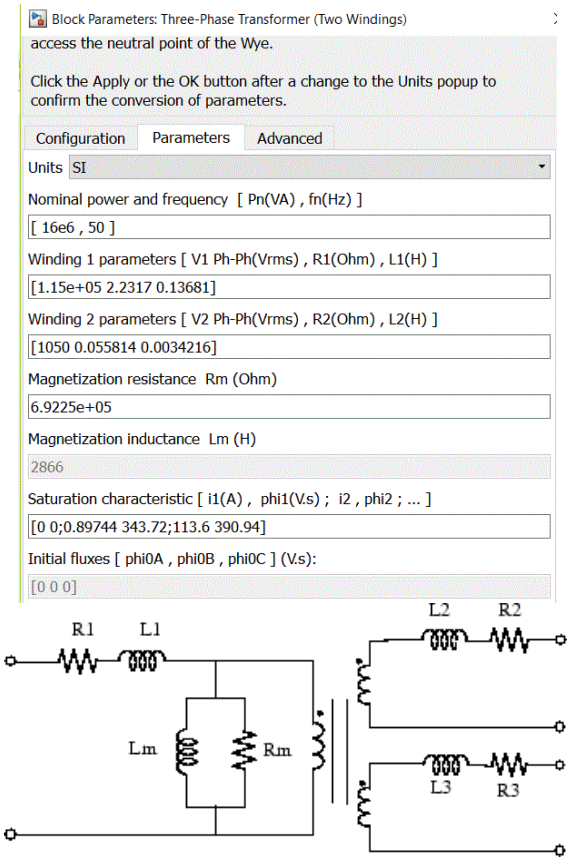

Fig. 3. Characteristics of transformer used in the model

In the absence of inter turn short circuits (secondary turns of the transformer *bc* are not closed), the transformer magnetization inductance is high (*Magnetization Inductance Lm (H)* in Fig. 3), consequently, the rate of magnetization current change is small (Fig. 4).

When a turn short circuit occurs (transformer secondary turns *bc* are closed), the model has two magnetization inductances: the primary circuit BC and the short circuit of *bc* turns. Moreover, the number of turns in the primary winding is much larger than the number of turns in the turn faults (as it can be seen in Fig. 3, from *Winding 1 parameters V1* and *Winding 2 parameters V2*). Therefore, the magnetization inductance of the primary BC circuit is much greater than the magnetization inductance of the inter turn short circuit *bc*. This is reflected in the rate of increase and decrease of the magnetization current (Fig. 5): first (up to a time of the order of 0.1 s), a rapid increase in current occurs in the inter turn short circuit bc.

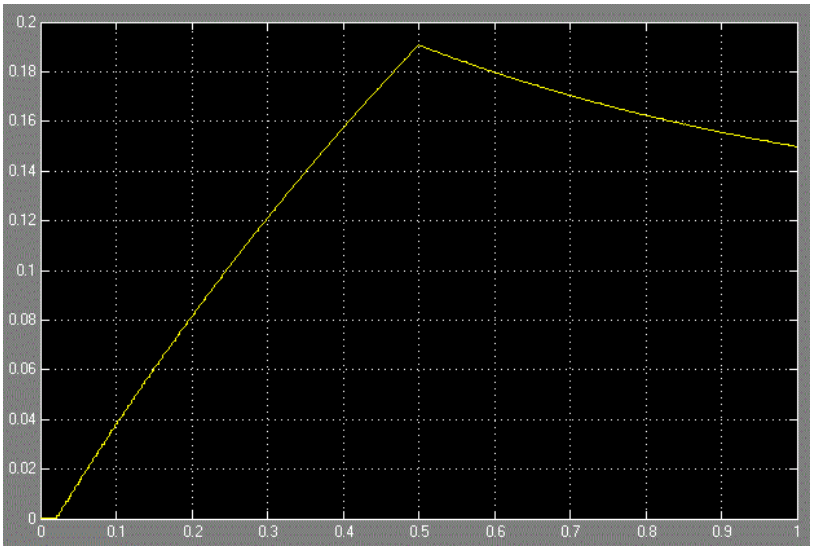

Fig. 4. Current in the primary winding BC in the absence of inter turn short circuits. Horizontal axis is time, s; vertical axis is current, A

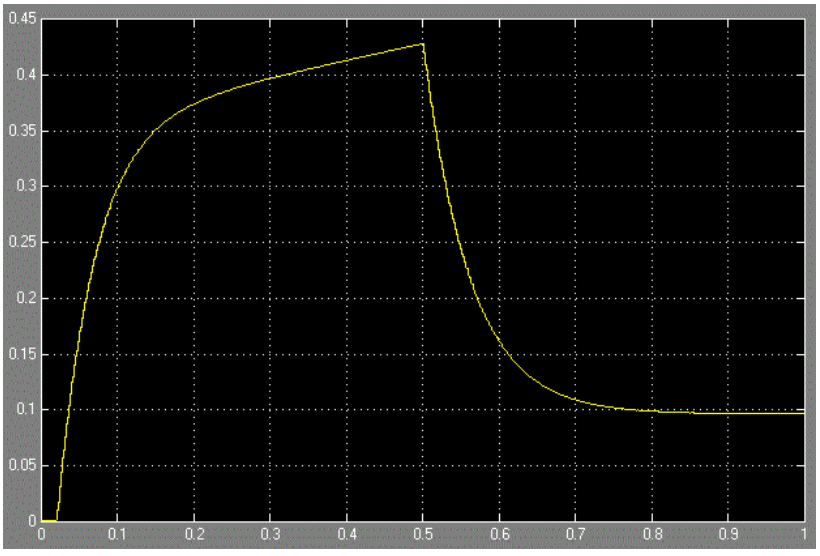

Fig. 5. Current in the primary winding BC in the presence of inter turn short circuits (the secondary transformer turns *bc* are closed). Horizontal axis is time, s; vertical axis is current, A

After current saturation in inter turn short circuit (as shown in Fig. 6), only the slow growth of the magnetization current component in the primary winding BC remains (at times from about 0.2 to 0.5 s). After the primary winding BC closes, a similar process occurs: a rapid decrease in the inter turn short circuit current (Fig. 6) (approximately in the range from 0.5 to 0.7 s), then a slow decrease in the current in the primary BC circuit (see Fig. 5).

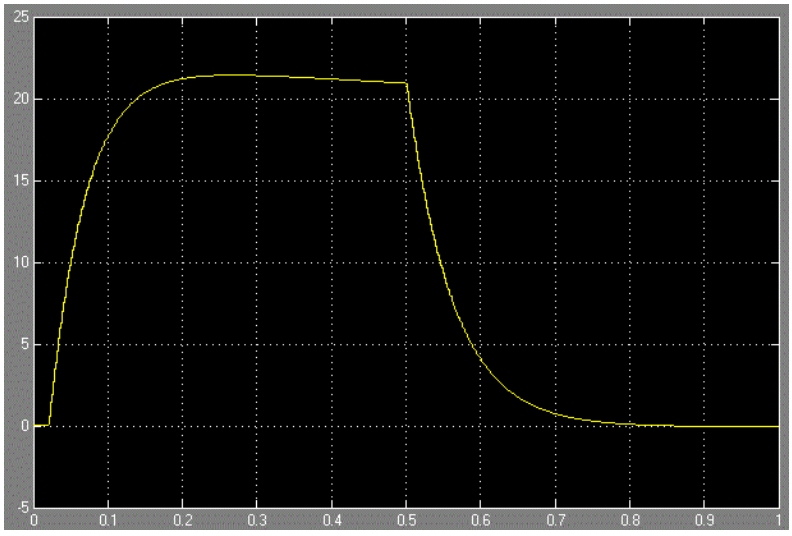

Fig. 6. Current in inter turn short circuits bc. Horizontal axis is time, s; vertical axis is current, A

Results

From the presented model of inter turn failures in transformers (Figs. 2 - 6), it can be seen that, based on the large difference in the rates of current change in the primary winding BC and in the inter turn short circuit *bc*, it becomes possible to create a device for detecting coil faults in transformer windings [10], using which the search for coil damage is significantly facilitated.

To verify and test the proposed methodology, transients were measured using an auxiliary transformer TSKS-40/145/10-UZ of Askold Electrotechnical Plant LLC (TU 3411-002-65653492-2010, the transformer idle run current is not more than 12%, power is 38 kVA, number of phases is 3, frequency is 50 Hz, degree of protection is IP 00, rated voltage of HV winding is 10 kV, rated voltage of HV winding is 0.4 kV, rated current of HV winding is 2.19 A, rated current of LV winding is 54.9 A , short circuit voltage is 1.48%, insulation class F, circuit and group connection is *Y/Yn-O*).

To record transients, the digital oscilloscope 6501 was used; the current in the transformer windings was measured by recording the voltage drop across the active resistance, connected in series with the measured transformer winding. Initially, a constant voltage of 8 V (through an active resistance of 47 Ohms) was applied to the primary HV winding of the transformer (BC pins). The current through the winding was measured by the voltage drop at a resistance of 10 Ohms, while the behavior of the transient process (with open - Fig. 7 and with closed - Fig. 8 turns of the secondary LV transformer windings) was similar to the picture observed in the Matlab/Simulink program (see Figs. 4, 5).

There are several ways for increasing the sensitivity of the proposed method:

1. By increasing DC voltage supplied to the transformer windings, while reducing the measurement time interval (to maintain the same current in the transformer winding).

2. By applying a constant voltage (measuring transient) in the windings of the lower voltage (LV).

3. By obtaining the reference measurements of the transient process in all windings of the undamaged (without winding short circuits) transformer. Further, during periodic measurements, the current transient measurements in the transformer windings should be compared with the saved reference measurements.

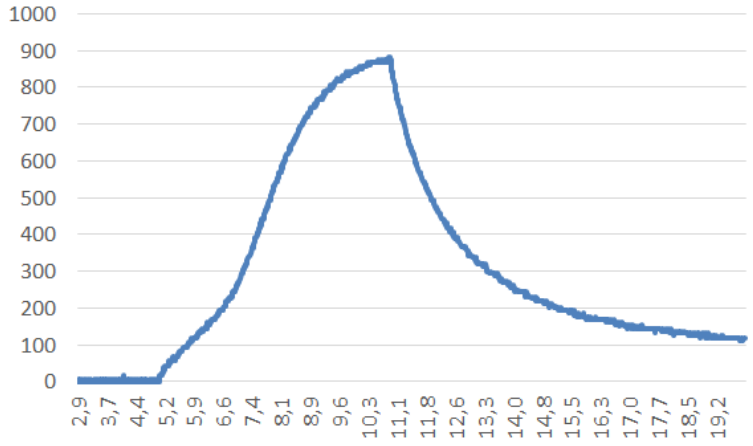

Fig. 7. The transient process in the primary HV winding (BC pins). At specific time (5 s) DC voltage of 8 V was connected to the HV; at time of 11 s HV winding was closed.
The X axis is time, s; the Y axis is voltage amplitude, mV, at a resistance of 10 Ohms
(current measurement in the HV primary winding)

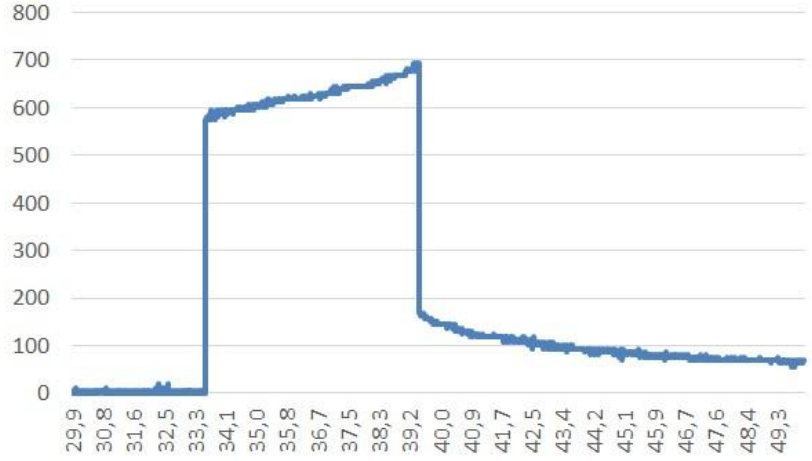

Fig. 8. The transient process in the primary HV winding (BC pins), the secondary LV winding (BC pins) are closed. At a time of 33.5 s, a DC voltage of 8 V was applied to the HV through a resistance of 47 Ohms; at a time of 39.5 s, the HV winding was closed.
The X axis is time, s; the Y axis is voltage amplitude, mV, at a resistance of 10 Ohms
(current measurement in the HV primary winding)

Further DC voltage of 8 V (through an active resistance of 10 Ohms) was applied to the secondary LV transformer winding (*bc* pins), the current through the winding was measured by the voltage drop at a resistance of 1 Ohm. A clear difference between the transient process in the absence (Fig. 9) and in the presence (Fig. 10) of inter turn fault (additionally wound one short-circuited turn on the B phase core) was observed.

Fig. 9. The transient process in the secondary LV winding (*bc* pins). At time of 0.02 s a constant voltage of 8 V through a resistance of 10 Ohms was applied to the LV; at time of 0.10 s, the LV winding was closed. The X axis is time, s; the Y axis is voltage amplitude, mV, at a resistance of 1 Ohms (current measurement in the LV secondary winding)

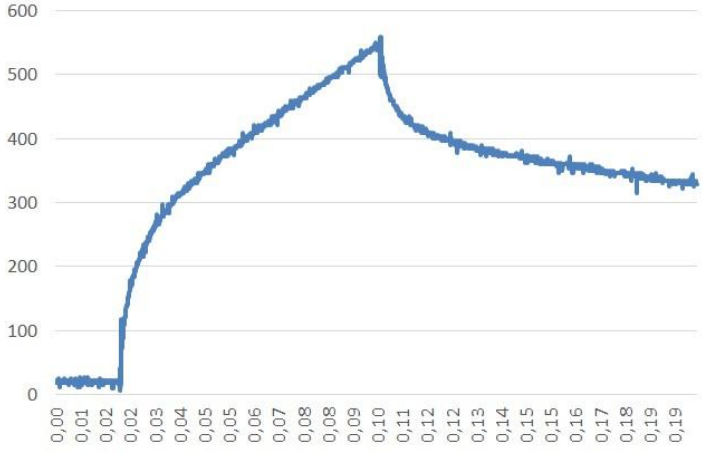

Fig. 10. The transient process in the secondary LV winding (*bc* pins) in the presence of inter turn fault (additionally wound one short-circuited turn on the B phase core).
At time of 0.02 s a constant voltage of 8 V through a resistance of 10 Ohms was applied to the LV; at time of 0.10 s, the LV winding was closed. The X axis is time, s; the Y axis is voltage amplitude, mV, at a resistance of 1 Ohms (current measurement in the LV secondary winding)

Conclusions

Thus, in the proposed method for detection the inter turn faults of transformed windings, the transients are measured in wide ranges of times, which allows tuning away from transformer magnetization currents, by measuring the transient in the fault itself, namely in the short-circuited turns of the transformer winding. This solves the task of detecting the inter turn faults in the transformer windings in a wide range of damaged (closed) turns.

The author expresses his gratitude to Badretdinov Nail (head of the laboratory of the educational and research center "Electric Power Engineering" of KSPEU) and Zapechelnyuk Eduard (head of the laboratory of the department “Relay protection and automation” of KSPEU) for assistance in measurements.

References

1. Bartley W. *Analysis of Transformer Failures. International Association of Engineering Insurers 36 th Annual Conference*. Stockholm, Sweden, 2003.
2. Pyatkov AV. Determination of inter turn fault in the windings of a power transformer with switching without excitation. In the collection: *Energetics - to the agro-industrial complex of Russia*. South-Ural State Agrarian University. 2017. pp. 156–160.
3. Oliveira L. Comparing Power Transformer Turn-to-Turn Faults Protection Methods: Negative Sequence Component Versus Space Vector Algorithms. Oliveira L, Cardoso AJM. *IEEE Transactions on Industry Applications*. 2017. Vol.53: 2817–2825.
4. Tytko O. Definition of turn-fault of stator winding induction motor on the basis of the compensation magnetic field. O Tytko, AV Khudiakov. *Технічна електродинаміка*. 2017. № 1. С. 58–61.
5. Fedotov GI. Turn fault of a power transformer and methods for diagnosing them. Fedotov G.I., Golgovskikh AV. *Society, science, innovations* (NPK-2016) Collection of articles 2nd ed, revised and updated. Vyatka State University. 2016. pp. 2080–2083.
6. Sheryazov SK. Monitoring Device for Power Transformers 6-10. 0.4 kV. Sheryazov S.K., Pyatkov A.V. *Proceedings of the LV Intern. Scientific. -Tech. conf. "Achievements of science - agro-industrial production*." Chelyabinsk: SUSU. 2016. P. 240–244.
7. Ivanova ZG. Development of a device for detecting inter turn fault in the windings of dry power transformers. Ivanova ZG, Makarova NL. *Vestnik Moskovskogo gosudarstvennogo agroinzhenernogo universiteta im. V.P. Goryachkina.* VP. 2013. № 1 (57). P. 30–31.
8. Makarova NL. *Diagnosing the state of isolation of power transformers of rural electric networks.* Makarova NL, Akhmetshin RS. monograph. M .: FGBOU VPO MSAU, 2012.pp 90 .
9. Stanley HH. *Power System Relayi*ng. Third Edition. Stanley H. Horowitz, Arun G. Phadke. doi:10.1002/9780470758786. 2008 Research Studies
10. Mustafin RG. *Utility model "Device for detecting windings short circuits of transformer windings* Patent. RF 07.11.2017 Bull. N 20 Accessed: 02.02.2017.

Литература

1. Bartley W. Analysis of Transformer Failures // International Association of Engineering Insurers 36th Annual Conference. Stockholm, Sweden, 2003.
2. Пятков А.В. Устройство определения витковых замыканий в обмотках силового трансформатора с переключением без возбуждения // Энергетика - агропромышленному комплексу РОССИИ. Южно-Уральский государственный аграрный университет, 2017. С. 156–160.
3. Oliveira L. Comparing Power Transformer Turn-to-Turn Faults Protection Methods: Negative Sequence Component Versus Space Vector Algorithms / L. Oliveira, A.J.M. Cardoso // IEEE Transactions on Industry Applications. 2017. Vol. 53. P. 2817–2825.
4. Tytko O. Definition of turn-fault of stator winding induction motor on the basis of the compensation magnetic field / Tytko O., Khudiakov A.V. // Технічна електродинаміка. 2017. № 1. С. 58–61.
5. Федотов Г.И. Витковые замыкания силового трансформатора и методы их диагностирования / Г.И. Федотов, А.В. Голговских // Общество, наука, инновации (НПК-2016):. 2-е издание, исправленное и дополненное. Вятский государственный университет. 2016. С. 2080–2083.
6. Шерьязов С.К. Устройство мониторинга силовых трансформаторов 6-10/0,4 кВ / С.К. Шерьязов, А.В. Пятков // Материалы LV Междунар.науч.-техн. конф. «Достижения науки - агропромышленному производству». Челябинск : ЮУрГАУ, 2016. С. 240–244.
7. Иванова З.Г. Разработка устройства для выявления витковых замыканий в обмотках сухих силовых трансформаторов / З.Г. Иванова, Н.Л.Макарова. //Вестник Московского государственного агроинженерного университета им. В.П. Горячкина. 2013. № 1 (57). С. 30–31.
8. Макарова Н.Л. Диагностирование состояния изоляции силовых трансформаторов сельских электрических сетей: монография / Н.Л. Макарова, Р.С. Ахметшин. М.: МГАУ, 2012. 90 с.
9. Stanley H. H. Power System Relaying, Third Edition / Stanley H. Horowitz, Arun G. Phadke // Print ISBN:9780470057124, |Online ISBN:9780470758786. 2008 Research Studies Press Limited.
10. Мустафин Рамиль Гамилович «Устройство обнаружения витковых замыканий обмоток

трансформаторов» Патент РФ 11.07.2017. Бюл. № 20 Ссылка активна на: 02.02.2017.

Authors of the publication

Ramil G. Mustafin– candidate of physical and mathematical sciences, the associate professor at "Relay protection and automation of electrical power systems", Kazan State Power Engineering University.

Received ***December 29, 2018***

UDC 620.97 **DOI:10.30724/1998-9903-2019-21-3-24-31**

CLOSED CYCLE OF AIR-STEAM MIXTURE IN THE DRYING SECTION OF PAPER MACHINE

V.G. Kazakov, E.N. Gromova

Higher School of Technology and Energy of St. Petersburg State University of Industrial Technologies and Design, St. Petersburg, Russia
gromova.gturp@mail.ru

Abstract: *The energy efficiency of the drying section of paper machine is determined by the technology of heat flows arrangements in it. Paper drying is the most energy-consuming stage of paper production. The thermal mode of the drying section is provided by the steam condensate system which is a part of it. Analysis of exergy increments shows that almost all elements of the drying thermal process are characterized by low exergy efficiency. The main ways for increasing the degree of thermodynamic perfection of the processes occurring in the drying section of the paper machine are identified based on the exergy analysis. It is assumed that the deep internal heat recovery of the steam-air mixture for heating the source air will increase the exergy efficiency of the heat recovery plant and reduce heat removal to the environment. The effectiveness of development and implementation of a closed cycle use of steam-air mixture in the drying section was examined. Building a closed cycle provides that the air mainly has a process duty, that is, it is a transport agent for the transfer of moisture and heat along a closed circuit. The calculations show that the exergy efficiency of the processes in the recovery unit of the drying section of the paper machine of the existing production is 28.6% against 66.29% for the proposed method.*

Keywords: *paper machine, paper drying, exergy analysis, energy saving, exergy efficiency, ventilation systems with heat recovery, heat exchanger, exergy, process ventilation, paper production, heat recovery, energy efficiency.*

For citation: Kazakov VG, Gromova EN. Closed cycle of air-steam mixture the drying section of paper machine. *Power engineering: research, equipment, technology* 2019; 21(3):24-31. (In Russ). doi:10.30724/1998-9903-2019-21-5-6-24-31.

ЗАМКНУТЫЙ ЦИКЛ ПАРОВОЗДУШНОЙ СМЕСИ В СУШИЛЬНОЙ ЧАСТИ БУМАГОДЕЛАТЕЛЬНОЙ МАШИНЫ

В.Г. Казаков, Е.Н. Громова

Высшая школа технологии и энергетики Санкт-Петербургского государственного университета промышленных технологий и дизайна, г. Санкт-Петербург, Россия
gromova.gturp@mail.ru

Резюме: *Энергетическая эффективность бумагоделательной машины определяется технологией организации тепловых потоков в ее сушильной части. Сушка бумаги является наиболее энергетически затратным этапом производства бумажной продукции, так как наибольшее количество водяных паров выделяется именно в сушильной части БДМ.*

Рациональное распределение потоков воздуха и паровоздушной смеси в сушильной части способствует повышению производительности и стабилизации работы машины.

Литературный обзор. Тепловой режим сушильной части обеспечивается входящей в её *состав пароконденсатной системой. Существующие системы теплоснабжения с каскадным распределением давления, в состав которых входят, как правило, двухступенчатые теплорекуперационные установки позволяют частично утилизировать низкопотенциальную теплоту отработавшего пара и сушильного воздуха*.

Материалы и методы: *Авторами были произведены расчеты сушильной части действующей бумагоделательной машины. Распределение энергии по функциональным частям БДМ в случае традиционной технологической схемы позволяет сделать следующий вывод: при незначительной доле удаляемой влаги в сушильной части БДМ (0,7 %), потребление энергии здесь максимально. Анализ приращений эксергии показывает, что практически все элементы теплового процесса сушки характеризуются низкими значениями эксергетических КПД. На основании эксергетического анализа в статье выделяются основные направления повышения степени термодинамического совершенства технологического процесса в сушильной части бумагоделательной машины.*

Результаты и обсуждение: *Предполагается, что глубокая внутренняя регенерация теплоты паровоздушной смеси для нагрева исходного воздуха позволит увеличить эксергетический КПД теплорекуперационной установки и снизить отвод теплоты в окружающую среду. Рассматривается эффективность разработки и реализации замкнутого цикла использования паровоздушной смеси в сушильной части. Организация замкнутого цикла предусматривает, что воздух, в основном, несет технологическую нагрузку, то есть является транспортным агентом в переносе влаги и теплоты по замкнутому контуру.*

Выводы: *Проведенные расчеты показывают, что эксергетический КПД процессов в рекуперационной установке сушильной части бумагоделательной машины действующих производств составляет 28,6 % против 66,29 % в предложенном способе. В целом, эксергетический КПД сушильной части БДМ в случае реализации замкнутого цикла паровоздушной смеси будет равен 72,4 %.*

Ключевые слова: *бумагоделательная машина; сушка бумаги; эксергетический анализ; энергосбережение; эксергетический КПД; системы вентиляции с рекуперацией теплоты; теплорекуператор; эксергия; технологическая вентиляция; производство бумаги; утилизация теплоты; энергетическая эффективность.*

Introduction

The energy efficiency of a paper machine (PM) is largely determined by the technology for heat flows arrangement in the drying section.

Modern paper machines are equipped with rather complex and high-performance ventilation systems and installations that ensure successful running of the paper manufacturing process. Along the entire paper motion from the headbox to the reel the necessary thermo-humid regime of the air surrounding the paper sheet is created using ventilation systems. PM includes wire, press and drying sections. The wire section is designed to remove the main part of moisture and formation of the paper web, the press part is aimed at removing the additional moisture by pressing. The remaining part of moisture is removed by drying in the drying section of the machine [1].

A large amount of moisture is released from the surface of the wet web. Ventilation units are used to remove the forming water vapors from the wire section outside the hall. At the same time, their condensation on the surrounding surfaces is prevented, and the necessary sanitary conditions for the staff are created. The highest water vapor emissions occur in the drying section

of the machine. The supply and removal of heat in this part of PM determines the heat consumption from external sources. That is why the drying section has long been the object of close attention of scientists and engineers as the object of the greatest expenditure of thermal energy.

Ensuring the necessary parameters of the air environment is achieved by the arranged supply of fresh and exhaust air.

The rational distribution of air flows, the optimal choice of parameters and the frequency of air exchange in the drying section contribute to increased productivity and stabilization of the machine operation, alignment of the moisture profile of the paper web.

Literature review

The thermal regime of the drying section is provided by the steam condensate system which is a part of it. Currently, the group heat supply system with cascade pressure distribution and steam bypass over individual groups of cylinders has gained predominant use. Such a heat supply system prevents the passage of steam into the condensate system [2,3].

The thermal circuit of the drying section consists of three functional groups: drying cylinders, water separators and heat recovery unit. A heat recovery unit is an integral part of the existing paper machines and includes three units, each of which consists of two recovery stages (heat exchangers) and a scrubber for heating the process water. The first stage of recovery provides pre-heating of the process (drying) air, the second one provides heating of the outside (ventilation) air. Thus, the low-grade heat of the exhaust steam and the drying air is partially used. From the press section of the machine, the wet paper web enters the first paper dryer cylinder. After passing 46 drying cylinders, 92% of the paper web dried to dryness is removed from the drying section for further processing.

From under the hood cap of the PM drying section the air-steam mixture *1* (Fig. 1) with a temperature of 100 °C is fed into the first recovery stage *2* (TU-1). The air-steam mixture gives some part of heat to the process (drying) air *17* supplied from the machine room with a temperature of 28 °C, and heats it up to 42 °C. Drying air from the recovery stage *2* is fed into the air heater *12* by centrifugal fan *8*, where it is heated to 100 °C, and after it is sent under the hood cap of the drying section of the machine *14*.

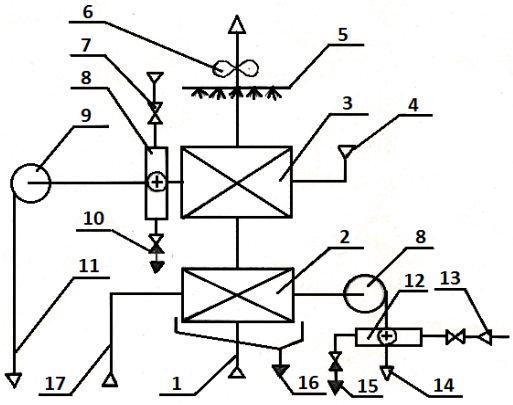

Fig. 1. Technological scheme of a traditional heat recovery unit:
1 - air-steam mixture; *2* - heat exchanger (heat trap) TU1;
3 - heat exchanger (heat trap) TU2; *4* - outside air;
5 - scrubber; *6* - axial fan; *7* - shutoff valve;
8 - air heater; *9* - centrifugal fan; *10* - check valve;
11 - ventilation air; *12* - air heater; *13* - steam; *14* - drying air;
15 - condensate; *16* - scrubber water and condensate from the exhaust air;
17 - air supplied from the machine room

Condensate *15* is discharged to the CHP, and scrubber water *16* is used to dilute the paper

pulp. Outside air in the winter period is heated in the second recovery stage *3* up to temperature of 0 °C, and then it is heated to 20 °C in a heater *8* by steam from the thermal power plant. From the heater *8*, the heated air is supplied to the machine hall *11*, where it assimilates the heat of equipment and reaches temperature of 28 °C, at which it enters the first recovery stage *2*.

The partially cooled air-steam mixture flows from the first recovery stage *2* (TU-1) to the second recovery stage *3* (TU-2), where it gives some part of its heat (up to the saturation temperature) to the outside air *4*. Next, the air-vapor mixture enters the scrubber *5*. The purpose of the scrubber is to separate moisture from the steam-air mixture by cooling it. The steam in it condenses. The temperature of the air discharged from the scrubber is 45 °C.

Materials and methods

The authors have calculated the drying section of the existing paper machine.

The drying section of the paper machine under consideration consists of 46 paper drying and one refrigerating cylinders. The drying cylinders are arranged in two rows, staggered, and are heated by condensing steam. Its dryness before drying is 43.5%, final dryness of paper is 92%. The temperature of the pulp after the wire frame is 50 °C. The consumption of drying air is 12 kg per 1 kg of evaporated water. The productivity is 13.1 tons of paper per hour.

Energy supply and dehumidification for various parts of PM are given in table 1.

Table 1

Energy distribution at PM

No.	Characteristics	Wire section		Press section		Drying section	
		Driver	Vacuum-pumps	Driver	Vacuum-pumps	Electrical energy	Steam
1	Energy distribution, %	6	5	6	11	3	69
2	Removed moisture, %	97.2		2.1		0.7	

Analysis of the results given in table 1 shows that only 0.7% of the total moisture removed in the paper machine is removed in the drying section of the machine. The amount of energy consumed to remove this moisture is 72% of the total energy supplied, of which 69% is energy consumption in the form of low pressure steam.

From table 1 it can also be concluded that, despite the relatively small amount of moisture removed in the drying section of the PM (0.7%), the energy consumption here is maximum, and the amount of heat input in the form of saturated steam from the CHP is determined by this particular section of PM.

During the study of the drying section of the existing paper machine it was established [4] that its exergy efficiency is only 52.6%. The low exergy efficiency of the drying section is determined by the exergy efficiency of the heat recovery unit of the drying section (57.5%) with the spent exergy amounted to 30% of the total exergy supplied.

This process is characterized by high irreversibility and, accordingly, low exergy efficiency. Analysis of the components of the exergy balance made it possible to identify the main directions for increasing the degree of thermodynamic perfection of the technological process in the drying section of PM.

1. Increasing the exergy efficiency of the heat recovery unit. Analysis of the exergy balance items shows that the exergy efficiency and the share of exergy spent in this process to the total exergy in the system are: $\eta = 57.5\%$ and $\gamma = 30\%$, respectively.

2. Reducing the heat flux discharged into the environment. As it follows from the heat balance, 60% of the heat flux is removed to the environment.

3. Increasing the potential of the drying air during the process of its absorption of the steam of the PM drying part.

4. Increasing the dryness of the paper web entering the dryer.

The practical implementation of the modernization of the drying section of PM in these areas becomes possible on the ground of the development of the following technical solutions [5, 6]:

- Intensification of the work of heat exchangers with a corresponding reduction in underheating between the heated air and the steam-air mixture (SAM). This measure will increase the exergy efficiency of the heat recovery unit;
- Development of a closed or almost closed SAM cycle of the PM drying section;
- Application of heat pump units in the PM ventilation system [7];
- Increasing the potential of drying air by optimizing the temperature of air directed under the PM cap, and the temperature of the source air [8];

The proposed technical solutions are not exhaustive. They can be considered as possible options for the modernization of the PM drying section.

Results and discussion

In this article, the authors considered one of the most promising ways to increase the exergy efficiency of the PM drying section, which also allows one to reduce energy costs in the steam-condensate system of the existing plants, namely the development of a closed cycle of a steam-air mixture.

Fig. 2 shows a scheme of a heat recovery unit of a paper machine with a closed drying air cycle.

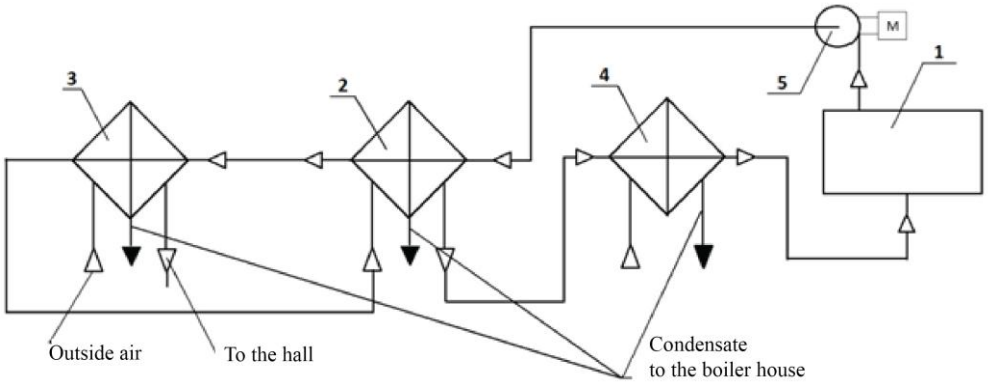

Fig. 2. The ventilation scheme of the drying section of the paper machine with a closed cycle of the drying air motion: 1 - closed hood over the drying part; 2 - air heater; 3 - aftercooler; 4 - mixing heat exchanger (MHE); 5 - centrifugal fan circulating air in a closed hood (drying chamber); 6 – moisture, removed from paper web during contact drying

The air-steam mixture (Fig. 2) with a temperature of 100 °C, removed from under the insulated hood *1* that covers the drying section of the machine (drying chamber), is sent to the heat exchanger TU *2*.

The air-steam mixture leaves the TU *2* heat exchanger at a saturation temperature of 45 °C and is sent to the mixing heat exchanger - aftercooler *3*, from where, at a temperature of 25 °C, dried and cooled, the air returns to TU *2*. Some part of the dried air, equal to the mass of cold air, used in the mixing heat exchanger is removed to the hall of the paper machine. In the heat exchanger TU 2, the air is heated to 80 °C, then it enters the air heater (AH) *4*, where its temperature rises to 100 °C, i.e. the temperature necessary for the ventilation process of the considered drying unit [9, 10].

In the aftercooler, the air temperature decreases due to the addition of outside air with an average annual temperature of 7 °C. In summer, a cooling machine is used [11].

Moisture released from the web during contact drying is absorbed by the drying air and removed from heat exchangers [12, 13]. All the heat released during condensation of the heating

steam in the cylinders, besides the heat carried away by the heated paper web, is absorbed by air and is used in heat exchangers of the regenerative circuit *2* and *3*. The air is circulated by a centrifugal fan *5*.

The thermodynamic process carried out in the proposed heat recovery unit is shown in Fig. 3 as an *i – d* diagram.

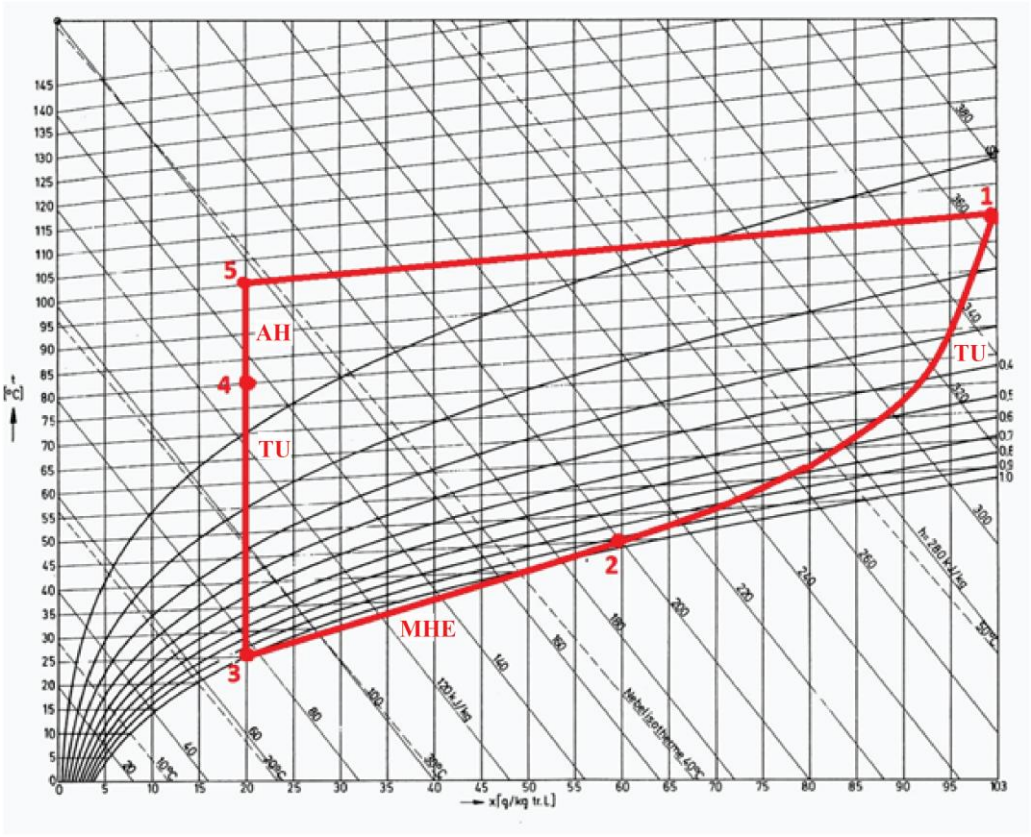

Fig. 3. Thermodynamic process of ventilation of the drying section of the machine for a closed cycle of air movement

The diagram (Fig. 3) shows the following processes:

1-2 - Cooling of the drying (technological) air in the heat exchanger TU to 45 °C, *d* = 60 g/kg of dry air;

2-3 - Cooling of the drying (technological) air in the aftercooler;

3-4 - Heating of dried and cooled air in a heat exchanger TU to 80 °C, d = 20 g/kg of dry air;

4-5 - Heating of the dried air in the heater t = 100 °C;

5-1 - Change of air parameters in the drying chamber t = 100 °C, d = 103 g/kg of dry air.

Exergy characteristics of the thermal process of heat and moisture transport by the proposed method are given in table. 2.

Analysis of thermal processes of functional groups by the proposed method shows that exergy efficiency is quite high [14, 15]. So the processes in the heat exchanger of the regenerative circuit and the heater, where 91% of the exergy of the total in the system is supplied, are characterized by exergy efficiency of 73.73% and 63.60%, respectively.

Table 2

Exergy characteristics of the heat recovery unit of the PM drying section for a closed cycle of drying air

Exergy characteristics	Regenerative circuit heat exchanger	Aftercooler	Air heater
Heat flow, ΔQ_i, kW	2947.98	1071.99	1071.99
Thermodynamic heating temperature, T_{Hi}, K	325.5	289	363
Received exergy, ΔE_{Hi}, kW	412.08	33.38	245.11
Thermodynamic cooling temperature, T_{Oi}, K	345.5	308	437.17
Spent exergy, ΔE_{Oi}, kW	558.88	97. 45	385.4
Exergy efficiency, $\eta_i=\Delta E_{Hi}/\Delta E_{Oi}$, %	73.73	34.26	63. 60

Thus, the exergy efficiency of processes in the recovery unit of the existing PM drying sections is 28.6% versus 66.29% for the proposed method.

Conclusions

Analysis of the exergy characteristics of the PM drying section during the implementation of the proposed method for heat arrangement in a heat recovery unit allows us to draw the following conclusions.

The smallest exergy efficiency have the third group of drying cylinders (59.6%), air heater (63.6%) and terminal cooler (34.3%). However, the total share of spent exergy in them is about 12% of the total spent exergy. Therefore, their influence on the overall efficiency of the PM drying section is not significant. In general, the exergy efficiency of PM drying section is 72.4%. As was indicated above [4], the exergy efficiency of the PM drying section for the existing modern plants is 52.6%. Such a significant increase in exergy efficiency was achieved by scientifically based heat technology in a heat recovery unit with a closed cycle of air movement.

References

1. Boykov LM. Energosberezhenie i uskorenie sushki bumagi i kartona. SPb.: SPbGUPTD, 2018.

2. Boykov LM, Prokhorov DA, Ionin EN. Modernizaciya sistem ventilyacii na predpriyatiyah CBP. Cellyuloza, bumaga, karton. 2015. Vol. 10.

3. Dincer I, Rosen MA. Exergy Analysis of Heating, Refrigerating and Air Conditioning: Methods and Applications.Elsevier Inc, J. Exergy 2015, 18 (2): 129. doi: 10.1016 / c2013-0-06800-4

4. Mateos-Espejel E, Paris J, Savulescu L, Maréchal F. Unified methodology for thermal energy efficiency improvement; application to kraft process. Chemical Engineering Science. 2011, 2 (66). doi: 10.1016 / j.ces.2010.09.032.

5. Belsky AP, Lotvinov MD. *Ventilyaciya bumagodelatel'nyh mashin.* M.:Lesnaya promyshlennost', 1990.(In Russ).

6. Brodyansky VM. *Eksergeticheskij metod i ego prilozheniya.* M.: Energoatomizdat, 1988. 7

Литература

1. Бойков Л.М. Энергосбережение и ускорение сушки бумаги и картона. СПб.: СПбГУПТД: Высш. шк. технологии и энергетики 2018. - 258с

2. Бойков Л.М., Прохоров Д.А., Ионин Е.Н. Модернизация систем вентиляции на предприятиях ЦБП // Целлюлоза, бумага, картон. 2015. №10.

3. Dincer I., Rosen M.A. Exergy Analysis of Heating, Refrigerating and Air Conditioning: Methods and Applications. Elsevier Inc, 2015//J. Exergy., 2015. Vol. 18, № 2.pp129.

4. Mateos-Espejel E., Paris J., Savulescu L., Maréchal F. Unified methodology for thermal energy efficiency improvement; application to kraft process. // Chemical Engineering Science. 2011. V. 66, N 2.

5. Бельский А.П., Лотвинов М.Д. Вентиляция бумагоделательных машин. М.: Лесная промышленность, 1990.

6. Бродянский В. М. Эксергетический метод и

7. Kurov VS. *Bumagodelatel'nye i kartonodelatel'nye mashiny. SPb:* SPbPU: 2008. (In Russ).
8. Bojkov LM. *Ventilyaciya bumago- i kartonodelatel'nyh mashin*. SPb.: SPbGUPTD, 2018.(In Russ).
9. Sukhodub IO, Deshko VI. Eksergeticheskij analiz sistem ventilyacii s utilizaciej polnoj teploty // *Inzhenerno-stroitel'nyj zhurnal*. 2014; 46 (2): 36-46 (In Russ). doi: 10.5862/MCE.46.5.
10. Hovey G, Allen DG, Tran H. *Drying kinetics of biosludge from pulp and paper mills.Pulping, engineering, environmental, recycling, sustainability conferenceJacksonville*, FL: TAPPI Press, 2019. 27-30 Oct 2019.
11. Nemirovskaya VV, Kuzovlev VA. Energosberezhenie s primeneniem utilizatorov teploty. *Nauchnyj zhurnal NIU ITMO.* Seriya: Holodil'naya tekhnika i kondicionirovanie. 2015. N2 (In Russ).
12. Plaznik U, Poredoš A, Kitanovski A, Vrabelj M, Kutnjak Z, et al. Electrocaloric cooling; the importance of electric-energy recovery and heat regeneration *EPL*. 2015. Vol. 111. (5). (In Russ). Available at :https://doi.org/10.1209/0295-5075/111/57009.
13. Gjennestad MA, Aursand E, Magnanelli E, et al. Perfomance analysis of heat and energy recovery ventilators using exergy analysis and nonequilibrium thermodynamics. Energy and Buildings. 2018. Vol.170. doi:10.1016/j enbuild 2018.04.013
14. Kazakov VG, Lukanin PV, Smirnova OS. *Eksergeticheskij analiz tekhnologicheskih skhem proizvodstva cellyulozy i bumagi* // *Promyshlennaya teploenergetika*. 2009. № 11.
15. Mikhailov VA, Sotnikova EV, Kalpina NYu. *Energosberezhenie v sistemah ventilyacii i kondicionirovaniya vozduha*. M. Ser. Nauchnaya mysl'. 2017.(In Russ).

его приложения. М.: Энергоатомиздат, 1988г.
7.В.С.Куров. Бумагоделательные и картоноделательные машины /. Под ред. В.С. Курова, Н.Н. Кокушина. СПб: Изд-во СПбПУ, 2008.
8 Бойков Л.М. Вентиляция бумаго- и картоноделательных машин. СПб.: СПбГУПТД, 2018.
9. Суходуб И.О., Дешко В.И. Эксергетический анализ систем вентиляции с утилизацией полной теплоты // Инженерно-строительный журнал. 2014. №2 (46).
10. Hovey G., Allen D.G., Tran H. Drying kinetics of biosludge from pulp and paper mills.Pulping, engineering, environmental, recycling, sustainability conference;. Jacksonville.FL: TAPPI Press, 2019 Ссылка активна на :27-30 октября 2019.
11.Немировская В.В., Кузовлев А.В. Энергосбережение с применением утилизаторов теплоты // Научный журнал НИУ ИТМО. Серия: Холодильная техника и кондиционирование. 2015. № 2
12. Plaznik U., Poredoš A., Kitanovski A., Vrabelj M., Kutnjak Z., Malič B. Electrocaloric cooling; the importance of electric-energy recovery and heat regeneration // EPL. 2015. Vol. 111. N 5.
13. Gjennestad M.A., Aursand E., Magnanelli E., et al. Perfomance analysis of heat and energy recovery ventilators using exergy analysis and nonequilibrium thermodynamics // Energy and Buildings. 2018. Vol. 170.
14. Казаков В.Г., Луканин П.В., Смирнова О.С. Эксергетический анализ технологических схем производства целлюлозы и бумаги // Промышленная теплоэнергетика. СПб ГТУРП. - СПб. 2013.-с 93 . № 11.
15. Михайлов В.А., Сотникова Е.В., Калпина Н.Ю. Энергосбережение в системах вентиляции и кондиционирования воздуха. М. Сер. Научная мысль. 2017.

Authors of the publication

Vladimir G. Kazakov – Department of Industrial Heat Power Engineering of the Higher School of Technology and Energy of St. Petersburg State University of Industrial Technologies and Design.

Ekaterina N. Gromova – Department of Industrial Heat Power Engineering of the Higher School of Technology and Energy of St. Petersburg State University of Industrial Technologies and Design.

Received ***March 28, 2019***

UDC 536.8 DOI:10.30724/1998-9903-2019-21-3-32-45

REGARDING THE APPLICATION LIMITATIONS OF THE CARNOT'S THEOREM

V.G. Kiselev

Peter the Great Saint-Petersburg Polytechnic University, St. Petersburg, Russia
ORCID: https://orcid.org/0000-0003-2308-1598, kis_vg@mail.ru

***Abstract**: The purpose of this article is to perform a comparative study of a reversible heat engine with an ideal or real gas as a working fluid and to determine the change in its efficiency depending on the thermodynamic characteristics of the working fluid. The main research method is the method of thermodynamic potentials, based primarily on the analysis of changes in the free and internal energy of an ideal and real gas in a cyclic process. The theory of thermodynamic potentials is used to consider the Carnot quasistatic heat engine. A comparative analysis of its operation is carried out, for a cycle with both an ideal and a real gas as a working fluid. The possibility of analyzing cyclic processes occurring in heat engines using the method of thermodynamic potentials has been identified and substantiated. The study has shown that the existing formulation of the Carnot's theorem is valid only for ideal gas as a working fluid. Based on the work carried out, the Carnot's theorem in the general case can be formulated, for example, as follows: the efficiency of the heat engine ηr, when it operates at the reversible Carnot cycle with real gas as a working fluid, is determined by the following expression:*

$$\eta_r = 1 - \frac{T_B}{T_A} + \varepsilon,$$

where T_A and T_B are the temperatures of the upper and lower isotherms of the Carnot cycle, respectively; ε is the correction term (positive or negative), depending on the thermodynamic properties of a real gas, which tends to zero as the properties of a real gas approach the properties of an ideal gas.

***Key words**: heat engine; thermodynamic potentials; characteristic functions; Gibbs energy; Helmholtz energy; Carnot's theorem; Carnot cycle; quasistatic process; reversible cyclic process; efficiency of the Carnot cycle; efficiency of heat engines; efficiency.*

For citation: Kiselev VG. Regarding the application limitations of the Carnot' s theorem. *Power engineering: research, equipment, technology*. 2019; 21(3): 32-45. (In Russ). doi:10.30724/1998-9903-2019-21-3-32-45.

ОБ ОГРАНИЧЕННОСТИ ОБЛАСТИ ПРИМЕНЕНИЯ ТЕОРЕМЫ КАРНО

В.Г. Киселёв

**Санкт-Петербургский политехнический университет Петра Великого,
г. Санкт-Петербург, Россия**
ORCID: https://orcid.org/0000-0003-2308-1598, kis_vg@mail.ru

***Резюме:** Целью написания данной статьи является сравнительное исследование обратимого теплового двигателя с идеальным или реальным газом в качестве рабочего тела и определение изменения его коэффициента полезного действия в зависимости от*

термодинамических характеристик рабочего тела. Основным методом исследования является метод термодинамических потенциалов, базирующийся, прежде всего на анализе изменения свободной и внутренней энергии идеального и реального газа в циклическом процессе. В статье на основе теории термодинамических потенциалов произведено рассмотрение квазистатического теплового двигателя Карно, в рамках которого осуществлен сравнительный анализ его работы, как для цикла с рабочим телом идеальный газ, так и для цикла с рабочим телом реальный газ. В работе выявлена и обоснована возможность анализа циклических процессов, протекающих в тепловых двигателях с использованием метода термодинамических потенциалов. На основе проведённого исследования установлено, что существующая формулировка теоремы Карно справедлива только для рабочего тела «идеальный газ». В общем случае, на основании проведённой работы, теорема Карно может быть сформулирована, например, следующим образом: коэффициент полезного действия тепловой машины η_r, при её функционировании по обратимому циклу Карно с рабочим телом реальный газ, определяется следующей формулой:

$$\eta_r = 1 - \frac{T_B}{T_A} + \varepsilon,$$

где T_A и T_B — температура, соответственно, верхней и нижней изотерм цикла Карно; ε – поправка (положительная или отрицательная), зависящая от термодинамических свойств реального газа, которая стремится к нулю при приближении свойств реального газа к свойствам газа идеального.

Ключевые слова: *тепловой двигатель; термодинамические потенциалы; характеристические функции; энергия Гиббса; энергия Гельмгольца; теорема Карно; цикл Карно; квазистатический процесс; обратимый циклический процесс; КПД цикла Карно; КПД тепловых двигателей; коэффициент полезного действия.*

Introduction

In a number of previous publications [1, 2, 3], the author used the method of thermodynamic potentials [4, 5] to analyze the simplest thermodynamic processes (mixing of ideal gases and isothermic equilibrium and non-equilibrium expansion of an ideal gas). This work explores the behavior of real gas in thermodynamic cycles and the influence of its properties on the efficiency of heat engines basing on the basic principles underlying the earlier publications. It should be noted that application of the theory of thermodynamic potentials to the “ideal gas mixture” system was a key factor in the appearance of an article entitled “The Gibbs Paradox and its Solution” [1]. So, the author poses the second task of the present work: to indirectly confirm the basic principles underlying this earlier publication. It should be noted that this problem is very actively discussed as a matter of modern thermodynamics, as evidenced, in particular, by the following works [6-10].

In accordance with I. Prigogin [11, p. 81], “Carnot showed that a reversible cyclic heat engine must perform the maximum work (driving force) ...”. Later he [11, p. 81] reports: “If any heat engine could perform more work than a reversible cyclic engine, then an infinite amount of work could be done. First, using a more efficient engine, it was necessary to transfer heat from the hot tank to the cold, then, using a reversible heat engine, return the same amount of heat to the hot tank. Since the direct process gives more work than it is required to complete the reverse process, the result is a gain in work. ... Carnot argued that this was impossible." Note that in this discussion there is a substitution of concepts. In fact, Carnot actually speaks only of volumetric-mechanical work (and only about it), into which the heat supplied to the system is converted (or vice versa, the work is converted to heat), and this phenomenon is observed only when a heat engine with an ideal gas as working fluid is used. At the same time, “Joule and Thomson showed that the vast majority

of gases studied by them are cooled during free expansion, since such expansion is associated with work against the internal forces of interaction between gas particles" [12, p. 35]. There is the possibility of heating real gases during expansion [p[1] . 249], however, an increase in gas temperature is a rather rare phenomenon, therefore, in the framework of this work we mainly restrict ourselves to considering the first case. Thus, when using non-ideal gas as a working fluid in the upper Carnot isotherm, the heat supplied to the system is spent both on the performance of volumetric-mechanical work and on maintaining a constant temperature of the "self-cooling" gas. As a result, the isotherm of the real gas will be below the isotherm of the ideal gas [13, p. 22], which should be interpreted as the presence of some internal compressive pressure of real gas. This thesis is illustrated by Fig. 1 "Isotherms for ideal (1) and real (2) gases."

Thus, it can be stated that under isothermal expansion of one mole of a real gas at relatively low pressures (when its volatility coefficient is less than one), the work performed by it will be less than that performed by one mole of an ideal gas at the same pressure change. This is driven by the fact that part of heat received by the non-ideal gas from the hot tank will be spent on maintaining its temperature, which is necessary for an isothermal process due to the presence of its "self-cooling" effect, that is, it is spent on chemical work against the Van der Waals forces. A similar situation, except for the sign, is also observed for the lower isotherm of the Carnot cycle. In this case, attraction of real gas molecules to each other takes place, so when it is compressed by external forces, in addition to heat generated due to mechanical work (as it is observed, for example, for an ideal gas) its self-heating occurs due to strengthening of Van der Waals bonds. So, in this case the chemical work will be performed by the substance itself. This leads to increased, in comparison with the amount of volumetric-mechanical work performed, heat transfer to the refrigerator of the system in question. In addition, we note that it is necessary to take into account the internal energy of a real gas, the change of which actually determines the volumetric-mechanical work of adiabats of the Carnot cycle. It is known that in the general case it depends on the volume of real gas [11, p. 163] and, therefore, the volumetric-mechanical work performed in adiabats (by the system and being done on the system) in this case is not subject to reduction. So it can be argued that when carrying out the Carnot cycle with the participation of real gas, along with the use of heat for performing volumetric-mechanical work, it is also used for performing chemical work, which has an influence on the system efficiency. This phenomenon will be considered in more detail in subsequent sections of this work. In addition, it should be noted that there are no doubts that the considered effects and their values depend on the type of reversible heat engine (thermodynamic cycle), which requires analysis of this factor, but is clearly beyond the scope of this work.

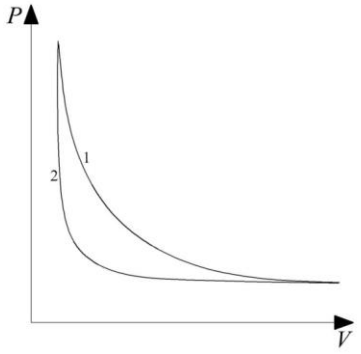

Fig. 1. Isotherms for ideal (1) and real (2) gases

We now return to the Carnot's theorem itself. Its traditional formulation, given, for example, in the monograph by I. Prigogin [11, p. 83], states that the discovery of Carnot "... comes

[1] Yavorsky B.M. Справочник по физике: справочник / B.M. Yavorsky, A.A. Detlaf. Moscow: Nauka, 1974. (In Russ).

down to the statement that the efficiency of a reversible heat engine is maximum, does not depend on the properties of the heat engine and is a function of only the temperatures of the hot and cold tanks:

$$\eta = 1 - \frac{Q_1}{Q_2} = 1 - f(t_1, t_2) \tag{1}$$

where $f(t_1, t_2)$ are the function of only temperatures t_1 and t_2 of hot and cold tanks."

Earlier we showed that in the case of real gas this statement is not true. Therefore, the aforecited conclusion of the Carnot's theorem should be attributed exclusively to the working fluid "ideal gas". In case of a real gas, expression (1) becomes simply incorrect, since there appears relationship between η and the gas properties. In the following sections of this article, we show the validity of the stated thesis using specific examples.

Materials and methods

Analysis of the work of the Carnot thermodynamic cycle with the "ideal gas" working fluid can be found in almost any course of thermodynamics. Therefore, we will use one of the variants for studying this issue, basing, for example, on the monograph of I. Prigogin [11, pp. 83–86]. Together with it, we will use the method proposed by the author and presented, in particular, in his work, "Philips and Carnot Heat Engines from the Point of View of the Theory of Thermodynamic Potentials" [3].

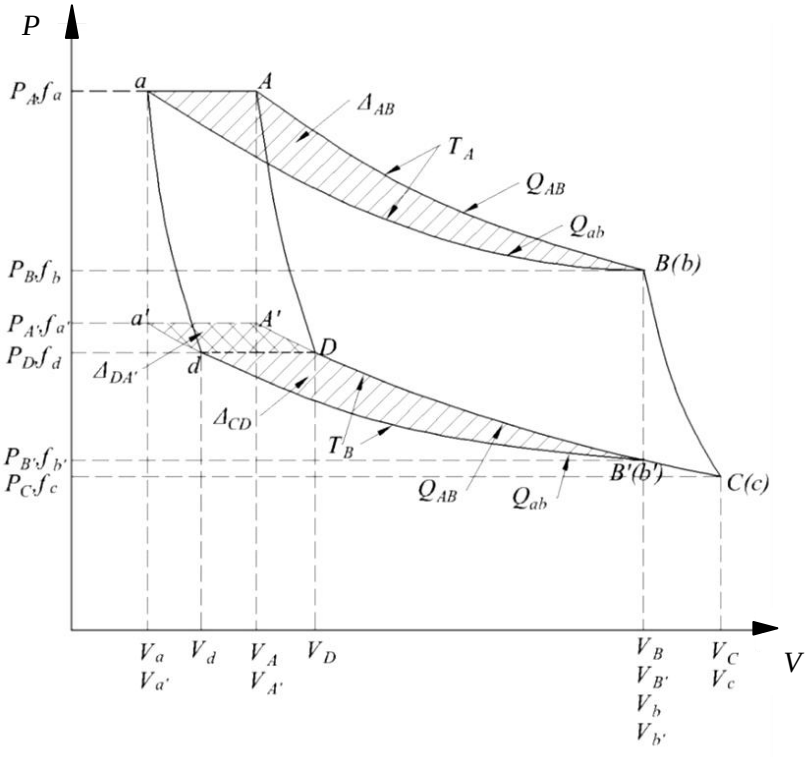

Fig. 2. Carnot cycle in P-V coordinates for ideal and real gas

Fig. 2 shows a graph of the cyclic operation of the Carnot machine in pressure-volume coordinates for one mole of ideal gas and one mole of real gas. Moreover, without loss of generality, it is accepted that the right adiabats and the right parts of isotherms of thermodynamic cycles of real and ideal gases coincide. In other words, the real gas in this case becomes ideal. Using this technique allows us to consider any Carnot cycle with the participation of the real gas

$a – ab – dc – d$ as the difference of two Carnot cycles ("large" $a – b – c –d$ and "small" $ab – b – c – dc$), in which, in their right part, the expansion of real gas is so significant that it becomes an ideal gas. An explanation of this thesis is presented in Fig. 3. In addition, in order to simplify further calculations, we assume that the device under consideration, operating with either ideal or real gas, is in vacuum, and to analyze its operation we use the theory of thermodynamic potentials, assuming that only one mole of gas is always used in the system.

Stage 1. Isothermal transitions at temperature T_A.

Ideal gas. Transition A - B.

In this case, in accordance with I. Prigogin [11, p. 84], external work performed by one mole of ideal gas A_{AB} is determined by the expression

$$A_{AB} = \int_A^B PdV = RT_A \ln \frac{V_B}{V_A}, \tag{2}$$

where P is the gas pressure; V is the current gas volume; V_A and V_B are the ideal gas volumes at the beginning and at the end of the upper isotherm of the Carnot cycle, respectively; T_A is the gas temperature of the upper isotherm of the Carnot cycle, R is the universal gas constant.

When using pressure as an independent variable, the last expression can be rewritten [14, p. 22] in the following form:

$$A_{AB} = \int_A^B VdP = -RT_A \ln \frac{P_B}{P_A}, \tag{3}$$

where P_A and P_B are the ideal gas pressures at the beginning and at the end of the upper isotherm of the Carnot cycle, respectively.

In such an isothermal process involving an ideal gas, heat Q_{AB} is absorbed from the reservoir, and the following equality is fulfilled:

$$A_{AB} = Q_{AB}. \tag{4}$$

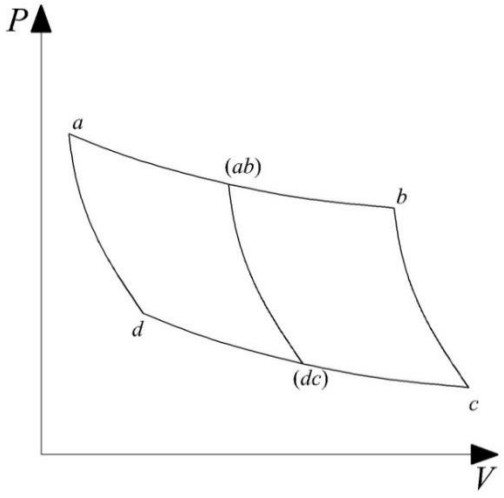

Fig. 3. The scheme of transformation of Carnot cycles with real gas as a working fluid

Real gas. Transition a - b.

In this case, external work performed by real gas A_{ab} is determined by the ratio [14, p. 22]

$$A_{ab} = \int_a^b VdP = -RT_A \ln \frac{f_b}{f_a} \tag{5}$$

where f_a and f_b are the volatilities of real gas at the beginning and end of the upper isotherm of the Carnot cycle, respectively.

Further, the difference between the volumetric-mechanical work of a real gas A_{real} and the volumetric-mechanical work of an ideal gas A_{ideal} will be a certain amount Δ_{AB}, which N. Izmailov calls the excessive work of expansion and is determined [13, p. 22], with the system of signs adopted by us, as follows :

$$\Delta_{AB} = RT_A \ln \frac{P_A}{f_A} = A_{\text{ideal}} - A_{\text{real}}, \tag{6}$$

where A_{ideal} is the isothermal work performed by ideal gas when expanding from pressure P_A to pressure P_B; A_{real} is the isothermal work performed by real gas when expanding from pressure P_A, corresponding to volatility f_a to pressure P_B, at which the real gas becomes an ideal one.

In this case, it can be stated (see Fig. 2) that heat received by the system with real gas (when volatility coefficient is less than one) is consumed both for performing external work A_{ab} and for working against internal pressure forces Δ_{AB}, i.e., the mutual attraction of gas particles. It should be noted that in the *a* - *b* isotherm the amount of heat absorbed by the real gas Q_{ab} remains unchanged, that is, it is equal to the heat absorbed by the ideal gas Q_{AB} in the isotherm *A* - *B*. Thus, for the upper isotherm of the Carnot cycle with alternating participation of the real and ideal gas it can be written:

$$Q_{AB} = Q_{ab}, \tag{7}$$

$$A_{AB} - A_{ab} = \Delta_{AB} > 0. \tag{8}$$

Stage 2. Adiabatic transition.
Ideal gas. Transition B - C.

It is known that the only source of energy for performing external work A_{BC}, under adiabatic expansion of an ideal gas, is a change in its internal energy ΔU [14, p. 42]. Therefore, in this case, we can write

$$-\Delta U = C_v(T_A - T_B) = A_{BC}, \tag{9}$$

where C_v is the heat capacity of an ideal gas at a constant pressure, and T_B is the gas temperature in the lower isotherm of the Carnot cycle.

Due to the preconditions imposed on the considered Carnot cycles, an analysis of the adiabatic transition *b* - *c* for a real gas is not required (all its parameters coincide with the parameters of an ideal gas), i.e. in particular $A_{BC} = A_{bc}$.

At the same time, for further research, we need to know the characteristics of an ideal gas at the moment of the end of the right adiabat at a temperature T_B (the beginning of the "lower" isotherm of ideal and real gas). For this purpose, the transition from point B to point C is carried out in two stages. In the first case, we move at a constant volume of ideal gas from point *B* to point *B′* located on the lower isotherm of the Carnot cycle, which will lead to a corresponding change in its internal energy [3]:

$$-\Delta U_{BB'} = C_v(T_A - T_B). \tag{10}$$

The heat released as a result of this process we will direct to a battery, which has a temperature T_B. It should be noted that the volumetric-mechanical work in this case, due to the constancy of the volume of gas, is zero. The further transition of one mole of ideal gas is carried out along the isotherm from point *B′* to point *C*. In this case, as we found out earlier, the external work performed is limited by the amount of heat supplied to the system and going to actually carry out this work (in our case, the amount of heat released as a result of a decrease in internal energy).

Thus, we can write [13, p. 22], taking into account the isothermal equivalence of the Helmholtz and Gibbs energy changes, the following expression:

$$A_{BC} = A_{B'C} = \int_{B'}^{C} PdV = RT_B \ln \frac{V_C}{V_{B'}} = -RT_B \ln \frac{P_C}{P_{B'}}. \quad (11)$$

In this case, a combination of equations (10) and (11) allows one to determine the values V_C and P_C corresponding to the volume and pressure of an ideal gas at point *C* of the lower isotherm. Indeed, from these expressions it follows that

$$C_v(T_A - T_B) = RT_B \ln \frac{V_C}{V_{B'}} = -RT_B \ln \frac{P_C}{P_{B'}}. \quad (12)$$

In these two equations, only V_C and P_C are unknown. In turn, the external work A_{BC} or A_{bc} of the considered system during its adiabatic transition from point *B* to point *C* will be equal to:

$$A_{BC} = A_{bc} = C_v(T_A - T_B). \quad (13)$$

Stage 3. Isothermal transitions at temperature T_B.

Ideal gas. Transition C - D.

We will consider this process by analogy with stage 1.

In this case, in accordance with I. Prigogin [11, p. 85], external work (negative) performed on an ideal gas is determined by the expression

$$A_{CD} = \int_{C}^{D} PdV = RT_B \ln \frac{V_D}{V_C}. \quad (14)$$

When using pressure as an independent variable, the last relation can be rewritten [13, p. 22] in the following form:

$$A_{CD} = \int_{C}^{D} VdP = -RT_B \ln \frac{P_D}{P_C}. \quad (15)$$

In such an isothermal process involving an ideal gas, heat Q_{CD} is transferred to the refrigerator, and the following equality is fulfilled:

$$A_{CD} = Q_{CD}. \quad (16)$$

Real gas. Transition c - d.

In this case, external work (negative) A_{cd} performed on real gas is determined by the equation

$$A_{cd} = \int_{c}^{d} PdV = RT_B \ln \frac{V_d}{V_c}. \quad (17)$$

When using pressure as an independent variable and volatility f, the last relation can be rewritten [13, p. 22]:

$$A_{cd} = \int_{c}^{d} VdP = -RT_B \ln \frac{f_d}{f_c} = -RT_B \ln \frac{f_d}{P_c}. \quad (18)$$

In turn, the difference between the values of the work of the real and ideal gases will be a certain amount Δ_{CD} (negative), which N. Izmailov calls the excess work of expansion and is determined in this case [13, p. 22] as follows:

$$\Delta_{CD} = -RT_B \ln \frac{P_D}{f_d} = A_{CD} - A_{cd}. \quad (19)$$

Therefore, the heat Q_{CD} generated by the system with real gas in the isothermal process *c* – *d* and transferred to the refrigerator can be decomposed into two components:

– Heat received as a result of the actual transformation of mechanical work with the participation of external forces acting on the system, and quantitatively equal to this work: $-RT_B \ln \frac{f_d}{P_c}$;

– Heat received as a result of work performed due to the attraction of molecules (Van der Waals forces), which is equal to Δ_{CD}.

Thus, it can be stated that in this case, external work is completely converted into heat; moreover, heat is also generated due to the work caused by the forces of Van der Waals.

Stage 4. Adiabatic transitions.

Perfect gas. Transition D - A.

In this subsection, we will use the results obtained by us when analyzing stage 2, which will have opposite signs due to the fact that the process under consideration proceeds in the opposite direction. All necessary explanations can be obtained from the analysis of Fig. 2: it can be seen that the considered transition is divided into two parts: isothermal *D* - *A′* and isochoric *A′* - *A*. It is known that under adiabatic compression of an ideal gas, a change in its internal energy is numerically equal to the volumetric-mechanical work performed on it [14, p. 42]. Therefore, in this case, an increase in internal energy is observed, and the following relation can be written:

$$\Delta U_{DA} = C_v(T_A - T_B) = -A_{DA}. \tag{20}$$

Thus, for transition *D* - *A*, given the the Helmholtz and Gibbs energies change equivalence in this case, we can write [15, p. 42]:

$$A_{DA} = A_{DA'} = \int_D^{A'} PdV = RT_B \ln \frac{V_{A'}}{V_D} = -RT_B \ln \frac{P_{A'}}{P_D}. \tag{21}$$

The combination of the last two equations allows one to determine V_D and P_D, corresponding to the volume and pressure of an ideal gas at point *D* of the lower isotherm. Indeed, from these equalities it follows that

$$-C_v(T_A - T_B) = RT_B \ln \frac{V_{A'}}{V_D} = -RT_B \ln \frac{P_{A'}}{P_D}. \tag{22}$$

In turn, from the latter expressions one can easily calculate the considered values V_D and P_D by means of simple algebraic transformations.

Real gas. Transition d - a

We will analyze this process by analogy with the *D* - *A* transition, replacing the corresponding pressures by volatilities, and the molar volumes of an ideal gas by molar volumes of real gas. All necessary explanations can be obtained by analyzing Fig. 2, from which it can be seen that the transition under consideration is divided into two parts: the isothermal *d* - *a′* and the isochoric *a′* - *a*.

It is known that during adiabatic compression of gas, a change in its internal energy is numerically equal to the volumetric-mechanical work performed on it [14, p. 42]. Therefore, in this case, an increase in internal energy is observed, and the following relation can be written:

$$\Delta U_{da} = C_r(T_A - T_B) = -A_{da} \tag{23}$$

where C_r is the heat capacity of real gas at a constant volume V_a, which in general case can be a function of both temperature and volume. In our discussions, without loss of generality, in order to simplify the analysis, we accept it depending only on the real gas volume. As for the previous discussions, the volumetric-mechanical work is concentrated in the section *d* - *a′*, and accordingly it is equal to zero in the section *a′* - *a*. Then, taking into account the comments made, we get:

$$A_{da} = A_{da'} = \int_d^{a'} PdV = RT_A \ln \frac{V_{a'}}{V_d} = -RT_A \ln \frac{f_{a'}}{f_d}. \tag{24}$$

The last two equations allow, using simple algebraic transformations, to calculate the parameters of the real gas V_d and f_d at the point *d*.

3. Results and discussion

3.1 Efficiency of the Carnot cycle with ideal gas

In accordance with I. Prigogin [11, p. 86], the efficiency of the Carnot cycle with an ideal gas η_i is determined by the formula

$$\eta_i = \frac{A_i}{Q_{AB}} = 1 - \frac{T_B}{T_A}, \tag{25}$$

where A_i is the total amount of work produced by the considered system.

We show that the results we obtained in the previous paragraph using the method of thermodynamic potentials coincide with the latter formula. To do this, we use fig. 2. The amount of heat entering the system in our case, as well as in the usual version of analysis of this process, is equal to Q_{AB} and equals to work performed at this stage A_{AB}.

To determine the work on the adiabat *B* - *C*, one can use the results of the previous paragraph (stage 2). In this case, the third-external work performed by the system is "concentrated" on the isotherm with temperature T_B and is determined by the following expression:

$$A_{BC} = C_v(T_A - T_B). \tag{26}$$

A similar situation, except for the sign, is observed when considering the transition along the adiabat *D* - *A*. External work performed on the system is concentrated on the isotherm with temperature T_B and is determined in this case by the formula

$$A_{DA} = -C_v(T_A - T_B) = -A_{BC}. \tag{27}$$

Thus, the total work performed on the upper isotherm and two adiabats, i.e., on the section D - A - B - C, will be equal to

$$A_{DABC} = A_{AB} + A_{BC} + A_{DA}. \tag{28}$$

However, knowing that

$$A_{DA} = -A_{BC}, \tag{29}$$

we obtain

$$A_{DABC} = A_{AB} = RT_A \ln\frac{V_B}{V_A}. \tag{30}$$

It is known that for negative external work performed on the lower isotherm of the Carnot cycle, we can write:

$$A_{CD} = RT_B \ln\frac{V_D}{V_C}. \tag{31}$$

In addition, consideration of the geometry of Fig. 2 allows us to state that the following equality is true

$$\ln\frac{V_B}{V_A} = \ln\frac{V_{B'}}{V_{A'}}. \tag{32}$$

At the same time, taking into account the fact that on the lower isotherm the same amount of work, determined by expression $A_{BC} = -A_{DA} = C_v(T_A - T_B)$ is added and subtracted to the work $A_{A'B'} = RT_B \ln\frac{V_{B'}}{V_{A'}}$, it becomes possible to assert that its value remains unchanged and, therefore, the following relation is true:

$$RT_B \ln\frac{V_B'}{V_A'} = RT_B \ln\frac{V_C}{V_D}. \tag{33}$$

And finally, compiling the last equation with the previous one, we get

$$\ln\frac{V_B}{V_A}=\ln\frac{V_C}{V_D}. \tag{34}$$

Taking into account the last three expressions and substituting the expressions for work A_{CD} and A_{DABC} into the expression that determines the efficiency of an ideal gas allows us to obtain the following formula:

$$\eta_i=\frac{RT_A\ln\frac{V_B}{V_A}+RT_B\ln\frac{V_D}{V_C}}{RT_A\ln\frac{V_B}{V_A}}=1-\frac{T_B}{T_A}. \tag{35}$$

This expression for the Carnot cycle efficiency completely coincides with a similar relation obtained in traditional way [1, p. 86], which confirms the correctness of the method of thermodynamic potentials for solving the problems under consideration. In the next subsection of this publication, we complicate the task somewhat by applying the method of thermodynamic potentials to analyze the efficiency of the Carnot cycle with the "real gas" working fluid.

3.2. Efficiency of the Carnot cycle with real gas

In case of Carnot cycle with a "real gas" working fluid, its efficiency η_r can be calculated using a formula similar to the corresponding formula for an ideal gas:

$$\eta_r=\frac{A_r}{Q_{ab}}. \tag{36}$$

However, the expression for the work, we denote it here A_r, will look somewhat different, since we have to use the concept of volatility instead of pressure in these calculation, and instead of the ideal gas volume, we use the real gas volume. In this case (see Fig. 2), the determination of the cycle efficiency can be carried out using the technique used in the previous paragraph of this paper. As before, we assume that the amount of heat Q_{ab} is equal to heat entering the system. And, in turn, the work performed by the system in the section *a* - *b* will be determined by the formula

$$A_{ab}=RT_A\ln\frac{V_b}{V_a}=-RT_A\ln\frac{f_b}{f_a}. \tag{37}$$

Note that in this case, in accordance with the analysis carried out in Paragraph 4, A_{ab} and Q_{ab} and are not equal to each other. To determine the work A_{bc} in section b - c from point b of the upper isotherm along the isochore, we descend to the intersection with the lower isotherm at point b′, and then we move along the lower isotherm to point *c*. Then the total work on the section *b* - *b′* - *c*, due to the constancy of the volume, on the isochore will be concentrated on the segment b′ - c and is equal to the following value:

$$A_{bb'c}=A_{b'c}=RT_B\ln\frac{V_c}{V_{b'}}=-RT_B\ln\frac{f_c}{f_{b'}}=-RT_B\ln\frac{P_c}{P_{b'}}=C_v(T_A-T_B). \tag{38}$$

Note that according to the terms of the problem, the properties of ideal and real gases coincide in this area, and the corresponding heat capacities are equal to each other. At the same time, the solution of the latter relation relative to f_c, P_c and V_c allows one to determine the properties of the considered gas at point *c*.

To determine the point *d* - the end of the lower isotherm of the Carnot cycle - we use the following technique. From point *a* of the upper isotherm *a* - *b*, along the isochor *a* - *a′* we descend to the point *a′* located on the continuation of the lower isotherm *c* - *d*, and then move along the isotherm *a′* - *c* to point *d*.

In fact, in the Carnot cycle, the movement along the adiabat under consideration proceeds in the opposite direction, which requires appropriate consideration by setting the signs in the following formula:

$$A_{da'a} = A_{da'} = -A_{a'd} = RT_B \ln\frac{V_{a'}}{V_d} = -RT_B \ln\frac{f_{a'}}{f_d} = -C_r (T_A - T_B) . \quad (39)$$

where C_r is the heat capacity of real gas, at a constant volume V_a .

We note that the solution of the last expression in relation to f_d and V_d allows one to determine the properties of a real gas at point *c*.

Thus, the total work performed on the upper isotherm and two adiabats, i.e., on the section *d* - *a* - *b* - *c*, will be equal to:

$$A_{dabc} = A_{ab} + A_{b'c} + A_{da'} . \quad (40)$$

However, due to the fact that in this case, for the adiabats *b* - *c* and *d* - *a*, the heat capacities are not equal to each other, i.e. $C_r \neq C_v$, so

$$A_{b'c} \neq -A_{da'} . \quad (41)$$

Thus, based on the last two formulas, we obtain the expression:

$$\begin{aligned} A_{dabc} &= RT_A \ln\frac{V_b}{V_a} + RT_B \ln\frac{V_c}{V_{b'}} + RT_B \ln\frac{V_{a'}}{V_d} = \\ &= -RT_A \ln\frac{f_b}{f_a} - RT_B \ln\frac{f_c}{f_{b'}} - RT_B \ln\frac{f_{a'}}{f_d} . \end{aligned} \quad (42)$$

At the same time, taking into account the data from the previous paragraph, for work (negative), which was performed on the system on the isotherm c - d, we obtain the following expression:

$$A_{cd} = RT_B \ln\frac{V_d}{V_c} = -RT_B \ln\frac{f_d}{f_c} . \quad (43)$$

It is more convenient to present the last two ratios in the form

$$A_{dabc} = RT_A \ln\frac{V_B}{V_A} - \Delta_{AB} + RT_B \ln\frac{V_C}{V_{B'}} - \Delta_{B'C} + RT_B \ln\frac{V_{A'}}{V_D} - \Delta_{DA'} , \quad (44)$$

$$A_{cd} = RT_B \ln\frac{V_D}{V_C} - \Delta_{CD} , \quad (45)$$

where Δ_{AB} , $\Delta_{B'C}$, $\Delta_{DA'}$ and Δ_{CD} is the corresponding redundant expansion work, and according to the conditions of the problem $\Delta_{B'C} = 0$.

Substitution of expressions for work A_{cd} and A_{dabc} in expression that determines the efficiency allows us to obtain the formula

$$\begin{aligned} \eta_r = &\frac{RT_A \ln\frac{V_B}{V_A} - \Delta_{AB} + RT_B \ln\frac{V_C}{V_{B'}} - \Delta_{B'C} + RT_B \ln\frac{V_{A'}}{V_D} - \Delta_{DA'}}{RT_A \ln\frac{V_B}{V_A}} + \\ &+ \frac{RT_B \ln\frac{V_D}{V_C} - \Delta_{CD}}{RT_A \ln\frac{V_B}{V_A}} = 1 - \frac{T_B}{T_A} + \varepsilon \end{aligned} . \quad (46)$$

It is more convenient to present the obtained equation in the form:

$$\eta_r = \eta_i + \varepsilon , \quad (47)$$

where

$$\varepsilon = \frac{-\Delta_{AB} + RT_B \ln \frac{V_C}{V_{B'}} - \Delta_{B'C} + RT_B \ln \frac{V_{A'}}{V_D} - \Delta_{DA'} - \Delta_{CD}}{RT_A \ln \frac{V_B}{V_A}}. \quad (48)$$

Analysis of the last formula allows us to state that the value ε that distinguishes the efficiency of the Carnot cycle with a working fluid "real gas" from the efficiency of the Carnot cycle with a working fluid "ideal gas" is a complex function of temperature of the cycle isotherms and the thermodynamic properties of the real gas that distinguish it from the ideal gas. In addition, it can be concluded that the efficiency of a real gas can, depending on the value of the volatility coefficient of a real gas, exceed or be less than the efficiency of an ideal gas. A more detailed analysis of the issue can be performed only taking into account the specific properties of the working fluid, that is, including the analysis of the contribution of various quantities Δ to the correction term ε.

An indirect confirmation of the validity of the obtained formula is the fact that when the equality $\Delta_{AB} = \Delta_{B'C} = \Delta_{DA'} = \Delta_{CD} = 0$ is true, that is, during the transformation of real gas into ideal gas, the following quantities are simultaneously reduced in the last formula: $RT_B \ln \frac{V_C}{V_{B'}}$ and $RT_B \ln \frac{V_{A'}}{V_D}$. Thus, in this case, the correction term ε becomes equal to zero, and the real gas is transformed into ideal gas.

Consequently, it can be stated that the efficiency of the quasistatic Carnot cycle is determined, in particular by the properties of a real gas. From the point of view of electrochemistry [15, p. 18], this result is quite expected, since it is known that with the equilibrium course of electrochemical reactions, the external work carried out by means of chemical energy can occur both with absorption and with the release of heat. In other words, a quasistatic system can perform additional, for example, volumetric-mechanical, work due to a chemical process that takes place with the absorption of heat from the environment or vice versa, with the release of heat into the environment. In this article this well-known principle is applied to a new object - the Carnot thermodynamic cycle.

4. Conclusions

Thus, based on the performed work, the following conclusions can be drawn:

1. The existing formulation of the Carnot – Clausius theorem is valid only for the "ideal gas" working fluid.

2. In general case, based on the presented calculations, the Carnot – Clausius theorem can be formulated, for example, as follows: the efficiency of a heat engine η_r when it is operated on a reversible Carnot cycle with a "real gas" working fluid is determined by the following formula:

$$\eta_r = 1 - \frac{T_B}{T_A} + \varepsilon \quad (49)$$

where T_A and T_B are the temperatures of the upper and lower isotherms of the Carnot cycle, respectively; ε is the correction term (positive or negative), depending on the thermodynamic properties of a real gas, which tends to zero as the properties of a real gas approach the properties of an ideal gas.

References

1. Kiselev VG. Paradoks Gibbsa i ego reshenie. *Power engineering: research, equipment, technology*. 2016 ;.(11-12):129–137. (In Russ).

2. Kiselev VG Izotermicheskoe rasshirenie ideal'nogo gaza i himicheskoe srodstvo. Kiselev VG.

Литература

1. Киселёв В.Г. Парадокс Гиббса и его решение // Известия высших учебных заведений. ПРОБЛЕМЫ ЭНЕРГЕТИКИ. 2016. № 11-12. С. 129–137.

2. Киселёв В.Г. Изотермическое расширение

Proceedings of the higher educational institutions. *Power engineering: research, equipment, technology*. 2017; (11-12):142–151. (In Russ).
3. Kiselev VG. Teplovye mashiny Filipsa i Karno s tochki zreniya teorii termodinamicheskih potencialov. Kiselev VG. Proceedings of the higher educational institutions. *Power engineering: research, equipment, technology*. 2018(9-10):154–165. (In Russ).
4. Gibbs J Willard; *The Collected Works*. Longmans, Green and Co (NY):1928;1: XXVIII + 434.
5. Thomson W. *Mathematical and Physical Papers.* Cambridge at the University: 1882. 1: 174-232.
6. Ihnatovych V. Study of the possibility of eliminating the Gibbs paradox within the framework of classical thermodynamics. Preprint available at: http://arxiv.org/pdf/1306.5737. Accessed: 2013.
7. Ihnatovych V. The logical foundations of Gibbs' paradox in classical thermodynamics. Preprint available at http://arxiv.org/pdf/1305.0742 Accessed (2013).
8. Ihnatovych V. On the incorrectness of the proof of the Gibbs theorem on the entropy of a mixture of ideal gases, which was given by J. W. Gibbs. Preprint available at http://arxiv.org/pdf/1804.08721 Accessed to:2018.
9. Ihnatovych V. Explanation of the Gibbs paradox.URL:https://zenodo.org/record/2908285.Accеseed (2019).
10. Ihnatovych V. Explanation of the Gibbs paradox 2019. Zenodo http://doi.org/10.5281/zenodo.2908285. Accessed to : May 18. 2018.
11. Prigogin I, Condepudi D. *Sovremennaya termodinamika. Ot teplovyh dvigatelej do dissipativnyh struktur:* monografiya. Moscow: Mir; 2002.(In Russ).
12. Glazov VM *Osnovy fizicheskoj himii:* monografiya. Moscow: Vyschaya Shkola, 1981. (In Russ).
13. Izmailov NA. *Elektrohimiya rastvorov*: monografiya. Izmailov NA. Moscow: Himiya, 1976. (In Russ).
14. Nikolaev LA. *Fizicheskaya himiya*: monografiya. Nikolaev LA. Moscow: Vyschaya Shkola, 1979. (In Russ).
15. Antropov LI. *Teoreticheskaya elektrohimiya*: monografiya . Moscow: Vyschaya Shkola, 1975. (In Russ).

идеального газа и химическое сродство // Известия высших учебных заведений. ПРОБЛЕМЫ ЭНЕРГЕТИКИ. 2017. № 11-12. С.142–151
3. Киселёв В.Г. Тепловые машины Филипса и Карно с точки зрения теории термодинамических потенциалов / В.Г. Киселёв // Известия высших учебных заведений. ПРОБЛЕМЫ ЭНЕРГЕТИКИ. 2018. № 9-10. С. 154–165.
4.Gibbs J Willard. The Collected Works. Longmans, Green and Co (NY):1928. Vol.1, pp. XXVIII + 434.
5.Thomson W. Mathematical and Physical Papers. Cambridge at the University:1882. Vol. 1. pp. 174-232.
6. Ihnatovych V. Study of the possibility of eliminating the Gibbs paradox within the framework of classical thermodynamics. Доступен по: http://arxiv.org/pdf/1306.5737. Ссылка активна на 2013.
7. Ihnatovych V. The logical foundations of Gibbs' paradox in classical thermodynamics. Доступно по: http://arxiv.org/pdf/1305.0742 Ссылка активна на 2013.
8. Ihnatovych V On the incorrectness of the proof of the Gibbs theorem on the entropy of a mixture of ideal gases, which was given by J. W.Gibbs. Preprintat http://arxiv.org/pdf/1804.08721 Ссылка активна на. 2018.
9.Ihnatovych V. Explanation of the Gibbs paradox.Доступно по: https://zenodo.org/record/2908285. Ссылка активна на 14 февраля 2019 г
10. Ihnatovych Volodymyr. Explanation of the Gibbs paradox. Zenodo. 2019.http://doi.org/10.5281/zenodo.2908285 Ссылка активна на 18 мая 2018г.
11. Пригожин И., Кондепуди Д. Современная термодинамика. От тепловых двигателей до диссипативных структур:. М.: Мир, 2002. 461 с.
12. Глазов В.М. Основы физической химии:.М.: Высшая школа, 1981.
13. Измайлов Н.А. Электрохимия растворов.М.: Химия, 1976. 488 с.
14. Николаев Л.А. Физическая химия. М.: Высшая школа, 1979. 372 с.
15. Антропов Л.И. Теоретическая электрохимия. М.: Высшая школа, 1975. 568 с.

Authors of the publication

Vladimir G. Kiselev – Professor of the department “Nuclear and Heat Power Engineering”, Peter the Great St. Petersburg Polytechnic University.

Received ***February 19, 2019***

UDC 621.311.16(0.75.8) **DOI:10.30724/1998-9903-2019-21-3-46-54**

OWER DISTRIBUTION NETWORKS WITH THE MAXIMAL NEARBY LOCATION OF TRANSFORMER SUBSTATIONS TO CONSUMERS

A.V. Lykin, E.A Utkin

Novosibirsk State Technical University, Novosibirsk, Russia
lykin@ngs.ru

Abstract: *The article considers the feasibility of changing the structure of a distribution electrical network by transferring points of electricity transformation as close to consumers as possible. This approach is based on installation of pole-mounted transformer substations (PMTS) near consumer groups and changes the topology of the electrical network. At the same time, for groups of consumers, the configuration of sections of the low-voltage network, including service drops, changes. The efficiency of approaching transformer substations to consumers was estimated by the reduction in electrical energy losses due to the expansion of the high-voltage network. The calculation of electrical losses was carried out according to twenty-four hour consumer demand curve. To estimate the power losses in each section of the electrical network of high and low voltage, the calculated expressions were obtained. For the considered example, the electrical energy losses in the whole network with a modified topology is reduced by about two times, while in a high-voltage network with the same transmitted power, the losses are reduced to a practically insignificant level, and in installed PMTS transformers they increase mainly due to the rise in total idle losses. The payback period of additional capital investments in option with modified topology will be significantly greater if payback is assessed only by saving losses cost. Consequently, the determination of the feasibility of applying this approach should be carried out taking into account such factors as increasing the reliability of electricity supply, improving the quality of electricity, and increasing the power transmission capacity of the main part of electrical network.*

Keywords: *power distribution network; electrical energy losses; quality of electricity; power transmission capacity; reliability of electricity supply; energy conservation; feasibility study; pole-mounted transformer substations.*

For citation: Lykin AV, Utkin EA. Ower distribution networks with the maximal nearby location of transformer substations to consumers. *Power engineering: research, equipment, technology.* 2019; 21(3):46-54. (In Russ). doi:10.30724/1998-9903-2019-21-3-46-54.

РАСПРЕДЕЛИТЕЛЬНЫЕ ЭЛЕКТРИЧЕСКИЕ СЕТИ 10/0,4 КВ С МАКСИМАЛЬНЫМ ПРИБЛИЖЕНИЕМ ТРАНСФОРМАТОРНЫХ ПОДСТАНЦИЙ К ПОТРЕБИТЕЛЯМ

А.В. Лыкин, Е.А Уткин

Новосибирский государственный технический университет, г. Новосибирск, Россия
lykin@ngs.ru

Резюме: *В статье рассматривается целесообразность изменения структуры распределительной электрической сети путем переноса пунктов трансформации электроэнергии как можно ближе к потребителям. Такой подход опирается на установку*

вблизи групп потребителей столбовых трансформаторных подстанций (СТП) и меняет топологию электрической сети. При этом для групп потребителей изменяется конфигурация участков сети низкого напряжения, включающих вводы в дома и здания. Эффективность приближения трансформаторных подстанций к потребителям оценивалась по величине снижения потерь электроэнергии за счет расширения сети высокого напряжения. Расчет потерь электроэнергии был выполнен по часовым интервалам типового суточного графика нагрузки потребителей. Были получены расчетные выражения, позволяющие вычислить потери мощности на всех участках электрических сетей низкого и высокого напряжения. Для рассмотренного примера потери электроэнергии в целом по сети с измененной топологией снижаются примерно в два раза, при этом в сети высокого напряжения с прежней передаваемой мощностью потери снижаются до практически незначимого уровня, а суммарные потери в трансформаторах возрастают в основном из-за роста общих потерь холостого хода. Срок окупаемости дополнительных капитальных вложений в вариант с изменённой топологией будет достаточно большим, если окупаемость будет оцениваться только за счет экономии при снижении потерь. Определение целесообразности применения данного подхода следует производить с учётом таких факторов, как увеличение надёжности электроснабжения, повышение качества электроэнергии и увеличение пропускной способности магистральной части электрической сети.

Ключевые слова: *распределительная сеть; потери электроэнергии; качество электроэнергии; пропускная способность; надежность электроснабжения; энергосбережение; технико-экономическое обоснование; столбовая трансформаторная подстанция.*

Introduction

The problem of high energy losses and low voltage levels in low-voltage distribution networks (secondary distribution networks) is discussed in many publications, for example [1-3]. To solve this problem, well-known methods are used [4, 5], namely: replacing overhead line (OHL) wires with larger cross-section wires, disaggregation of lines, reactive power compensation and installation of control transformers. The transfer of electrical network to a higher rated voltage for low-voltage networks is not applied, since power receivers are connected directly to this network.

For suburban and rural networks, overhead lines are used, which account for the majority of the load losses. Load losses also occur in a step-down transformer of a transformer substation (TS) and inputs to houses and buildings. Transfer to a higher rated voltage in such networks is possible on the sections of the overhead line and on branches from it when moving the transformation closer to consumers using pole-mounted transformer substations (PMTS). This approach is used in many countries, in particular the USA and Canada [6, 7], where three-phase distribution (12.47/0.416 kV) and single-phase (7.2/0.24 kV) transformers are usually installed near consumers.

In the Russian literature, there appear proposals for the use of the so-called innovative network in which pole-mounted transformer substations (PMTS) are as close to the consumer as possible [8, 9]. The innovative project of Rosseti[1] considers the use of 6–10/0.4 kV PMTS with capacities from 25 to 100 kVA, installed in close proximity to consumers and allowing one to minimize the length of 0.4 kV OHL. The project aims to increase the reliability of electricity supply to consumers through the use of simpler design solutions: the use of PMTS installed on

[1] Innovation and evolution. Rosseti // Electrical energy. Transmission and distribution. 2017

standard supports; replacement of disconnectors and fuses by reclosers installed on branches from OHL 10 kV lines and ensuring their protection up to PMTS installed.

For electrical networks of external power supply with a voltage of 0.4-10 kV for agricultural purposes, the new construction is recommended to be carried out by transferring transformation points (several PMTS 10/0.4 kV with a capacity of up to 40 kV·A with single-phase and three-phase transformers) directly to the consumer.

The benefits of PMTS using near consumers are:

- Improving the quality of electricity at the consumer;
- Reduction of electricity load losses;
- Reduction of commercial electricity losses;
- Reduction of operating costs;
- Simplification of the installation of automated electricity metering;
- Simplification of the installation of protective equipment;
- Increasing the transmitting capacity of main OHL;
- Improving the reliability of power supply.

We should also note the following disadvantages of expanding the 10 kV network, replacing the 0.4 kV network:

- Increasing the OHL cost;
- Increasing the total cost of distribution transformers;
- Increasing the idle losses.

The feasibility study of the new network topology can give various results, which are determined by the specifics of consumers' location, their capacity and daily load schedules, as well as by the lengths of the main line and branches from it. PMTS power and the number of consumers connected to them are also of importance.

Materials and methods

Consider one approach to justifying a project to build a 10/0.4 kV electrical network with TS transfer as close to electricity consumers as possible.

To justify this approach, we adopt a method for comparing network construction variants.

New construction can be performed in 2 options:

Option 1. The network is constructed by steel insulated wires (the Russian SIP type) at a voltage of 0.4 kV. The cost of TS is included in the capital investment of the option (traditional option).

Option 2. The network is constructed by protected wires (SIP3) at a voltage of 10 kV with PMTS being placed near a group of consumers (1-6 and more) and inputs into buildings at a voltage of 0.4 kV. There is no centralized TS, and a new 10 kV line connects to the existing 10 kV network.

For simplicity, we assume that consumers have the same power and the same configuration of the daily load schedule, the main line does not have branches and consumers are evenly distributed along the main line on both sides of it, and the length of the inputs to them from one support on both sides of the main line is the same.

As a comparison criterion, we take the total discounted costs for the eight-year life of the facility. Schemes of the options are shown in Figs. 1 and 2.

We accept the cost of construction of 1 km of 0.4 kV OHL with SIP2 wires 3x50+1x54.6 - 1200 ths. rubles, and for 10 kV OHL with SIP3 50 wires - 1885 ths. rubles[2]. Given the market cost of 4 PMTS with transformers of 25 kV·A and TS with a transformer of 100 kV·A, as well as the cost of SIP4 wires 2x25 for inputs to buildings, we get the cost of constructing 0.4 and 10 kV network options, respectively, 1103 and 1654 ths. rubles.

[2] Integrated price standards for typical technological solutions for capital construction of electrical power facilities in terms of electrical grid facilities. Approved by order of the Ministry of Energy of Russia dated February 8, 2016 No. 75.

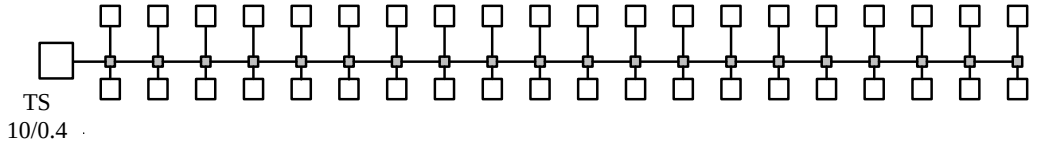

Fig. 1. Scheme of the 0.4 kV network option

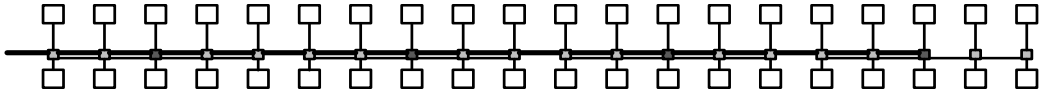

Fig. 2. Scheme of a 10 kV network option using PMTS (version with 10 consumers at PMTS). The supports on which the PMTS are mounted are indicated by dark gray.

Electricity losses ΔW for the two options are determined using the formula:

$$\Delta W = \Delta W_{OHL} + \Delta W_{in} + \Delta W_T + \Delta W_{idle},$$

where ΔW_{OHL} is the losses in overhead line; ΔW_{in} is the losses for inputs to buildings; ΔW_T is the load losses in transformers; ΔW_{idle} is the losses of idling in transformers.

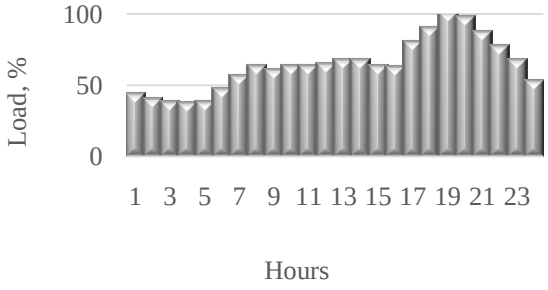

Fig. 3. A twenty-four hour load chart for private houses

A significant share of power losses for a low-voltage network occurs in the OHL network sections, for example, according to [10], losses in OHL are 91.8%, and at inputs (connections) of consumers it is 8.2%. Therefore, by changing OHL to 10 kV voltage can have a very large impact on reducing line losses.

A 10 kV OHL with a function of power distribution to consumers with PMTS will be characterized by low load and low current density. Replacing a 0.4 kV line with a maximum current of about 200 A at the head section (current density of about 4 A/mm^2) with OHL of 10 kV, we have a 25-fold decrease in current and current density (with the same wire section): 0.16 A/mm^2, which entails a huge reduction in power losses: 25^2 times. The load losses in such OHL become negligible. It is natural to believe that a 10 kV network can and should cover much more consumers and it should be used where 2 or more TS are using a traditional power supply scheme with a 0.4 kV network.

For numerical estimation of losses reduction, we compare losses in the schemes shown in Figs. 1 and 2. To calculate the losses, we take the daily schedule of the private houses load shown in Fig. 3.

The monthly electricity consumption of a residential building in which three people live can be taken 470 kWh, therefore, the average power consumed by one house is: *P*av=0.654 kW. Assuming that the daily load schedule of one month is the same for all days of the month, we get the average power equal to 63.4%, so the schedule fill factor β=0.634 and the maximum power *P*max=1.03 kW. It should be noted that the considered load shedule refers to the total power of the line, and for each house individually or several houses, the fill factor will be less, and the energy losses in the OHL end sections and at the inputs will be more. For simplicity, we accept the same schedule for all parts of the network.

Losses calculation for networks with 0.4 kV OHL

Power losses in a single-phase input into the building at the considered time *i* are:

$$\Delta P_{in\_i} = \frac{P_i^2 \left(1 + \mathrm{tg}^2\varphi\right) r_{0,in}\, 2 l_{in}}{U_{ph}^2},$$

where P_i is the power consumed by the house during the considered hour; $\mathrm{tg}\varphi$ is the reactive power coefficient; $r_{0,in}$ is the linear resistance of the input conductor, l_{in} is the length of inputs from a certain pole; U_{ph}^2 is the network phase voltage.

Power losses in inputs to the entire building at the considered time *i*:,

$$\Delta P_{\Sigma in\_i} = n_h \Delta P in\_i,$$

where n_h is the amount of houses.

Power losses at the OHL section *k* at the considered time *i*:

$$\Delta P_{\text{sec.}OHL\, i,k} = \frac{\left\{\left[\left(P_i + \Delta P_{in\_i\, -}\right) n_i k + \sum_{m=1}^{k} \Delta P_{\text{sec. OHL}\, i,m-1}\right]^2 + \left[1 + \mathrm{tg}^2\varphi\right]^2\right\} r_{0,OHL}\, l_{\text{sec. OHL}}}{U^2} k_n$$

where k is the section number, starting from the furthest from TS , $\sum_{m=1}^{k} {}^{\Delta P}_{\text{sec. OHL}\, i,m-1}$ is the sum of losses at the previous OHL sections; n_i is the amount of houses connected to one PMTS; $r_{0,OHL}$ is the specific resistance of the OHL wire; $l_{\text{sec. OHL}}$ is the length of one OHL section; U = 0.4 kV is the linear network voltage k_n = 1.2 is the non-uniformity coefficient, which takes into account the increase in power losses caused by the imbalance of the OHL phase load currents [11].

In this formula losses of reactive power for simplicity are not taken into account due to the low values of SIP inductive resistances.

OHL power losses at the considered time *i*:

$$\Delta P_{OHL,i} = \sum_{n} \Delta P_{\text{sec.OHL}\, i,k},$$

Load losses in transformer at the considered time

$$\Delta P_{\mathrm{T}\, i} = \frac{\left\{\left[n_n P_i + \Delta P_{\Sigma \mathrm{в}\, i} + \Delta P_{OHL\, i}\right]^2 \left[1 + \mathrm{tg}^2\varphi\right]\right\} R_{\mathrm{T}}}{U_{HV}^2},$$

where R_{T} is the transformer resistance; U_{HV} is the voltage of high-voltage winding of transformer.

Daily power losses in the inputs, OHL and transformers are determined by summing 24 values of hourly power losses, the idle energy losses in the transformer is equal to the product of the idle power losses by 24 hours.

Methodology for calculating network losses with 10 kV OHL and PMTS

We accept the condition that there is a separate input for each building connected to the PMTS, while the length of the inputs for houses remote from the PMTS can be large, and neighboring supports are used to suspend them.

It is convenient to determine the power losses at the inputs to the buildings and 0.4 kV OHL, going from one PMTS in the considered hour through the average length for the inputs of one PMTS:, l_{in-av} $\Delta P_{in\_i} = n_{\text{h.PMTS}} \dfrac{P_i^2 \left(1+\text{tg}^2\varphi\right) r_{0,in} 2lin\_av}{U_{ph}^2}$,

where P_i is the power consumed by the house during the considered hour; tgφ is the reactive power coefficient; $r_{0,in}$ is the linear resistance of the input conductor; l_{in_av} is the average length for the inputs of this PMTS; $n_{\text{h.PMTS}}$ is the amount of houses connected to one PMTS; U_{ph} is the network phase voltage.

Power losses at the PMTS transformer windings at the considered time i:

$$\Delta P_{Ti} = n_{PMTS} \frac{\left[\left(P_i n_{h.PMTS} + \Delta P_{in\_n}\right)^2 (1+tg\varphi) RT \right]}{U_{HV}^2},$$

where n_{PMTS} is the amount of PMTS.

Transformer idle power losses are:.

$\Delta P_{Ti} = n_{PMTS} \Delta P_{idle}$.

Power losses at the 10 kV OHL section k at the considered time i:,

$$\Delta P_{\text{sec.OHL}\,i,k} = \frac{\left[\left(P_i n_{\text{h.PTMS}} + \Delta P_{T\,i} + \Delta P_{idle}\right) k + \sum_{m=1}^{k} \Delta P_{\text{sec.OHL}\,i,m-1} \right]^2 \left(1+\text{tg}^2\varphi\right) r_{0,OHL} l_{\text{sec.OHL}}}{U^2},$$

where $l_{\text{sec.OHL}}$ is the length of the 10 kV section between two PMTS; U =10 kV is the linear OHL voltage.

OHL power losses at the considered time i:. $\Delta P_{OHL} = \sum_k \Delta P_{\text{sec.OHL}\,i,k}$.

Daily power losses in the inputs, OHL and transformers are determined by summing 24 values of hourly power losses, the idle energy losses in the transformer is equal to the product of the idle power losses by 24 hours.

The following values are taken in the calculations [12]: the linear resistance of the SIP2 wire is 3x50+1x54.6: 0.641 Ohm/km, the linear resistance of the SIP-3 wire 50 is: 0.72 Ohm/km, the linear resistance of the SIP-4 wire 2x25 is: 1.2 Ohm/km

Active resistances of transformers [13]:

TMG-100/10: $R_{\text{T}} = \dfrac{P_к \cdot U_{rat}^2}{S_{rat}^2} = \dfrac{1970 \cdot 10^2}{100^2} = 19,7 Ohm$

TMG -25/10: $R_{\text{T}} = \dfrac{P_к \cdot U_{rat}^2}{S_{rat}^2} = \dfrac{600 \cdot 10^2}{25^2} = 96 Ohm$

Results

For the first option, losses in the network with 0.38 kV OHL (Fig. 1) amounted to 31.83 kWh (4.83% of the transmitted energy); for the second option, the losses in the network with 10 kV OHL and PMTS (Fig. 2) amounted to 15.7 kWh (2.44% of the transmitted power). Thus, losses decreased by 2 times when using a network with PMTS. The structure of losses is shown in Figs. 4 and 5.

The payback period of the option with large capital investments (10 kV network) will be long enough if the payback is estimated only by saving losses. Approximately accepting annual electricity losses as daily losses multiplied by the number of days in a year, for the given example,

additional capital investments in the second option will pay off by saving losses for 31 years. At the same time, taking into account an increase in the reliability of power supply, an increase in the quality of voltage among consumers, as well as a number of other indicators, the electrical network of 10 kV should be considered more preferable. A similar assessment is given by the authors [14], arguing that such reconstruction or new construction provides significant savings in network losses compared to any other method under consideration, but the initial high investment outweighs the benefits offered for the remaining part of the evaluation period.

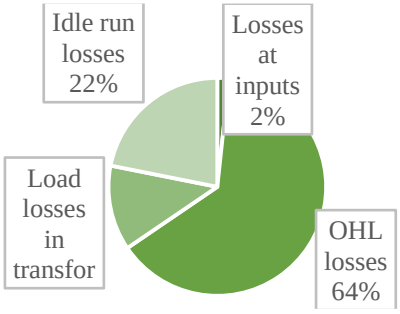

Fig. 4. The structure of losses in the network with an 0.38 kV OHL with the head TS

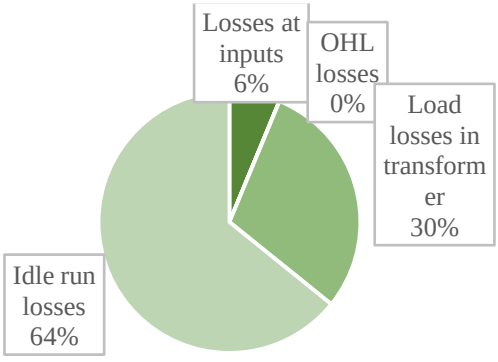

Fig. 5. The structure of losses in the network with an 10 kV OHL with PMTS

Calculations of electrical energy losses made for cases of installation of 5, 6, and 8 PMTS (the number of connected houses to one PMTS, respectively, are 8, 6, and one PMTS with 4 houses and 5) showed an increase in losses with an increase in the number of PMTS. Since that losses for a 10 kV network are determined only by losses in transformers (Fig. 5), with a decrease in the load per one PMTS (number of houses), the total load losses in transformers decrease, while the total idle losses increase as the number of transformers increases. In this case, idle run losses prevail over load losses, and the total losses in transformers increase.

Comparing the economic efficiency of construction of distribution networks using PMTS in Russia and North America, where such networks are widespread, it is worth noting that in Russia the cost of electricity for the population is about two times lower than in the United States. And the energy consumption by one house in the USA is 897 kWh [15], which is almost twice as much as in Russia.

Conclusions

1. In an electrical network with PMTS located as close to the consumer as possible, the losses in medium-voltage OHL become insignificant, while the losses in PMTS transformers increase. In general, losses are mostly reduced.

2. The more consumers (houses) are connected to one PMTS, the lower the total power losses in the transformers and in the network as a whole are, while losses at the inputs increase due to an increase in their length.

3. The rationale for building a network with PMTS as close to the consumer as possible cannot be done taking into account only the reduction of electrical energy losses in the network; one should evaluate the improvement of electrical energy quality, the reliability of power supply and the reduction of operation costs. Improving the quality of electrical energy, first of all, will affect the reduction of negative voltage deviation among consumers, as well as the voltage asymmetry coefficient in the zero sequence. It should be expected that an increase in the reliability of power supply will occur due to a decrease in the failure rate of a total network of 10/0.4 kV, by switching off only PMTS with damaged sections of the 0.4 kV network, as well as due to a higher level of 10 kV OHL reliability as compared to 0.4 kV OHL.

References

1. Vorotnitskii VE, Zagorskii YaT, Apryatkin VN, Zapadnov AA. Calculations, norming and reducing of electrical energy losses in city electrical networks. *Electrical power stations*, 2000. N5. (In Russ).

2. Kalambe S, Agnihotri G. Loss minimization techniques used in distribution network: bibliographical survey. *Renewable and sustainable energy reviews*, 2014. N29. pp. 184-200.

3. Orlov AI, Karchin VV. Approaches to electrical energy losses reduction and quality of electrical energy improvement in 0.4 kV electrical networks. *Materials of the Eighth International Scientific School «Science and innovation»*. Yoshkar-Ola: «Mari Institute of Education», 2013. (In Russ).

4. Agüero JR. Improving the efficiency of power distribution systems through technical and non-technical losses reduction. *PES T&D* – IEEE, 2012. pp 1-8.

5. Zhelezko YuS. Vy`bor meropriyatij po snizheniyu poter` e`lektroe`nergii v e`lektricheskix setyax: Rukovodstvo dlya prakticheskix raschyotov [Selection of procedures to reduce electrical energy losses in electrical networks: A guide for practical calculations]. Moscow, Ehnergoatomizdat ., 1989. (In Russ).

6. William H. Kersting Distribution System Modeling and Analysis. – Second Edition. CRC Press, 2007.

7. Short TF. Electric power distribution handbook / Tom Short. – 2004 by CRC Press LLC.

8. Knyazev VV. The main directions of increasing the reliability of power supply in countryside. Electro, 2006, N5. (In Russ).

9. Fursanov, MI. Circuit-design solutions and information support of urban electrical networks in terms of SMART GRID. *Power industry. Proceedings of the higher educational institutions and power industry associations CIS*, 2017; 5(60):393-406. (In Russ).

Литература

1. Воротницкий В. Э. Анализ динамики, структуры и мероприятий по снижению потерь электроэнергии в электрических сетях России и за рубежом //Энергоэксперт. – 2017. №. 5-6. С. 24.

2. Kalambe S., Agnihotri G. Loss minimization techniques used in distribution network: bibliographical survey // Renewable and sustainable energy reviews. 2014. Т. 29. С. 184-200.

3. Орлов А.И., Карчин В.В. Способы снижения потерь и повышения качества электрической энергии в электрических сетях 0,4 кВ // Материалы 8 международной научной школы «Наука и инновации». Йошкар-Ола: ГБОУ ДПО (ПК) С «Марийский институт образования», 2013.

4. Agüero J. R. Improving the efficiency of power distribution systems through technical and non-technical losses reduction // PES T&D 2012. – IEEE, 2012. С. 1-8.

5. Железко Ю.С. Выбор мероприятий по снижению потерь электроэнергии в электрических сетях. М.: Энергоатомиздат, 1989.

6. William H. Kersting Distribution System Modeling and Analysis. Second Edition. CRC Press, 2007.

7. Short T.F. Electric power distribution handbook / Tom Short. 2004 by CRC Press LLC.

8. Князев В.В. Основные направления повышения надёжности электроснабжения потребителей в сельской местности // ЭЛЕКТРО. 2006. №5.

9. Фурсанов, М. И. Схемно-конструктивные решения и информационное обеспечение городских электрических сетей в условиях SMART GRID // Энергетика. Известия высших учебных заведений и энергетических объединений СНГ. 2017. Т. 60, № 5. С. 393-406.

10. Lasso, H., Ascanio, C., Guglia, M. A model for calculating technical losses in the secondary energy distribution network // IEEE/PES Transmission &

10. Lasso H, Ascanio C, Guglia MA. model for calculating technical losses in the secondary energy distribution network. *IEEE/PES Transmission & Distribution Conference and Exposition*: Latin America. 2006. pp 1–6.
11. Zhelezko YuS. Electrical energy losses. Reactive power. Quality of electrical energy: guidance for practical calculations. Moscow, ENAS Publ., 2009. pp 456. (In Russ).
12. Bodin AP, Pyatakov FYu. Electrical installations of consumers. Moscow, ZAO Energoservis Publ., 2006. 616 p. (In Russ).
13. Makarov EF. *0.4-35 i 110-1150 kV*. Electrical networks 0.4-35 and 110-1150 kV handbook. Moscow :ENERGIYA., 2006. pp 624. (In Russ).
14. Vegunta SC, Hawkins D, Clifton F, Steele A, S. Reid A. Distribution network losses and reduction opportunities from a UK DNO's perspective. – CIRED, 23 International Conference on Electricity Distribution, Lyon, 15-18 June 2015, pp 0068.
15. U.S. Energy Information Administration 2017. Frequently asking questions. «How much electricity does an American home use?»: InfoCtr@eia.gov Accessed to: Octomber2, 2019.

Distribution Conference and Exposition: Latin America. 2006. pp 1–6.
11. Железко Ю.С. Потери электроэнергии. Реактивная мощность. Качество электроэнергии: Руководство для практических расчетов. – М.: Изд-во НЦ ЭНАС, 2009. С. 420.
12. Бодин А.П., Пятаков Ф.Ю. Электроустановки потребителей.. – М.: ЗАО «Энергосервис», 2006. 616 с.
13. Макаров Е.Ф. Электрическая сеть 0,4-35 и 110-1150 кВ. – М.: ИД «ЭНЕРГИЯ», 2006. 624 с.
14. S. C. Vegunta, D. Hawkins, F. Clifton, A. Steele, S. A. Reid Distribution network losses and reduction opportunities from a UK DNO's perspective / // CIRED, 23rd International Conference on Electricity Distribution, Lyon, 15-18 June 2015, Paper 0068.
15. U.S. Energy Information Administration 2017. Frequently asking questions. How much electricity does an American home use? (RECS) InfoCtr@eia.gov .Accessed to:Octomber 2, 2019.

Authors of the publication

Anatoliy V. Lykin – PhD in Engineering sciences, Associate Professor, Department "Automated Electrical Power Systems", Novosibirsk State Technical University.

Evgeniy A. Utkin –Master's programme student, Novosibirsk State Technical University, in the field of study 13.04.02 electrical and power engineering (specialization: electrical power systems and networks).

Received ***February 20, 2019***

UDC 541.183 **DOI:10.30724/1998-9903-2019-21-3-55-62**

APPLICATION OF X-RAY FLUORESCENCE SPECTROMETRY IN ASSESMENT OF ULTRAFILTRATION MEMBRANE SURFACE CONDITION AT WATER PRE- TREATMENT UNITS OF THERMAL POWER PLANTS

E.V. Veselovskaya, E.N. Voloshina, S.E. Lysenko
Platov South-Russian State Polytechnic University (NPI), Novocherkassk, Russia

Abstract: *The objects of the study were the Doy Chemical hollow-fiber ultrafiltration membranes which were use for preparation of make-up water for the Novocherkasskaya Regional Thermal Power Plant (RTPP).*

We tried out a possibility of applying the X-ray fluorescence spectrometry to study the condition of the spent non-recoverable ultrafiltration membranes in order to identify the causes of their irreversible destruction. The ARL Quant'X X-ray fluorescence energy dispersive spectrometer of Thermo Scientific (USA) was used in the study.

Thin cuts of the Doy Chemical hollow-fiber ultrafiltration membranes were used in the experiments, which had worked for more than three years in the field conditions of the feed water of the Don River, Russia.

The analysis of the obtained samples spectra allowed us to assume that the membranes were irreversibly contaminated by iron bacteria. Basing on the conclusions made during the analysis of X-ray fluorescence spectra we developed and tested in field conditions one of the optimization variants for technological pretreatment scheme. This scheme enables a significant increase in the service life of ultrafiltration membranes, even when the feed water is heavily contaminated by bacteria. Field tests of the modernized technology were carried out at Novocherkasskaya RTPP during 2016-2018 and showed a significant increase in the service life of the membrane modules. At the same time, the quality of the filtrate, productivity and pressure drops at the cascades of ultrafiltration units fully corresponded to the normative values even in conditions of deteriorated quality of the feed river water.

It has been proved that aggressive regeneration of ultrafiltration membranes that have worked for a long time under the conditions of feed water having increased values of the total microbial number and high values of permanganate oxidation does not allow one to restore their initial state. In this case the main cause of ultrafiltration membranes contamination is iron, which is present in colloidal and bacterial forms in the pores and on the membranes surfaces. In the conditions of the Novocherkasskaya RTPP, in addition to timely flushing and chemical regeneration of ultrafiltration membranes, the necessity of organizing a preliminary treatment of the feed water with reagents having a prolonged bactericidal effect is accepted.

Keywords: *thermal power plants; water pre-treatment; water use; water regimes; water treatment units; water desalination; ultrafiltration membranes; X-ray fluorescence spectrometry; iron bacteria; water disinfection.*

For citation: Veselovskaya EV, Voloshina EN, Lysenko SE. Application of x-ray fluorescence spectrometry in assesment of ultrafiltration membrane surface condition at water pre- treatment units of thermal power plants. *Power engineering: research, equipment, technology*. 2019; 21 (3): 55-62. (In Russ). doi:10.30724/1998-9903-2019-21-3-55-62.

ПРИМЕНЕНИЕ РЕНТГЕНОФЛУОРЕСЦЕНТНОЙ СПЕКТРОМЕТРИИ ДЛЯ ОЦЕНКИ СОСТОЯНИЯ ПОВЕРХНОСТИ УЛЬТРАФИЛЬТРАЦИОННЫХ МЕМБРАН ВОДОПОДГОТОВИТЕЛЬНЫХ УСТАНОВОК ТЭС

Е.В. Веселовская, Е.Н. Волошина, С.Е. Лысенко

"Южно-Российский государственный политехнический университет (НПИ) имени М.И. Платова", г. Новочеркасск, Россия

Резюме: *Объектом исследования являлись половолоконные ультрафильтрационные мембраны производства Doy Chemical, использованные при подготовке добавочной воды для Новочеркасской ГРЭС.*

Опробована возможность применения метода рентгенофлуоресцентной спектрометрии для исследования состояния отработанных, не подлежащих регенерации, ультрафильтрационных мембран с целью выявления причин, приводящих к их необратимой деструкции. Исследования проводили с помощью рентгенофлуоресцентного энергодисперсионного спектрометра ARL Quant'X производства Thermo Scientific (USA).

В эксперименте были использованы тонкие срезы образцов половолоконных ультрафильтрационных мембран производства Doy Chemical, проработавших в производственных условиях более трех лет на исходной воде реки Дон.

Анализ полученных спектров образцов позволил предположить необратимое загрязнение мембран железобактериями. На основе выводов, сделанных при анализе рентгенофлуоресцентных спектров, разработан и опробован в производственных условиях один из вариантов оптимизации технологической схемы предочистки, позволяющий значительно увеличить срок службы ультрафильтрационных мембран, в том числе при значительном бактериальном загрязнении исходной воды. Производственные испытания модернизированной технологии проводились на Новочеркасской ГРЭС в течение 2016-2018 годов и показали значительное увеличение срока службы мембранных модулей. При этом качество фильтрата, производительность и перепады давления на каскадах ультрафильтрационных установок полностью соответствовали нормативным значениям даже в условиях снижения качества исходной речной воды.

Доказано, что проведение агрессивной регенерации ультрафильтрационных мембран, отработавших длительный срок в условиях исходной воды с повышенными значениями общего микробного числа и высокими значениями перманганатной окисляемости, не позволяет восстановить их исходное состояние. Основной причиной загрязнения ультрафильтрационных мембран в данном случае является железо, присутствующее в коллоидной и бактериальной формах в порах и на поверхности мембран. В условиях Новочеркасской ГРЭС помимо своевременных промывок и химических регенераций ультрафильтрационных мембран признана необходимость организации предварительной обработки исходной воды реагентами, обладающими пролонгированным бактерицидным действием.

Ключевые слова: *тепловые электрические станции; водоподготовка; водоиспользование; водные режимы; водоподготовительные установки; обессоливание воды; ультрафильтрационные мембраны; рентгенофлуоресцентная спектрометрия; железобактерии; обеззараживание воды.*

Introduction

In recent decades, membrane technologies for natural waters treatment have been increasingly widely used in the practice of water treatment of thermal power plants (TPP), due to their environmental friendliness, high quality of water purification, compact size of units and the possibility of their full automatization [1–6]. Ultrafiltration membrane units successfully replace multi-stage technological schemes, which include clarifiers. This allows one to avoid the deposition of contaminants by reagent methods and, consequently, to exclude the formation of precipitation of high humidity. This circumstance is extremely important, since efficient dewatering of precipitates involves the use of additional reagents and finishing dehydration units.

The main disadvantages of ultrafiltration methods for water pre-treatment are the membranes high cost, the significant consumption of wash water, and the sensitivity of membranes to the impact of certain specific impurities present in natural waters that can cause their irreversible destruction. Therefore, we believe that it is important to use highly informative methods for analyzing the surface condition of membranes, which allow one to predict possible negative changes of the membrane condition in the presence of certain impurities in the feed water.

Energy dispersive X-ray fluorescence spectrometry (EDXRF) was chosen as one of the methods for obtaining objective information about the surface condition of the spent ultrafiltration membrane. This method allows simultaneous recording the entire range of energies of the secondary (characteristic) radiation from the sample [7–9]. Fluorescence radiation is decomposed into the spectrum using Si-based semiconductor detectors that record all radiation from the sample and convert it into electrical pulses, forming a spectrum in the form of relationship between the number of pulses and the energy of each element. Further, the spectra are processed by mathematical methods and statistical analysis, allowing obtaining quantitative and qualitative data.

According to our data, the EDXRF method has not yet been applied for assessing the condition of spent ultrafiltration membranes used at the pre-treatment stage at water treatment facilities of thermal power plants. We have chosen this research method as it has certain advantages, namely the relatively low requirements for sample preparation and the possibility of analysis in wide range of concentrations.

Problem statement

In recent years, at PJSC OGK-2 Novocherkasskaya Regional Thermal Power Plant (RTPP) ultrafiltration clarification is used as a water pre-treatment technology, which was introduced by the specialists of NPK Mediana-Filter. Initially, the technological scheme of water treatment included the direct supply of raw water after preliminary mechanical filtration to ultrafiltration units. However, this technology resulted in reduction of the filter cycle and premature failure of the membranes. Therefore, as an experiment, a technology for preliminary disinfection of raw water by chlorine-containing reagents was developed, successfully tested on stand-alone modular units by the specialists of NPK Mediana-Filter under the direct supervision of the head of the chemical workshop of PJSC OGK-2 Novocherkasskaya RHPP S.E. Lysenko.

This article presents the EDXRF study of the surface condition of the spent ultrafiltration membranes, which were operated according to the technology without preliminary disinfection of water. In addition, a detailed description is given of an improved technological scheme of ultrafiltration, implementation of which has shown positive results.

Experimental technique

The surface conditions of ultrafiltration membranes were studied at the Platov South-Russian State Polytechnic University using the ARL Quant'X X-ray fluorescence energy dispersive spectrometer from Thermo Scientific (USA). The device has the following characteristics:

- Silicon-lithium detector with electric cooling;
- Measurements sensitivity is in the range from 0.0001 to 100%;
- The measurement time for one element is from 10 to 60 seconds;

- Adjustable size of the X-ray beam from 1 to 10 mm.

The thin cuts of samples of hollow-fiber ultrafiltration membranes from Doy Chemical, which had worked under real conditions for more than three years at the feed water of the Don River were used in the experiments. Slice No. 1 is the initial sample in dry condition; slice No. 2 is the sample subjected to soaking for 48 hours in distilled water; slice No. 3 is the sample in contact with a 4% solution of citric acid for 48 hours with continuous shaking and subjected to subsequent washing with distilled water for 6 hours.

Unfortunately, according to the terms of supply for the membranes, it is impossible to obtain a sample based on a "fresh" membrane (before its commissioning) to perform a comparative analysis. Therefore, the EDXRF method was used to study samples based on membranes decommissioned due to the impossibility of restoring their original flow capacity, that is, the so-called "spent" membranes.

Before being placed in cuvettes, the slices, which contacted with liquids, were held in air for 10 min. To detect characteristic radiation, semiconductor solid-state detectors were used, the operation of which is based on ionization inside the semiconductor, the detector type is Si (Li).

The anode material of the analyzer tube is Rh (optionally Ag). The maximum radiation power was 50 W at voltage supplied in 1 kV increments in the range from 4 to 50 kV. The selectivity of the recording was provided by 7 filters and additional direct excitation of electrons. The maximum counting speed was up to 100,000 pulses per second with an optimal value of about 50,000. The radiation stability is 0.25% for 8 hours for the device sensitivity in the range from 0.0001 to 100%.

Experimental results

Quantitative and qualitative results of the conducted experiments are presented in Table 1 and Figs.1,2.

Table 1

Quantitative results of the initial sample study by X Energy dispersive X-ray fluorescence y

Oxides concentration, %		Element concentration, %	
SO_3	19.02	Sx	7.62
CI	4.92	CI	4.92
TiO_2	19.52	Ti	11.70
MgO	-	Mg	-
CaO	7.95	Ca	5.69
P_2O_5	6.29	Px	2.74
K_2O	25.65	K	21.29
Fe_2O_3	0.501	Fe	0.350
ZnO	0.400	Zn	0.322
Sb_2O_3	0.0850	Sb	0.0710
Al_2O_3	14.62	Al	7.74
MnO	0.956	Mn	0.740
WO_3	0.061	W	0.048
Br	0.0203	Br	0.0203
PdO	0.0097	Pd	0.0084

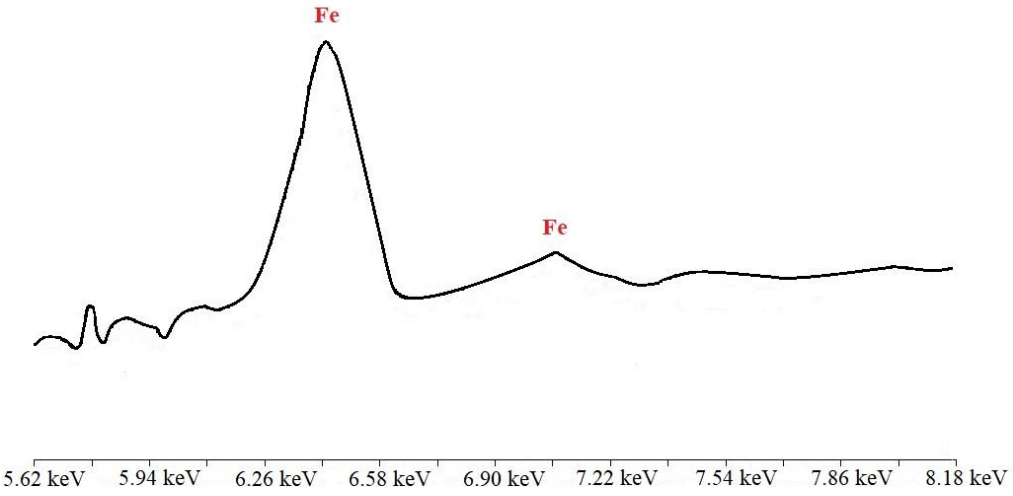

Fig. 1. X-ray fluorescence spectra of the initial sample of ultrafiltration membrane, fabricated using palladium filter.

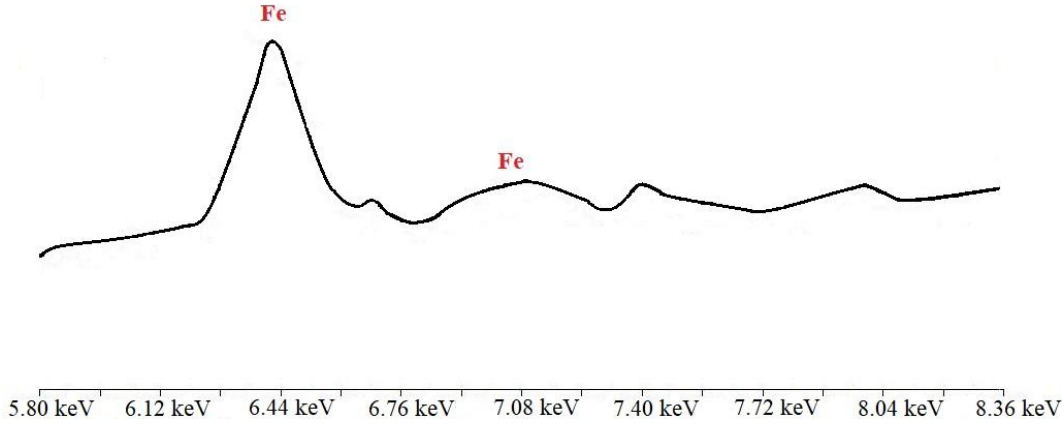

Fig. 2. X-ray fluorescence spectra of the initial sample of ultrafiltration membrane after chemical washing, fabricated using palladium filter

For the sample No.2, which was in contact with distilled water, no significant changes were revealed, so we can conclude that washing with water without the use of aggressive reagents does not lead to positive changes in the surface of the worked ultrafiltration membranes. Therefore, further studies were performed for the initial sample and sample No.3. The figures show the most characteristic parts of spectra for these samples.

Comparison of the spectra of the initial sample and the sample after aggressive chemical washing allows us to conclude that even chemical regeneration does not contribute to a fundamental change in the condition of the ultrafiltration membrane. In order to understand in

more detail the reasons leading to an irreversible deterioration of the membrane, we consider the composition of the initial water entering the ultrafiltration unit (Table 2).

Table 2

Composition of the initial river water supplied to the ultrafiltration plant, according to the data from the chemical workshop of the Novocherkasskaya RHPP for 2014 - 2016

Characteristics	Meas. unit	Value
Total salt content	mg/l	500–1000
Particles percentage	mg/l	3–50
Iron concentration	mg/l	0.1–2.1
Permanganate oxidizability	mgO_2/l	3–32
Total stiffness	mg- equ/L	5–10
Alcalinity	mg- equ/L	2.3–4.5
Hydrosilicic acid concentration	mg/l	4–16
Oil products concentration	mg/l	0.05–1.1
pH		7.5–8.5
Temperature	^0C	7–34

Besides this, the increased values of the total microbial number were periodically recorded in the feed water. The presence of bacterial water pollution, together with high permanganate oxidizability, allows us to conclude that there is a bacterial film on the surface of the membranes [10, 11].

Analysis of the obtained spectra shows that the spent ultrafiltration membranes are characterized by the presence of iron, which remains even after acid chemical washing. Bacterial iron or iron bacteria are typical representatives of surface water bodies. Iron bacteria are represented, as a rule, by filamentous forms that can effectively be fixed on the surface of water treatment equipment, in particular on the surface of ultrafiltration membranes. In addition, iron oxides accumulate on the surface of bacterial cells, both as a result of absorption by ferrous bacteria of ferrous ions from the feed water, and as a result of oxidation of the bacterial film itself, accompanied by the deposition of insoluble ferric oxides and hydroxides. The absence of the effect of acid washing of the spent ultrafiltration membrane can apparently be explained by the fact that iron (III) hydroxide, which is a product of the activity of iron bacteria, under the proposed conditions of membrane regeneration forms a colloidal gel capable of accumulating in the membrane pores, reducing their cross-sectional area.

Thus, taking into account the increased permanganate oxidizability of the feed water and the high probability of bacterial contamination of ultrafiltration membranes, it was concluded that it is advisable to continuously disinfect water using sodium hypochlorite as a disinfecting reagent. To ensure the longest possible exposure time of free chlorine, the point of introduction of sodium hypochlorite, as a result of field experiments, was chosen in front of contact filters located in the technological scheme immediately before the ultrafiltration units.

Taking into account the transport lag from the point of introduction of sodium hypochlorite in the feed water pipeline to the point of control of free chlorine in the ultrafiltered water supply line to reverse osmosis plants (the location of reverse osmosis units in the process flow diagram is immediately after the ultrafiltration units), which is from 50 to 60 minutes, and inconstancy of chlorine absorption of the feed water, the selection of the optimal dose of sodium hypochlorite was carried out step by step with a dose change interval of not less than 1 hour.

The concentration of free chlorine at the inlet to reverse osmosis plants was monitored using the *Burkert* free chlorine control system, as well as by titration. For dosing of commercial sodium hypochlorite in a wide range of concentrations of active chlorine (from 20 to 190 g/l), a metering pump for the SEV-1 dosing station and the SEV-1 consumption tank were used.

Implementation of these technical measures had a positive effect on the condition of ultrafiltration units: the cartridges replacement time increased from 4 to 6 weeks, and during the

inter-flood period it was about 8 weeks. The quality of the filtrate, productivity and pressure drops on the cascades of ultrafiltration plants during 2016–2018 never went beyond the regime charts.

Conclusions

Analysis of X-ray fluorescence spectroscopy data shows that even aggressive regeneration of ultrafiltration membranes that have spent a long time (more than 5 years) does not lead to restoration of their initial condition. This, possibly, is a consequence of exceedance of the critical transmembrane pressure during operation of the ultrafiltration unit, which causes irreversible mechanical changes in the structure of the membrane fiber. Taking into account the characteristics of the feed water, we can conclude that the main cause of contamination of ultrafiltration membranes, apparently, is iron, which is present mainly in colloidal and bacterial forms. Given the developed surface of ultrafiltration membranes, it can be assumed that the deposition and fixing of these forms of iron will occur both on the membrane surface and in its pores. As a result of these processes, the pore cross-sectional area of ultrafiltration membranes will decrease, causing a decrease in the flow through the membrane and, accordingly, an increase in transmembrane pressure, leading to its destructive changes.

Thus, based on the data of X-ray fluorescence analysis, we consider it expedient to carry out not only timely washing and chemical regeneration of ultrafiltration membranes, but also to organize preliminary disinfection of water entering the ultrafiltration unit, for example, by solution of sodium hypochlorite, which has a prolonged bactericidal effect.

References

1. Apel PYu, Bobreshova OV, Volkov AV, et al. Perspektivy razvitiya membrannoj nauki. *Razvitiya membrannoj nauki* 2019; 9(2): 59-80. (In Russ).

2. Veselovskaja EV, Shishlo AG. Povyshenie ekologicheskih pokazatelej vodopodgotovitel'nyh ustanovok teploenergeticheskih predpriyatij. University News. North-Caucasian Region. Technical Sciences Series. 2016.-N. 4. pp 36-41.

3. Veselovskaya EV, Shishlo AG. Opyt primeneniya perspektivnyh tekhnologij vodopodgotovki na otechestvennyh teplovyh elektrostanciyah// *Izvestiya vuzov, Sev.-Kavk. region. Tekhnologiya nauki.* 2016; (2):31-34.(In Russ).

4. Shishlo AG. Issledovanie processa obessolivaniya dobavochnoj vody blochnoj TES metodom nano-fil'tracii. *Izvestiya vuzov. Tekhnicheskie nauki.* 2013; 4: 38-41.(In Russ).

5 Fazullin DD, Mavrin GV, Shajhiev IG, Nizameev IR Ul'trafil'traciya vodomaslyanyh emul'sij dinamicheskoj membranoj nejlon–polistirol. Membrany i membrannye tekhnologii, 2019;8(1): 51-58.

6. Roldugin VA. Bazhenov VI, Plisko SD, T.V. Modelirovanie vneshnego massoperenosa v polovolokonnyh membrannyh kontaktorah Kirsh Membrany i membrannye tekhnologii 2019; 5(4): 261-268.(In Russ).

7. Jose A.C. Broekaert. Editors .Adolescent pregnancy.*2*-nd ed. Wiley-VCH: Verlag CmbH & Co. KGaA:,2002.

Литература

1. Апель П.Ю., Бобрешова О.В., Волков А.В., Волков В.В., Никоненко В.В., Стенина И.А., Филиппов А.Н., Ямпольский Ю.П., Ярославцев А.Б. Перспективы развития мембранной науки //*Мембраны и мембранные технологии* .2019. №2(9). С.59-80.

2. Веселовская Е.В., Шишло А.Г. Повышение экологических показателей водоподготовительных установок теплоэнергетических предприятий // *Известия Вузов.* Сев.-кавк. Регион, науч.-центр высш. Шк.-техн. Науки.2016.- № 4.- С. 36-41.

3. Веселовская Е.В., Шишло А.Г. Опыт применения перспективных технологий водоподготовки на отечественных тепловых электростанциях// *Известия вузов*, Сев.-Кавк. регион. Технология науки. 2016. №2. С. 31-34.

4. Шишло А.Г. Исследование процесса обессоливания добавочной воды блочной ТЭС методом нано- фильтрации // *Известия вузов. Технические науки*. 2013 г., вып. 4, с. 38-41.

5. Ультрафильтрация водомасляных эмульсий динамической мембраной нейлон–полистирол/ Фазуллин Д.Д., Маврин Г.В., Шайхиев И.Г., Низамеев И.Р. // *Мембраны и мембранные технологии*, 2019. том 8. №1. С. 51-58.

6. Кирш В.А., Ролдугин В.И., Баженов С.Д., Плиско Т.В.Моделирование внешнего массопереноса в половолоконных мембранных контактора // *Мембраны и мембранные*

8. Becker Y. *Spektroskopiya.* - Moscow: Tehnosphera; 2009. (In Russ).
9 Lazarev SI, Golovin YuM., Lazarev DS, Polikarpov VM. Issledovaniya sostoyaniya vody v acetatcellyuloznoj membrane MGA-95 metodami infrakrasnoj spektrometrii i termogravimetrii. Membrany i membrannye tekhnologii 2019; 5(4):278-281. (In Russ).
10. Pasmore M, Todd P, Smith S, Baker D, Silverstein J, Coons D, Bowman CN. Effects of ultrafiltration membrane surface properties on Pseudomonas aeruginosa biofilm initiation for the purpose of reducing biofouling. J. *Membrane Science*. 2002;194:, 15-32.
11. Wilf I. New membrane research and development achievements. *Desalination and Water Reuse.* 2001;10(1): 28-33.

технологии, 2019,№4(5) 261-268.
7. Jose A.C. Broekaert. Analytical Atomic Spectrometry with Flames and Plasmas. Wiley-VCH: Verlag CmbH & Co. KGaA, 2002. 375p.
8. Беккер Ю. *СПЕКТРОСКОПИЯ.* - М.: Техносфера, 2009. 528 с.
9. Лазарев С.И., Головин Ю.М., Лазарев Д.С., Поликарпов В.М Исследования состояния воды в ацетатцеллюлозной мембране МГА-95 методами инфракрасной спектрометрии и термогравиметрии. // Мембраны и мембранные технологии .2019., №4 (5).с. 278-281.
10. Pasmore M., Todd P., Smith S., Baker D., Silverstein J., Coons D., Bowman C.N. Effects of ultrafiltration membrane surface properties on Pseudomonas aeruginosa biofilm initiation for the purpose of reducing biofouling. // *J. Membrane Science.* 2002. Vol. 194, pp 15-32.
11. Wilf I. New membrane research and development achievements. // *Desalination and Water Reuse*. 2001. Vol. 10/1, pp. 28-33.

Authors of the publication

Elena V. Veselovskaya – Dr.Sc. in Engineering sciences, Professor, Department "Thermal Power Stations and Heat Transfer Engineering", Platov South-Russian State Polytechnic University, Novocherkassk. E-mail: elenaveselovsckaja@yandex.ru.

Elena N. Voloshina – engineer of the center for collective use "Nanotechnology", Platov South-Russian State Polytechnic University.

Sergey E. Lysenko – Department "Thermal Power Stations and Heat Transfer Engineering", Platov South-Russian State Polytechnic University.

Received ***March 23, 2019.***

UDC621.311.001.57 **DOI:10.30724/1998-9903-2019-21-3-63-72**

DEVELOPMENT OF THE WAVE METHOD OF CALCULATION OPERATIONAL PARAMETERS OF A DOUBLE-CIRCUIT POWER TRANSMISSION LINE WITH KNOWN VALUES OF OUTPUT VOLTAGES AND CURRENTS AT THE END OF THE LINE

G.A. Bolshanin, M.P. Plotnikov

Bratsk State University, Bratsk, Russia
ORCID: https://orcid.org/0000-0003-0218-7334, bolshaning@mail.ru*
https://orcid.org/0000-0002-0877-4727, plotnikov_m.p@mail.ru

Abstract: *Electrical energy from the place of its generation is transmitted to consumers of various capacities. The distance from the source of electrical energy to the consumer can vary from several meters to several thousand kilometers. In this regard, the accurate determination of the operating parameters of the power transmission line (PTL) is a mandatory and necessary condition for the PTL normal functioning. In the current-carrying parts of the double-circuit PTL there are six incident and six reflected waves of the electromagnetic field. They determine voltages and currents. A scheme is proposed for the distribution of these waves along linear wires of a homogeneous section of a double-circuit PTL. This scheme shows that the current-carrying parts of the adjacent wires have a significant impact on voltages and currents in one wire. This scheme illustrates the distribution of the amplitude values of electromagnetic field waves, defined as the integration constant. Using the integration constants, the propagation constants of electromagnetic waves along the linear wires of the PTL and the corresponding wave impedances, one can obtain the amplitude values of the incident and reflected waves at any point of the double-circuit PTL, and hence the currents and voltages in the double-circuit PTL. The article presents a method for determining the currents and voltages in a double-circuit PTL according to the load. The proposed method will allow determining the qualitative and quantitative indicators of electrical energy (induced voltage) appearing from each wire separately and provide the possibility of their elimination, which will improve the quality of electrical energy.*

Keywords*: development of methodology for calculation the operating parameters of a double circuit power transmission line; incident and reflected waves; self and mutual wave impedances.*

For citation: Bolshanin GA, Plotnikov MP. Development of the wave method of calculation operational parameters of a double-circuit power transmission line with known values of output voltages and currents at the end of the line. *Power engineering: research, equipment, technology*. 2019; 21(3): 63-72. (In Russ). doi:10.30724/1998-9903-2019-21-3-63-72.

РАЗРАБОТКА ВОЛНОВОЙ МЕТОДИКИ РАСЧЕТА РЕЖИМНЫХ ПАРАМЕТРОВ ДВУХЦЕПНОЙ ЛИНИИ ЭЛЕКТРОПЕРЕДАЧИ ПРИ ИЗВЕСТНЫХ ВЫХОДНЫХ ЗНАЧЕНИЯХ НАПРЯЖЕНИЙ И ТОКОВ В КОНЦЕ ЛИНИИ

Г.А. Большанин, М.П. Плотников
Братский государственный университет, г. Братск, Россия
ORCID: https://orcid.org/0000-0003-0218-7334, bolshaning@mail.ru*
https://orcid.org/0000-0003-4017-6732, plotnikov_m.p@mail.ru

Резюме: *Электрическая энергия от места ее генерации передается потребителям различной мощности. Расстояние от источника электрической энергии до потребителя может быть от нескольких метров до нескольких тысяч километров. В связи с этим точное определение режимных параметров линии электропередачи (ЛЭП) является обязательным и необходимым условием для нормального функционирования ЛЭП. В токоведущих частях двухцепной ЛЭП присутствуют шесть падающих и шесть отраженных волн электромагнитного поля. Именно они определяют значения напряжений и токов. Для учета взаимного влияния проводов в статье предложена схема распределения этих волн по линейным проводам однородного участка двухцепной ЛЭП. Из этой схемы видно, что на величину напряжений и токов в одном проводе оказывает существенное влияние токоведущие части соседних проводов. Эта схема иллюстрирует распределение амплитудных значений волн электромагнитного поля, которые являются постоянными интегрирования. С помощью постоянных интегрирования, постоянных распространения электромагнитных волн по линейным проводам ЛЭП и соответствующих волновых сопротивлений можно получить наглядное представление об амплитудных значениях падающих и отраженных волн в любой точке двухцепной ЛЭП, а значит, и о токах и напряжениях в двухцепной ЛЭП. В статье представлена методика определения токов и напряжений в двухцепной ЛЭП по нагрузке. Предлагаемая методика позволит определять качественные и количественные показатели электрической энергии (наведенное напряжение), появляющиеся от каждого провода в отдельности и обеспечит возможность их устранения, что позволит повысить качество электрической энергии.*

Ключевые слова: *разработка методики расчета режимных параметров двухцепной ЛЭП; падающая и отраженная волна; собственные и взаимные волновые сопротивления.*

Introduction

Usually, electrical energy is delivered from power plants where it is generated, to consumers using the overhead power transmission lines (PTL), which are characterized by transmission capacity, length and design.

Most consumers of high power are located far from the places of electricity generation. So, the transportation of electrical energy has to be carried out by overhead power lines of voltage of 35 kV and higher. Often such PTL are double-circuit. The use of double-circuit power transmission lines allows one to save raw materials (material for new supports), reduce the exclusion zone, improve the environmental situation, etc.

Electricity supplying organizations are obliged to provide consumers with high-quality electrical energy that meets the requirements of current regulatory documents[1]. For load planning, it is necessary to calculate the modes for each PTL. In this case, it is advisable to take into account the largest number of factors affecting the transmission of electrical energy along power lines.

The calculation of electric networks modes is crucial for electric power systems. One of the main tasks is to calculate the modes of double-circuit overhead power lines, in particular, to determine currents and voltages at any point on the power line wires. To solve this task it is necessary to know voltages and currents either at the beginning of the power line or at its end, in addition to the primary parameters of the analyzed PTL.

The article provides an option for calculation operational parameters at known voltages and currents at the end of power lines. This information can be obtained at the substation under consideration.

Experimental technique

[1] GOST 32144-2013. Electric Energy. Electromagnetic compatibility of technical equipment. Standards of quality of electrical energy in general-purpose power supply systems. Moscow: Standardinform, 2014. 16 p.

The transmission of electrical energy is accompanied by directional distribution of electromagnetic field [1], which propagates through an unloaded power transmission line according to harmonic laws [2].

Typically, analysis of transmission of high-quality electrical energy is performed for a single line wire. This is true, since the process of such energy transmission through each linear wire is the same. In this case, the electromagnetic connections between the PTL linear wires are so insignificant that taking them into account does not make sense [3, 4]. But this is true only for high-quality electrical energy. Otherwise, these electromagnetic interconnections should be taken into account.

Electricity is transported through each linear wire of a homogeneous section of a double-circuit power transmission line by six incident waves of the electromagnetic field and six reflected waves [1]. This fact is confirmed by the equations of distribution of phase voltage and linear current [5]. For a line wire, they have the following form:

$$\dot{U}_{A'} = \frac{1}{6}\sum_{i=1}^{6}\left(A_{A'(2i-1)}e^{\gamma_i l} + A_{A'2i}e^{-\gamma_i l}\right), \tag{1}$$

$$\dot{I}_{A'} = \frac{1}{6}\left[\sum_{i=1}^{6}\left(\frac{A_{A'2i}e^{-\gamma_i l}}{\underline{Z}_{cA'i}} - \frac{A_{A'(2i-1)}e^{\gamma_i l}}{\underline{Z}_{cA'i}} + \frac{A_{B'2i}e^{-\gamma_i l}}{\underline{Z}_{cA'B'i}} - \frac{A_{B'(2i-1)}e^{\gamma_i l}}{\underline{Z}_{cA'B'i}} + \frac{A_{C'2i}e^{-\gamma_i l}}{\underline{Z}_{cC'A'i}} - \frac{A_{C'(2i-1)}e^{\gamma_i l}}{\underline{Z}_{cC'A'i}} + \right.\right.$$

$$\left.\left. + \frac{A_{A''2i}e^{-\gamma_i l}}{\underline{Z}_{cA'A''i}} - \frac{A_{A''(2i-1)}e^{\gamma_i l}}{\underline{Z}_{cA'A''i}} + \frac{A_{B''2i}e^{-\gamma_i l}}{\underline{Z}_{cA'B''i}} - \frac{A_{B''(2i-1)}e^{\gamma_i l}}{\underline{Z}_{cA'B''i}} + \frac{A_{C''2i}e^{-\gamma_i l}}{\underline{Z}_{cC''A'i}} - \frac{A_{C''(2i-1)}e^{\gamma_i l}}{\underline{Z}_{cC''A'i}}\right)\right], \tag{2}$$

where $A_{A'2i}$ and $A_{A'(2i-1)}$, $A_{B'2i}$ and $A_{B'(2i-1)}$, $A_{C'2i}$ and $A_{C'(2i-1)}$, $A_{A''2i}$ and $A_{A''(2i-1)}$, $A_{B''2i}$ and $A_{B''(2i-1)}$, $A_{C''2i}$ and $A_{C''(2i-1)}$ are the integration constants for the *i-th* pair of electromagnetic field waves; γ_i is the propagation constant for the same pair of electromagnetic field waves; $\underline{Z}_{cA'i}$, $\underline{Z}_{cB'i}$, $\underline{Z}_{cC'i}$, $\underline{Z}_{cA''i}$, $\underline{Z}_{cB''i}$, $\underline{Z}_{cC''i}$ are the self-wave impedances; $\underline{Z}_{cA'B'i}$, $\underline{Z}_{cC'A'i}$, $\underline{Z}_{cA'A''i}$, $\underline{Z}_{cA'B''i}$, $\underline{Z}_{cC''A'i}$, $\underline{Z}_{cB'C'i}$, $\underline{Z}_{cB'A''i}$, $\underline{Z}_{cB'B''i}$, $\underline{Z}_{cB'C''i}$, $\underline{Z}_{cC'A''i}$, $\underline{Z}_{cA''B''i}$, $\underline{Z}_{cC''A''i}$ are the mutual wave impedances.

The distribution of phase voltages and linear currents in other linear wires is described in a similar way.

Equations (1) and (2) indicate the presence of a double-circuit design of six incident and six reflected waves of an electromagnetic field in each linear wire of a power transmission line. Moreover, one incident and one reflected waves of them can be considered as normal waves of the considered linear wire. The remaining ten waves in this case should be considered as induced from neighboring linear wires. All this is considered in the distribution scheme of the electromagnetic field wave amplitudes along the linear wire of a homogeneous section of a double-circuit power transmission line, shown in Fig. 1. The following notation is used in the scheme: *1* and *2* are the normal incident and reflected waves of the electromagnetic field; *3, 5, 7, 9,* and *11* are the incident waves of electromagnetic field induced from neighboring wires; *4, 6, 8, 10* and *12* are the reflected waves of the electromagnetic field induced from adjacent wires.

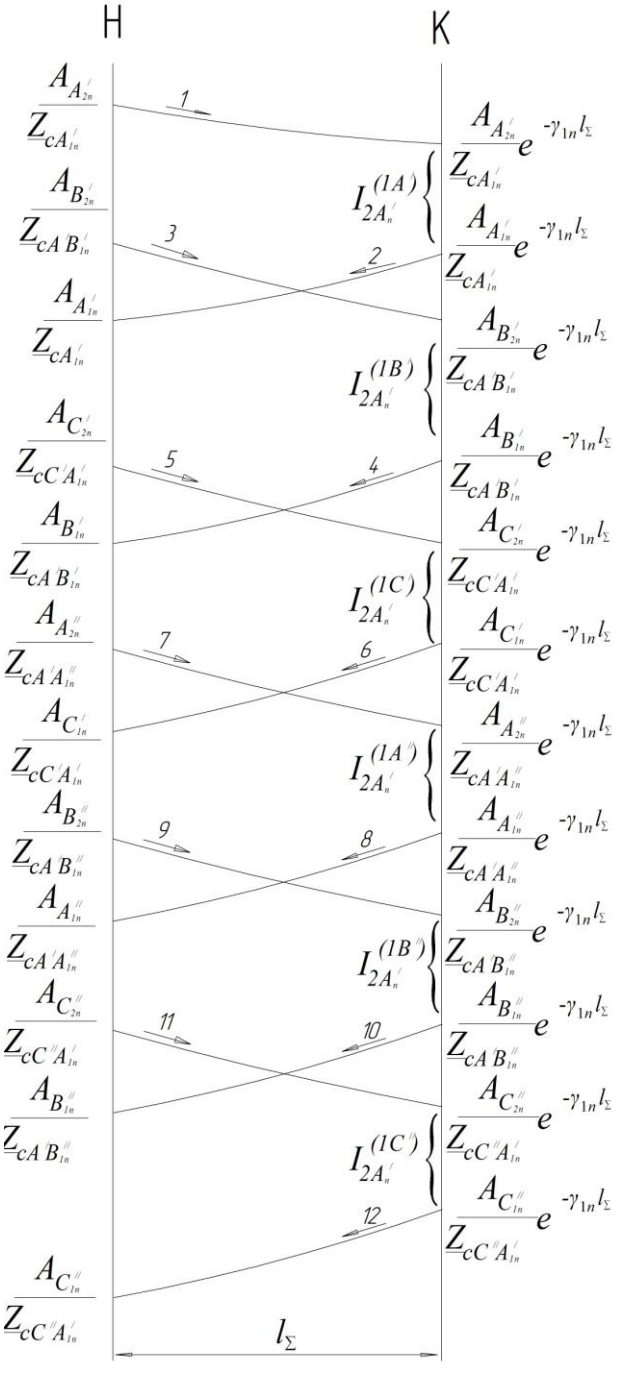

Fig. 1. The distribution scheme of the electromagnetic field wave amplitudes along the linear wire of a homogeneous section of a double-circuit power transmission line

In the distribution scheme of the electromagnetic field wave amplitudes the currents $\dot{I}_{2A'}^{(1A')}$, $\dot{I}_{2A'}^{(1B')}$, $\dot{I}_{2A'}^{(1C')}$, $\dot{I}_{2A'}^{(1A'')}$, $\dot{I}_{2A'}^{(1B'')}$, $\dot{I}_{2A'}^{(1C'')}$ illustrate part of the electrical energy entering the load.

Integration constants illustrate the amplitudes of the waves of the electromagnetic field. Odd integration constants $A_{A'1} - A_{A'11}$, $A_{B'1} - A_{B'11}$, $A_{C'1} - A_{C'11}$, $A_{A''1} - A_{A''11}$, $A_{B''1} - A_{B''11}$, $A_{C''1} - A_{C''11}$ illustrate the reflected waves, and even integration constants $A_{A'2} - A_{A'12}$, $A_{B'2} - A_{B'12}$, $A_{C'2} - A_{C'12}$, $A_{A''2} - A_{A''12}$, $A_{B''2} - A_{B''12}$, $A_{C''2} - A_{C''12}$ – illustrate the incident waves. The integration constants illustrating the incident waves of electromagnetic field exceed the values of integration constants illustrating the reflected waves.

The implementation of equations (1) and (2) allows us to predict currents and voltages at any point in a double-circuit PTL. For this, one should know reliable information about the primary and secondary parameters of power lines and voltages and currents at the end of the analyzed power lines.

Parameters of the equivalent circuit of power line are usually taken as primary parameters, and self and mutual wave resistances, attenuation coefficients, phase coefficients, etc are usually taken as the secondary parameters. Secondary parameters can be calculated if there is reliable data on the primary parameters. Such information can be taken from the reference literature[2]., but it is not exact.

Gerasimova VG, et al. Production, transmission and distribution of electrical energy. Under total ed. professors of MEI VG , 9nd ed., Sr. Moscow: Publishing House MEI, 2004.

More accurate information can be obtained as a result of appropriate calculations [6 - 13]. But it is a cumbersome procedure, requiring consideration of many factors affecting the amount of the transported electrical energy. The primary parameters of PTL can be determined experimentally [14, 15]. But such an operation also requires implementation of a number of organizational and technical measures. But the obtained information will be reliable. Self-wave impedances illustrate the influence of the intrinsic parameters of a linear wire on the transmission of electrical energy. Mutual wave impedances illustrate the influence of electromagnetic links between the current-conducting parts of power lines on the same process of electrical energy transmission.

Self- and mutual wave impedances are calculated by the formulas:

$$\left.\begin{aligned} &\underline{Z}_{cA'i}=\frac{\Delta}{\gamma_i\Delta_{1A'}};\ \underline{Z}_{cA'B'i}=\frac{\Delta}{\gamma_i\Delta_{2A'}};\ \underline{Z}_{cC'A'i}=\frac{\Delta}{\gamma_i\Delta_{3A'}};\\ &\underline{Z}_{cA'A''i}=\frac{\Delta}{\gamma_i\Delta_{4A'}};\ \underline{Z}_{cA'B''i}=\frac{\Delta}{\gamma_i\Delta_{5A'}};\ \underline{Z}_{cC''A'i}=\frac{\Delta}{\gamma_i\Delta_{6A'}}, \end{aligned}\right\} \tag{3}$$

where Δ, $\Delta_{1A'}$, $\Delta_{2A'}$, $\Delta_{3A'}$, $\Delta_{4A'}$, $\Delta_{5A'}$, $\Delta_{6A'}$ are the determinants of the system of equations that make up the mathematical model of distribution of electrical energy over a homogeneous section of a double-circuit power line [4].

The following equality confirms that the current at the end of the linear wire A' is derived from six pairs of waves of the electromagnetic field:

$$\dot{I}_{2A'}=\frac{1}{6}\left(\dot{I}_{2A'}^{(1)}+\dot{I}_{2A'}^{(2)}+\dot{I}_{2A'}^{(3)}+\dot{I}_{2A'}^{(4)}+\dot{I}_{2A'}^{(5)}+\dot{I}_{2A'}^{(6)}\right), \tag{4}$$

where $\dot{I}_{2A'}^{(1)}$, $\dot{I}_{2A'}^{(2)}$, $\dot{I}_{2A'}^{(3)}$, $\dot{I}_{2A'}^{(4)}$, $\dot{I}_{2A'}^{(5)}$ and $\dot{I}_{2A'}^{(6)}$ are the current shares at the end of a linear wire A' from each pair of waves of electromagnetic field. The equation for the first current component in expression (4) is the following:

$$\dot{I}_{2A'}^{(1)}=\dot{I}_{2A'}^{(1A')}+\dot{I}_{2A'}^{(1B')}+\dot{I}_{2A'}^{(1C')}+\dot{I}_{2A'}^{(1A'')}+\dot{I}_{2A'}^{(1B'')}+\dot{I}_{2A'}^{(1C'')}, \tag{5}$$

where $\dot{I}_{2A'}^{(1A')}$ is the self-current at the end of the linear wire A' from the first pair of waves of electromagnetic field; $\dot{I}_{2A'}^{(1B')}$, $\dot{I}_{2A'}^{(1C')}$, $\dot{I}_{2A'}^{(1A'')}$, $\dot{I}_{2A'}^{(1B'')}$, $\dot{I}_{2A'}^{(1C'')}$ are the currents at the end of the linear wire A', induced from neighboring wires from the first pair of electromagnetic field waves. For the remaining components of current in expression (4), the current shares will be found in a similar way.

By substituting equation (5) into equation (4) we obtain:

$$\begin{aligned} \dot{I}_{2A'}=\frac{1}{6}\Big(&\dot{I}_{2A'}^{(1A')}+\dot{I}_{2A'}^{(1B')}+\dot{I}_{2A'}^{(1C')}+\dot{I}_{2A'}^{(1A'')}+\dot{I}_{2A'}^{(1B'')}+\dot{I}_{2A'}^{(1C'')}+\\ &+\dot{I}_{2A'}^{(2A')}+\dot{I}_{2A'}^{(2B')}+\dot{I}_{2A'}^{(2C')}+\dot{I}_{2A'}^{(2A'')}+\dot{I}_{2A'}^{(2B'')}+\dot{I}_{2A'}^{(2C'')}+\\ &+\dot{I}_{2A'}^{(3A')}+\dot{I}_{2A'}^{(3B')}+\dot{I}_{2A'}^{(3C')}+\dot{I}_{2A'}^{(3A'')}+\dot{I}_{2A'}^{(3B'')}+\dot{I}_{2A'}^{(3C'')}+\\ &+\dot{I}_{2A'}^{(4A')}+\dot{I}_{2A'}^{(4B')}+\dot{I}_{2A'}^{(4C')}+\dot{I}_{2A'}^{(4A'')}+\dot{I}_{2A'}^{(4B'')}+\dot{I}_{2A'}^{(4C'')}+\\ &+\dot{I}_{2A'}^{(5A')}+\dot{I}_{2A'}^{(5B')}+\dot{I}_{2A'}^{(5C')}+\dot{I}_{2A'}^{(5A'')}+\dot{I}_{2A'}^{(5B'')}+\dot{I}_{2A'}^{(5C'')}+\\ &+\dot{I}_{2A'}^{(6A')}+\dot{I}_{2A'}^{(6B')}+\dot{I}_{2A'}^{(6C')}+\dot{I}_{2A'}^{(6A'')}+\dot{I}_{2A'}^{(6B'')}+\dot{I}_{2A'}^{(6C'')}\Big), \end{aligned} \tag{6}$$

The distribution scheme of the electromagnetic field wave amplitudes (Fig. 1) shows that for the end of the linear wire A' the following relation will be valid, which is found as the ratio of the integration constants to the wave impedance:

$$\dot{I}_{2A'}^{(1A')}=\frac{A_{A'2}}{\underline{Z}_{cA'1}}e^{-\gamma_1 l_\Sigma}-\frac{A_{A'1}}{\underline{Z}_{cA'1}}e^{\gamma_1 l_\Sigma}; \tag{7}$$

To simplify the subsequent presentation, we perform a replacement using the symbol B:

$$B_{A'1} = A_{A'1}e^{\gamma_1 l_\Sigma};\ B_{A'2} = A_{A'2}e^{-\gamma_1 l_\Sigma}, \tag{8}$$

The remaining integration constants are reduced to equations of the form (8).

By substitution of equation (8) into expression (7), we obtain:

$$\dot{I}_{2A'}^{(1A')} = \frac{B_{A'2}}{\underline{Z}_{cA'1}} - \frac{B_{A'1}}{\underline{Z}_{cA'1}}.$$

Thus, the integration constants from the end of a double-circuit power transmission line are defined as the sum of the product of the current and wave impedance and the integration constant:

$$B_{A'2} = \dot{I}_{2A'}^{(1A')}\underline{Z}_{cA'1} + B_{A'1}.$$

This equality establishes a quantitative relationship between the integration constants at the beginning and at the end of a double-circuit power transmission line. To calculate the integration constants, it is necessary to know the numerical values of almost all components of the output current. To find them, one can use the fact that each component of current is inversely proportional to the corresponding wave resistance. In this case, taking into account formulas (3), the following equality is true:

$$\left.\begin{gathered}\frac{\dot{I}_{2A'}^{(1A')}}{\dot{I}_{2A'}^{(2A')}} = \frac{\underline{Z}_{cA'2}}{\underline{Z}_{cA'1}} = \frac{\gamma_1}{\gamma_2};\ \frac{\dot{I}_{2A'}^{(1A')}}{\dot{I}_{2A'}^{(3A')}} = \frac{\underline{Z}_{cA'3}}{\underline{Z}_{cA'1}} = \frac{\gamma_1}{\gamma_3};\ \frac{\dot{I}_{2A'}^{(1A')}}{\dot{I}_{2A'}^{(4A')}} = \frac{\underline{Z}_{cA'4}}{\underline{Z}_{cA'1}} = \frac{\gamma_1}{\gamma_4};\\ \frac{\dot{I}_{2A'}^{(1A')}}{\dot{I}_{2A'}^{(5A')}} = \frac{\underline{Z}_{cA'5}}{\underline{Z}_{cA'1}} = \frac{\gamma_1}{\gamma_5};\ \frac{\dot{I}_{2A'}^{(1A')}}{\dot{I}_{2A'}^{(6A')}} = \frac{\underline{Z}_{cA'6}}{\underline{Z}_{cA'1}} = \frac{\gamma_1}{\gamma_6}.\end{gathered}\right\} \tag{9}$$

The derived equations (9) allow us to express all currents through the current $\dot{I}_{2A}^{(1A')}$:

$$\dot{I}_{2A'}^{(2A')} = \frac{\gamma_2}{\gamma_1}\dot{I}_{2A'}^{(1A')};\ \dot{I}_{2A'}^{(3A')} = \frac{\gamma_3}{\gamma_1}\dot{I}_{2A'}^{(1A')};\ \dot{I}_{2A'}^{(4A')} = \frac{\gamma_4}{\gamma_1}\dot{I}_{2A'}^{(1A')};\ \dot{I}_{2A'}^{(5A')} = \frac{\gamma_5}{\gamma_1}\dot{I}_{2A'}^{(1A')};\ \dot{I}_{2A'}^{(6A')} = \frac{\gamma_6}{\gamma_1}\dot{I}_{2A'}^{(1A')}. \tag{10}$$

By substitution expression (10) into equations (6), we obtain an equation in one unknown. In this case unknown is the current $\dot{I}_{2A'}^{(1A')}$. Solution of this equation makes it possible to determine the formula for calculating this current:

$$\dot{I}_{2A'}^{(1A')} = \frac{6\dot{I}_{2A'}\gamma_1\Delta_{1A'} + 0}{(\gamma_1+\gamma_2+\gamma_3+\gamma_4+\gamma_5+\gamma_6)(\Delta_{1A'}+\Delta_{2A'}+\Delta_{3A'}+\Delta_{4A'}+\Delta_{5A'}+\Delta_{6A'})}. \tag{11}$$

Voltage at the end of the line wire A', taking into account equalities (8), can be rewritten as follows:

$$\begin{gathered}6\dot{U}_{1A'} = 2B_{A'1} + 2B_{A'3} + 2B_{A'5} + 2B_{A'7} + 2B_{A'9} + 2B_{A'11} + \\ + \frac{6\dot{I}_{2A'}\Delta_{1A'}(\gamma_1\underline{Z}_{cA'1} + \gamma_2\underline{Z}_{cA'2} + \gamma_3\underline{Z}_{cA'3} + \gamma_4\underline{Z}_{cA'4} + \gamma_5\underline{Z}_{cA'5} + \gamma_6\underline{Z}_{cA'6})}{(\gamma_1+\gamma_2+\gamma_3+\gamma_4+\gamma_5+\gamma_6)(\Delta_{1A'}+\Delta_{2A'}+\Delta_{3A'}+\Delta_{4A'}+\Delta_{5A'}+\Delta_{6A'})} = \\ = 2B_{A'1} + 2B_{A'3} + 2B_{A'5} + 2B_{A'7} + 2B_{A'9} + 2B_{A'11} + a.\end{gathered} \tag{12}$$

The initial task was to obtain integration constants, which make it possible to determine voltage and current anywhere in the double-circuit power transmission line. There are six of them in equation (12). To calculate them, one needs another 5 (five) equations. They can be obtained using the derivatives of equation (1) with respect to variable *l*.

The second derivative of equation (1) with respect to variable *l* for the end of the linear wire A' taking into account expression (12) takes the form:

$$\begin{gathered}\frac{d^2\dot{U}_{2A'}}{dl^2} = \frac{1}{6}\Big[2\gamma_1^2B_{A'1} + 2\gamma_2^2B_{A'3} + 2\gamma_3^2B_{A'5} + 2\gamma_{4n}^2B_{A'7} + 2\gamma_5^2B_{A'9} + \\ + 2\gamma_6^2B_{A'11} + \frac{6\dot{I}_{2A'}\Delta_{1A'}(\gamma_1^3\underline{Z}_{cA'1} + \gamma_2^3\underline{Z}_{cA'2} + \gamma_3^3\underline{Z}_{cA'3} + \gamma_4^3\underline{Z}_{cA'4} + }{(\gamma_1+\gamma_2+\gamma_3+\gamma_4+\gamma_5+\gamma_6)(\Delta_{1A'}+\Delta_{2A'}+\Delta_{3A'}+\Delta_{4A'}+ \rightarrow\end{gathered}$$

$$\rightarrow \frac{+\gamma_5^3 \underline{Z}_{cA'5} + \gamma_6^3 \underline{Z}_{cA'6})}{+\Delta_{5A'} + \Delta_{6A'})}\Big] = \frac{1}{6}\big(2\gamma_1^2 B_{A'1} + 2\gamma_2^2 B_{A'3} + 2\gamma_3^2 B_{A'5} +$$
$$+ 2\gamma_4^2 B_{A'7} + 2\gamma_5^2 B_{A'9} + 2\gamma_6^2 B_{A'11} + b\big). \quad (13)$$

When analyzing the results of transmission of electrical energy through power lines, it is necessary to solve differential equations of the second order. This solution is associated with the search for numerical values of the propagation constants. The second derivative of the phase voltage in a linear wire A' with respect to variable l can be determined through the primary parameters of a double-circuit power transmission line [4, 5]:

$$\frac{d^2\dot{U}_{2A'}}{dl^2} = \big[\underline{Z}_{0A'}\big(\underline{Y}_{0A'0} + \underline{Y}_{0A'B'} + \underline{Y}_{0A'A''} + \underline{Y}_{0A'B''} + \underline{Y}_{0C'A'} +$$
$$+ \underline{Y}_{0C''A'}\big) - \underline{Y}_{0A'B'}\underline{Z}_{0A'B'} - \underline{Y}_{0A'A''}\underline{Z}_{0A'A''} - \underline{Y}_{0C'A'}\underline{Z}_{0C'A'} - \underline{Y}_{0A'B''}Z_{0A'B''} -$$
$$- \underline{Y}_{0C''A'}\underline{Z}_{0C''A'n}\big]\dot{U}_{2A'} + \big[Z_{0A'B'}\big(\underline{Y}_{0B'0} + \underline{Y}_{0B'C'} + \underline{Y}_{0B'B''} + \underline{Y}_{0B'C''} +$$
$$+ \underline{Y}_{0B'A''} + \underline{Y}_{0A'B'}\big) - \underline{Y}_{0A'B'}\underline{Z}_{0A'} - \underline{Y}_{0B'C'}\underline{Z}_{0C'A'} - \underline{Y}_{0B'A''}\underline{Z}_{0A'A''} -$$
$$- \underline{Y}_{0B'B''}\underline{Z}_{0A'B''} - \underline{Y}_{0B'C''}\underline{Z}_{0C''A'}\big]\dot{U}_{2B'} + \big[\underline{Z}_{0C'A'}\big(\underline{Y}_{0C'0} + \underline{Y}_{0C'A''} +$$
$$+ \underline{Y}_{0C'A'} + \underline{Y}_{0C'C''} + \underline{Y}_{0B'C'} + \underline{Y}_{0B''C'}\big) - \underline{Y}_{0C'A'}\underline{Z}_{0A'} - \underline{Y}_{0B'C'}\underline{Z}_{0A'B'} -$$
$$- \underline{Y}_{0C'A''}\underline{Z}_{0A'A''} - \underline{Y}_{0B''C'}\underline{Z}_{0A'B''} - \underline{Y}_{0C'C''}\underline{Z}_{0C''A'}\big]\dot{U}_{2C'} +$$
$$+ \big[\underline{Z}_{0A'A''}\big(\underline{Y}_{0A''0} + \underline{Y}_{0A''B''} + \underline{Y}_{0A'A''} + \underline{Y}_{0C''A''} + \underline{Y}_{0B'A''} + \underline{Y}_{0C'A''}\big) -$$
$$- \underline{Y}_{0A''B''}\underline{Z}_{0A'B''} - \underline{Y}_{0C''A''n}\underline{Z}_{0C''A'} - \underline{Y}_{0A'A''}\underline{Z}_{0A'} - \underline{Y}_{0B'A''}\underline{Z}_{0A'B'} -$$
$$- \underline{Y}_{0C'A''}\underline{Z}_{0C'A'}\big]\dot{U}_{2A''} + \big[\underline{Z}_{0A'B''}\big(\underline{Y}_{0B''C''} + \underline{Y}_{0B''0} + \underline{Y}_{0B''C'} +$$
$$+ \underline{Y}_{0A'B''} + \underline{Y}_{0B'B''} + \underline{Y}_{0A''B''}\big) - \underline{Y}_{0B''C''}\underline{Z}_{0C''A'} - \underline{Y}_{0A'B''}\underline{Z}_{0A'} -$$
$$- \underline{Y}_{0B'B''}\underline{Z}_{0A'B'} - \underline{Y}_{0B''C'}\underline{Z}_{0C'A'} - \underline{Y}_{0A''B''}\underline{Z}_{0A'A''}\big]\dot{U}_{2B''} +$$
$$+ \big[\underline{Z}_{0C''A'}\big(\underline{Y}_{0C''0} + \underline{Y}_{0C''A'} + \mathrm{Y}_{0C''A''} + \mathrm{Y}_{0B'C''} + \mathrm{Y}_{0C'C''} +$$
$$+ \mathrm{Y}_{0B''C''}\big) - \mathrm{Y}_{0C''A'}Z_{0A'} - \mathrm{Y}_{0B'C''}Z_{0A'B'} - \underline{Y}_{0C'C''}\underline{Z}_{0C'A'} -$$
$$- \underline{Y}_{0C''A''}\underline{Z}_{0A'A''} - \underline{Y}_{0B''C''}\underline{Z}_{0A'B''}\big]\dot{U}_{2C''} =$$
$$= b_1\dot{U}_{2A'} + b_2\dot{U}_{2B'} + b_3\dot{U}_{2C'} + b_4\dot{U}_{2A''} + b_5\dot{U}_{2B''} + b_6\dot{U}_{2C''}.$$

For the end of the line wire A', this equation can be rewritten as follows:

$$\frac{d^2\dot{U}_{2A'}}{dl^2} = b_1\dot{U}_{2A'} + b_2\dot{U}_{2B'} + b_3\dot{U}_{2C'} + b_4\dot{U}_{2A''} + b_5\dot{U}_{2B''} +$$
$$+ b_6\dot{U}_{2C''} = b_0. \quad (14)$$

When combining equation (14) with equation (13), the following expression is obtained:

$$6b_0 - b = 2\gamma_1^2 B_{A'1} + 2\gamma_2^2 B_{A'3} + 2\gamma_3^2 B_{A'5} + 2\gamma_4^2 B_{A'7} +$$
$$+ 2\gamma_5^2 B_{A'9} + 2\gamma_6^2 B_{A'11}. \quad (15)$$

The fourth derivative of equation (1) with respect to variable l for the beginning of a linear wire taking into account equalities (8) takes the form:

$$\frac{d^4\dot{U}_{2A'}}{dl^4} = \frac{1}{6}\big(2\gamma_1^4 B_{A'1} + 2\gamma_{2n}^4 B_{A'3} + 2\gamma_3^4 B_{A'5} + 2\gamma_4^4 B_{A'7} +$$
$$+ 2\gamma_5^4 B_{A'9} + 2\gamma_6^4 B_{A'11} + c\big). \quad (16)$$

The fourth derivative of voltage at the end of the linear wire with respect to variable l can be represented as follows:

$$\frac{d^4\dot{U}_{2A'}}{dl^4} = c_1\dot{U}_{2A'} + c_2\dot{U}_{2B'} + c_3\dot{U}_{2C'} + c_4\dot{U}_{2A''} + c_5\dot{U}_{2B''} + c_6\dot{U}_{2C''} = c_0. \quad (17)$$

By combining expression (17) with equation (16) we obtain:

$$6c_0 - c = 2\gamma_1^4 B_{A'1} + 2\gamma_2^4 B_{A'3} + 2\gamma_3^4 B_{A'5} + 2\gamma_4^4 B_{A'7} + 2\gamma_5^4 B_{A'9} + 2\gamma_6^4 B_{A'11}. \quad (18)$$

The sixth derivative of equation (1) with respect to variable *l* for the beginning of a linear wire, taking into account equalities (8), will take the form:

$$\frac{d^6 \dot{U}_{2A'}}{dl^6} = \frac{1}{6}\left(2\gamma_1^6 B_{A'1} + 2\gamma_2^6 B_{A'3} + 2\gamma_3^6 B_{A'5} + 2\gamma_4^6 B_{A'7} + 2\gamma_5^6 B_{A'9} + 2\gamma_6^6 B_{A'11} + d\right). \quad (19)$$

The sixth derivative of voltage at the end of the linear wire A' with respect to variable *l* can be also written as follows:

$$\frac{d^6 \dot{U}_{2A'}}{dl^6} = d_1 \dot{U}_{2A'} + d_2 \dot{U}_{2B'} + d_3 \dot{U}_{2C'} + d_4 \dot{U}_{2A''} + d_5 \dot{U}_{2B''} + d_6 \dot{U}_{2C''} = d_0. \quad (20)$$

The combination of equation (20) with equation (19) gives the following expression:

$$6d_0 - d = 2\gamma_1^6 B_{A'1} + 2\gamma_2^6 B_{A'3} + 2\gamma_3^6 B_{A'5} + 2\gamma_4^6 B_{A'7} + 2\gamma_5^6 B_{A'9} + 2\gamma_6^6 B_{A'11}. \quad (21)$$

The eighth derivative of equation (1) with respect to variable *l* for the beginning of a linear wire A', taking into account equalities (8), takes the form:

$$\frac{d^8 \dot{U}_{2A'}}{dl^8} = \frac{1}{6}\left(2\gamma_1^8 B_{A'1} + 2\gamma_2^8 B_{A'3} + 2\gamma_3^8 B_{A'5} + 2\gamma_4^8 B_{A'7} + 2\gamma_5^8 A B_{A'9} + 2\gamma_6^8 B_{A'11} + f\right). \quad (22)$$

The eighth derivative of voltage at the end of the linear wire A' with respect to variable *l* can be written as follows:

$$\frac{d^8 \dot{U}_{2A'}}{dl^8} = f_1 \dot{U}_{2A'} + f_2 \dot{U}_{2B'} + f_3 \dot{U}_{2C'} + f_4 \dot{U}_{2A''} + f_5 \dot{U}_{2B''} + f_6 \dot{U}_{2C''} = f_0. \quad (23)$$

Equation (23) together with equation (22) form the following expression:

$$6f_0 - f = 2\gamma_1^8 B_{A'1} + 2\gamma_2^8 B_{A'3} + 2\gamma_3^8 B_{A'5} + 2\gamma_4^8 B_{A'7} + 2\gamma_5^8 B_{A'9} + 2\gamma_6^8 B_{A'11}. \quad (24)$$

The tenth derivative of equation (1) with respect to variable *l* for the beginning of a linear wire A', taking into account equalities (8), will take the following form:

$$\frac{d^{10} \dot{U}_{2A'}}{dl^{10}} = \frac{1}{6}\left(2\gamma_1^{10} B_{A'1} + 2\gamma_2^{10} B_{A'3} + 2\gamma_3^{10} B_{A'5} + 2\gamma_4^{10} B_{A'7} + 2\gamma_5^{10} B_{A'9} + 2\gamma_6^{10} B_{A'11} + h\right). \quad (25)$$

So, the tenth derivative of voltage at the end of the linear wire A' with respect to variable *l* takes the form:

$$\frac{d^{10} \dot{U}_{2A'}}{dl^{10}} = h_1 \dot{U}_{2A'} + h_2 \dot{U}_{2B'} + h_3 \dot{U}_{2C'} + h_4 \dot{U}_{2A''} + h_5 \dot{U}_{2B''} + h_6 \dot{U}_{2C''} = h_0. \quad (26)$$

By combining equation (26) with equation (25) we get the following:

$$6h_0 - h = 2\gamma_1^{10} B_{A'1} + 2\gamma_2^{10} B_{A'3} + 2\gamma_3^{10} B_{A'5} + 2\gamma_4^{10} B_{A'7} + 2\gamma_5^{10} B_{A'9} + 2\gamma_6^{10} B_{A'11}. \quad (27)$$

The joint solution of equations (12), (15), (18), (21), (24) and (27) will allow us to form equalities for calculating the odd integration constants from $A_{A'1}$ to $A_{A'11}$. The even constants of integration from $A_{A'2}$ to $A_{A'12}$ are calculated by formulas (8).

In a similar way, the remaining integration constants for each linear wire of a double-circuit power transmission line are determined. This can be carried out under the condition of availability of reliable information about the numerical values of the primary parameters of a homogeneous section of a three-phase power transmission line of double-circuit design and output voltages and currents at the frequency of each harmonic component.

Results

A method has been developed for determining the numerical values of integration constants at known output phase voltages and linear currents. The integration constants calculated in this way will provide insight into the propagation of electromagnetic field waves in the linear wires of power lines. In addition, the information obtained allows predicting the results of transmission of electrical energy through a double-circuit power transmission line.

Conclusion

The result of this study can be applied in engineering practice at the stage of design, reconstruction and operation of double-circuit power transmission lines. Calculation of the integration constants, currents and voltages, and the operational parameters as a whole, will make it possible to predict the result of electrical energy transmission along the homogeneous sections of a double-circuit power transmission line.

With a minor modification, the proposed methodology for calculating the integration constants, and therefore the design of electrical energy transmission results, can be extended to heterogeneous sections of power lines, and to the entire transmission line as a whole. It can serve as an example of the development of similar techniques for power lines of other versions.

References

1 Yakushev AYa. Analysis of electromagnetic processes in a homogeneous long line. *Electrical Engineering*. 2017; 10:23-28. (In Russ).

2. Vedernikov AC. Mathematical model of the electromagnetic field of a wire of a multi-circuit overhead transmission line in a steady state. *Bulletin of the Samara State Technical. University*. 2013; 4(36):150-154. (In Russ).

3. Fereira VH, et al. A servey on intelligent system transmission lines. *Electric Power System Research*. 2016; 136:135-153.

4. Plotnikov MP, Bolshanin GA Algorithm for constructing a mathematical model of a homogeneous section of a double-circuit transmission line under conditions of low quality electrical energy. *Electrotechnical complexes and control systems*. 2012; 4:34-40. (In Russ).

5. Plotnikov MP. Voltage distribution on a double-circuit power line. *Systems. Methods Technology*. 2012; 4(16):66-70. (In Russ).

6. Mühlbaer AA Features of the calculation of the induced voltage on the disconnected circuit of a double-circuit overhead power line. Scientific Bulletin of NSTU. 2016; 64(3):146-160.

7. Panova EA Specified electrical parameters of double-circuit transmission lines of 110 kV for remote determination of the location of damage. *Electrotechnical systems and complexes*. 2016; 4(33):35-40. (In Russ).

8. Panova EA Determination of specific electrical parameters of overhead power lines. *Electrical equipment, operation and repair*. 2014; 10:16-22. (In Russ).

9. Bulatnikov MV, Kadomskaya KP, Kandakov SA, et al. Determination of the primary longitudinal parameters of overhead and underground power lines based on the calculation of the electromagnetic field. *Electricity*. 2016; 5:17-24. (In Russ).

10. Heo J-YA simulator for calculating normalized voltage on communication line. J-Y Heo, H-C Seo,

Литература

1. Якушев А.Я., А.Г. Середа, М.Н. Василенко, П.Е. Булавский, В.Л. Белозеров. Анализ электромагнитных процессов в однородной длинной линии // Электротехника. 2017. №10. С. 23–28.

2. Ведерников А.С. Математическая модель электромагнитного поля провода многоцепной воздушной линии электропередачи в установившемся режиме. // Вестник Самарского государственного технического. университета.. 2013. №4(36). С. 150–154.

3 Fereira V.H. Zanghi R, Fortez M.Z., Sotelo G.G.,. Silva R.B.M,. Souza J.C.S, Guimarâes C.H.C., Gomes. S.Jr.. A servey on intelligent system transmission lines // Electric Power System Research. 2016. N136. pp. 135–153.

4. Плотников М.П. Алгоритм построения математической модели однородного участка двухцепной линии электропередачи в условиях пониженного качества электрической энергии. / М.П. Плотников, Г.А. Большанин // Электротехнические комплексы и системы управления. 2012. №4. С. 34–40.

5. Плотников М.П. Распределение напряжения по двухцепной линии электропередачи. / М.П. Плотников, Г.А. Большанин // Системы. Методы. Технологии. 2012. № 4 (16). С. 66–70.

6. Мюльбаер А.А. Особенности расчета наведенного напряжения на отключенной цепи двухцепной воздушной линии электропередачи // Научный вестник НГТУ. 2016. Т 64. №3. С. 146–160.

7. Панова Е.А. Уточненные удельные электрические параметры двухцепных ЛЭП 110 кВ для дистанционного определения места повреждения // Электротехнические системы и комплексы. 2016. №4 (33). С. 35–40.

8. Панова Е.А. Определение удельных электрических параметров воздушных линий электропередачи // Электрооборудование,

S-J Lee, YS Kim, C-H Kim. Journal of Electrical Engineering and Technology. 2014; 9(4);1394-1400.
11. Wang SV, W Hu, G Zou, Z Wu, S Li, Z Sun. Dianwang Jishu. 2014; 38(5):1162-1168.
12. Selivanov VN, Danilin AN, Zalesova OV, Kolobov VV. Study of the frequency characteristics of the mutual influence of overhead power line.. *Bulletin of MSTU*. 2016; 19(4):744-752. (In Russ).
13. Bolsanin GA, Bolshanin LYu. Parameters of three-wire power lines. The eight-pole method. Bratsk: BrGU Publishing House, 2013. pp 265. (In Russ).
14. Bolsanin GA. Transmission of electrical energy through power transmission lines of one-, two- and three-wire versions / GA Bolshanin. Bratsk: BrSU publishing house, 2016.pp 313. (In Russ).
15. Bolsanin GA, Bolsanina LYu. The method of determining the primary and generalized secondary parameters of a homogeneous section of a three-wire transmission line by the method of an eight-port network.; applicant and patent holder. Patent RUS №2522829. IPC G 01 R 27/02. №2013101260/28; 01.10.2013. Accessed: 20 Jul.2014. (In Russ).

эксплуатация и ремонт. 2014. №10. С. 16–22.
9. Булатников М.В., Кадомская К.П., Кандаков С.А., и др. Определение первичных продольных параметров воздушных и подземных линий электропередачи на основе расчета электромагнитного поля // Электричество. 2016. №5. С. 17–24.
10. Heo J.-Y. A simulator for calculating normal induced voltage on communication line // Journal of Electrical Engineering and Technology. 2014. Vol. 9, N4. pp. 1394–1400.
11. Wang S. Influece of neighboring transmission lines on the measurement transmission line UVN options at the operating frequeney // Dianwang Jishu. 2014. Vol. 38, N5. pp. 1162–1168.
12. Селиванов В.Н. Данилин А.Н,. Залесова О.В, Колобов В.В.. Исследование частотных характеристик взаимного влияния воздушных линий электропередачи // Вестник МГТУ. 2016. Т. 19. №4. С. 744–752.
13. Большанин Г.А. Параметры трехпроводной ЛЭП. Метод восьмиполюсника. Братск: Изд-во БрГУ, 2013. 265 с.
14. Большанин Г.А. Передача электрической энергии по ЛЭП одно-, двух- и трехпроводного исполнений. Братск: Изд-во БрГУ, 2016. 313 с.
15. Большанин Г.А, Большанина Л.Ю. Способ определения первичных и обобщенных вторичных параметров однородного участка трехпроводной линии электропередачи методом восьмиполюсника. Патент 2522829. Российская Федерация. МПК G 01 R 27/02. №2013101260/28; Ссылка активна на :20 июля 2014.

Authors of the publication

Georgy A. Bolshanin – Department of Electrical Power Engineering and Electrical Engineering, Bratsk State University.

Mikhail P. Plotnikov – Department of Electrical Power Engineering and Electrical Engineering, Bratsk State University.

Received ***November 6 2018.***

UDC 658.264 DOI:10.30724/1998-9903-2019-21-3-73-85

MATHEMATICAL MODELING OF THE FORECAST AND STANDBY HEATING MODES

V.A. Tarasov [1], V.V. Tarasova [2], V.V. Afanasyev [1], V.G. Kovalev [1], V.N. Orlov[1]

[1]Chuvash State University, Cheboksary, Russia
[2]LLC Engineering and Technical Center GORISS, Cheboksary, Russia

Abstract*: The aim of the work is the development and study of methods for reducing the cost of heat energy for heating buildings and constructions by means of usage of automated control systems based on a programmable logic controller.* ***Methods****: In contrast to the known methods, the proposed mathematical model of non-stationary processes in heat-intensive enclosures makes it possible, according to the adaptive control algorithm, to perform forecast and standby heating taking into account the time dependence of the outdoor air temperature.* ***Results:*** *The algorithm ensures the equality of the heating system power and the heat losses power, allows one to maintain the desired indoor air temperature in the room when the outdoor air temperature changes. The heat loss compensation mode is achieved without using the temperature chart parameters of the network water and the parameters of proportional-integral-differential control laws that are necessary to set up at common automatic heating control systems. When calculating the forecast and standby heating modes, the mathematical model allows, at given initial and final temperatures of the internal air, determining the heating system power, which provide the desired temperature at the end of a specified period of time. The adaptive control algorithm allows setting the calculated outdoor temperature and the desired internal air temperature at any time. Under the forecast control, the mathematical model allows determining the system power at which the internal air temperature will remain almost constant when the outdoor air temperature changes.* ***Conclusions:*** *The developed algorithm of adaptive control allows one to create an energy-efficient heating system that provides the desired room temperature with minimum consumption of thermal energy taking into account all parameters affecting the heat loss power and the heating system power.*

Keywords: mathematical model, power of the heating system, forecast temperature, outside air, forecast control, standby heating, adaptive control algorithm, programmable logic controller.

For citation: Tarasov VA, Tarasova VV, Afanasyev VV, Kovalev VG, Orlov VN. Mathematical modeling of the forecast and standby heating modes. *Power engineering: research, equipment, technology*. 2019; 21(3):73-85. (In Russ). doi:10.30724/1998-9903-2019-21-3-73-85.

МАТЕМАТИЧЕСКОЕ МОДЕЛИРОВАНИЕ РЕЖИМОВ ПРОГНОЗНОГО И ДЕЖУРНОГО ОТОПЛЕНИЯ

В.А. Тарасов[1], **В.В. Тарасова**[2], **В.В. Афанасьев[1], В.Г. Ковалев[1], В.Н. Орлов[1]**

[1]Чувашский государственный университет им. И.Н.Ульянова, г.Чебоксары, Россия
[2]ООО «Инженерно-технический центр ГОРИСС», г.Чебоксары, Россия

Резюме. Цель: *Целью работы является разработка и исследование методов снижения затрат тепловой энергии на отоплениезданий и сооружений за счет применения систем автоматизированного управления*

Методы: *Методом математического моделирования нестационарных тепловых процессов в системах отопленияозданаметодика расчета режимов прогнозного и дежурного отопления и алгоритмадаптивного управления системой отопления, который реализован на программируемом логическом контроллере. В отличие от известных методов предложенная математическая модель нестационарных процессов в теплоемких ограждениях позволяет осуществлять по алгоритму адаптивного управления прогнозное и дежурное отопление с учетом изменения во времени температуры наружного воздуха.*

Результаты*: Алгоритм обеспечивает равенство мощности системы отопления и мощности тепловых потерь, позволяетподдерживать заданную температуру внутреннего воздуха в помещении при изменениитемпературы наружного воздуха. Выход на режим компенсации тепловых потерь достигается без использования параметров температурного графика сетевой воды и параметров пропорционально-интегрально-дифференциальных законов регулирования, которые необходимы для настройки широко распространенных систем автоматического управления отоплением. При расчете режимов прогнозного и дежурного отопления математическая модель позволяет при заданных начальных и конечных температурах внутреннего воздуха определить значения мощности системы отопления, обеспечивающие желаемую температуру в конце заданного промежутка времени. Алгоритм адаптивного управления позволяет в любой момент времени задатьзначения расчетной температуры наружного воздуха и требуемой температуры внутреннего воздуха.При прогнозном управлении математическая модель позволяет определить значения мощности системы,при которых температура внутреннего воздуха будет оставаться практически постоянной при изменении температуры наружного воздуха.*

Выводы*: Разработанный алгоритм адаптивного управления позволяет создать энергоэффективную систему отопления, обеспечивающую при минимальном расходе тепловой энергии заданную температуру в помещениях здания с учетом всех параметров, влияющих на мощность тепловых потерь и мощность системы отопления.*

Ключевые слова: *математическая модель, мощностьсистемы отопления, прогнозная температура, наружный воздух,прогнозное отопление,дежурноеотопление, алгоритм адаптивного управления, программируемый логический контроллер*.

Introduction

In developed countries, the global energy crisis of the 70s of the 20th century accelerated the development and implementation of energy-saving technologies, contributed to a large-scale structural economy reorganization to reduce the share of energy-intensive industries by their transfer to developing countries. All of this taken over the past quarter of the 20th century led to a decrease in the energy intensity of economy in developed countries by 2–2.5 times. The policy of energy-saving and energy efficiency continues in the 21st century. According to the State report on the state of energy-saving and energy efficiency in the Russian Federation in 2017 (http://www. economy. gov.ru) over the past ten years, the energy intensity of the economy of the advanced countries has decreased by 15–20%, while the previously adopted plans are being revised towards tightening. For example, by 2020 it is planned to reduce the economy energy intensity in the United States by 25% as compared to that in 2005, in the EU countries by 20% as compared to that in 2007, and in the P. R. China by 49% as compared to that in 2006. Therefore, the task of energy saving and improving energy efficiency for our country is very relevant.

Buildings and constructions are among the main consumers of heat energy, which account for up to 20% of the total balance of global energy consumption [1]. According to the Forecast of the scientific and technological development of the sectors of the fuel and energy complex of Russia for the period up to 2035 (https://www/minenergo.gov.ru) the centralized heat supply systems form the core of heat supply in Russia, the share of which in the total volume of heat energy production reaches 82% ($1.3 \cdot 10^9$ Gcal per year). The expert estimations show that the housing and utilities sector solely, excluding the budget sphere, accounts for about 20% of the total energy saving potential in the Russian Federation [2]. At the same time, in the public sector, about 82% of the total amount of operated buildings have a reduced, low and very low energy efficiency class, which indicates a significant potential for energy saving in this sector. One of the most efficient ways to reduce the consumption of thermal energy for heat supply is the automation of heating systems and the improvement of heat supply control algorithms [3,4,5].

In Russia, the regulation of the heat supply regime of the vast majority of buildings and constructions is carried out centrally from the heat source (boiler room, CHP) according to the temperature schedule of network water supply depending on the outdoor temperature. In this case, control is carried out depending on factors common to all buildings in the area of heat supply source. The group stage of regulation has a similar drawback, when management is carried out from factors common to fewer buildings [6,7,8,9].

Thus, centralized and group heating control systems do not take into account the individual static and dynamic heating characteristics of individual buildings, the effects of insolation and wind, do not enable efficient management of heat carrier parameters, and the organization of forecast and standby heating. Therefore, they often do not provide optimal temperature regime in the premises and result in irrational overspending of thermal energy, especially in autumn and spring. The technological capabilities of individual heat points (IHP) with automatic weather regulation are much higher, since they allow one to take into account almost all the factors affecting a single building. Therefore, the task of increasing the energy efficiency in the heat supply of buildings can be solved only by widespread introduction of IHP with automatic weather regulation [8, 10, 11, 12].

The aim of this work is to develop a mathematical model of the unsteady thermal regime of a building, which describes the dynamics of real processes occurring in buildings and constructions during the transition from one state to another, taking into account the actual specific heating characteristics of the enclosing structures, the thermal inertia of buildings, external disturbances in the form of outdoor temperature air changes [4.13]. The model is implemented in an adaptive heating system control algorithm for a programmable logic controller (PLC).

Materials and methods

The object of simulation is a centralized heat supply system of a typical four-story educational building D of Chuvash State University, consisting of a heating station, main supply and outlet pipes, stacks and connections to heating units, as well as shut-off and control valves. The housing is supplied with heat in accordance with the temperature schedule 130/70 °C. The IHP scheme includes forced pump circulation with coolant mixing from the return pipe [4,13]. The automatic weather control system includes: PLC-150 programmable logic controller, water temperature sensors in the supply line, at the inlet and outlet of the heating system, outdoor and indoor air temperature sensors, electromagnetic water flow converter, full pressure transmitters at the inlet and outlet of heat point, circulation pump that controls a two-way valve with an electric actuator. Signals from the sensors enter the control cabinet for further processing by the controller and its peripherals. The main thermo-technical characteristics of the case are: mass of heat-resistant enclosures M=1460 t; the average heat capacity of the heat-resistant enclosure material c=800 J/(kg·K); the generalized thermal characteristic of the building, determined by the statistical processing of data from an automated heat point [4], qV=2.843 kW/K; indoor heat transfer coefficient α_v = 7.8 W/(m^2·K), outdoor winter heat transfer coefficient α_n =23 W/(m^2·K); time constant: T =$1.728 \cdot 10^5$ s=48 hours.

Comfortable conditions in the premises with minimum consumption of heat energy for heating are achieved at the heat balance of the building or construction, when the heating system provides compensation for heat losses taking into account technological and domestic heat and insolation. To calculate the forecast and standby heating modes and the emergency response modes for heating, it is necessary to study the relationship between the temperatures of indoor and outdoor air and the power of the heating system during non-stationary processes.

In order to ensure a predetermined air temperature inside a heated room, the actual power of the heating system P_{heat} should compensate the calculated heat loss of the building P_{loss}, taking into account the technological and domestic heat energy input into the heated building, as well as insolation.

The calculated heat loss power depends on the thermal characteristics of the building and the temperatures of the indoor and outdoor air:

$$P_{\text{loss}} = qV(t_{\text{calc.in}} - t_{\text{calc.out}}), \quad (1)$$

where V is the external total structural volume of the building; q is the specific heating characteristic of the building, which should take into account the real thermophysical characteristics of the enclosures, the shape and orientation of the building, the infiltration and the wind impact. The product qV is a generalized thermal characteristic of the building.

The difference between the actual or desired temperature of the air inside the building and the continuously measured actual or set outdoor temperature $(t_{\text{calc.in}} - t_{\text{calc.out}})$ is the main disturbing factor for the heating system. The heating system power required to compensate heat loss depends on the temperatures of the direct and return water and the water flow in the heating system:

$$P_{\text{heat}} = G_2 \rho c(t_{\text{dir}} - t_{\text{ret}}) = P_{\text{loss}} - P_{\text{ext}}, \quad (2)$$

where G_2 is the volume water consumption in the building heating circuit; ρ is water density; c is the specific water heat capacity; $t_{\text{dir}}, t_{\text{ret}}$ are the temperatures of direct and return water in the building heating circuit; P_{ext} is the power of technological and domestic heat sources including insolation.

The most common method of heating system control is to control perturbation (according to the temperature of the outdoor air or using the temperature difference between the indoor and outdoor air). The control system may provide feedback using the temperature of coolant entering the building, or using the coolant temperature in the return pipe [3,5,6]. In this case, only coolant temperatures are usually used, through which, using a number of assumptions, the power of the heating system is determined by mathematical modeling. High-quality control by changing the temperatures of the direct and return water in accordance with the temperature schedule with a constant flow rate of water cannot fully compensate heat losses, since the influence of wind and insolation is not taken into account. The network water temperature at the heat source is determined by the air temperature for a certain period, taking into account the forecast and the available heat capacity of the source. Transport lag leads to a mismatch between the consumer network water temperature and the current outdoor temperature. In addition, the heat source often fails to comply with the temperature schedule of the network water, therefore widespread heating control algorithms that use only the temperature of the external and internal air, as well as the water temperature in the heating pipes and heating systems cannot provide timely and full compensation of heat losses. It should also be noted that for the implementation of well-known control algorithms for network water temperature, reference points of the heating system schedule and parameter values of proportional-integral and proportional-integral-differential laws of regulation are necessary.

The existence of water flow meters in modern heating centers allows one to determine the actual heating system power and to perform control not according to the temperature schedule, but directly by the power of the heating system, based on equality (2) using the adaptive control algorithm [4,13].

The algorithm for adaptive heat supply of buildings and construction, created on the basis of the automated heat point of building D, Chuvash State University, which takes into account weather, climatic and functional conditions, is implemented in the CODESYS environment on the PLC-150 programmable logic controller with registration and visualization of all measured and calculated values at an automatic operator workstation (AOW) [4]. The algorithm provides a quick access to the mode of compensation for heat loss without using the parameters of the network water temperature schedule and the parameters of proportional-integral and proportional-integral-differential laws of regulation [4,13].

To study the dynamics of thermal processes in heating systems, a model based on the heat balance of internal air and enclosures using quasistationary approximations can be applied [14]. The differential heat balance equation for the temperature of the internal air has the form [14] when written using the notation adopted in the theory of automatic control:

$$T_{\text{in\_air}} \frac{dt_{\text{in\_air}}}{d\tau} + t_{\text{in\_air}} = kP_{\text{heat}} + T_{\text{out\_air}} \frac{dt_{\text{out\_air}}}{d\tau} + t_{\text{out\_air}}, \qquad (3)$$

where $T_{\text{in\_air}}$ is the time constant for the indoor air temperature $t_{\text{in\_air}}$; $T_{\text{out\_air}}$ is the time constant for the outdoor air temperature $t_{\text{out\_air}}$; P_{heat} is the actual power of the heating system; $k = 1/qV$ is the coefficient for transmission via the channel “heating system power - indoor air temperature”.

The product of the building specific heating characteristic q and the external total structural volume of the building V is a generalized thermal characteristic qV that can be determined by statistical processing of metering nodes data [4]. The time constant $T_{\text{in\_air}}$ can be expressed in terms of mass of heat-resistant enclosures and the generalized thermal characteristic qV:

$$T_{\text{in\_air}} = \frac{cM}{2qV} U,$$

where c is the average specific heat of heat-resistant enclosures; U is the correction factor taking into account the difference in the values of heat transfer coefficients from the outer surface of the wall to the outside air α_{out_air} and from the inner air to the inner surface of the wall α_{in_air} [14]:

$$U = \frac{R_{\text{wall}} + 2R_{\text{out\_air}}}{R_{\text{in\_air}} + R_{\text{wall}} + R_{\text{out\_air}}},$$

where $R_{\text{wall}} = \delta / \lambda$ is the wall thermal resistance; $R_{\text{in\_air}} = 1/\alpha_{\text{in\_air}}$ is the resistance to heat transfer from internal air to the inner surface of the wall; $R_{\text{out\_air}} = 1/\alpha_{\text{out\_air}}$ is the resistance to heat transfer from the outer surface of the wall to the outside air

In stationary mode at heat loss compensation:

$$P_{\text{heat}} = P_{\text{loss}} = qV(t_{\text{calc.in}} - t_{\text{calc.out}})$$

In non-stationary modes, with forecast control and standby heating, the actual power of the heating system may differ from the heat loss power

$$P_{\text{heat}} = KP_{\text{loss}}.$$

Equation (3) is easily solved for the time-independent outdoor air temperature [14]. However, in reality, this temperature can vary significantly, which must be taken into account when calculating the forecast, standby and emergency control heating modes [15,16]. To simulate the cooling or warming processes, it was assumed that the outdoor temperature at the initial time τ =0 is equal to $t_{\text{out\_air0}}$, and then began to change in time according to the law

$$t_{\text{out\_air}} = B\tau^2 + t_{\text{out\_air0}},\ B = \frac{t_{\text{out\_air}k} - t_{\text{out\_air0}}}{\tau_k^2},$$

where $t_{\text{out\_air0}}$, $t_{\text{out\_air}k}$ are the outdoor temperatures at the beginning and end of the period τ_k. In addition, the outdoor air temperature change rate at the initial time is zero. In this case, B<0 for the predicted cooling, B>0 for the predicted warming and B=0 for the constant outdoor air temperature.

For this law of the outdoor temperature change in time, equation (3) has the form

$$T_{\text{in\_air}}\frac{dt_{\text{in\_air}}}{d\tau} + t_{\text{in\_air}} = kP_{\text{heat}} + 2T_{\text{out\_air}}B\tau + B\tau^2 + t_{\text{out\_air0}}. \quad (4)$$

The initial conditions for solving equation (4) are:

$$\tau = 0,\ t_{\text{in\_air}} = t_{\text{in\_air0}},\ t_{\text{out\_air}} = t_{\text{out\_air0}}. \quad (5)$$

The solution of equation (4) under the initial conditions (5) has the form

$$t_{\text{in\_air}}(\tau) = C\exp(-\frac{\tau}{T_{\text{in\_air}}}) + y(\tau),$$

where $C = t_{\text{in\_air0}} - 2BT_{\text{in\_air}}^2 + 2BT_{\text{in\_air}}T_{\text{out\_air}} - K(t_{\text{in\_air0}} - t_{\text{out\_air0}}) - t_{\text{out\_air0}}$;

$$y(\tau) = B\tau^2 - 2BT_{\text{in\_air}}\tau + 2BT_{\text{in\_air}}^2 + 2BT_{\text{out\_air}}\tau - 2BT_{\text{in\_air}}T_{\text{out\_air}} + K(t_{\text{in\_air0}} - t_{\text{out\_air0}}) + t_{\text{out\_air0}}. \quad (6)$$

In the particular case for the stationary mode with $B = 0$ and $K = 1$, the actual power of the heating system is equal to the heat loss power

$$P_{\text{heat}} - P_{\text{ext}} = P_{\text{loss}}.$$

If the actual power of the heating system is greater than the heat loss power, the temperature of the internal air will increase, if it is less, the temperature of the internal air will decrease. The internal air temperature change rate depends on the coefficient K. When the heating is turned off and $K = 0$, the mathematical model allows estimating the temperature cooling time inside the room taking into account changes in the temperature of the outdoor air.

During non-working hours (holidays, weekends and night time), the temperature of the indoor air can be reduced by decreasing the heating power to the standby heating mode in order to reduce heating costs. To ensure a decrease or an increase in air temperature from temperature $t_{\text{in\_air0}}$ to a predetermined level $t_{\text{in\_air}k}$ during time τ_k, the power of the heating system P_{heat} is determined from solution of the following equation with respect to the coefficient K

$$t_{\text{in\_air}k}(\tau_k) = C\exp(-\frac{\tau_k}{T_{\text{in\_air}}}) + y(K,\tau_k,t_{\text{in\_air0}},t_{\text{in\_air}k}). \quad (7)$$

Then, the calculated power of the heating system is determined as

$$P_{\text{heat}} = KP_n,$$

where P_n is the power at the beginning of the room temperature cooling or heating period.

Results

The proposed mathematical model makes it possible to determine the coefficient K for a given indoor air cooling or heating rate and the required power of the heating system during stand-by heating, taking into account the outdoor air temperature change in time. Tables 1 and 2 show the calculations results for changes in heating power and heat energy consumption during two days when switching to standby heating mode and vice versa, and also without switching to standby mode at a constant outdoor temperature $t_{out\_air} = -15$ °C (Table 1) and when changing outdoor temperature from $t_{out\_air} = -15$ °C to -17 °C (Table 2). It can be concluded that the specific value of thermal energy savings due to standby heating on non-working days substantially depends on the outdoor air temperature and for $t_{out\_air} = -15$ °C it is 11%. The calculation data show that when the heating is completely turned off and the outdoor temperature is -15 °C, the air in the room will cool down to 14.6 °C in 8 hours (Fig. 2*a*, curve 2). If the outdoor air temperature during this period decreases to -17 °C, then the indoor air will cool down to 12.6 °C (Fig. 2*a*, curve 3), and if the outdoor temperature rises to -13 °C, the indoor temperature will decrease for only 3.4 °C.

Table 1

Changes in the heating system power and the thermal energy consumption at a constant outdoor temperature $t_{out\_air} = -15$ °C

Mode	Time, hours	Heating system power, kW	Thermal energy consumption, kW·h
Cooling of indoor air to15 °C	8	6.91	55.28
Operation with reduced heat losses (standby heating)	28	85.3	2388
Extra-heating (increase in the internal air temperature to 20 °C)	12	149.65	1795
Total	48		4238.28
Operation without standby heating	48	99.5	4776
Thermal energy savings			537.72

Table 2

Changes in the heating system power and the thermal energy consumption when changing the outdoor temperature from $t_{out\_air} = -15$ °C to -17 °C (Fig.1)

Mode	Time, hours	Heating system power, kW	Thermal energy consumption, kW·h
Cooling of indoor air to15 °C	8	43.95	351.6
Operation with reduced heat losses (standby heating)	28	90.97	2547.16
Extra-heating (increase in the internal air temperature to 20 °C)	12	155.24	1862.88
Total	48		4761.64
Operation without standby heating	48	105.2	5049.6
Thermal energy savings			287.96

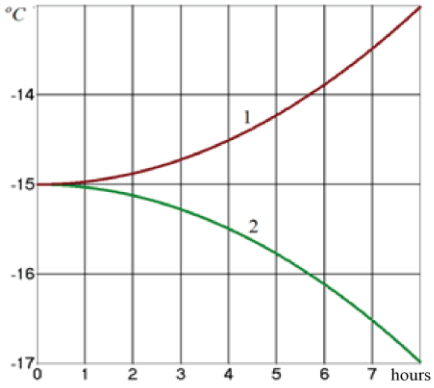

Fig. 1. Change in outdoor temperature over time:
1 - during warming; 2 - during cooling

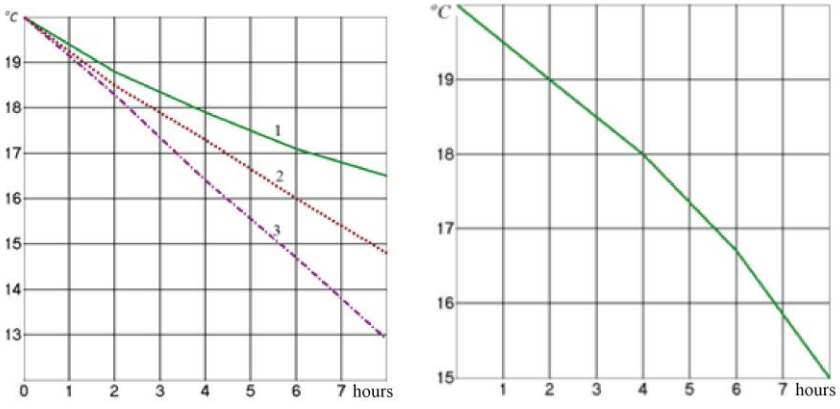

a) *b*)

Fig. 2. Changes in indoor temperature during 8 hours:
a) for a complete heating shutdown; b) for standby heating.

Curve *1* was obtained when outdoor air temperature increased from $t_{out\_air} = -15$ °C to -13 °C;

curve *2* is for $t_{out\_air} = -15$ °C; curve *3* was obtained when outdoor air temperature decreased from

$t_{out\_air} = -15$ °C to -17 °C

From experimental relationships between the indoor air temperature and time, obtained when the heating was completely turned off, time constants T can be determined [14,15,16]. Indoor air temperature maintenance at a given level should be ensured in a wide range of the outdoor air temperature changes due to a corresponding change in the temperature of direct network water according to the temperature schedule. It should be noted that the temperature of direct water will vary with a certain delay in time due to the inertia of the heating system and transport delay. Therefore, in the existing control algorithms according to the network water temperature schedule, the required power of the heating system is achieved using proportional-integral and proportional-integral-differential laws of regulation not immediately, but with some delay [16, 17, 18].

The mathematical model developed in this work allows studying the operation modes at constant and variable power of the heating system. The adaptive control algorithm allows one to reach any given heating mode, including during standby and forecast control, without using the parameters of the temperature schedule and the parameters of proportional-integral and proportional-integral-differential laws of regulation.

To maintain a constant room temperature for a given time interval τ_k, the coefficient K and calculated power of the heating system can be determined by solving equation (7) from the condition that the indoor air temperature is equal at the beginning and at the end $t_{\text{in\_air}k} = t_{\text{in\_air}0}$ of a certain time interval τ_k. During this interval, the power of the heating system is assumed to be constant over time. Table 3 shows the forecasted heat loss power and the estimated power of the heating system during cooling and warming.

Figure 3 presents the calculated relationships between the internal air temperatures during cooling and warming and time at the heating system power determined using the mathematical model (curves 1) and the heating system power equal to the heat loss power at the beginning (curves 3) and at the end (curves 2) of the considered time interval .

Table 3

Changes in the forecast and calculated power of the heating system during the outdoor air cooling and warming

Change in outdoor temperature over a specified time interval τ_k (8 hours)	Outdoor temperature at the beginning of the calculation interval, °C	Outdoor temperature at the end of the calculation interval, °C	Predicted heat loss power at the beginning of the calculation interval, kW	Predicted heat loss power at the end of the calculation interval, kW	Estimated power determined from a mathematical model, kW
Cooling	-15	-17	99.5	105.9	135
Warming	-15	-13	99.5	93.8	62.5

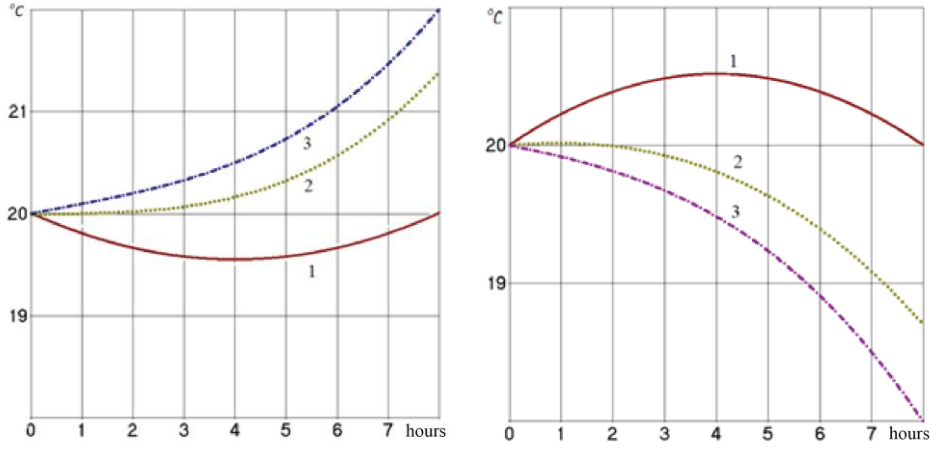

a) *b*)

Fig. 3. Dependence of indoor air temperature on time during warming (a) and cooling (b)for various heating system powers: 1 – power, determined from a mathematical model; 2 - power equal to losses at the end of the time interval; 3 - power equal to losses at the beginning of the time interval

From fig. 3b (curve 2) it can be seen that setting the heating system power equal to the heat loss power at the end of the cooling interval does not provide a constant indoor air temperature of 20 °C and causes under-heating; during warming, setting the heating system power equal to the loss power at the end of the selected interval (Fig. 3a, curve 2) causes the set temperature to be exceeded, i.e. extra-heating. Similar phenomena, but more pronounced are observed when the power of the heating system is set equal to the heat loss power at the beginning of the interval. Therefore, in case of forecast heating, to stabilize the temperature of the indoor air, it is necessary

to set not the powers corresponding to the predicted temperatures of the outside air at the end of the considered time interval, but the power determined using mathematical model, which takes into account the thermal inertia of the enclosing structures. During cooling, the calculated power is greater than the heat loss power at the end of the period under consideration, during warming it is less, which is explained by the influence of heat accumulated by the building envelope. Therefore, forecast heating control [16,17,18] should be proactive taking into account the thermal inertia of the building. Studies using a mathematical model showed that in order to maintain a constant temperature of indoor air in a room, it is necessary to set not the forecasted temperatures of the outdoor air, but the calculated ones $t_{\text{calc.out}}$, which, under cooling, are lower than the forecasted outdoor air temperature at the end of the considered time interval, but under warming they are higher. The calculated outdoor temperature can be determined from the expression

$$t_{\text{calc.out}} = \frac{qVt_{\text{calc.in}} - KP_{\text{loss}}}{qV},$$

where P_{loss} is the heating network power at the beginning of the considered interval.

The calculated outdoor temperatures necessary to maintain the indoor air temperature at a given level are greatly influenced by the time constants of buildings and construction. So, for example, for a time constant T =48 hours, when the outdoor temperature decreases by 2 degrees from -15 °C to -17 °C, the calculated temperature $t_{\text{calc.out}}$ =-28 °C, and when it is increased by 2 degrees $t_{\text{calc.out}}$ = -1.97 °C. With a decrease in the time constant to 24 hours for the same conditions, the calculated outdoor temperatures are -22 °C and -7.97 °C, respectively. Thus, with a decrease in the time constant, which occurs with a decrease in the mass and thermal resistance of the building enclosures, the calculated temperatures approach the outdoor air temperatures at the end of the considered time interval, and the coefficient K tends to 1.

Mathematical models, algorithms for standby heating and maintaining at a given level the heating system power during forecast control can be implemented using PLC. The adaptive control algorithm uses continuously measured temperatures of indoor and outdoor air, and also allows setting the calculated temperature of the outdoor air and the required temperature of the indoor air to provide a comfortable temperature in the room as settings for air temperatures [4,13]. With forecast control, the mathematical model allows determining the heating system power and the ambient temperature settings, at which the indoor air temperature will remain almost constant when the outdoor temperature changes without under-heating and extra-heating.

Conclusions

The proposed mathematical model of unsteady processes in heat-resistant enclosures allows the forecast and standby heating to be adapted according to the adaptive control algorithm, taking into account the change in the temperature of the outdoor air over time. When calculating the modes of forecast and standby heating, the mathematical model allows, at given initial and final temperatures of the internal air, determining heating system power that provide the desired temperature at the end of a given period of time. For the standby heating, this is the temperature at the end of the cooling or warming interval. The developed adaptive control algorithm allows one to provide any design conditions and create an energy-efficient heating system that provides a given temperature in the building's premises with minimal heat consumption, taking into account all the parameters that affect the heat loss power and the heating system capacity.

The created experimental installation for monitoring and controlling the heat supply regimes of a building allows, faster than the known algorithms, achieving equality of the actual power of the heating system and the power of heat losses when weather conditions change, to implement any adaptive control algorithms without setting the temperature parameters of the network water.

References

1. Oldewurtel F, Sturzenegger D, Morari M. Importance of building climate control. *Applied energy*. 2013; 101 (1):521-532.
2. Livchak VI. The choice of priority in the automatic regulation of heat transfer from heating systems of residential buildings. *Engineering systems*. 2016 AVOK North-West. 2016;. (1):38–45.
3. Panferov VI, Trenin NA, Panferov SV. On the assessment of heat saving reserves in the automation of building heating systems. *News of heat supply*. 2017; (9):46–49. (In Russ).
4. Tarasova VV, Afanasyev VV, Kovalev VG, Tarasov VA, Kalinin AG. Adaptive control of the mode of heat supply of a building with the help of an automated heat supply station. *Vestnik chuvashskogo universiteta*. 2016; (3):117–123. (In Russ).
5. Cherkasova OA, Malkin VV, Sabischansky IA, Merkulov PN. Automatic control of optimal hydraulic modes of heating systems. *News of heat supply*. 2019; (1):21–25. (In Russ).
6. Puhkal VA. Analysis of heat consumption for heating residential buildings in operation. *Fundamental research*. 2017; (1):106–111. Available at the journal.URL: http://fundamental-research.ru/ru/article/view?id=41323 Accessed to: 31 March 2019.
7. Shaikh PH, Nor NM, Nallagownden P, Elamvazuthi I., Ibrahim T. *of Smart Sustainable Buildings. Renewable and Sustainable Energy Reviews*, 2014;34:409-429. doi: 10.1016 / j.rser.2014.03.027
8. Zakharov AA, Zakharova IG, Romazanov AR, Shirokikh AV. Thermal mode modeling and heat supply management of the premises of a smart building. *Bulletin of Tyumen State University*. Physical and mathematical modeling. Oil, gas, energy. 2018; 4(2):105-119. doi: 10.21684 / 2411-7978-2018-4-2-105-119.
9. Anvari-Moghaddam A, Monsef H, Rahimi-Kian A. Cost-Effective and Comfort-Aware Residential Energy Management under Different Pricing Schemes and Weather Conditions. *Energy and Buildings.* 2015. (86): 782-793. doi: 10.1016 / j.enbuild.2014.10.017.
10. Ascione F, Bianco N, Stasio CDe, Mauro GM, Vanoli GP. Simulation-Based Model of the Predictive Control of Energy and Thermal Comfort. *Energy and Buildings*. 2016; (111):131-

Литература

1. Oldewurtel F., Sturzenegger D., Morari M. Importance of occupancy information for building climate control // Applied energy. 2013. 101(1). pp.521–532.
2. ЛивчакВ.И. Выбор приоритета в авторегулировании и теплоотдачи систем отопления жилых зданий // Инженерные системы. 2016 АВОКСеверо-Запад. 2016. № 1. С.38–45.
3. Панферов В.И., Тренин Н.А., Панферов С.В. К оценке резервов экономии теплоты при автоматизации систем отопления зданий // Новости теплоснабжения. 2017. №9. С.46–49.
4. Адаптивное управление режимом теплоснабжения здания с помощью автоматизированного теплового пункта/ В.В. Тарасова, В.В. Афанасьев, В.Г. Ковалев, В.А. Тарасов, А.Г. Калинин // Вестник Чувашского университета. 2016. № 3. С.117–123.
5. Черкасова О.А., Малкин В.В., Сабищанский И.А., Меркулов П.Н. Автоматическое управление оптимальными гидравлическими режимами систем теплоснабжения // Новости теплоснабжения. 2019. №1.С.21–25.
6. Пухкал В.А. Анализ режимов теплопотребления на отопление эксплуатируемых жилых зданий // Фундаментальные исследования. 2017. № 1. С. 106–111. Доступно по URL: http://fundamental-research.ru/ru/article/view?id=41323. Ссылка активна на: 31марта 2019.
7. Shaikh P.H., Nor N.M., Nallagownden P., Elamvazuthi I., Ibrahim T. A Review on Optimized Control Systems for Building Energy and Comfort Management of Smart Sustainable Buildings. Renewable and Sustainable Energy Reviews, 2014. Vol. 34. pp. 409–429.
8. Захаров А.А., Захарова И.Г., Ромазанов А.Р., Широких А.В. Моделирование теплового режима и управление теплоснабжением помещений умного здания // Вестник Тюменского государственного университета. Физико-математическоемоделирование. Нефть, газ, энергетика. 2018. Т4. № 2. С. 105-119.
9. Anvari-Moghaddam A, Monsef H, Rahimi-Kian A. Cost-Effective and Comfort-Aware Residential Energy Management under Different Pricing Schemes and Weather Conditions // Energy and Buildings. 2015. Vol. 86. pp. 782-793.
10. Ascione F. Simulation-Based Model Predictive Control by the Multi-Objective Optimization of Building Energy Performance and Thermal Comfort /

144. doi: 10.1016 / j.enbuild.2015.11.033.
11. Ock J, Issa RRA, Flood I. Smart building energy management systems (BEMS) simulation conceptual framework. *Proceedings of the 2016 Winter Simulation Conference*. IEEE Press, 2016. pp. 3237-3245. doi: 10.1109 / WSC.2016.7822355.
12. Senave MA. Reynders G, Verbeke S, Saelens D. Simulation exercise to improve building energy performance characterization via on-board monitoring. *Energy Procedia*. 2017; 132:969-974. doi: 10.1016/j.egypro.2017.09.687.
13. Tarasova VV, Tarasov VA, Kalinin AG, Afanasyev VV, Kovalev VG. Study of the dynamic characteristics of the automatic heating control system of a building. *Bulletin of the Chuvash University.Natural and Technical Sciences*. 2015; 3:122-128. (In Russ).
14. Panferov VI, Anisimova EYu, Nagornaya AN. To the theory of mathematical modeling of the thermal regime of buildings. *Bulletin of the South Ural State University. Chelyabinsk*. 2006. 14:128-133. (In Russ).
15.Abdullin VV, Shnayder DA, Basalaev AA. Building Heating Feed-Forward Control Based on Indoor Air Temperature Inverse Dynamics Model. *Lecture Notes in Engineering and Computer Science: Proceedings of The World Congress on Engineering and Computer Science 2014*, WCECS 2014, 22–24 October, 2014, San Francisco, CA, USA, pp. 886–892.
16. Akhmetov ER. Analysis of the model of duty heating as an energy-saving measure. *Energy saving and energy efficiency*. 2014. 5(59): 25–28. (In Russ).
17. Dobrotin SA, Prokopchuk EL. Synthesis of a system of anticipatory control of the process of supplying heat to a building's heating. *Problems of Regional Publisher: Institute of Energy of the Academy of Sciences of Moldova Energy (Kishinev)*. 2011. N2 .pp. 53-65. (In Russ).
18. Rumyantsev D.V., Tverskoy M.M. Algorithm of proactive control of thermal processes of a building with a combined heating system. *Basic Research*. 2015.2(24):5371–5376. Available at: http://fundamental-research.ru/ru/article/view?id=38352. Accessed to 27 March 2019.

F. Ascione, N. Bianco, C. De Stasio, G. M. Mauro, G. P. Vanoli // Energy and Buildings. 2016. Vol. 111. pp. 131-144.
11.Ock J. Smart building energy management systems (BEMS) simulation conceptual framework / J. Ock, R. R. A. Issa, I. Flood // Proceedings of the 2016 Winter Simulation Conference. IEEE Press, 2016. pp. 3237-3245. doi: 10.1109/WSC.2016.7822355.
12.Senave M. A Simulation exercise to improve building energy performance characterization via on-board monitoring / M. Senave, G. Reynders, S. Verbeke, D. Saelens // Energy Procedia. 2017. Vol. 132. pp. 969-974.
13.Тарасова В.В., Тарасов В.А., Калинин А.Г., Афанасьев В.В., Ковалев В.Г. Исследование динамических характеристик системы автоматического регулирования отопления здания. Вестник Чувашского университета. Естественные и технические науки 2015. № 3, С.122-128
14.Панферов В.И., Анисимова Е.Ю., Нагорная А.Н. К теории математического моделирования теплового режима зданий // Вестник Южно-Уральского государственного университета. Челябинск. 2006. №14. С.128-133.
15.Abdullin V.V., Shnayder D.A., Basalaev A.A. Building Heating Feed-Forward Control Based on Indoor Air Temperature Inverse Dynamics Model. Lecture Notes in Engineering and Computer Science: Proceedings of The World Congress on Engineering and Computer Science 2014, WCECS 2014, 22–24 October, 2014, San Francisco, CA, USA, pp. 886–892.
16.Ахметов Э.Р. Анализ модели работы дежурного отопления как энергосберегающего мероприятия // Энергоресурсосбережение и энергоэффективность. 2014. № 5 (59). С.25–28.
17.Добротин С. А. , Прокопчук Е. Л. Синтез системы упреждающего управления процессом подачи тепла на отопление здания // Проблемы региональной энергетики. 2011. №2. С. 53-65 Издательство: Институт энергетики Академии наук Молдовы (Кишинев).
18.Румянцев Д.В., Тверской М.М. Алгоритм упреждающего управления тепловыми процессами здания при комбинированной системе отопления // Фундаментальные исследования. 2015. № 2-24. С. 5371–5376. Доступен по URL: http://fundamental-research.ru/article/view?id=38352 .Ссылка активна на: 27 марта 2019.

Authors of the publication

Vladimir A. Tarasov – PhD in Engineering sciences, Associate Professor Chuvash State University, Cheboksary, Russia. E- mail: vladimir_tarasov@inbox.ru.

Valentina V. Tarasova – software engineer LLC Engineering and Technical Center GORISS, Cheboksary, Russia. E- mail: charming_cerl@rambler.ru

Vladimir V. Afanasyev – Grand PhD in Engineering sciences, Associate Professor Chuvash State University, Cheboksary, Russia. E- mail: avvteo@mail.ru.

Vladimir G. Kovalev – PhD in Engineering sciences, Associate Professor Chuvash State University, Cheboksary, Russia. E- mail: espp21@mail.ru

Viktor N. Orlov – PhD in Physico-mathematical sciences, Professor Chuvash State University, Cheboksary, Russia. E- mail: orlov.vick@yandex.ru.

Received ***April 03, 2019***

UDC 620.9 **DOI:10.30724/1998-9903-2019-21-3-86-96**

SUPERSONIC FLOW OF TWO-PHASE GAS-DROPLET FLOWS IN NOZZLES

A.I. Sharapov, A.A. Chernykh, A.V. Peshkova

Lipetsk State Technical University, Lipetsk, Russia

Abstract: *For practical applications, the description of processes occurring during the flow of two-phase gas-liquid mixtures requires a simple physical and mathematical model that describes the behavior of a two-phase medium in the entire range of phase concentrations changes and in a wide range of pressure changes. Problems of this kind arise in various branches of industry and technology. In the space industry, one often has to deal with the movement of various gases in rocket nozzles, consider the combustion, condensation of various vapors on the nozzle walls and their further impact on the velocity sublayer at the nozzle wall. The large acoustic effect arising from the engines affects the gas-liquid mixture in the nozzles of rocket engines. In the metal industry, metal cooling occurs with the help of nozzles in which the emulsion mixture is supplied under high overpressure. But this is only a short list of applied issues in which one has to deal with a problem of this type. The paper presents the results and directions of study of the problems of two-phase dispersed gas-droplet flows in the nozzles. The main methods of investigation of two-phase heterogeneous flows are described. The main characteristics of heterogeneous two-phase flows in the nozzles, which were confirmed by experimental results, are presented. The calculation of the air-droplet flow in the Laval nozzle is given. The technique, which is based on integral energy equations for two-phase dispersed flows, is described. The main problems and questions concerning the further description and studying of two-component flows are stated.*

Keywords: *gas-droplet flows, heterogeneous medium, sound propagation, sound velocity, Laval nozzle, quasi-equilibrium flow, critical parameters, medium compressibility, Witoszynskyj nozzle, acoustics of dispersed medium.*

For citation: Sharapov AI, Chernykh AA, Peshkova AV. Supersonic flow of two-phase gas-droplet flows in nozzles. *Power engineering: research, equipment, technology*.2019; 21(3):86-98. (In Russ). doi:10.30724/1998-9903-2019-21-3-86-98.

СВЕРХЗВУКОВОЕ ТЕЧЕНИЕ ДВУХФАЗНЫХ ГАЗОКАПЕЛЬНЫХ ПОТОКОВ В СОПЛАХ

А.И. Шарапов, А.А. Черных, А.В. Пешкова

Липецкий государственный технический университет, г. Липецк, Россия
sharapov-lipetsk@yandex.ru, Peshkova_Nastja@mail.ru

Резюме: *Для практических приложений описания процессов, происходящих при течении двухфазных газожидкостных смесей, необходима простая физико-математическая модель, описывающая поведение двухфазной среды во всем диапазоне изменения концентраций фаз и в широком диапазоне изменения давлений. Проблемы такого рода встают в разных отраслях промышленности и техники. В космической промышленности часто приходится сталкиваться с движением различных газов в соплах ракет, рассматривать сгорание, конденсацию различных паров на стенках сопел и дальнейшее их*

влияние на скоростной подслой у стенки сопла. Большой акустический эффект, исходящий от двигателей, влияет на газожидкостную смесь в соплах ракетных двигателей. В металлопромышленности имеет место охлаждение металла с помощью форсунок, в которых эмульсионная смесь подаётся под высоким избыточным давлением. Но это лишь краткий перечень прикладных задач, в которых приходится сталкиваться с проблемой такого типа. В работе приведены результаты и направления исследования проблематики течения двухфазных дисперсных газокапельных потоков в соплах за последнее время. Изложены основные методы исследования двухфазных гетерогенных потоков. Приводятся основные характеристики протекания гетерогенных двухфазных потоков в соплах, которые были подтверждены опытными результатами. Приводится расчёт течения воздушно-капельного потока в сопле Лаваля. Изложена методика, которая опирается на интегральные энергетические уравнения для двухфазных дисперсных потоков. Изложены основные проблемы и вопросы, касающиеся дальнейшего описания и изучения двухкомпонентных потоков. В расчетах пренебрегается структура двухфазного потока и рассматривают его течение как односкоростной однотемпературный континуум.

Ключевые слова: *газокапельные потоки, гетерогенная среда, распространение звука, скорость звука, сопло Лаваля, квазиравновесное течение, критические параметры, сжимаемость среды, сопло Витошинского, акустика дисперсных сред*

Introduction

To describe the processes occurring during the two-phase gas-liquid mixtures flow, a simple physical and mathematical model is needed that shows the behavior of a two-phase medium in the entire range of changes in phase concentrations and in a wide range of pressure changes. Problems of this kind arise in various branches of industry and technology. In the space industry, one often has to deal with the movement of various gases in rocket nozzles, consider their combustion, condensation of various vapors on the nozzle walls and their further impact on the velocity sublayer near the nozzle wall. The large acoustic effect arising from the engines affects the gas-liquid mixture in the nozzles of rocket engines. In metal industry, metal cooling is made using nozzles in which the emulsion mixture is supplied under high overpressure.

The study of motion of various two-phase media is currently of great interest for the aircraft industry, engineering, and for the design of water circuit of nuclear reactors. Due to the complexity of the processes of interphase interaction, the general approaches for these types of two-phase mixtures are not formalized due to the peculiarities of their behavior. This issue was already addressed in the 30-40s of the last century, but issues related to determination the speed of sound [1-4], description the flow in the presence of phase transitions, etc., are still not systematized and have not been properly studied. This interest is mainly caused by finding universal relations [2] for describing various flow parameters in dispersed multicomponent media, since motion of such flows, for example, in nozzles is associated with various heat transfer processes, as well as processes accompanied by phase transitions. This can be attributed to various gas-droplet media in which the dispersed phase in the form of liquid droplets is in suspension.

It is also worth noting that a small number of works [2, 4] are devoted to the study of gas-droplet systems at sufficiently high mass contents of the droplet phase ($\varphi \geq 5\%$).

The study of propagation of sound waves in various media is inextricably linked with heat and mass transfer processes, but the authors [1, 5, 6] state that heat transfer processes are not involved in the propagation of acoustic waves in stationary two-phase media. As for the unjustified increase in speed at $\varphi < 0.5$, the situation has an inverse physical formulation. The gaseous medium itself begins to prevail over the liquid one, and the gaseous medium, which begins to fill the entire volume, becomes a source of waves itself. As a result of long-range order destruction by

perturbations, a state with slowly decreasing waves arises, therefore, the energy that the surface layer of the δ-droplet begins to emit is amplified, and two wave fronts are obtained.

As was noted above, an interpretation based on linear theory can no longer be applied [1, 5], since the so-called dispersion phenomena are observed during the propagation of sound waves: reflection, absorption, etc. If one considers the "liquid – gas" interface, an abrupt change in the speed of sound will be observed at its boundary [5-10].

We address a two-phase medium of the "droplets–gas" type in which a wave propagates with a length comparable to the free-path length between the droplets. The concept of the speed of sound should be taken into account. It is appropriate to use the methods of molecular kinetic theory, in which molecules will be replaced by small droplets (heterogeneous medium). Knudsen's criterion will be applicable to such a system. The description of a system with sufficiently large liquid droplets requires another approach: not from the point of view of compressibility, but with consideration of such a process as a two-component one [1, 6, 10, 11-16]. The system should be divided into separate "droplets-gas" transitions, which together will characterize the entire system. The wave propagation process is similar to the Brownian motion of molecules, as a result of which some assumptions become applicable. Based on these formulas, a comparison of different gas-liquid systems was made.

As a result, methods of probabilistic description of the process or a separate description of the liquid – gas boundary become feasible. There exists the scaling method, when the system is compared with the free path length between individual dispersed inclusions. In this case, for example, a sound wave of a certain frequency flies onto a drop, which generates a series of fronts (also acoustic waves) that begin to propagate from the source in different directions [17, 18]. The generation of waves is associated with a change in the continuum, and therefore in acoustic waves the main change is made by the liquid, which, due to its diffusion motion, is a very good refractive component. Therefore, based on this point of view, one should subdivide the degree of intensity of the wave propagation through such dispersive homogeneous media.

Research method

Consider the equations for equilibrium and frozen flows. We will proceed from the basic kinetic integral equation for a two-component medium. After simple transformations, it reduces to the equation

$$w = \sqrt{w_0^2 + \frac{2c_p\left(T_0 - T\right)}{\left(1+\varphi^2 d\right)}} \tag{1}$$

During a polytropic process, in case when there are heat exchange processes, relation (1) takes the form

$$w = \sqrt{w_0^2 + \frac{2c_p T_0\left(1-\beta^m\right)}{\left(1+\varphi^2 d\right)}} \tag{2}$$

For an inhibited process, one can obtain the ratio

$$w = \sqrt{w_0^2 + \frac{2c_p T_0\left(1-\beta^m\right)}{\left(1+ d\right)}} \tag{3}$$

Several conclusions can be drawn from these two equations. Firstly, the Mach number for the inhibited flow, with the same pressure and temperature drops, is greater than the Mach number for the equilibrium flow. This is true for any ratio of phase slip coefficients φ.

Laval nozzle calculation

We give an example of the Laval nozzle calculation for a two-phase vapor-air medium. The pressure change profile is shown in Fig. 1. The initial pressure is 1.2 bar, the output pressure is 0.5 bar.

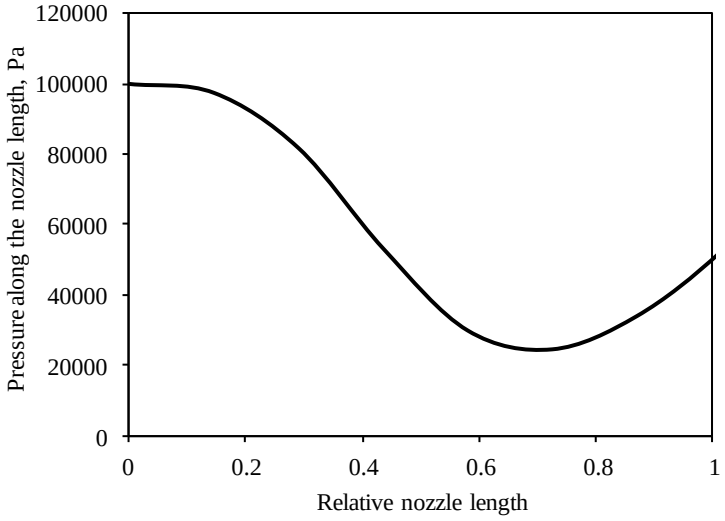

Fig. 1. The profile of pressure changes along the entire length of the Laval nozzle

Consider the change in velocity over the entire nozzle profile for the case of equilibrium air flow. An example of calculation is shown in Fig. 2 for different exponents *m*.

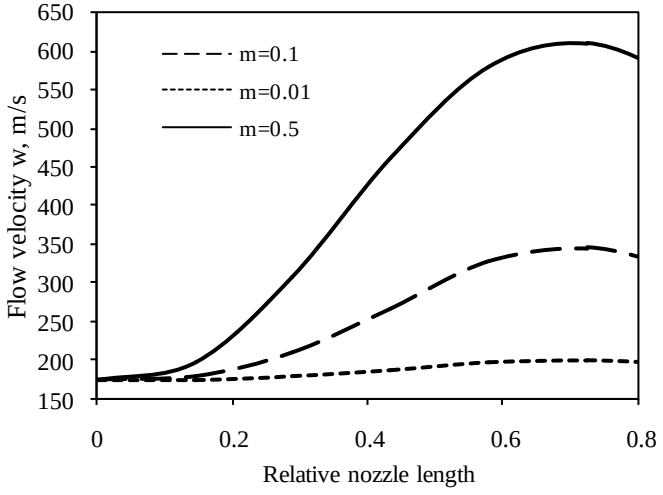

Fig. 2. Change in the air quasi-equilibrium flow rate at different exponents *m*

It is seen that for the case m=0.1, the speed of sound is reached in the critical section. For the case m=0.5, the speed of sound is reached well before the flow reaches the critical section of the nozzle. But such a case is not realized in practice, because the adiabatic index cannot be negative.

Now consider the flow distribution with a small amount of gradually mixed moisture Δd=0.4 kg/kg. The initial flow velocity at the entrance to the nozzle is taken equal to 10 m/s. From the graphs in Fig. 3, it can be seen that for m=0.5 the flow rates are different in the critical section, and for the frozen flow this value is greater than for the equilibrium one. The speed of sound is reached later at equilibrium flows in comparison with the frozen flow, as shown in Fig. 3. This figure shows the establishment of the speed of sound for both equilibrium and frozen flows. In this case, a gradual mixing of moisture deforms the velocity profile, and the achievement of the speed of sound for a frozen flow occurs long before the minimum nozzle cross section is reached. As the

exponent *m* decreases, the flow continues to expand, passing through the critical section of the Laval nozzle.

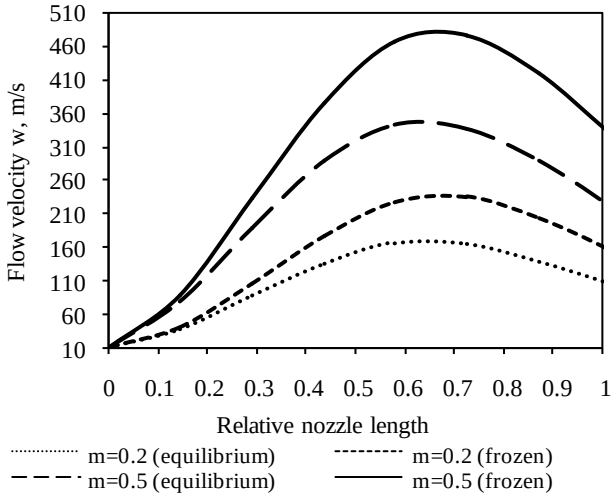

Fig. 3. Change in the gas-droplet flow with a gradually mixed moisture Δd= 0.4 kg moist./kg at different exponents *m*. For the inhibited flow the speed of the liquid component is two times lower

Figures 4 and 5 show the results of calculating the change in the rates of the frozen and equilibrium two-phase droplet-air flow. These dependences show how the slip coefficient φ affects the flow propagation in the nozzle. An increase in the velocity of the droplet component in the main flow leads to a shift in the maximum of the velocity profile towards the output section, and the case with the opposite effect leads to a shift in the maximum to the input section. Moreover, such an effect is observed only if there is a mixing of small portions of moisture.

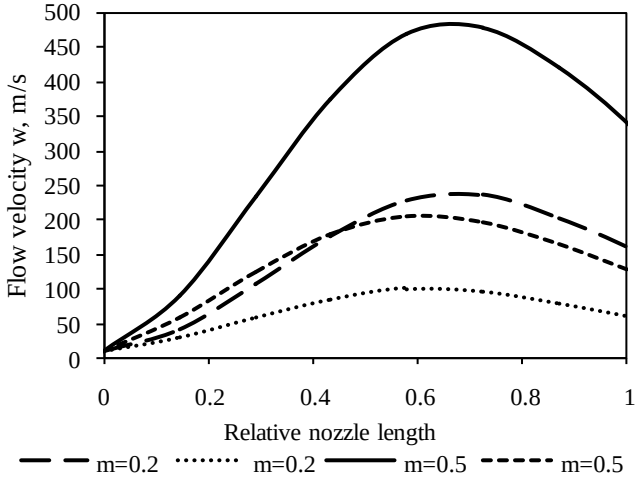

Fig. 4. Change in the gas-droplet inhibited flow with a gradually mixed moisture Δd= 0.4 kg moist./kg at different exponents *m*. For *m*=0.2 the speed of the liquid component is two times lower than the gas one, and for m=0.5 the reversed dependence is observed

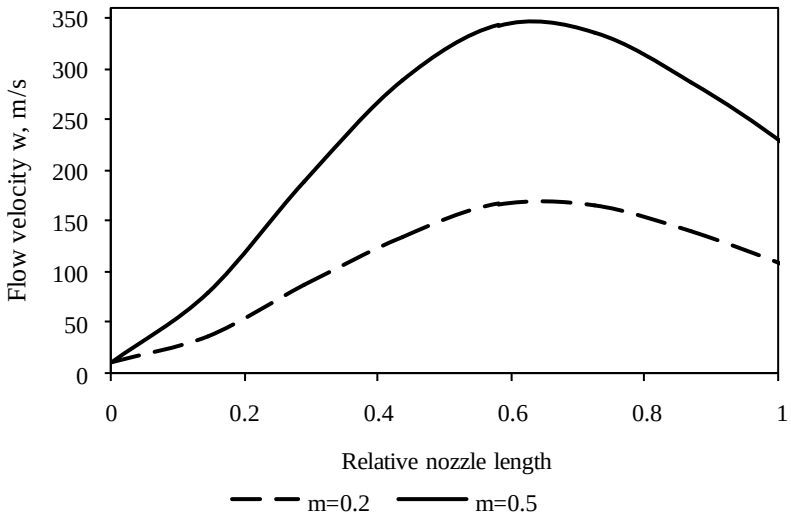

Fig. 5. Change in the gas-droplet quasi-equilibrium flow with a gradually mixed moisture Δd= 0.4 kg moist./kg at different exponents *m*.

Consider a gas-droplet flow with a moisture content of 1 kg. moist./kg. In fig. 6 it can be seen that for two-phase gas-droplet media the flow velocity does not approach the sonic one in a critical section. Note that the critical velocity for a two-phase flow does not correspond to the speed of sound in gas. The critical velocity becomes equal to the speed of sound only in a gas in which there is no moisture or dispersed inclusions. Since the critical velocity is equal to the speed of sound only for an ideal gas and isoentropic flow, such a property is no longer applicable for a polytropic flow.

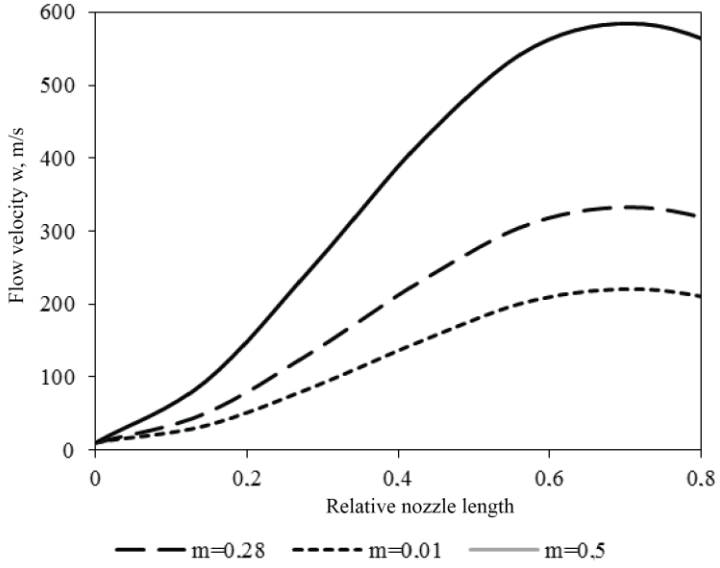

Fig. 6. Change in the gas-droplet equilibrium flow with *d*=1 kg moist./kg at different exponents *m*.

Taper nozzle calculation

If the area is known, then the speed of each phase can be found, since the gas phase consumption is known, G=20 kg/s, and the phase densities are known. In this case, the droplet phase velocity can be found using the moisture content ratio (3). The remaining graphs were constructed using the iteration method using formula (3). The main ratios that were used in this task are:

$$w_i = \frac{G}{\rho_в F_i} \quad \text{and} \quad w_{i+1} = \frac{G}{\rho_в F_{i+1}} \tag{4}$$

We find the temperature from relation (3), which can be represented by the iteration method as follows:

$$w_{i+1} = \sqrt{w_i^2 + \frac{2c_p\left(T_{i+1} - T_i\right)}{\left(1+\varphi^2 d\right)}} \tag{5}$$

The pressure is found from the Mendeleev-Klaiperon equation of gas state in the form

$$\Delta p_i = \rho R_\mu \Delta T_i . \tag{6}$$

Further, one can set the distribution of the nozzle cross-sectional area over its entire dimensionless length, and from here find the flow velocity, since the amount of air *M* supplied to the nozzle is known. Then, using formula (6), one can find the temperature difference at each iteration by setting the velocity coefficient. In this case, the velocity coefficient was taken equal to 0.8. It was indicated that in the course of solving the problem the phase pressures were taken equal to each other. In this case, the law of distribution of the cross-sectional area, which was used in solving this problem *F=f (x)* is:

$$F = Ax^2 + B ,$$

where *x* is the dimensionless nozzle length, *A* and *B* are the constants, which are found from the conditions: for $F_1 = 0.9\ \text{m}^2$, $x_1 = 0$, and for $F_2 = 0.5\ \text{m}^2$, $x_1 = 1$.

Further the main calculation is presented. The pressure change along the entire dimensionless nozzle length is set by the following laws, which are shown in Figs. 7 and 8.

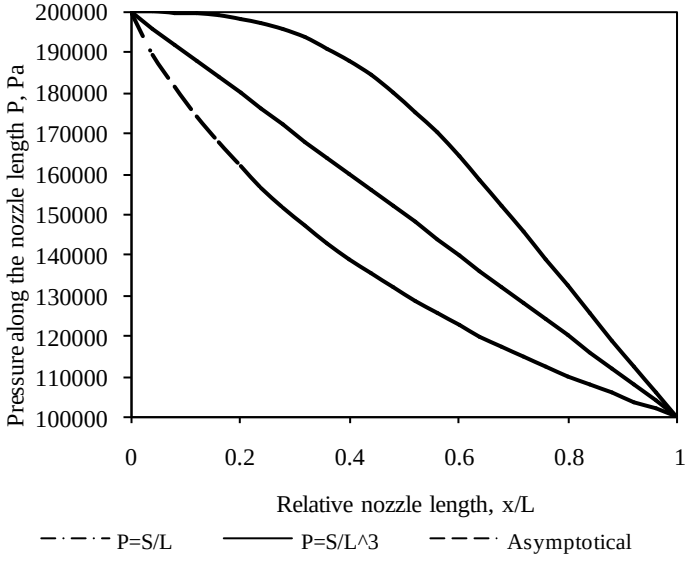

Fig. 7. Pressure change along the entire dimensionless nozzle length

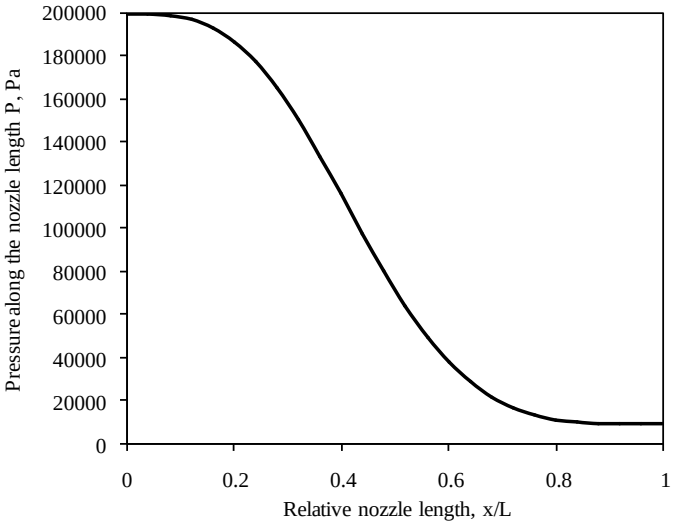

Fig. 8. Pressure change along the entire dimensionless nozzle length according to the exponential law (Witoszynskyj)

Since the temperature in the gas is equal to the temperature in the liquid, the temperature change in the media will be adiabatic:

$$T = T_0 \left(\frac{P}{P_0} \right)^{\frac{k-1}{k}} \tag{7}$$

Temperature distribution in the equilibrium flow is different. Such flows are characterized by polytropic gas compression, therefore, we use the formula:

$$T = T_0 \left(\frac{P}{P_0} \right)^{\frac{n-1}{n}} . \tag{8}$$

For convenience, the polytropic index is taken as 1.2.

Thus, the task of propagation of a two-phase flow of the “liquid droplets-gas” type in nozzles of different geometries was solved and graphs of distribution of the two-phase flow velocity over the dimensionless length of the nozzle were obtained (Figs. 9-11). The solid line in figures for the law, which is shown by the solid line in Fig. 8; small strokes and dash-dotted lines show the approximations for the law depicted in Fig. 7.

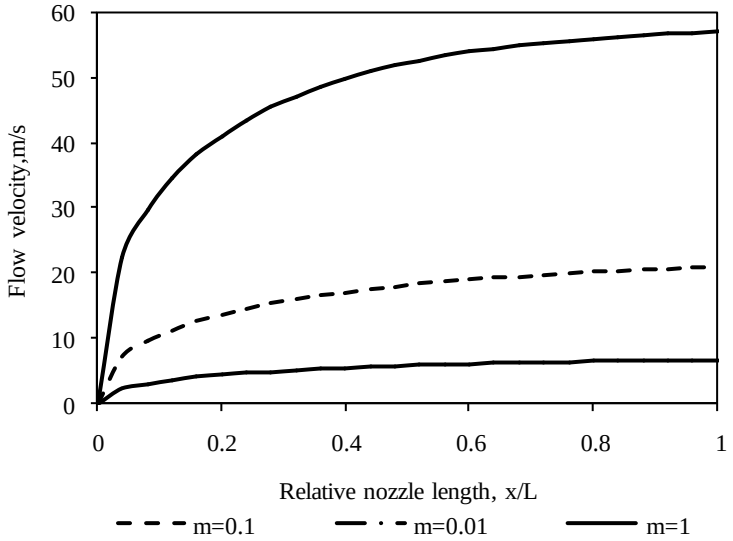

Fig. 9. Relationship between change in the inhibited flow velocity and dimensionless nozzle length at different exponents *m* when pressure is distributed according to the hyperbolic law

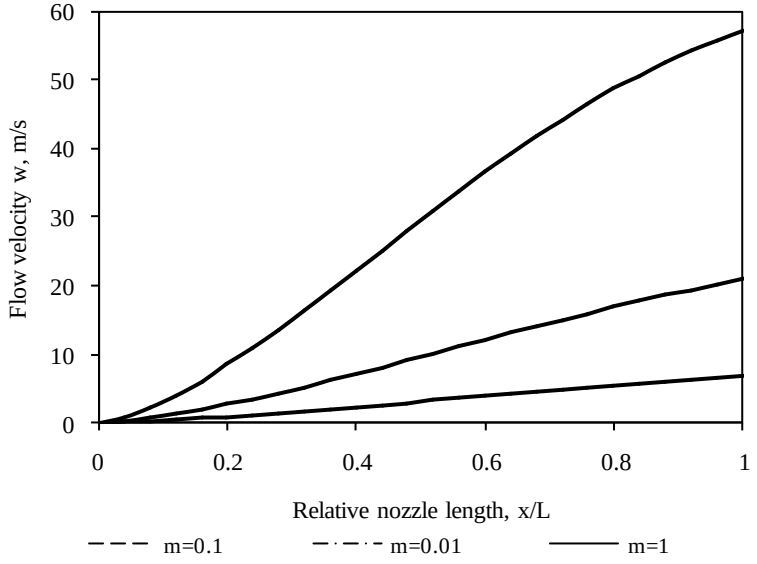

Fig. 9. Relationship between change in the inhibited flow velocity and dimensionless nozzle length at different exponents *m* when pressure is distributed according to the cubic law

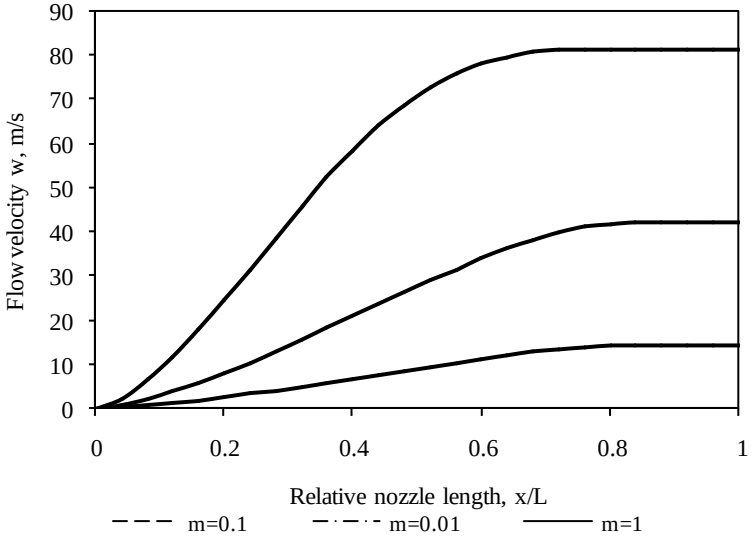

Fig. 10. Relationship between change in the inhibited flow velocity and dimensionless nozzle length at different exponents *m* when pressure is distributed according to the exponential law

The dimensionless length is presented as the ratio of the variable value to the maximum one, and the dimensionless diameter in relation to the minimum value. The initial temperature was taken equal to 70 ºC, the initial pressure was 200 kPa.

The obtained results show that the most acceptable profile for achieving a high flow velocity is the exponential profile. The same can be said about the achievement of the speed of sound: during profiling the most suitable nozzle, an exponential nozzle is more preferable from the point of view of critical flow parameters. These dependences were obtained for quasi-equilibrium flow. In each case the prevalence of equilibrium or frozen methods of mixture compressibility will be determined by the non-stationary process conditions. Thus, there arises a problem for describing a two-phase system with the same component parts from the point of view of acoustics. And here it is necessary to emphasize that a clear answer on how to describe such a medium in terms of compressibility [1, 10, 11, 14, 16] has not been received yet. Therefore, the concept of sound speed for such a system is no longer applicable. It is worth noting another one property of the Vitoshinsky profile. When x/L=0.75 is reached, the flow velocity remains constant, i.e. critical flow rate was reached at 0.75. The remaining tapering nozzles need to set a large degree of pressure reduction in order to increase the speed of the working jet.

It remains to consider one more question about the applicability of all thermodynamic equations to heterogeneous gas-droplet media, but with rather small droplets. The theoretical and experimental studies for superheated vapor were also carried out, which resulted in formulation of conditions for the applicability of the gas state equation. As a result, for $M \leq 3$ and a pressure of 1 MPa, it is possible to use the thermodynamic equations of gas state for such gas-droplet flows.

Under certain properties, superheated or saturated vapor can be considered as a homogeneous medium, but the applicability of the basic thermodynamic equations is violated at high supersonic speeds [11, 12]. Therefore, it is worth pointing out that a similar picture of applicability of thermodynamic relations for an ideal gas will be observed for vapor-gas media under the condition that this medium does not contain dispersed inclusions in the form of droplets.

Conclusions

A two-phase medium is a system that has certain specific features that appear as a result of the propagation of acoustic waves of different frequencies. In this connection, several questions arise that need to be considered: how to characterize such a system from the point of view of sound theory and what is meant by the speed of sound; how to describe the characteristics of such

a system, which includes such critical parameters as *P*cr and *t*cr? Therefore, the question about the inapplicability of the concept of the speed of sound to multiphase media is raised, since it is ultimately necessary to consider in each phase its speed of sound. In this case, the analysis of the two-phase flow should be based on the general integral energy equations, taking into account the fact that the gas and condensed phases can have different temperatures, pressure and velocity using a two-fluid flow model; the predominance in each case of equilibrium or frozen methods of compressibility of the mixture will be determined by the conditions of an unsteady process. A two-phase or some other multicomponent system must be described using equation (2); at the same pressure and temperature the Mach number for the inhibited flow is greater than the Mach number for the equilibrium flow. With a high content of the liquid component, the condition of local thermodynamic equilibrium is violated, and one should not use the equations applicable to the gas component.

References

1. Chernyh A.A., Peshkova A.V. Nachal'nye svedeniya o teorii rasprostraneniya zvuka v dvuhkomponentnyh smesyah. 3 Mezhdunarodnaya nauchnaya konferenciiya studentov i molodyh uchenyh. «Molodezh' i sistemnaya modernizaciya strany»; 22-23 may 2018; Kursk, Russia. 2018. pp. 207–211. (In Russ).

2. Nakoryakov VE., Pokusaev BG. Schreiber, IR. Rasprostranenie voln v gazovyh i parozhidkostnyh sredah. Novosibirsk: Institut teplofiziki SO AN SSSR, 1983. (In Russ).

3. Gubarev VYa.. Gazozhidkostnye techeniya v soplah. *Vestnik Rybinskoj gosudarstvennoj aviacionnoj tekhnologicheskoj akademii im. P.A. Solov'eva*.2017; 43(4):61–68. (In Russ).

4. Chernyh AA., Sharapov AI., Peshkova AV. Akusticheskie processy v gazokapel'nyh sredah.. *Vestnik Tambovskogo gosudarstvennogo tekhnicheskogo universiteta*. 2018; 24(2):281–286 (In Russ).

5. Nigmatulin RI., Aganin AA., Toporkov DYu., Il'gamov MA. Obrazovanie skhodyashchihsya udarnyh voln v puzyr'ke pri ego razrushenii. DOKLADY FIZIKI. 2014; 59(9): 431-435. (In Russ). doi: 10.1134/S1028335814090109

6. Nigmatullin RI., Aganin AA., Ilgamov MA. et al. Sil'noe szhatie para v kavitacionnyh puzyr'kah v vode i acetone. *Vestnik Bashkirskogo universiteta.* 2017; 22 (3): 580-585.(In Russ).

7. Chernykh AA., Peshkova AV., Sharapov AI. Chernyh AA., Peshkova AV., Sharapov AI. Osnovnye polozheniya teorii akustiki dvuhfaznyh sred 5 Mezhdunarodnaya mmolodezhnaya nauchnaya konferenciya. 2018. Pp 302-305. (In Russ).

8. Gubarev V.Ya. Skorost' zvuka v gazozhidkostnyh sredah. V sbornike: Energosberezhenie i effektivnost'

Литература

1. Черных А.А., Пешкова А.В. Начальные сведения о теории распространения звука в двухкомпонентных смесях// Труды 3-й Международной научной конференции студентов и молодых ученых. «Молодежь и системная модернизация страны»; 22-23 мая 2018., Курск, 2018. С. 207–211.

2. Накоряков В.Е., Покусаев Б.Г., Шрейбер И.Р. Распространение волн в газовых и парожидкостных средах. Новосибирск ИТФ СО АН СССР, 1983. 237 с.

3. Губарев В.Я. Газожидкостные течения в соплах. // Вестник Рыбинской государственной авиационной технологической академии им. П.А. Соловьева. 2017. № 4 (43). С. 61–68.

4. Черных А.А., Шарапов А.И., Пешкова А.В. Акустические процессы в газокапельных средах. // Вестник Тамбовского государственного технического университета. 2018.№ 2(24). С. 281-286.

5. Нигматулин Р.И., Аганин А.А., Топорков Д.Ю., Ильгамов М.А. Образование сходящихся ударных волн в пузырьке при его разрушении. ДОКЛАДЫ ФИЗИКИ. 2014. Т.59. № 9. С. 431-435.

6. Нигматулин Р.И., Аганин А.А., Ильгамов М.А., Топорков Д.Ю. Сильное сжатие пара в кавитационных пузырьках в воде и ацетоне. // Вестник Башкирского университета. 2017.№ 3.(22) С. 580-585.

7. Черных А.А., Пешкова А.В., Шарапов А.И. Основные положения теории акустики двухфазных сред. // Труды 5-й Международной молодежной научной конференции. 2018. С. 302-305.

8. Губарев В.Я. Скорость звука в газожидкостных средах. В сборнике: Энергосбережение и

v tekhnicheskih sistema ..Mezhdunarodnaya nauchno-tekhnicheskaya konferenciya studentov, molodyh uchenyh i specialistov. Russia 2017.10-12 Jul; Tambov, Russia. Tambovskij gosudarstvennyj tekhnicheskij universitet.(In Russ).

9.Nigmatulin RI., Bolotnova RH. Shirokoe uravnenie sostoyaniya vody i para v uproshchennoj forme. *Teplofizika vysokih temperatur*.2011;49(2):303-306. (In Russ).

10.Pokusaev BG., Tairov EA., Vasil'ev SA. Nizkochastotnye volny davleniya v parozhidkostnoj srede s fiksirovannym sloem sfericheskih chastic. *Akusticheskaya fizika.* 2010; 56(3):306-312.(In Russ).

11. Fedotovsky VS., Prokhorov YuP., Vereshchagina TN.Dinamicheskaya plotnost' i skorost' rasprostraneniya voln davleniya v dispersnyh sredah // *Teploenergetika* 2001; 48(3): 70–74.(In Russ).

12. Doncov VE., Nakoryakov VE. Processy obrazovaniya i rastvoreniya gidratov za udarnoj volnoj v zhidkosti, soderzhashchej puzyr'ki gaza .*Zhurnal prikladnoj mekhaniki i tekhnicheskoj fiziki.* 2009; 50(2):318-326. (In Russ).

13. Shagapov VI. Vliyanie teplomassobmennyh processov mezhdu fazami na rasprostranenie malyh vozmushchenij v pene. Teplofizika vysokih temperatur. //*Vestnik Bashkirskogo Universiteta*. 1985; 23(1):126-132.(In Russ).

14. Chernyh AA., Gubarev VYa. Rasprostranenie zvukovyh voln v dvuhfaznyh sredah. 5 Mezhdunarodnoj nauchno-tekhnicheskoj konferencii studentov, molodyh uchyonyh i specialistov «Energosberezhenie i effektivnost' v tekhnicheskih sistemah». 2018. pp. 272–273. (In Russ).

15. Nakoryakov VE., Doncov VE., Pokusaev BG. Rasprostranenie voln davleniya v zhidkosti s tverdymi chasticami i puzyr'kami gaza. *Inzhenernaya teplofizika*. 1994 ; 4(2):173–188.(In Russ).

16. Nigmatulin RI., Aganin AA., Toporkov DYu., Ilgamov MA. The formation of converging shock waves in a bubble during its compression. *Reports of the Academy of Sciences*. 2014. 458(3):282.(In Russ). doi: 10.7868/S0869565214270115

17. Nigmatulin RI., Gubajdullin DA., Fedorov YuV. Akusticheskie volny raznoj geometrii v polidispersnyh puzyr'kovyh zhidkostyah. *Teoriya i eksperiment.*.2013;450(6): 665(.In Russ).

18. Nigmatulin RI., Aganin AA., Il'gamov MA., Toporkov DYu. Evolyuciya vozmushchenij sfericheskoj formy kavitacionnogo puzyr'ka. *Uchenye zapiski Kazanskogo universiteta*.. 2014; 156

эффективность в технических система // Труды Международной научно-технической конференции студентов, молодых ученых и специалистов. Тамбовский государственный технический университет. 10-12 июля 2017.Тамбов.

9. Нигматулин Р.И., Болотнова Р.Х. Широкое уравнение состояния воды и пара в упрощенной форме.// *Теплофизика высоких температур* .2011. Т.49. № 2 С. 303-306.

10. Покусаев Б.Г., Таиров Е.А., Васильев С.А. Низкочастотные волны давления в парожидкостной среде с фиксированным слоем сферических частиц. // Акустическая физика.. 2010.56. № 3(56). С. 306-312.

11. Федотовский В.С., Прохоров Ю.П., Верещагина Т.Н. Динамическая плотность и скорость распространения волн давления в дисперсных средах // Теплоэнергетика. 2001. № 3(48). С. 70–74.

12. Донцов В.Е., Накоряков В.Е., Донцов Е.В. Процессы образования и растворения гидратов за ударной волной в жидкости, содержащей пузырьки газа //. *Журнал прикладной механики и технической физики.* 2009; № 2(50) .С. 318-326.

13. Шагапов В.И. Влияние тепломассобменных процессов между фазами на распространение малых возмущений в пене. Теплофизика высоких температур. //Вестник Башкирского Университета.. 1985 Т.23.№ 1. С.126-132.

14. Черных А.А., Губарев В.Я. Распространение звуковых волн в двухфазных средах// Труды 5 Международной научно-технической конференции студентов, молодых учёных и специалистов «Энергосбережение и эффективность в технических системах». 2018. С. 272-273.

15. Накоряков В. Е., Донцов В. Е., Покусаев Б. Г. Распространение волн давления в жидкости с твердыми частицами и пузырьками газа // Инженерная теплофизика. 1994. Т.4.№ 2. С. 173–188.

16. Нигматулин Р.И., Аганин А.А., Топорков Д.Ю., Ильгамов М.А. Образование сходящихся ударных волн в пузырьке при его сжатии. Доклады академии наук. 2014.Т.458. № 3. С.282.

17. Нигматулин Р.И., Губайдуллин Д.А., Федоров Ю.В. Акустические волны разной геометрии в полидисперсных пузырьковых жидкостях. Теория и эксперимент. 2014. Т.450. № 6 . С.665.

18. Нигматулин Р.И., Аганин А.А., Ильгамов

(1): 79-108.(In Russ).

М.А., Топорков Д.Ю. Эволюция возмущений сферической формы кавитационного пузырька. Ученые записки Казанского университета. 2014.Т.156. № 1. С. 79-108.

Authors of the publication

Aleksei I. Sharapov – Department of industrial heat power engineering, Lipetsk State Technical University.

Anton A. Chernykh – Department of industrial heat power engineering, Lipetsk State Technical University.

Anastasia V. Peshkova – Department of industrial heat power engineering, Lipetsk State Technical University.

Received ***April 09, 2019***

UDC621.039.524.44:621.311.25 DOI:10.30724/1998-9903-2019-21-3-99-108

ON THE POSSIBILITY OF PARTICIPATION OF NPPS WITH VVER IN EMERGENCY FREQUENCY REGULATION IN POWER SYSTEMS

V.A. Khrustalev*[1], M.V. Garievskii[2], I.A. Rostuntsova[1], A.V. Portyankin[1]

[1]Yuri Gagarin State Technical University of Saratov, Saratov, Russia
[2]Saratov Scientific Center, Russian Academy of Sciences, Saratov, Russia
ORCID: http://orcid.org/0000-0002-1630-926X, khroustalevva@mail.ru

Abstract: *The purpose of the article is to study the possibility and feasibility of participation of nuclear power plants (NPPs) with VVER in emergency frequency control in power systems with a high proportion of nuclear power units and, at the same time, of reducing the power consumption for the own needs of the main circulation pumps during modes with power below nominal. To solve these problems, it was proposed to increase the achievable speeds of power gain (load increase) due to the installation of frequency controlled drives of the MCP. Large system frequency variations (caused by large imbalances between generation and demand) may jeopardize electrical equipment, in terms of maintaining stable and reliable operating conditions. For NPPs, the task of preventing or localizing accidents is even more important than for TPPs, since in case of major system accidents, it is possible to completely stop external power supply of the NPPs own needs. Thus, besides the requirements for the primary control of the frequency of NPPs with VVER, today we need more stringent requirements for their emergency acceleration and mobility. The operation of NPPs with long-term non-recoverable active power shortage causes a decrease in the speed of the main circulation pumps of NPPs with VVER and a decrease in the coolant flow rate. It is shown that the installation of variable frequency drives of the MCPs at NPP with VVER is appropriate not only to save energy consumption for their drive in partial modes, but also to increase the power of NPP above the nominal (without reducing the reserve before the heat exchange crisis in the reactor core) for the elimination of system accidents, and thus to improve the safety of the NPPs included in the power system.*

Keywords: *nuclear power plant, power system, frequency, emergency control, main circulation pump, variable frequency drive*.

Acknowledgments: *The work was funded by the Russian Foundation for Basic Research (grant no. 17-08-00220 A).*

For citation: Khrustalev VA, Garievskii MV, Rostuntsova IA, Portyankin AV. On the possibility of participation of npps with vverin emergency frequency regulation in power system. *Power engineering: research, equipment, technology*.2019; 21(3): 99-108. (In Russ). doi:10.30724/1998-9903-2019-21-3-99-108.

О ВОЗМОЖНОСТИ УЧАСТИЯ АЭС С ВВЭР В ПРОТИВОАВАРИЙНОМ ЧАСТОТНОМ РЕГУЛИРОВАНИИ В ЭНЕРГОСИСТЕМАХ

В.А. Хрусталев*[1], М.В. Гариевский[2], И.А. Ростунцова[1], А.В. Портянкин[1]
[1]Саратовский государственный технический университет им. Ю.А. Гагарина, г. Саратов, Россия

[2]Саратовский научный центр РАН, г. Саратов, Россия
ORCID: http://orcid.org/0000-0002-1630-926X, khroustalevva@mail.ru

Резюме: *Целью статьи является изучение возможности и целесообразности участия АЭС с ВВЭР в противоаварийном частотном регулировании в энергосистемах с высокой долей атомных энергоблокови, одновременно, снижения расхода электроэнергии на собственные нужды главных циркуляционных насосов на режимах с мощностью ниже номинальной. Для решения этих задач предложено повысить достижимые скорости набора мощности (наброса нагрузки) за счет установки частотно регулируемых приводов ГЦН. Изменение частоты в энергосистеме, вызванное большим дисбалансом между генерацией и потреблением, может поставить под угрозу электрическое оборудование с точки зрения поддержания стабильных и надежных условий эксплуатации. Для атомных электростанций задача предотвращения или локализации аварий представляется еще более важной, чем для ТЭС, т.к. при крупных системных авариях возможно полное прекращение внешнего энергоснабжения собственных нужд АЭС. Таким образом, кроме требований к первичному регулированию частоты АЭС с ВВЭР нужны более жесткие требования к их аварийной приемистости и мобильности. Работа АЭС при длительном невосстанавливаемом дефиците активной мощности вызывает снижение числа оборотов главных циркуляционных насосов АЭС с ВВЭР и уменьшение расхода теплоносителя. Показано, что установка частотно-регулируемых приводов главных циркуляционных насосов на АЭС с ВВЭР целесообразна, в перспективе, не только для экономии расхода энергии на их привод на частичных режимах, но и для повышения мощности энергоблоков АЭС выше номинальной (без уменьшения запаса до кризиса теплообмена в активной зоне реактора) для ликвидации системных аварий, а значит, и для повышения безопасности входящих в ОЭС энергоблоков АЭС.*

Ключевые слова: *атомная электростанция; энергосистема; частота; противоаварийное регулирование; главный циркуляционный насос; частотно-регулируемый привод.*

Благодарности: *Исследование выполнено при финансовой поддержке РФФИ в рамках научного проекта № 17-08-00220 А.*

Introduction

Attempts to normatively involve nuclear power plants (*NPPs*) in the regulatory process, including emergency ones, have been implemented for a long time. One of them was undertaken in 2002 by *RAO UES* Order No. 524 dated September 18, 2002. In accordance with *RAO UES Order* No. 544 “On improving the quality of primary and secondary frequency regulation of electric current in the *UES* of Russia”, the main condition for connecting power plants, including the nuclear ones to the power system is their participation in the primary frequency regulation in the power system.

The requirement for the participation of nuclear power units in the dispatch load schedule has recently been accompanied by the requirement to involve *NPPs* in the primary regulation of the current frequency in the network [1, 2]. In accordance with the standard of the organization of *JSC “SO UES”* (Company's Code STO 59012820.27.120.20.004-2013. Norms for the participation of power units of nuclear power plants in the normalized primary frequency regulation), the maximum required change in power is ± 2% of N_{nom} for the normalized primary regulation of frequency (*NPRF*) and –8 % of N_{nom} for the general primary regulation (*GPRF*), moreover, in the first 10 seconds at least 50% of the required power change should be fulfilled.

However, due a number of reasons noted earlier in the Russian studies [3], this,

apparently, is also not enough, since the requirements do not stipulate the gradually growing need for participation of large nuclear power units in emergency frequency control in the UPS. For such participation, the speeds and ranges mentioned in [3] are clearly not enough. Large hydroelectric power stations (*HPS*) and even hydroelectric pumped storage power stations (*HPSPS*) do not possess maneuvering properties previously assigned to them, mainly due to the large inertial delay at the derivative spillways, as well as due to their overregulation by numerous requirements of the System Operator.

With the development of accidents with a steady decrease of *UPS* current frequency, a serious contradiction is that in *UPS* with a high proportion of nuclear power plants during accidents with a decrease in the frequency, NPPs should increase generation. Unfortunately, *MCPs* make it impossible, since they reduce power and flow rate of the pumped coolant proportionally to the decrease in mains supply frequency. This was noted in [4]. In case of emergencies with increasing frequency (increased generation over the consumer load), such nuclear power plants also run the risk of stopping external and then internal power supply.

One of the most efficient technologies that can fundamentally solve the problem of maneuverability of nuclear power plants with *VVER* is a smooth change in the flow rate of the coolant by controlling the rotation frequency of the *MCP* electric drives (Fig. 1) [5–8].

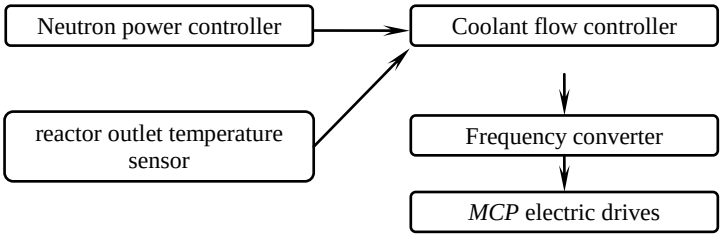

Fig. 1. The block diagram of the flow rate control

Theoretical basis

The *NPP* operation with a long unreplaceble shortage of active power causes a decrease in the number of *MCP* revolutions and a decrease in the coolant flow rate. The use of special frequency converters can eliminate this contradiction [9], since the operation of thyristor converters does not depend on the mains supply frequency. When using them, the power of the unit can be increased to a supernominal value to eliminate system accidents without reducing the supply before the heat transfer crisis in the reactor core [10]. Moreover, this maneuver can be implemented in the long-term mode (monitoring the load) and during participation in the regulation of the emergency frequency drop (dynamic load surge).

Studies have shown that a smooth change in the coolant flow rate by controlling the rotational speed of the *MCP* electric drives allows one to obtain the specified steam parameters and, due to this, the efficient energy characteristics of the turbines during the *NPP* modes of partial power, start and stop, and significantly reduce temperature and pressure fluctuations in the main circuits. This leads to a decrease in the ranges of changes in the average temperature of the core and mitigation of neutron-physical disturbances in the core. At the same time, resource-saving internal devices are achieved, reliability, durability and efficiency are improved by reducing low-cycle fatigue of metal of power equipment and increasing the efficiency of the net unit in the power range of 60–100% of N_{nom} and above the nominal one [11].

The most important *MCP* advantage achieved with a variable frequency drive (*VFD*) is the possibility of an additional (to 4% of N_{nom} achieved by today) power increase up to 7-10% above the nominal level. It is based on the possibility of maintaining the same safety factor before the heat transfer crisis *DNBR (Departure from nuclear boiling ratio)* by

correspondingly increasing the coolant weight velocity [11].

The main circulation pumps are most strictly regulated for operation in case of emergency frequency deviations in the network (for power units with a *VVER*-1000 reactor unit):

A) From 50 to 51 Hz - up to 10 s and not more than 60 s or 10 times in total per year;

B) From 49 to 48 Hz - up to 5 minutes and not more than 26 minutes or 20 times in total per year;

C) From 48 to 47 Hz - up to 1 min and not more than 6 min or 15 times in total per year;

D) From 47 to 46 Hz - up to 10 s and not more than once every three years.

The literature gives an example [3] of the need to increase the rate of the generation shortage elimination in order to maintain the stability of power units operation. This problem becomes especially urgent in connection with the increase in the share of *NPPs* in many *UPSs*, since it is known that in case of system accidents with breakdown of external power supply, there arises a task of reliable and long-term (up to 72 hours) removal of residual heat generation from the reactor core due to internal power supply. Many *NPP* sites with reactor units (RU) of Russian architecture, namely *Akkuyu NPP* (Turkey), *Ruppur NPP* (Bangladesh), *Kudankulam NPP* (India), Jordan, Egypt, Finland, etc. turn out to be "inside" energy regions with relatively weak transmission capacities of electrical connections.

At the same time, it is known that reserves of transmission capacities above 20% of P_{max}, when implemented, can "shift" the calculated phase angle to an unacceptable zone $\Theta>70\div80°$ with occurrence of amplitude fluctuations and even flow vectors, which can cause an avalanche-like accident. If the initial phase angle Θ is 60° and there is a generation shortage in comparison with consumption, and the generators rotors in the *UPS* receiving part are "slowed down a little" when entering the dead zone of the turbine regulators (for example, Δh=–1 rpm), then the receiving system rotors will "turn around" due to a lag to the critical value of the phase angle of 90°. If it is 1 rpm (360° per minute), then a thirty-degree (30°) limit excess of the angle Θ will be achieved in just 5 s [60/(360/30)=5 s], which requires very high loading speeds to prevent a system accident [3].

On the other hand, the relationship between active power N_{act} and frequency in the case of rotating *MCP* injection machines is established from simple reasons:

$$N_{act} = af^3 \text{ or } \frac{dN_{act}}{df} = 2af^2 df = 3\frac{af^3}{f}df = 3N_{act}\frac{df}{f}, \text{ but as } af^3 = N_{act}, \frac{dN_{act}}{N_{act}} = 3\frac{df}{f}.$$

Modern *VVER* reactors also have a certain maneuverability with stabilizing negative feedback between the average temperature of the active zone and reactivity [12–13]. This connection is much more stable today during the operation time due to the addition of gadolinium to the fuel compositions, so the fuel rods today are often called gadolinium fuel rods. Such fuel and the active zone based on it are much more stable and safer during operation.

With tertiary regulation in such *UPSs*, a high emergency response rate (rate of shortage or load surge) should be provided and there should be a margin for the upper power level [3]. However, this reduces the installed capacity utilization factor (*ICUF*). But if *ICUF* is determined by the initial level of nominal power, then its value is sometimes greater than 1. This was shown by the operational practice of a number of *NPP* units in separate temporary operation areas during operation at 104% N_{nom}.

This problem can also be successfully solved when the power units will have a significant margin to increase power above the nominal. Such a reserve is quite real when equipping a *MCP* with a converter with a high-voltage variable frequency drive (converter with *HVVFD*).

In the absence of adjustment range and the occurrence of an unforeseen power shortage

under conditions of full load of the units (generators), an unrecoverable decrease in frequency occurs (Table 1, Fig. 2):

$$f_2 - f_1 = -\Delta f\left(1-\mathrm{e}^{-t/T_f}\right) \text{ or vice versa } f_2 - f_1 = +\Delta f\left(1-\mathrm{e}^{-t/T_f}\right),$$

where T_f is the frequency constant of the power system, T_f =10÷15 s; Δf is the final value of the frequency change due to a shortage (–) or an excess (+) of power, i.e. the difference between generation and load $\Delta P = P_g \pm P_{load}$ in % or infractions $\Delta f\,\% = \frac{\Delta P\%}{K} = \frac{100}{K}\cdot\frac{\Delta P}{P_{load.nom}}$; K =1÷3 is the frequency factor of the power system [14]

$$f_2 - f_1 = -\frac{\Delta P\%}{K}\left(1-\mathrm{e}^{-t/T_f}\right) = \frac{100}{K}\times\frac{\Delta P}{P_{load.\,nom}}\left(1-\mathrm{e}^{-t/T_f}\right)$$

Table 1

Frequency drop in UPS at various factors K and resulting shortage

Power shortage ΔP, %	Frequency drop Δf, Hz (%)		
	K=1	K=2	K=3
2	1 (2%)	0.5 (1%)	0.33 (0.7%)
4	2 (4%)	1 (2%)	0.67 (1.3%)
6	3 (6%)	1.5 (3%)	1.00 (2%)
8	4 (8%)	2 (4%)	1.33 (2.7%)
10	5 (10%)	2.5 (5%)	1.67 (3.3%)

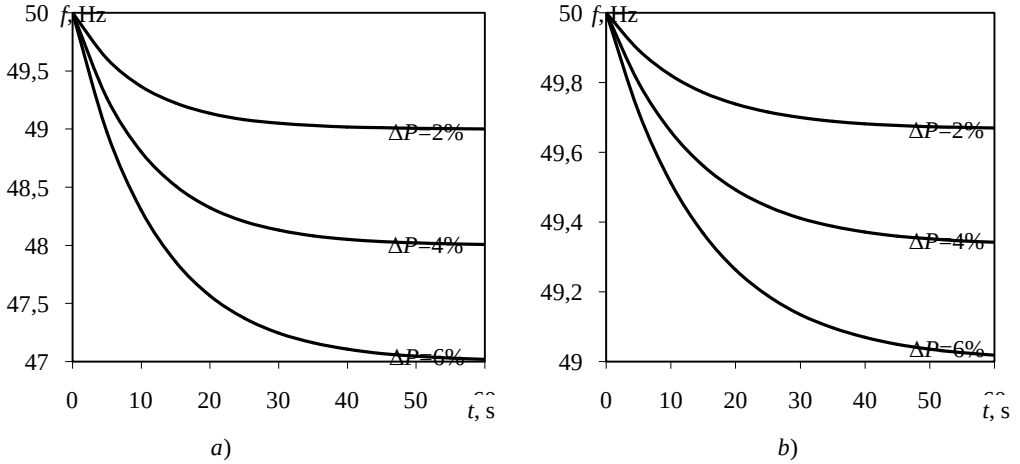

a) *b*)

Fig. 2. The frequency drop after an accident with nonrecoverable power shortage (2, 4 and 6%) for various power systems: a - frequency factor of the power system K=1; b - K=3

Operational experience shows that in most power systems, a sudden loss of 5% of the generating power will not lead to an unacceptably low frequency, while a loss of 20% of the generating power will almost certainly cause the system collapse. The practical limit of sudden losses and, therefore, the maximum power of one generating unit is about 10% of the minimum system demand [15]. Figure 3 shows the change in frequency when a 10% power shortage occurs in the power system (according to [15]).

The transition time from one mode to another when working on a schedule is minutes. In emergency situations that may occur in the power system or at the plant with its equipment, a limited change in power is required in a very short time (gaining up to 10% of the nominal power in no more than 2 s; short-term pulse unloading of the turbine) or a complete shutdown of the unit. Moreover, temperature limitations do not play such an important role [3]. The rate of

change of power is determined mainly by the dynamic characteristics of the units and automatic control systems. The ways to increase the emergency intakes of blocks are fundamentally different from the ways to improve the remaining maneuverable characteristics, and in some cases the improvement of the latter is accompanied by a significant deterioration in the emergency intake. Therefore, although throttle response is certainly one of the components of maneuverability, often maneuverability and throttle response (which is understood as emergency throttle response) are considered as independent characteristics [3].

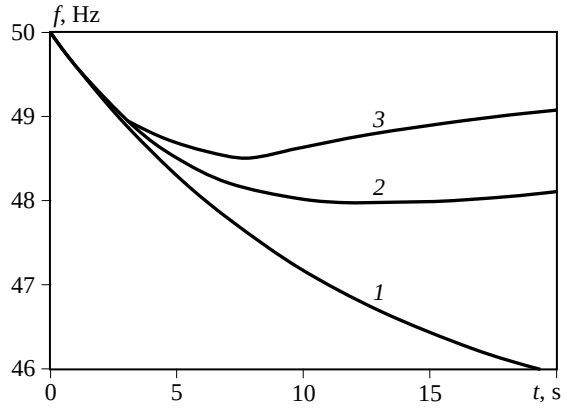

Fig. 3. Frequency change when a 10% power shortage occurs in the power system:

1 - frequency drop; 2 - frequency change with increasing production at operating power units; 3 - with an increase in production and disconnection of a group of consumers

Obviously, a compromise is needed between the growing need for the active participation of *NPP* units with *VVER* reactors in the regulation of load schedules and the desire to keep their average annual installed capacity utilization factor (*ICUF*) high and economically-acceptable [16]. In this regard, in most cases, it may turn out to be economically more profitable to transfer the regulation region to the near-base, that is, to the sub- and supernominal range of permissible power [17, 18]. The speed of power gain by *NPP* power units during the elimination of emergency power shortages in receiving power systems or systems that are separated from the power connection with the power shortage is to ensure a rapid increase in the generated power by 10% in 1–2 s.

For *NPP* units, the task of preventing or localizing systemic accidents seems even more important than for TPPs [15]. This is due to the need for emergency cooling of the reactor after it is stopped. As the lessons of major system accidents show, it is possible to completely stop the external power supply of the station's own needs. Thus, it is obvious that in addition to the requirements for *NPRF NPPs* with *VVER*-1000, 1200 (projects of *NPP*-2006, *NPP-TOI*) nowadays it is necessary to present more stringent requirements for emergency intake and mobility.

In this regard, it is also advisable to transfer the *MCP* in the Ist circuit to a variable frequency drive through a converter device and provide a bypass contactor to return to the normal network in the event of a scheduled repair or failure.

Results

The results of calculations of characteristic values when changing the frequency of the supplying *MCP* current in the range from 46 to 53 Hz are presented in Table. 2. Figures 4 and 5 show the relationships between the coolant flow rate and power of the *VVER*-1000 and *VVER*-1200 power units and the frequency of converter with *HVVFD MCP* in the range of load reduction with the *MCP* frequency drive from ~ 0.92 and increase to ~ 1.06.

Note that, the results shown in rows 5 and 6 of table 2 prove that the formula of *MCP* power proportionality to the 3rd power of frequency gives a fairly accurate result. At the same

time, it should be borne in mind that K=1÷3 is the conditional frequency factor of the power system, depending on the composition of the consumer equipment.

Table 2

The results of calculations of characteristic values when changing the frequency of the supplying MCP current

Characteristics	Frequency, Hz (AC current at MPC)							
	46	47	48	49	50	51	52	53
1. Relative coolant consumption	0.92	0.94	0.96	0.98	1	1.02	1.04	1.06
2. Flow through MPC (*VVER*-1000):								
m^3/h	20010	20445	20880	21315	21750	22185	22620	23055
kg/h*	14407	14720	15034	15347	15660	15973	16286	16600
3. Network pressure, m								
Network 1	59.2	61.9	64.5	67.2	70	72.8	75.7	78.7
Network 2	71.9	75.1	78.3	81.6	85	88.4	91.9	95.5
Network 3	76.2	79.5	82.9	86.4	90	93.6	97.3	101.1
4. Relative power of *MPC*	0.78	0.83	0.88	0.94	1	1.06	1.12	1.19
5. *MPC* power (*VVER*-1000), kW	3582	3821	4070	4329	4600	4882	5174	5479
6. *MCP* pump power according to the exact formula for the network 3	3590	3827	4075	4341	4608	4889	5182	5488
7. *MPC* electrical power (*VVER*-1000), kW**	5840	6229	6636	7059	7500	7959	8436	8933
8. *NPP* power, MW***								
for *VVER* -1000	920	940	960	980	1000	1020	1040	1060
for *VVER* -1200	1104	1128	1152	1176	1200	1224	1248	1272
9. *NPP* power taking into account changes in the *MCP* power, MW								
for *VVER* -1000	925	944	963	981	1000	1019	1037	1056
for *VVER* -1200	1110	1133	1155	1178	1200	1222	1245	1267

* the density of water at p=160 at, t_{av}=305ºC
** power was determined for the ration N_{el}/N_{MPC} for the designed frequency of 50 Hz
*** η_{NPP}=const adopted for a relatively small range of frequency and load conditions 0.92–1.06 of N_{nom}

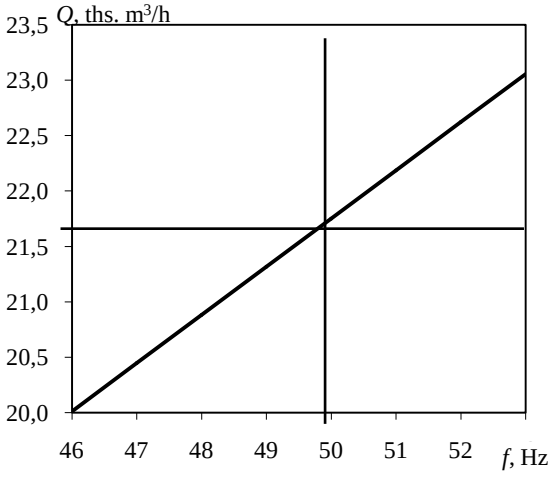

Fig. 4. Relationship between coolant consumption and the frequency of converter with a high-voltage variable frequency MPC drive of the *VVER*-1000 power unit

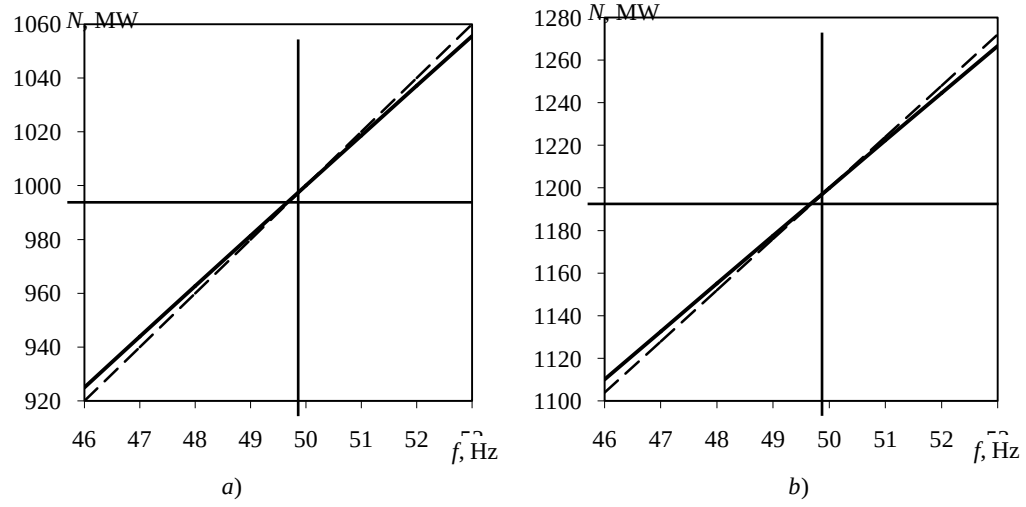

Fig. 5. Relationship between power of the VVER-1000 (a) and the VVER-1200 (b) power units and the frequency of the MCP supply current: —— – taking into account MPC power change; - - - – without taking into account MPC power change

Conclusions

1. If the frequency-controlled drive is used only for saving expenses for pumping the coolant in the load range below N_{nom}, then the *MCP* and the converter are selected according to N_{nom}, and the savings depend on the area below N_{nom} and are associated only with the energy consumption for drive of 4 *MCP*.

2. A greater impact can be achieved when installing MCP and converter devices with high-voltage frequency-controlled drive, providing increased power above N_{nom} and even higher than those achieved today at *VVER*-1000 without *MCP* replacing. This is acceptable due to the fact that with an increase in the coolant flow rate above the calculated (nominal) one, an additional reserve is formed before the heat transfer crisis of the second kind *DNBR*. At the same time, the expenses of *MCP* supplying above N_{nom} will increase, and when adjusting schedules below N_{nom}, they will fall. The final effect in this case will be significantly greater due to the replacement (in a less capital-intensive way) of new construction, as well as due to displacement of gas from the Russian energy sector, as a more valuable export resource. However, in this case, it is necessary to select the *MCP* and *HVVFD* of the highest power.

3. When the frequency changes by 1 Hz, the coolant flow through the *MCP* changes in direct proportion to this change in the 1st degree, that is, through the active zone of the reactor (*VVER*-1000) 4 × 435=1740 m^3/h or at a water density of 720 kg/m^3 for 1253 t/h. Since at the first stage of the assessment it is possible to take the efficiency of nuclear power plants to be constant in a close to basic mode, it is easy to see that such a decrease in flow rate also causes a corresponding change in the thermal power transmitted from the Ist to IInd circuit, i.e. 1 Hz corresponds to 1253/62646=0.02 or a 2% change in thermal power. For a unit with a 1000 MW RU, this corresponds to (at η_{AES}=const) 2% of electric power or 20 MW, for a *VVER-TOI* unit it is equal to 24 MW.

References

1. Non-baseload Operation in Nuclear Power Plants: Load Following and Frequency Control Modes of Flexible Operation. *Nuclear Energy Series*, 2018;NP-T-3.23:173.
2. Technical and Economic Aspects of Load Following with Nuclear Power Plants. Nuclear Development Division. Paris: OECD NEA, 2011. pp 53.
3. Ivanov VA. *Rezhimy moshchnyh paroturbinnyh ustanovok.*. 2nd ed. Leningrad: Energoatomizdat, 1986. 248 p. (In Russ).
4. Bazhanov VV., Loshchakov I.I., Shchuklinov AP. Issledovanie vozmozhnosti ispol'zovaniya na AES akkumulyatorov teplovoj energii pri regulirovanii chastoty toka v seti. *Izvestiya vysshih uchebnyh zavedenij*. YaDERNAYa ENERGETIKA 2013(4): 29–36. (In Russ).
5. Lazarev GB., Novakovskij AN., Sultanov AT. Energoeffektivnoe upravlenie raskhodom teplonositelya v glavnyh konturah reaktornyh ustanovok energoblokov AES. Energiya Edinoj Seti 2015;4(21):70–88. (In Russ).
6. Anishev EY., Lazarev GB. Specific features of the application of frequency converters in power electric drives of circulation pumps *Russian Electrical Engineering.* 2007; 78:560–564. doi: 10.3103/S1068371207100100.
7. Ciufu L., Popescu MO. Introducing energy efficiency in nuclear power plants by using variable medium voltage frequency drives // Advanced Topics in Electrical Engineering (ATEE), 2015 9th International Symposium on. IEEE, 2015. pp. 873-876. doi: 10.1109/ATEE.2015.7133924
8. Barie EZ., Chang C. Application of variable frequency drive on the condensate pump motors of APR1400 nuclear power plants for energy savings .*Journal of International Council on Electrical Engineering*. 2018. 8(1): 179–189. doi: 10.1080/22348972.2018.1515691
9. Basharat A., Korolev VI., Loshchakov II. Sistema upravleniya energoblokom AES s regulirovaniem proizvoditel'nosti glavnyh cirkulyacionnyh nasosov. Izvestiya RAN. Energetika. 2006; 5: 120–130. (In Russ).
10. Hrustalev VA., Garievskij MV. Povyshenie moshchnosti dejstvuyushchih energoblokov s vodo-vodyanymi reaktorami: sostoyanie, problemy i perspektivy. *Academenergo.* 2017; 4:77–88. (In Russ).
11. Lazarev GB., Hrustalyov VA., Garievskij MV.

Литература

1. Non-baseload Operation in Nuclear Power Plants: Load Following and Frequency Control Modes of Flexible Operation, // *Nuclear Energy Series*, 2018.No. NP-T-3.23. p 173.
2. Technical and Economic Aspects of Load Following with Nuclear Power Plants. Nuclear Development Division. Paris: OECD NEA, 2011. pp 53.
3. Иванов В.А. Режимы мощных паротурбинных установок. 2-е изд., перераб. и доп. Л.: Энергоатомиздат. Ленингр. отд-ние, 1986. 248 с.
4. Бажанов В.В., Лощаков И.И., Щуклинов А.П. Исследование возможности использования на АЭС аккумуляторов тепловой энергии при регулировании частоты тока в сети // Известия высших учебных заведений. ЯДЕРНАЯ ЭНЕРГЕТИКА. 2013. № 4. С. 29–36.
5. Лазарев Г.Б., Новаковский А.Н., Султанов А.Т. Энергоэффективное управление расходом теплоносителя в главных контурах реакторных установок энергоблоков АЭС // Энергия Единой Сети. 2015.№ 4(21). С.70–88.
6. Anishev E.Y., Lazarev G.B. Specific features of the application of frequency converters in power electric drives of circulation pumps // *Russian Electrical Engineering*. 2007. Vol. 78, pp. 560–564.
7. Ciufu L., Popescu M.O. Introducing energy efficiency in nuclear power plants by using variable medium voltage frequency drives Advanced Topics in Electrical Engineering (ATEE), 2015 9th International Symposium on. IEEE, 2015. pp. 873–876.
8. Barie E.Z., Chang C. Application of variable frequency drive on the condensate pump motors of APR1400 nuclear power plants for energy savings // *Journal of International Council on Electrical Engineering*. 2018. Vol. 8. N. 1. pp. 179–189.
9. Башарат А., Королев В.И., Лощаков И.И. Система управления энергоблоком АЭС с регулированием производительности главных циркуляционных насосов // Известия РАН. Энергетика. 2006. №5. С. 120–130.
10. Хрусталев В.А., Гариевский М.В. Повышение мощности действующих энергоблоков с водо-водяными реакторами: состояние, проблемы и перспективы // Труды Академэнерго. 2017. №4. С. 77–88.
11. Лазарев Г.Б., Хрусталёв В.А., Гариевский М.В. Перспективы и проблемы применения

Perspektivy i problemy primeneniya chastotnogo regulirovaniya glavnyh cirkulyacionnyh nasosov reaktornyh ustanovok VVER v manevrennyh rezhimah raboty AES .Energetik. 2018; 9:9–14. (In Russ).
12. S.P. Averyanova, AA. Dubov, KB. Kosourov, P E. Filimonov. Temperature regulation and maneuverability of VVER-1000. *Atomic Energy*. 2011; 109(4):246-251. doi:10.1007/s10512-011-9352-1.
13. Aver'yanova SP., Dubov AA ., Kosourov KB., Semchenkov YuM., Filimonov PE. VVER-1200/1300 operation in a daily load schedule. *Atomic Energy*. 2013; 113. (5): 305–313. doi: 10.1007/s10512-013-9637-7.
14. Barzam AB. Avarijnye rezhimy energeticheskih sistem i ih dispetcherskaya likvidaciya. M.: Energiya, 1970. (In Russ).
15. Electric Grid Reliability and Interface with Nuclear Power Plants, Nuclear Energy Series, No. NG-T-3.8, Vienna: International atomic energy agency, 2012. 78 p.
16. Panov S. AES nauchat manevrirovat' Atomnyj ekspert. 2016; 51 (9):26–29. (In Russ).
17. Hrustalev VA., Bashlykov DO., Garievskij MV. Voprosy effektivnosti vysokovol'tnyh chastotno-reguliruemyh privodov GCN energobloka AES s VVER .*Proceeding of the higher educational institutions. ENERGYSECTOR PROBLEMS.* 2017; 19 (7-8):94–104. (In Russ.) doi: 10.30724/1998-9903-2017-19-7-8-94-104.
18. Hrustalev VA., Garievskij MV. Sistemnye preimushchestva modernizacii glavnyh cirkulyacionnyh nasosov AES s VVER ustanovkoj chastotno-reguliruemyh privodov. Trudy Akademenergo. 2019; (1):36–45. (In Russ).

частотного регулирования главных циркуляционных насосов реакторных установок ВВЭР в маневренных режимах работы АЭС // Энергетик. 2018. №9. С. 9–14.
12. S.P. Averyanova, A.A. Dubov, K.B. Kosourov, P.E. Filimonov. Temperature regulation and maneuverability of VVER-1000. Atomic Energy. 2011; 109(4):246-251.
13. Aver'yanova S.P., Dubov A.A., Kosourov K.B., Semchenkov Yu.M., Filimonov P.E. VVER-1200/1300 operation in a daily load schedule // *Atomic Energy*. 2013; Vol. 113. N5. pp. 305–313.
14. Барзам А.Б. Аварийные режимы энергетических систем и их диспетчерская ликвидация. М.: Энергия, 1970. 184 с.
15. Electric Grid Reliability and Interface with Nuclear Power Plants, Nuclear Energy Series, No. NG-T-3.8, Vienna: International atomic energy agency, 2012. 78 p.
16. Панов С. АЭС научат маневрировать // Атомный эксперт. 2016. № 9(51). С. 26–29.
17. Хрусталев В.А., Башлыков Д.О., Гариевский М.В. Вопросы эффективности высоковольтных частотно-регулируемых приводов ГЦН энергоблока АЭС с ВВЭР // Известия высших учебных заведений. ПРОБЛЕМЫ ЭНЕРГЕТИКИ. 2017. №7–8. С. 94–104.
18. Хрусталев В.А., Гариевский М.В. Системные преимущества модернизации главных циркуляционных насосов АЭС с ВВЭР установкой частотно-регулируемых приводов // Труды Академэнерго. 2019. №1. С. 36–45.

Authors of the publication

Vladimir A. Khrustalev – Professor of the Department of Thermal and Nuclear Power Engineering, Yuri Gagarin State Technical University of Saratov.

Michael V. Garievskii – researcher of the Saratov Scientific Center of the Russian Academy of Sciences.

Irina A. Rostuntsova – assistant lecturer of the Department of Thermal and Nuclear Power Engineering, Yuri Gagarin State Technical University of Saratov.

Alexey V. Portyankin – Associate Professor of the Department of Thermal and Nuclear Power Engineering, Yuri Gagarin State Technical University of Saratov.

Received ***April 16, 2019***

UDC 662.611 **DOI:10.30724/1998-9903-2019-21-3-109-116**

FEATURES OF APPLICATION OF THE METHANE-HYDROGEN FRACTION AS FUEL FOR THERMAL POWER PLANT BOILERS

M.A. Taymarov, V.K. Ilyin, E.G. Chiklyaev, R.G. Sungatullin

Kazan State Power Engineering University

Abstract: *The methane-hydrogen fraction is a gaseous hydrocarbon by-product during oil processing for obtaining petroleum products. Until recently, the methane-hydrogen fraction was used as furnace oil in internal technological processes at a refinery. Some of the low-calorie methane-hydrogen fraction was burned in flares. Driven by the prospect of the methane-hydrogen fraction use as a fuel alternative to natural gas for burning in thermal power plants boilers, it became necessary to study the methane-hydrogen fraction combustion processes in large volumes. The conversion of ON-1000/1 and ON-1000/2 furnaces from the combustion of the methane-hydrogen fraction with combustion heat of 25.45 MJ/m^3 to the combustion of the composition with combustion heat of 18.8 MJ/m^3 leads to a decrease in temperature in the flame core for 100 °C as an average. The intensity of flame radiation on the radiant tubes decreases. Therefore, the operation of furnaces during combustion of methane-hydrogen fraction with a low heat of combustion at the gas oil hydro-treating unit is carried out only with a fresh catalyst, which allows lower flame temperatures in the burner.*

The experiments to determine the concentration of nitrogen oxides NOx and the burning rate w of the methane-hydrogen fraction in the ON-1000/1 furnace and natural gas in the TGM-84A boiler, depending upon the heat of combustion Q_n^r were carried out. The obtained results showed that the increase in the hydrogen content H_2 from 10.05 % to 18.36% (by mass) results in an increase in the burning rate w by 45%. The burning rate of natural gas with methane CH_4 content of 98.89% in the TGM-84A boiler is 0.84 m/s, i.e. it is 2.5 times lower than the burning rate of the methane-hydrogen fraction with H_2 content of 10.05%. The distributions of heat flux from the flame q_f over the burner height h in the TGM-84A boiler were obtained in case of natural gas burning and calculation of burning of the methane-hydrogen fraction with a hydrogen content of 10.05% and methane of 28.27%. The comparison of the obtained data shows that burning of methane-hydrogen fraction causes an increase in the incident heat flux q_f at the outlet of the burner.

Keywords: thermal power plants; methane-hydrogen fraction; burning; combustion; heating oil; vacuum gas oil; power boilers; burning rate; temperature; natural gas; heat; flame; burners; boiler.

For citation: Taymarov MA, Ilyin VK, Chiklyaev EG, Sungatullin RG. Features of application of the methane-hydrogen fraction as fuel for thermal power plant boiler. *Power engineering: research, equipment, technology*. 2019; 21(3):109-116. (In Russ). doi:10.30724/1998-9903-2019-21-3-109-116.

ОСОБЕННОСТИ ПРИМЕНЕНИЯ МЕТАНО-ВОДОРОДНОЙ ФРАКЦИИ В КАЧЕСТВЕ ТОПЛИВА ДЛЯ КОТЛОВТЭС

М.А. Таймаров, В.К. Ильин, Е.Г. Чикляев, Р.Г. Сунгатуллин

Казанский Государственный Энергетический Университет, г. Казань, Россия.

***Резюме*:** *Метано-водородная фракция является побочным газообразным углеводородным продуктом при переработке нефти с получением конечных нефтепродуктов. До последнего времени метано-водородной фракция использовалась как печное топливо на НПЗ во внутренних технологических процессах. Некоторая часть низкокалорийной метано-водородной фракции сжигалась в факелах. В связи с перспективной использования метано-водородной фракции как топлива альтернативного природному газу для сжигания в энергетических котлах тепловых электростанций возникла необходимость изучения процессов горения метано-водородной фракции в больших объемах. Перевод печей ОН-1000/1 и ОН-1000/2 с сжигания метано-водородной фракции с теплотой сгорания 25,45 МДж/м^3 на сжигание состава с теплотой сгорания 18,8 МДж/м^3 приводит к снижению температуры в ядре факела в среднем на 100 ℃. Интенсивность излучения факела на радиантные трубы уменьшается. Поэтому эксплуатация печей при сжигании метано-водородной фракции с низкой теплотой сгорания на установке гидроочистки газойля проводится только при свежем катализаторе, допускающем более низкие температуры факела в топке.*

Полученные авторами результаты экспериментов по определению концентрации оксидов азота NO_x и скорости горения w метано-водородной фракции в печи ОН-1000/1 и природного газа в котле ТГМ-84А в зависимости от теплоты сгорания $Q_н^p$ показали, что увеличение содержания водорода H_2 с 10,05 % (по массе) до 18,36 % приводит к росту скорости горения w на 45 %. Скорость горения природного газа с содержанием метана CH_4 98,89 % в котле ТГМ-84А составляет 0,84 м/с, то есть в 2,5 раза ниже скорости горения метано-водородной фракции с содержанием H_2 10,05 %. Распределение тепловых потоков от факела $q_ф$ по высоте топки h в котле ТГМ-84А при сжигании природного газа в сравнении с расчетными данными при сжигании метано-водородной фракции при содержании водорода 10,05 % и метана 28,27 % показывает, что сжигание метано-водородной фракции вызывает рост падающих тепловых потоков $q_ф$ на выходе из топки.

Ключевые слова: *тепловые электрические станции; метано-водородная фракция; сжигание; горение; печное топливо; вакуумный газойль; энергетические котлы; скорость горения; температура; природный газ; теплота; факел; горелки; котел*

Introduction

The methane-hydrogen fraction is formed at the refinery during the process of deep oil processing. It is a by-product that, at its large production volumes is used as fuel for technological furnaces, depending on the composition and its calorific value, and at small production volumes it is burned in flames [1–5]. Nowadays, it is planned to use the methane-hydrogen fraction as a gaseous alternative fuel for power boilers of thermal power plants (*TPP*). However, there are some features of the chemical composition and combustion process of the methane-hydrogen fraction associated with the hydrogen content. This circumstance does not allow utilizing the methane-hydrogen fraction as a substitute for natural gas without a detailed study of its heat and energy characteristics during combustion. Therefore, the study on this topic is relevant.

Object description

The properties of the methane-hydrogen fraction were experimentally studied using the operating furnace equipment *ON*-1000/1 and *ON*-1000/2 of the vacuum gas oil hydrotreatment unit of workshop No. 2 at JSC Ryazan Oil Refining Company. *TGM*-84A boilers were considered as research objects where it is planned to use the methane-hydrogen fraction as fuel instead of natural gas. During the experiments, the *TERA*-50 total radiation radiometers were used to measure the heat fluxes, and dual chromel-alumel thermocouples [6] and the *ThermaCAMP-50F* thermographic camera were used to determine the flame temperature. The composition of the samples of the methane-hydrogen fraction was analyzed in the central factory laboratory. The experimental procedure for measuring the operation parameters of furnaces and the boiler is described in [7]. The operation parameters of the *TGM-84B* boilers during combustion of the

methane-hydrogen fraction were calculated using [8–12]. The scheme of the *ON*-1000/1 and *ON*-1000/2 furnaces, which were used to study the regime parameters of the combustion process of the methane-hydrogen fraction, is shown in Fig. 1.

The dimensions of the burners of the *ON*-1000/1 and *ON*-1000/2 furnaces are: length is 8.6 m, width is 3.3 m, height is 5.5 m. *LE-CFSG-2W* bottom gas burners *1* in the amount of 40 pcs. are made as single pipes with an outlet diameter of gas supply openings of 6.3 mm and provide a flow rate of methane-hydrogen fraction per furnace in the amount from 1000 to 1500 m^3/h.

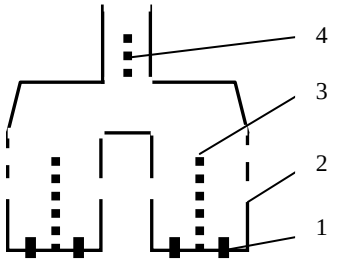

Fig. 1. Cross section of the ON-1000/1 and ON-1000/2 furnaces:
1 - burners; 2 – hatches; 3 – radiate coil; 4 – convective coil

Research methodolo

The heat fluxes and temperatures incident from the flame were measured through the side hatches 2. The heat of combustion of the methane-hydrogen fraction is received in the burner by radiating coils 3 (see Fig. 1), which provide heating of vacuum gas oil in the amount of 177 t/h in a mixture with hydrogen-containing gas in the amount of 97.4 thousand m^3/h and convective coils *4* in the chimney.

The product is heated from 322 °C to 347 °C. The temperature of the outer surface of the radiant coils as measured by *ThermaCAMP-50F* thermographic camera is 530 °C.

The scheme of the *TGM-84A* boiler, for which the possibility of using the methane-hydrogen fraction as a fuel instead of natural gas is considered, is shown in Fig. 2.

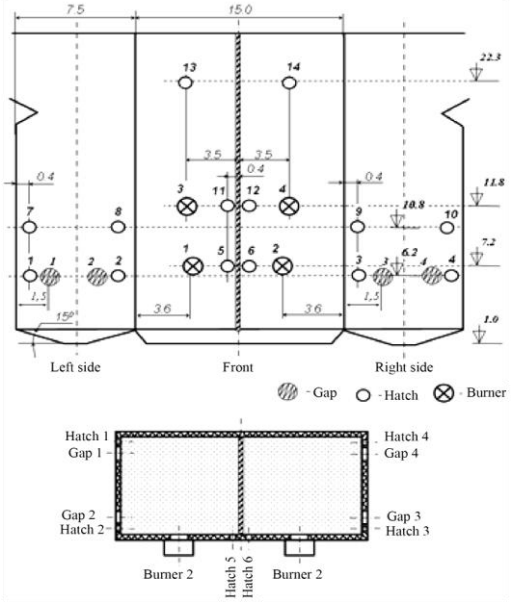

Fig. 2. The scheme of the *TGM-84A* boiler

The *TGM-84A* boiler is a gas-oil drum boiler, which is characterized by steam capacity of 420 t/h, steam parameters of 560 °C and pressure of 14 MPa. The furnace is divided in height into two halves by a partition wall. The burner has the following dimensions: width is 15 m, depth is 7.5 m, height is 27 m. Burners of 2 pcs. are located at heights of 7.2 and 11.8 m. The natural gas consumption for the *TGM-84A* boiler at a nominal capacity of 420 t/h is 32.5 thousand m^3/h for the lower calorific value Q_n^r=34.24 MJ/m^3 and the following gas composition: methane CH_4=98.89% (by mass), ethane C_2H_6=0.47%, propane C_3H_8=0.18%, nitrogen N_2=0.76%. The *HF-TsBK-VTI-TKZ* vortex burners are installed at the *TGM-84A* boiler, with a unit power of 76.7 MW when operating on gas, with peripheral tubular gas distribution: 12 pcs. of the ∅23, and 12 pcs. of the ∅33. The air swirl is dual-flow in hot air and consists of two sections of the axial (central) swirl and one section of the tangential (peripheral) swirl.

Research results

The compositions of the methane-hydrogen fraction used as fuel for the *ON*-1000/1, *ON*-1000/2 furnaces for heating vacuum gas oil at JSC Ryazan Oil Refining Company are given in Table. 1.

Table 1

Compositions of samples of methane-hydrogen fraction used as fuel for furnaces ON-1000/1 and ON-1000/2 for heating of vacuum gas oil at a hydrotreating unit

Sample No.	Density ρ at 760 mm Hg and 0 °C, Q_n^r	Hydrogen, % by mass	Methane, % by mass	Ethene, % by mass	Ethane, % by mass	Propene, % by mass	Propane, % by mass	I-Butane, % by mass	N-Butane, % by mass	Sum of butylenes, % by mass
1	0.440	14.75	18.53	2.06	12.45	3.34	13.26	5.40	9.95	0.71
2	0.380	18.36	18.28	0.86	10.74	1.00	13.34	4.55	12.94	0.20
3	0.444	14.33	24.41	0.54	10.50	0.73	14.45	4.87	13.39	0.35
4	0.431	13.76	36.71	0.55	9.86	0.66	12.48	2.88	7.03	0.36
5	0.481	11.04	44.18	0.50	8.08	0.36	10.56	3.15	8.44	0.00
6	0.400	15.42	31.51	1.07	8.43	0.57	8.04	2.17	4.67	0.06
7	0.445	15.99	3.64	0.03	7.26	0.04	16.54	6.13	18.46	0.00
8	0.434	14.59	24.82	0.73	10.85	1.72	14.71	5.05	8.85	0.24

Sample No.	I-Pentane, % by mass	N-Pentane, % by mass	Hexane and higher, % by mass	Oxygen, % by mass	Nitrogen, % by mass	Carbon oxide, % by mass	Carbon dioxide, % by mass	Hydrogen sulfide, % by mass	Calorific value Q_n^r, MJ/m^3
1	4.21	2.39	0.00	2.95	9.27	0.11	0.58	0.03	20.91
2	4.96	4.78	0.23	1.91	7.25	0.03	0.36	0.20	22.83
3	3.94	4.10	0.19	1.35	5.98	0.03	0.36	0.48	21.27
4	2.39	2.76	0.60	1.79	7.65	0.06	0.18	0.28	23.98
5	3.50	3.06	0.27	1.57	4.93	0.03	0.25	0.10	22.96
6	1.20	1.14	0.00	6.18	19.19	0.03	0.20	0.12	25.45
7	7.32	5.03	0.39	5.06	13.93	0.00	0.18	0.00	18.80
8	3.40	2.58	0.20	3.03	8.29	0.06	0.23	0.67	21.88

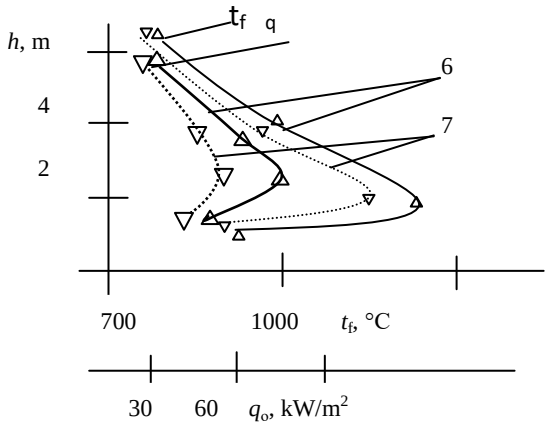

Fig. 3. Distribution of flame temperature t_f and heat flux from internal lining q_o along the height h of ON-1000/1 and ON-1000/2 furnaces when burning methane-hydrogen fraction with the sample compositions No. 6 and 7 at an excess air coefficient of 1.3

The obtained experimental data of the nitrogen oxides NOx concentration and the burning rate *w* of methane-hydrogen fraction in the *ON*-1000/1 furnace and natural gas in the TGM-84A boiler, depending on the calorific value Q_n^r, are given in Table. 2.

Table 2

The obtained experimental data of the burning rate *w* of methane-hydrogen fraction in the ON-1000/1 furnace and natural gas in the TGM-84A boiler, depending on the calorific value Q_n^r

Calorific value Q_n^r, MJ/m^3	Density ρ, kg/m^3	H_2 content, % by mass	CH_4 content, % by mass	Excess air coefficient α	Fuel consumption, m^3/h	Temperature at the outlet from burner T_b, °C	NO_x concentration, mg/m^3 (in terms of α=1.4)	Burning rate *w*, m/s
25.43	0.540	10.1	28.3	1.3	1115	802	84.8	2.02
26.68	0.536	10.05	28.27	1.1	1375	881	63.6	2.11
22.83	0.38	18.36	18.28	1.1	1458	884	56.1	3.07
33.94	0.69	-	98.89	1.1	32500	1150	136	0.84

The distribution of heat fluxes from flame q_f over the burner height *h* in the *TGM-84A* boiler during the combustion of natural gas is shown in Fig. 4. The calculated data for the combustion of the methane-hydrogen fraction with a hydrogen content of 10.05% and methane 28.27% is also presented in Fig.4.

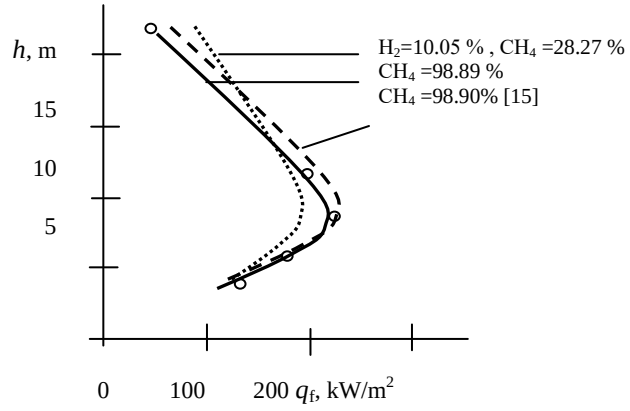

Fig. 4. Heat fluxes from flame q_f over the burner height h in the TGM-84A boiler during the combustion of natural gas (CH_4 =98.89 %) in comparison with the calculated data for the combustion of the methane-hydrogen fraction (H_2=10.05 %, CH_4 =28.27 %) for steam load of 255 t/h and with data [13] for the boiler PK-41

Discussion

As it is seen from table 1, the calorific value of the methane-hydrogen fraction is 55.5–75.1% of the calorific value of natural gas used as fuel for *TPP* boilers. The experimentally obtained distribution of the flame temperature and heat fluxes q_o incident from the inner lining over the height h of the burners in the *ON*-1000/1 and *ON*-1000/2 furnaces when burning the methane-hydrogen fraction with the samples composition No. 6 and 7 at an excess air ratio of 1.3 is shown in fig. 3.

As it can be seen from fig. 3, the conversion of *ON*-1000/1 and *ON*-1000/2 furnaces from the combustion of the methane-hydrogen fraction with combustion heat of 25.45 MJ/m^3 (sample No.6) to the combustion of the composition with combustion heat of 18.8 MJ/m^3 (sample No.7) leads to a temperature decrease in the flame core for 100 °C as an average. Heat fluxes q_o also significantly decrease; therefore, the operation of furnaces during the combustion of the methane-hydrogen fraction with low heat of combustion at the gas oil hydrotreatment unit is carried out only with a fresh catalyst that allows lower flame temperatures in a burner.

As it can be seen from table 2, an increase in the hydrogen H_2 content from 10.05% to 18.36% (by mass) leads to an increase in the burning rate w by 45%. The burning rate of natural gas with methane content of 98.89% in the *TGM-84A* boiler is 0.84 m/s, i.e. 2.5 times lower than the burning rate of the methane-hydrogen fraction with H_2 content of 10.05%. Due to the low heat of combustion of the methane-hydrogen fraction, the concentration of nitrogen oxides NO_x is on average 2 times lower compared to that during combustion of natural gas.

As it can be seen from fig. 4, the burning of the methane-hydrogen fraction (H_2=10.05 %, CH_4=28.27 %) causes an increase in the incident heat fluxes q_f at the outlet of the furnace, which is accompanied by an increase in heat loads of the *TGM-84A* boiler superheater and leads to a decrease in efficiency, compared to that during operation of this boiler on natural gas. However, the distribution of heat fluxes of flame over height h during combustion of the methane-hydrogen fraction is most suitable for a direct-flow boiler *PK-41* [13] of supercritical pressure having a burner chamber pinch.

Conclusions

1. The burning of the methane-hydrogen fraction with a high, over 10% (by mass), hydrogen content instead of natural gas in the *TPP* power boilers is accompanied by increased values of the incident heat fluxes at the outlet of the burner.

2. To reduce the amount of incident heat fluxes at the outlet from the boiler burner, it is necessary to increase the methane share in the methane-hydrogen fraction, which will reduce the rate of fuel combustion and ensure fuel combustion within the burner volume.

References

1. Tajmarov MA., Kuvshinov NE., Stepanova TO. Optimizaciya raboty pechej P-101 i P-101A na ustanovke L-24-600. *Vestnik Kazanskogo tekhnologicheskogo universiteta.2015*.18 (22):50–53 (In Russ).

2. Tanatarov MA., Ahmetshina MN., Faskhutdinov RA. *Tekhnologicheskie raschety ustanovok pererabotki nefti.* M: Himiya, 1987. (In Russ).

3. Sardanashvili AG., L'vova AI. *Primery i zadachi po tekhnologii pererabotki nefti i gaza.* M: Himiya, 1980. 256. (In Russ).

4Manovyan AK. *Tekhnologiya pervichnoj pererabotki nefti i prirodnogo gaza* .M: Himiya, 2001. 568. (In Russ).

5. Tajmarov MA., Dodov IR. Ustanovka dlya proizvodstva sinteticheskogo motornogo topliva.. *Vestnik kazanskogo tekhnologicheskogo universiteta*. 2015; 18(8):162–166.

6. Trembovlya VI., Finger ED., Avdeeva AA. Teplotekhnicheskie ispytaniya kotel'nyh ustanovok.2 nd ed. Moscow: Energiya 1977. (In Russ).

7. Tajmarov MA., Ahmetova RV., Lavirko YuV. Sungatullin RG., Zheltuhina ES. Snizhenie vrednyh vybrosov v atmosferu oksidov azota kotlami TES. *Izvestiya KGASU* 2017.39(1):180–188. (In Russ).

8. Zel'dovich YaB., Sadovnikov PYa., Frank-Kameneckij DA. Okislenie azota pri gorenii. M.-L: ANSSSR 1947 (In Russ).

9. Knorre GF., Aref'ev KM., Bloh AG., Nahapetyan EA., Paleev II., Shtejnberg VB. Teoriya topochnyh processov. M.-L.: Energiya 1966. (In Russ).

10. Bloh AG. Teploobmen v topkah parovyh kotlov. L.: Energoatomizdat 1984. (In Russ).

11. Aksyutin O., Ishkov A., Romanov K., et al. New Methane-Hydrogen Fuel Technology and its Potential Application in the Gas Industry. Development and Innovation in Focus All Eyes Turn to Perth for LNG 18. Report of the International Gas Union, April–September 2016, P. 74–76.

12. Kim JJ. Adsorption equilibria and kinetics of propane and propylene on zeolite 13x pellets. Microporous and mesoporous materials. 2019; 274: 286-298.

13. Mirel I., Pentia D., Florescu C., et al.. Water treatment from swimming pool, piscine and swimming basins. *Scientific Bulletin of Politechnica*

Литература

1. Таймаров М.А., Кувшинов Н.Е., Степанова Т.О. Оптимизация работы печей П-101 и П-101А на установке Л-24-600 //Вестник Казанского технологического университета. 2015. №.22(18).С.50–53.

2. Танатаров М.А., Ахметшина М.Н., Фасхутдинов Р.А. Технологические расчеты установок переработки нефти. М: Химия,1987. 352 с.

3. Сарданашвили А.Г., ЛьвоваА.И. Примеры и задачи по технологии переработки нефти и газа. М: Химия, 1980. 256 с.

4. Мановян А.К. Технология первичной переработки нефти и природного газа .М: Химия, 2001. 568 с.

5. Таймаров М.А., Додов И.Р. Установка для производства синтетического моторного топлива.// Вестник казанского технологического университета.2015. № 8(18). С.162–166.

6. Трембовля В.И., Фингер Е.Д., Авдеева А.А. Теплотехнические испытания котельных установок. 2-е изд., перераб. и доп. М.: Энергия, 1977, 297с.

7. Таймаров М.А., Ахметова Р.В., Лавирко Ю.В. Сунгатуллин Р.Г., Желтухина Е.С. Снижение вредных выбросов в атмосферу оксидов азота котлами ТЭС. // Известия КГАСУ. 2017. №1(39). С.180–188.

8 Зельдович Я.Б., Садовников П.Я., Франк-Каменецкий Д.А. Окисление азота при горении. М.-Л.: Издательство АНСССР, 1947. 147 с.

9. Кнорре Г.Ф., Арефьев К.М., Блох А.Г., Нахапетян Е.А., Палеев И.И., Штейнберг В.Б. Теория топочных процессов. М.-Л.: Энергия, 1966. 492 с.

10.Блох А.Г. Теплообмен в топках паровых котлов. Л.: Энергоатомиздат, 1984. 240 с.

11. Аксютин О., Ишков А., Романов К., у ал. Новая технология метано-водородного топлива и ее потенциальное применение в газовой промышленности. Развитие и инновации в фокусе для СПГ 18. Доклад Международного газового союза, апрель-сентябрь 2016 г.С. 74–76.

12. Kim J.J. Adsorption equilibria and kinetics of propane and propylene on zeolite 13x pellets. Microporous and mesoporous materials. 2019. Vol.

University of Timisoara. 2015; 60(2):79-83.
14. World Energy Outlook / International Energy Agency 2018:46.
15. Steadier Boom for the Oil Sands // Petroleum Economist. 2016. June. P. 8–10.
16. Short-term Canadian Natural Gas Deliverability 2015–2018. P. 6

274. P. 286-298.
13. Mirel I., Pentia D., Florescu C., Ionescu D. Water treatment from swimming pool, piscine and swimming basins/ Scientific Bulletin of Politechnica University of Timisoara. 2015. Vol. 60, № 2.pp 79-83.
14. World Energy Outlook / International Energy Agency. 2018 pp 146.
15.Steadier Boom for the Oil Sands // Petroleum Economist. 2016. June. Pp. 8–10.
16.Short-term Canadian Natural Gas Deliverability 2015–2018. P. 63.

Authors of the publication

Mikhail A. Taymarov – Kazan State Power Engineering University.

Vladimir K. Ilyin – Kazan State Power Engineering University.

Evgeniy G. Chiklyaev– Kazan State Power Engineering University.

Rais G. Sungatullin– Kazan State Power Engineering University.

Received ***December 11, 2018***

UDC 631.344 (088.8) **DOI:10.30724/1998-9903-2019-21-3-117-125**

MODELING OF THERMAL STRESSES DESTROYING THE POROUS COATING OF HEAT-EXCHANGE SURFACES OF POWER PLANTS

A.A. Genbach[1], D.Yu. Bondartsev[1,2]

[1]Almaty University of Power Engineering and Telecommunications, Almaty, Republic of Kazakhstan
[2]JS Trest Sredazenergomontazh, Almaty, Republic of Kazakhstan
d.bondartsev@saem.kz

Abstract: *Modeling of the low heat conductive low-porous capillary porous coatings and metal (copper, stainless steel) surfaces (base layer) was studied. Heat and mass transfer in the porous coatings moved with excessive liquid due to the combined action of capillary and mass forces. The dynamics of vapor bubble was described along with their heat-dynamic properties, which were observed by the optic research methods. Finding solution for the thermoelasticity allowed to reveal the influence of the specific heat flow and heat tension of compression and stretching depending on time of supply and sizes of pulled particles at the time of the system limit state as to "porous coating - base layer". The theory was confirmed by the trial, which was observed by camcorder SKS-1M.*

Keywords: *capillary-porous coatings, thermoelasticity, compression stresses, tensile stresses, model.*

For citation: Genbach AA, Bondartsev DYu. Modeling of thermal stresses destroying the porous coating of heat-exchange surfaces of power plants. *Power engineering: research, equipment, technology*. 2019; 21(3):117-125. (In Russ). doi:10.30724/1998-9903-2019-21-3-117-125.

МОДЕЛИРОВАНИЕ ТЕРМИЧЕСКИХ НАПРЯЖЕНИЙ, РАЗРУШАЮЩИХ ПОРИСТЫЕ ПОКРЫТИЕ ТЕПЛООБМЕННЫХ ПОВЕРХНОСТЕЙ ЭНЕРГОУСТАНОВОК

А.А. Генбач[1], Д.Ю. Бондарцев[1,2]

[1]Алматинский Университет Энергетики и Связи, г. Алматы, Казахстан
[2]АО «Трест Средазэнергомонтаж», г. Алматы, Казахстан
d.bondartsev@saem.kz (http://orcid.org/0000-0001-8778-7851)

Резюме: *Исследовано моделирование плохотеплопроводных малопористых капиллярно-пористых покрытий и металлических (медь, нержавеющая сталь) поверхностей (подложка). Тепломассоперенос в капиллярно - пористых покрытиях протекал с избытком жидкости за счет совместного действия капиллярных и массовых сил. Описана динамика паровых пузырей и их термогидравлические характеристики, наблюдаемые оптическими методами исследования. Разработана физическая модель процесса тепломассопереноса в реальной пористой структуре. Для такой модели решена задача термоупругости и определено предельное состояние системы хорошо - и плохотеплопроводных материалов*

(пористое покрытие на металлической подложке). Определены тепловые потоки, подводимые к поверхности, время их воздействия на создание разрушающих напряжений, размеры отрывающихся частиц и глубины проникновения температурной волны в подложку. Тепловые потоки подсчитывались от времени взрывообразного появления первого зародыша (10^{-8} с) до времени разрушения материалов (10^{2} - 10^{3} с), т.е. от времени релаксации до времени, описывающего микропроцесс. С увеличением величины q в нагреваемом слое и, следовательно, уменьшением времени нагрева τ, растет роль напряжения сжатия. Несмотря на высокую сопротивляемость сжатию, разрушение от сжимающих термонапряжений происходит в более благоприятных условиях мгновенного и в малых объёмах. Теория подтверждена экспериментом, полученным в результате наблюдения камерой СКС-1М. Разрушение капиллярно-пористых покрытий происходит в результате потери устойчивости в тонком слое, прилежащим к свободной поверхности. Поэтому рассматривалось напряженное состояние верхнего слоя, толщина которого зависит от коэффициента теплоотдачи, структуры покрытия и подложки (металлической парогенерирующей поверхности).

Ключевые слова: *капиллярно-пористые покрытия, естественные минеральные среды, термоупругость, напряжения сжатия, напряжения растяжения, модель, элементы энергоустановок, тепломассообмен.*

The actual task in power plants is to create the degree of cooling of high-tension parts and assemblies. Modeling of capillary porous coatings and analogy of the processes taking place in them allow to reveal the mechanism of heat transfer at vaporization of liquids, to establish the zones of fatigue cracks occurrence and development in the centers of steam embryo activation, to study natural and artificial porous coatings applied to metal fences (substrates) up to the onset of the ultimate state of materials.

In our works [1-3] it is shown that different models given in [4-12] describe different modes of boiling and do not contradict each other.

On the basis of experimental and theoretical studies [4-12] dynamic models of heat transfer intensification at boiling on a porous surface are constructed. Developed surfaces contain tied internal cavities in the form of rectangular channels and small pores connecting the channels with the volume of liquid.

The ratio of the latent heat flow $\left(\frac{\pi}{6}\bar{D}\,r\rho\,\bar{n}\bar{f}\right)$ to the total heat flow could be larger (2 to 5) times for a developed surface than for a conventional surface with a specific heat flow up to 1×10^4 W/m^2. At high heat flows, this ratio decreased. The deviation of some data from estimated data reached 300%. The following indications are used in the formula: $\bar{D}$ – average detachable diameter of vapor bubbles in the porous structure; r – specific heat of evaporation; p_v - vapor density; $\bar{n}$ – average nucleation centers density; $\bar{f}$ – average frequency of vapor bubble generation and silence.

Let's develop a physical model for transferring the specific heat flow q through the steam-generating surface (wall or substrate) which is covered by a capillary-porous structure (Fig. 1).

Processes of heat and mass transfer in the porous coating take place with the liquid overflow $\tilde{m} = m_l / m_v$ due to the action of the potential of pressure developed by capillary and mass forces ΔP_{cap+g}.

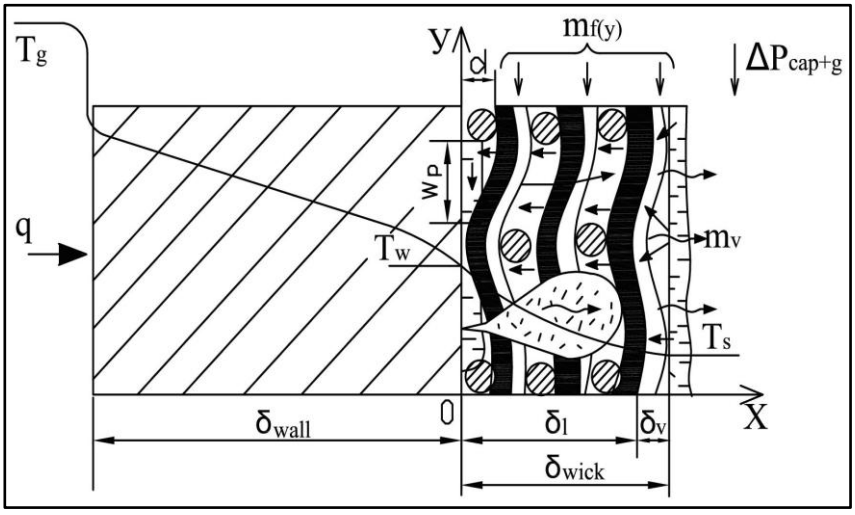

Fig. 3 Physical model of the heat and mass transfer in the real porous structure of coatings under the liquid overflow: Straight lines – fluid movement; wavy lines – steam movement: q – specific heat flow, W/m^2; T_g, T_w, T_s – temperatures of gases, wall (substrate) and saturation (^oC); δ_{wall}, δ_l, δ_v, δ_{wick} – thicknesses of wall, liquid, vapor, wick (m); m_f (y), m_v – flows of liquid and steam, (kg/s); ΔP_{cap+g} – current dynamic capillary and mass pressure (N/m^2);d – grain size (m); w_p – width of the porous material cell (m).

In the cooling system under investigation, with small heat flows, heat is transfered due to conductive heat transmission; its value is the higher, the greater the effective thermal conductivity of the structure moistened with the liquid and the thermal conductivity of the shell. The fluid flow has a smooth nature; there are no vapor bubbles and related perturbation processes on the liquid surface. The liquid intensely evaporates from the menisci with small excesses of the coolant; when a liquid overflow increases, the evaporation begins from the surface of the flowing films.

In a certain heat flow that is smaller than the parameter $\tilde{m} = m_l / m_v$, a disruption in the smooth wavy flow of the liquid film begins, and separate vapor bubbles appear. Several active structure cells are constantly acting generation centers. The onset of liquid boiling ($\Delta T_{o.b.}$) depends on a lot of conditions and design parameters and is determined by the equation for this variation $\Delta T_{o.b.}$, which corresponds to the heat flow $q_{o.b.}$ The decrease in the flow rate of the cooling liquid $m_{l(y)}$ or the increase in the heat inflow q lead to a rapid growth of evaporation centers $\bar{n}$.

A zone of transition to the developed bubble boil is not high due to the high rate of growth of the active vapor generation centers $\bar{n}$. A further growth of the heat load q leads to the stable operation of a large number of active bubble generation centers and their uniform distribution throughout the steam-generating surface. However, certain critical conditions lead to a burnt-out and a surface burn-over. Therefore, the analogy in the processes of deliberate destruction of brittle materials and the burnt-out allows to model such processes and identify the mechanism thereof [1-3].

To learn the destruction process mechanism, experiments were carried out with the use of photoelasticity and holography methods [1]. The stress state of the models was estimated at similar times by photographic recording of isochromic patterns and counting the band order n at different points in the directions under study.

The solution of the problem of thermoelasticity makes it possible to determine the limit state of the medium for a porous coating and a metal vapor-generating surface [1-2].

In case of thermal destruction of poorly heat-conducting coatings with low porosity and a a metal wall (substrate), it is required to identify the effect of the specific heat flux (q) applied to the surface and the time of its action τ on the formation of destructive stresses (σ), the granulometric

composition of shell (size of detached particles), as well as the depth of penetration of the temperature perturbation (δ) for the metal.

If q increases in a very short time interval (τ), the dynamic effects become very significant and compression stresses (σ_c) reach large values which are often several times higher than the tensile strength of the material in compression. Therefore, it is necessary to take into account these stresses in the mechanism of thermal destruction of the material. We have to find out what type of stress σ_i reaches before its limit values.

Let's consider a plate with the thickness of 2h. The constant ultimate heat flux (q) is supplied to the surface z =+h, starting from the timepoint t = 0. The bottom surface z = -h and the plate side edges are thermally insulated.

Thermal conductivity equation with limiting and initial conditions can be written in the form:

$$\alpha_w \frac{\partial T}{\partial z} = \frac{\partial T}{\partial \tau}, \; T = 0, \tau < 0 \tag{1}$$

$$\lambda_w \frac{\partial T}{\partial z} = q, \quad z = +h;$$

$$\lambda_w \frac{\partial T}{\partial z} = 0, \quad z = -h,$$

where α_w, λ_w – coefficients of thermal diffusivity and thermal conductivity of the wall (substrate).

The temperature distribution along the thickness depends on thermophysical properties of the material, its heat flux value and feeding time [2]:

$$T\left(\frac{z}{h};\tau\right) = q\left\{\frac{M}{2(c\lambda\rho)}\tau + \frac{\frac{3z}{h}+\frac{6z}{h}-1}{12M} - \frac{4}{\pi M}\sum\frac{(-1)}{n}\exp\left[-n\,\frac{\pi M}{4(c\lambda\rho)}\tau\right]\cos\left[\frac{n\pi}{2}\left(\frac{z}{h}+1\right)\right]\right\}, \tag{2}$$

where $M = \frac{\lambda_w}{h}$; n – positive numbers; c – heat capacity; ρ – wall density.

Using the known temperature distribution in the plate, we can find the thermal tension and compression stresses arising at a certain time t at various depths from the surface δ_i = (h = z_i) for a given value of the heat flux (q), since the plate with a variable temperature is in the plain stress condition.

$$\sigma_{xx} = \sigma_{yy} = -\frac{\alpha E}{(1-\nu)}T\left(\frac{z}{h};\tau\right) + \frac{1}{(1-\nu)2h}\int \alpha E T\left(\frac{z}{h};\tau\right)dz, \tag{3}$$

where the first term is the component of the compression stress, and the second term is the tension stress. α – linear expansion factor; E – Young's modulus (elasticity modulus); ν – Poisson ratio (lateral contraction);

If we are given the limit values of tension ($\sigma_{lim.tens.}$) and compression ($\sigma_{lim.comp.}$) stresses for coating and metal, we obtain the dependence of the heat flux (q) required for destruction, based on the time of supply (τ) and the depth of penetration (δ). In addition, when we equate temperatures on the plate surface to the melting temperature $T_{m.}$ of coating and metal, we find the values of specific heat fluxes necessary to melt the surface layer for a different period of action thereof (q_1), i.e. in each case, we have functional dependences of the heat flux on the time it affects the coating and the metal surface.

The causes of the destruction of boiler-turbine parts depend on the prehistory of the development of cracks in the stress raiser (relaxation zone) [4-8, 9-12]. Counting must be conducted from the time of the explosive appearance of the nucleating center of vapor (the time interval is 10^{-8} s to 10^{-3} s). The energy of the spontaneous appearance of a vapor bubble is a value close to the value which is constant (invariant) with respect to time of its growth. It is spent to maintain the nucleating center with a radius of R_{kr} and prevents it from collapsing (q reaches up to 10^8 W/m^2). At this time interval, a thermodynamic equilibrium is established for the transition from microprocesses (microparticles and clusters with sizes of (10^{-7}÷10^{-8}) m (nanoparticles) of separate (single) individual bubbles to processes described by the behavior of a large number of bubbles, using integrated characteristics ($\bar{q}, \bar{\alpha}, \overline{\Delta T}, \overline{\Delta P}, \bar{w}$), where $\bar{\alpha}, \overline{\Delta T}, \overline{\Delta P}, \bar{w}$ is average values of heat transfer coefficients, temperature and hydro-gas dynamic pressures and flow velocity. The presence of stress concentrators where the active vapor phase is generated, significantly reduces the $\sigma_{lim.comp.}/\ \sigma_{lim.tens.}$ ratio, and this value can be equal (1÷2), including for energy steels. We have also to take into account the presence of other stress raiser, the cyclicity of loads during starting and stopping modes of equipment operation, which lead to fatigue cracks (stresses).Consequently, there's a high possibility that $\sigma_{lim.tens.} \approx \sigma_{lim.comp.}$, and $\sigma_{lim.tens.}$ reaches 10 MPa and becomes of the same order for porous coatings.

The processes of death as well as the nucleation have also explosive nature ($\tau = 10^{-8}$÷10^{-6} s), which leads to the emergence of cumulative phenomena, which along with the corrosive and electrical processes destroy the stress raiser (active generation center) due to erosion processes, bringing its size to the critical crack. In the case of instant condensation of vapor in the cavity (hole), its volume instantaneously disappears and a powerful cumulative effect (cavitation) is formed. In this case, shock waves penetrate into the the parts and cracks develop, where an oxygen enters.

At the moment of "birth" of a bubble or a drop, α is up to 1x10^5 W/m^2 at a vapor temperature (500 ÷ 565) ^{o}C, ΔT reaches 500 ^{o}C, and q values acting at the bottom of the bubble ("dry" spot zone) is up to 5x10^7 W/m^2. If we take into account that the individual vapor bubble generates q 10 times more than its integral value [3], then the total q is 5x10^8 W/m^2, which is represented in q = q (τ, δ) in the figures. The greater the penetration depth of the heat wave (or δ of the detached particle from the porous coating), the longer it will take to destroy the parts by stresses (Figures 2-4).

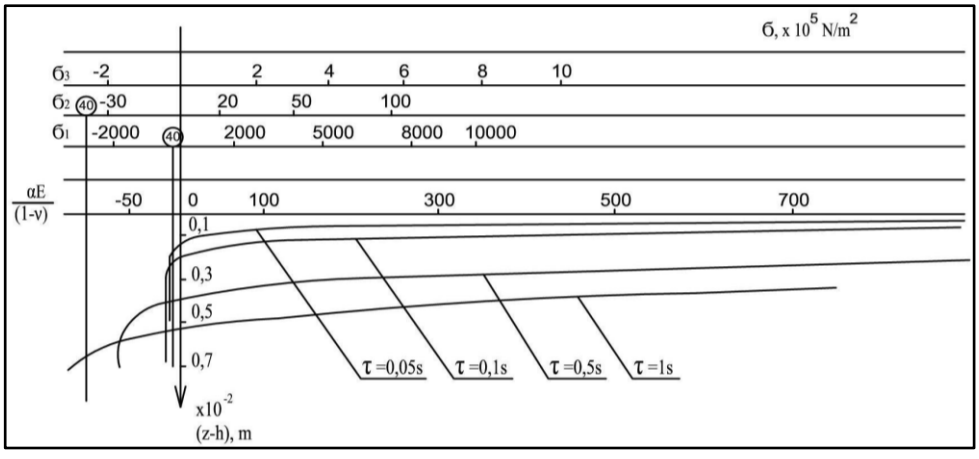

Fig. 2 Stress diagrams σ_i for the quartz plate (coating) thickness for various heat fluxes q_i and the time of their action τ: q_1 = 8.8x10^7 W/m^2; q_2 = 0.12x10^7 W/m^2; q_3 = 0.008x10^7 W/m^2;
40 – yield strength

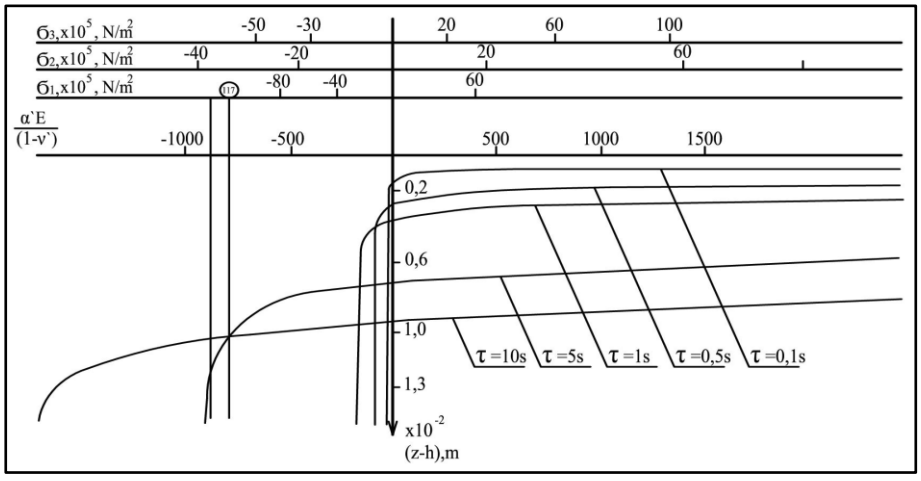

Fig. 3 Stress diagrams for granite coating thickness for different heat fluxes q_i and time τ of their action: $q_1 = 0.142x10^7$ W/m^2; $q_2 = 0.042x10^7$ W/m^2; $q_3 = 0.0075x10^7$ W/m^2; 117 – yield strength: σ_i, = $x10^5$ H/m^2, E = $x10^5$ H/m^2.

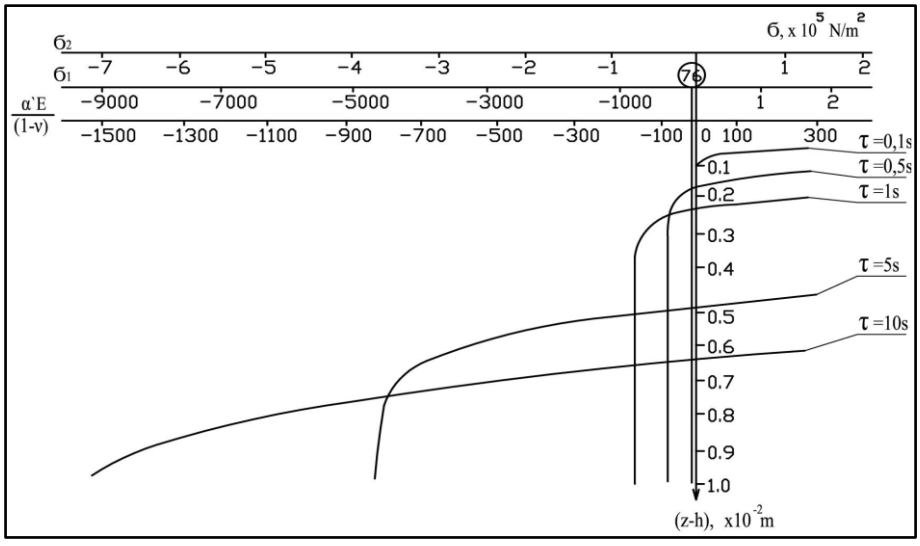

Fig.4 Stress diagrams for the teschenite plate (coating) thickness for different q_i and τ values: $q_1 = 6.6x10^6$ W/m^2; $q_2 = 0.1x10^4$ W/m^2; 76 – yield strength

The relationship between compressive and tensile stresses is shown in Fig. 2-4. It is stress diagrams (coating) within the plate for various time intervals from the beginning of the process under consideration. At small values of τ and order of 10^{-2} s, only compression stresses arise. Starting from $\tau \sim 10^{-1}$ s, in some region of Δ ($h-z_i$), the compression stress turns into a tensile stress, and for different time intervals it is at different depths from the plate surface.

With an increase in q in the heated layer, and consequently a decrease in the heating time τ, the role of the compression stress increases. Despite the high resistance to compression, the destruction from compressive thermal stresses occurs under more favorable conditions of instantaneously and in small volumes.

For heated vapor-generating surfaces, the film boiling was established and the temperature of the surface increased sharply to a value $T_{m.}$, as a result of the change in the boiling condition.

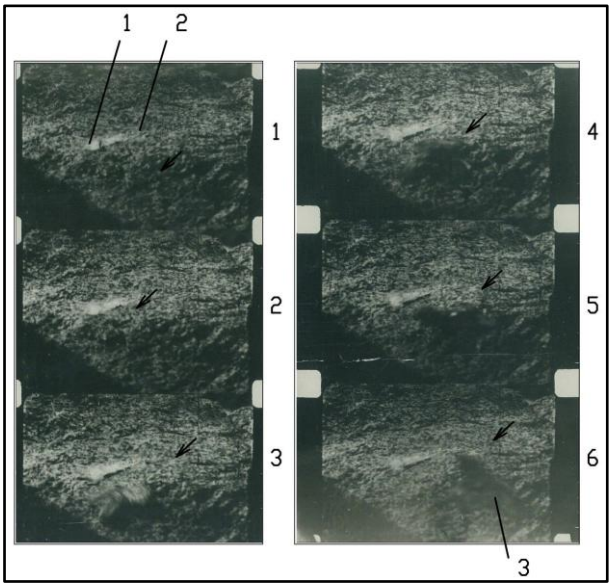

Fig. 5. Fragment of a high-speed shooting of the destruction of a teshenite with a rocket flame-jet burner with a specific heat flux equal to 1.2×10^6 W/m^2. A shell with a size of $2.5x10^{-3}$ forms for 2.2 s.

A line of destruction of "equal possibilities" is clearly visible (arrow): 1 – capillary-porous coating; 2 – particle (shell) detached from the coating; 3 – line of destruction of "equal possibilities". Cinemagram of particle flight in time: τ_1 to τ_6: 1 = 0 s; 2 = 5/1500 s; 3 = 10/1500 s; 4 = 15/1500 s; 5 = 20/1500 s; 6 = 25/1500 s.

A calculation was made of the specific energy (Q) of the destruction of a unit volume of quartz, granite, and teshenite coatings. The energy Q was calculated, depending on the thickness δ of the detached particles. Curves have pronounced minima.

For quartz coating, the minimum energy loss is $Q=0.5x10^9$ J/m^3 for $\tau = (0.1 \div 1)$ s, $\delta_i = (0.1 \div 0.25)x10^{-2}$ m.

For granite coating: $Q=2.5x10^9$ J/m^3 for $\tau = (0.1 \div 5)$ s, $\delta_i = (0.1 \div 0.3)x10^{-2}$ m. For $q=0{,}1x10^7$ W/m^2 and $\delta = (0.2 \div 1.5)\ x10^{-2}$ m, $Q = 2.5x10^9$ J/m^3.

For teshenite coating: $Q=0.5x10^9$ J/m^3 for $\tau = (0{,}1 \div 5)$ c, $\delta_i = (0{,}1 \div 0{,}4)x10^{-2}$ m, where the ratio of limit normal compression and tensile stresses varied from 20 to 30. The presence of microcracks in the coating monolith reduces its compressive strength in the vicinity of this crack so that the compressive strength can be only 2 times greater than the tensile strength.

Curves (Q = f (q)) with their minima with increasing of δ_i move in the direction of the decrease in q, and for the thermal destruction of brittle coatings, a lower energy capacity Q is required.

Conclusion

The danger of the appearance of limit thermal stresses is great at the moment of startup and shutdown of power equipment at power plants. These stresses arise primarily in the places of concentrators, which are active vapor phase centers or condensate formation centers. The capillary-porous structure can be both of natural origin (salt deposits, tarnishes) and artificially created with well and poorly heat-conducting materials in a wide range of porosity and permeability of 3% to 90%. Structures can play a modeling role and serve as a high-intensity and forced cooling system. For example, teschenite porous coatings with a 5-fold greater lineal expansion coefficient and a 10-fold lower thermal conductivity factor and approximately the same melting point in comparison with energy steels serve as a modeling material. They are the most viscous with a porosity of up to 30%.

References

1. Genbach AA., Bondartsev DYu., Iliev IK. Heat transfer crisis in the capillary-porous cooling system of elements of heat and power installations. Thermal Science2019;23(Pt2):849-860.
https://doi.org/10.2298/TSCI171016139G
2. Genbach AA., Bondartsev DYu., Iliya K. Iliev. Investigation of a high-forced cooling system for the elements of heat power installations. *Journal of machine Engineering* . 2018; 18 (2):106-117.
3. Genbach AA., Bondartsev DYu., Iliev IK. Modelling of capillary coatings and heat exchange surfaces of elements of thermal power plants. *Bulgarian Chemical Communications*. 2018; 50:133-139.doi:10.5604/01.3001.0012.0937.
4. Jamialahmadi M. Experimental and Theoretical Studies on Subcooled Flow Boiling of Pure Liquids and Multicomponent Mixtures, Intern. J *Heat Mass Transfer*. 2008; 51 (9-10): 2482–2493 doi: 10.1016 / j.ijheatmasstransfer.2007.07.052.
5. Ose Y., Kunugi T. Numerical Study on Subcooled Pool Boiling, Progr. In Nucl. Sci. and Technology, 2011; 2:125–129.
6. Krepper E. CFD Modeling Subcooled Boiling-Concept, Validation and Application to Fuel Assembly Design, Nucl. Eng. and Design, 2007; 237 (7.):716–731.doi: 10.1016 / j.nucengdes.2006.10.023
7. Ovsyanik AV. Modelirovanie processov teploobmena v kipyashchih zhidkostyah, Gomel'skij gosudarstvennyj tekhnicheskij universitet im. P.O. Suhogo, Gomel': Belarus', 2012. (In Russ).
8. Alekseik OS., Kravets VYu. Physical Model of Boiling on Porous Structure in the Limited Space.Eastern-European *Journal of Enterprise Technologies.* 2013; 64 (4):26–31.
9. Polyaev VM., Majorov VA., Vasil'ev LL. *Gidrodinamika i teploobmen v poristyh elementah konstrukcij letatel'nyh apparatah.* M.: Mashinostroenie 1998. (In Russ).
10.Kovalev SA., Solov'ev SL. *Isparenie i kondensaciya v teplovyh trubah*. M.: Nauka, 1989. (In Russ).
11 Kupetz M., Heiew Jeni E., Hiss F. Modernization and prolongation of operation of steam turbine power plants in Eastern Europe and Russia / *Thermal Engineering.* 2014; 6: 35–43. (In Rus.)
12. Grin' EA. Vozmozhnosti mekhaniki razrusheniya primenitel'no k zadacham prochnosti, resursa i obosnovaniya bezopasnoj ekspluatacii teplomekhanicheskogo energooborudovaniya .*Teploenergetika*. 2013; 1:25–32. (In Russ).

Литература

1. Genbach A.A., Bondartsev D.Yu., Iliev I.K. Heat transfer crisis in the capillary-porous cooling system of elements of heat and power installations .// Thermal Science. 2019. Vol. 23, Pt 2 A, pp. 849-860.
2.Genbach A.A., Bondartsev D.Yu., Iliev I.K. Investigation of a high-forced cooling system for the elements of heat power installations, Journal of machine Engineering, 2018.Vol. 18, №2. pp. 106-117.
3.Genbach A.A., Bondartsev D.U., Iliev I.K. Modelling of capillary coatings and heat exchange surfaces of elements of thermal power plants. // Bulgarian Chemical Communications, 2018.Vol. 50, Special Issue G. pp. 133 – 139.
4.Jamialahmadi M.. Experimental and Theoretical Studies on Subcooled Flow Boiling of Pure Liquids and Multicomponent Mixtures, Intern. // Heat Mass Transfer. 2008. Vol.51, № 9-10. pp. 2482-2493.
5. Ose Y., Kunugi T. Numerical Study on Subcooled Pool Boiling, Progr. In Nucl. Sci. and Technology 2011.Vol 2, pp. 125-129.
6. Krepper E. CFD Modeling Subcooled Boiling-Concept, Validation and Application to Fuel Assembly Design, Nucl. Eng. and Design2007, Vol 237. N7. pp. 716-731.
7.Овсяник А.В. Моделирование процессов теплообмена в кипящих жидкостях, Гомельский государственный технический университет им. П.О. Сухого, Гомель: Беларусь, 2012.260 с.
8. Alekseik, O.S., Kravets V. Yu. Physical Model of Boiling on Porous Structure in the Limited Space. // Eastern-European Journal of Enterprise Technologies, 2013 64(4), pp. 26-31.
9.Поляев В.М., Майоров В.А., Васильев Л.Л. Гидродинамика и теплообмен в пористых элементах конструкций летательных аппаратах. М.: Машиностроение, 1998. – 168 с.
10.Ковалев С.А., Соловьев С.Л. Испарение и конденсация в тепловых трубах. – М.: Наука, 1989. 112 с.
11 Kupetz M., Jeni Heiew E., Hiss F. Модернизация и продление срока эксплуатации паротурбинных электростанций в Восточной Европе и в России.// Теплоэнергетика. 2014. № 6. С.35-43.
12. Гринь Е.А. Возможности механики разрушения применительно к задачам прочности, ресурса и обоснования безопасной эксплуатации тепломеханического энергооборудования // Теплоэнергетика. 2013. №1. С. 25-32.

Authors of the publication

Alexsandr A. Genbach - doctor of technical sciences, professor, department of thermal power plants, "Almaty University of Power Engineering and Telecommunications" (AUPET).

David Yu. Bondartsev - doctoral PhD, department of thermal power plants, "Almaty University of Power Engineering and Telecommunications" (AUPET), lead engineer of JS "Trest Sredazenergomontazh" (production planning and control department).

Received ***November 02, 2018***

UDC 696.41 **DOI:10.30724/1998-9903-2019-21-3-126-134**

DEVELOPMENT OF TECHNIQUE AND PROGRAM FOR ANALYSIS OF OPTIONS FOR TRANSITION TO A CLOSED HOT-WATER SUPPLY SCHEME FOR HEAT SUPPLY SYSTEMS

F.N. Gazizov, I.G. Akhmetova

[1]LLC "Neva Energy", St. Petersburg, Russia
[2]Kazan State Power Engineering University

Abstract: *The article describes the prerequisites for development of methodology for integrated assessment of options for transition to a closed hot-water supply scheme. For analysis of promising options for transition to a closed system of hot water supply, criteria have been proposed that influence the choice of possible solutions. Block diagrams of boundary conditions and independent variables were created. A pyramid of indicators which affect the operating costs of heating system over 25 years of its operation was formulated. A method and a program for selecting the optimal transition scheme to a closed hot-water supply system with calculation of weighting factors have been developed.*

Key words: *heat networks, hot water supply, heat supply system, method of selecting the optimal solution, weighting factors.*

For citation: Gazizov FN, Akhmetova IG. Development of technique and program for analysis of options for transition to a closed hot-water supply scheme for heat supply systems. *Power engineering: research, equipment, technology*. 2019; 21(5-6):126-134. (In Russ). doi:10.30724/1998-9903-2019-21-3-126-134.

РАЗРАБОТКА МЕТОДИКИ И ПРОГРАММЫ АНАЛИЗА ВАРИАНТОВ ПЕРЕВОДА НА ЗАКРЫТУЮ СХЕМУ ГВС СИСТЕМЫ ТЕПЛОСНАБЖЕНИЯ

Ф. Н. Газизов[1], И.Г. Ахметова[2]

[1]ООО «Невская Энергетика», Санкт-Петербург, Россия
[2]ФГБОУ ВО «КГЭУ», Казань, Россия

Резюме*: в статье рассмотрены предпосылки разработки методики укрупненной оценки вариантов перевода на закрытую схему ГВС. Для анализа перспективных вариантов перехода на закрытую систему ГВС предложены критерии, влияющие на выбор возможных решений. Составлены блок-схемы граничных условий и независимых переменных. Сформулирована пирамида показателей, влияющих на эксплуатационные затраты системы теплоснабжения за 25 лет ее применения. Разработана методика и программа выбора оптимальной схемы перехода на закрытую систему ГВС с расчетом весовых коэффициентов.*

Ключевые слова*: тепловые сети, горячее водоснабжение, система теплоснабжения, методика выбора оптимального решения, весовые коэффициенты.*

Introduction

From July 27, 2010 the Federal Law No. 190 “On Heat Supply” (hereinafter FZ-190) entered into force, so most heat supply organizations and local self-government bodies were faced with the issue of transition of subscribers connected to hot water supply (HWS) through an open circuit to a closed circuit of HWS preparation [1, 2]. This obligation is enshrined in paragraph 9 of Article 29 of FZ-190. Taking into account the fact that more than half of the heat supply systems operating in Russia today are open, the question of choosing the most appropriate method for switching to a closed DHW preparation scheme is quite acute [3 - 6].

To date, there is no approved methodology for an integrated assessment of options for transition to a closed hot water supply scheme at the scale of settlements/cities. The only possible method for comparing options and assessing the cost of measures to organize a closed hot water supply system is the technical and economic study of each option for a given city. This work in itself requires significant costs, and therefore, local authorities are not ready to carry it out. As a result, the solutions included in the designed heat supply schemes are either not sufficiently substantiated, or there is no justification for the decisions taken.

Development of choice criteria for options of transition to closed HWS system

To analyze perspective options of transition to closed HWS scheme it is necessary to evaluate the criteria that affect the choice of each of the possible solutions [7]. Table 1 presents the main criteria and characteristic that they affect.

Table 1

The main criteria for choosing an option for transition to a closed HWS system

Criterion	Characteristic	Note
Heating season degree-day (HSDD)	Heat losses from the surface of the pipeline/hydraulic losses in the networks	The four-pipe system in comparison with the two-pipe one has a larger surface of heat exchange with the environment and a larger total length of the heating networks.
Source type	CHPP/boiler house	For a CHPP, the use of a four-pipe system is economically unreasonable.
Availability of space for additional equipment at consumer	Dimensions of basement of residential buildings	In case of lack of free space or inability to access it, installation of individual heating unit (IHU) is not possible.
Population density	The specific heat load of the region (Gcal/km^2)	At low population density, options with a developed heating network (four-pipe system or central heating system) are more expensive.
Capacity of cold water supply (CWS) networks	Hydraulic losses in the networks	When switching to IHU/central heat supply station (CHSS) options, the load on CWS networks significantly increases. In this case, for HWS, either a separate branch with cold water is required, or the option of connecting via a four-pipe system becomes appropriate.

Continuation of the table

The presence of HWS cut on the temperature chart	Temperature chart of the heating network	An additional factor in the transition to the four-pipe system, where the temperature cut can be abandoned.
The real heat load of the district	The presence or absence of a reserve capacity of the heating network	The increase in network water consumption for CHSS/IHU options compared with the four-pipe system and, as a result, the need for new networks.
The ratio of peak load for heating and hot water supply	Heat losses from the surface of the pipeline/hydraulic losses in the networks	The four-pipe system in comparison with the two-pipe one has a larger surface of heat exchange with the environment and a larger total length of the heating networks.
Soil type and the possibility of work performance	The density of urban development, improvement of the district, access to communications, etc.	The cost of pipeline laying directly depends on the complexity of construction and installation works.
The existing connection schemes	The ratio of the existing load connection schemes for HWS: open system/IHU/CHSS/four-pipe system.	Availability at the heat supply source of the appropriate equipment and experience of working with it of the operating organization.
Operation costs	Service life of pipelines and main equipment.	The four-pipe system, unlike CHSS/IHU, does not require regular technical inspection and replacement of the main equipment.

Table 1 considers exclusively basic assessing criteria of transitioning options to a closed HWS system. In a real project, this list can be reduced or expanded depending on the current situation in the considered project. Nevertheless, it is appropriate to divide the proposed criteria into two categories:

• Boundary conditions (according to the type of logical variables “true/false”);

• Independent variables (the value of which will vary in different projects and will be converted into natural or monetary equivalents).

Drawing up a block diagram of boundary conditions and independent variables

The positions 2, 3, 6, and 10 of the basic criteria shown in Table 1 can be proposed as boundary conditions. Figure 1 shows an explanatory block diagram for accounting these boundary conditions.

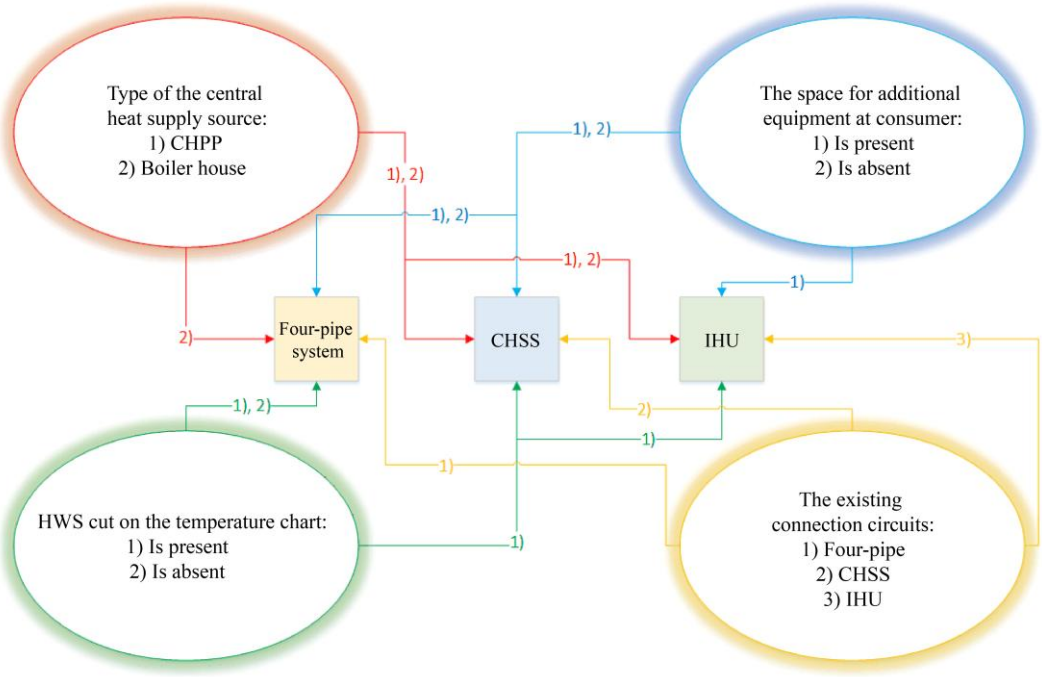

Fig. 1. Block diagram of boundary conditions

The other criteria presented in Table 1 (1, 4, 5, 7, 8, 9, 11) have a quantitative assessment (toe, kW·h, rub.) and are considered as independent variables. Fig. 2 shows an explanatory block diagram for accounting of independent variables data. The considered criteria include: heating season degree-day (HSDD), population density, capacity of cold water supply networks (CWS), real heat load of the district, the ratio of the peak load on heating and hot water supply, soil type, as well as the possibility of work performance and operating costs. These independent variables are presented in the diagram as gray squares and are connected to the indicators they affect.

A significant difference between the criteria of Fig. 2 from the positions shown in Fig. 1 is the presence of a natural and, as a result, cash equivalent, allowing one to quantify the impact of each position on the decision to choose a priority scheme for the district HWS. An important feature of this block diagram is separation of costs for capital investments and annual costs. The second indicator becomes extremely relevant when comparing heat and hydraulic losses, as well as the cost of repair work and replacement of the main equipment. It is further recommended that all economic indicators be added over a period of 25 years. Such an approach will allow a more objective assessment of the options for the CHSS/IHU and the four-pipe system, as it takes into account the nominal life of pipeline equipment, which is 25 years for metal products. In addition, the announced period will include major repairs and replacement of heat exchange equipment for options with installation of heating units according to the type of CHSS/IHU.

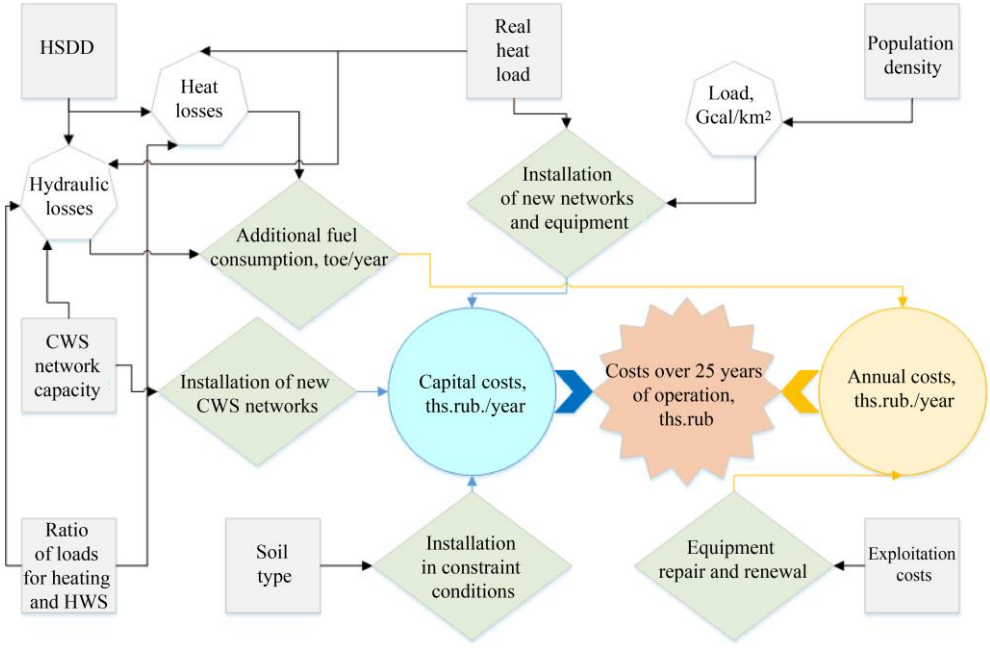

Fig. 2. Block diagram of independent variables

Thus, it is possible to compile an enlarged block diagram for assessing the options for transition to a closed HWS system taking into account the indicators presented in Figs. 1 and 2. Below is the basic calculation scheme in the framework of the developed methodology (Fig. 3).

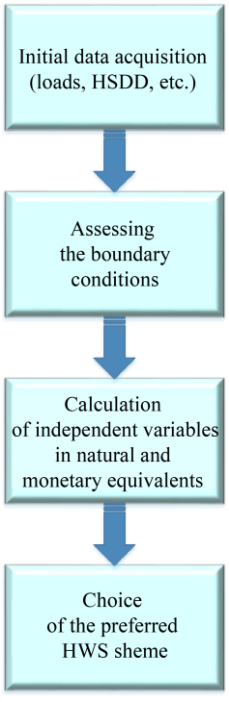

Fig. 3. Basic scheme for choosing the optimal HWS system

Development of a program for choosing the optimal HWS scheme

The final indicator for choosing the option of switching to a closed system, as noted in Fig. 2, are the cash costs over 25 years of operation of a newly introduced or reconstructed heat supply system. However, due to inflation, changes in market prices for equipment and other indicators that affect the final project cost, it is difficult to use accurate quantitative indicators to select the optimal solution. For this reason, the developed methodology is based on the analysis of a variety of relevant feasibility studies for various projects with selection of qualitative weighting factors for each of the criteria.

Based on these assumptions, a pyramid of indicators can be formulated that affects the operating costs of the heat supply system for 25 years of its application. Figure 4 presents this scheme, which is based on indicators that are affected by all 7 previously considered criteria (Fig. 2).

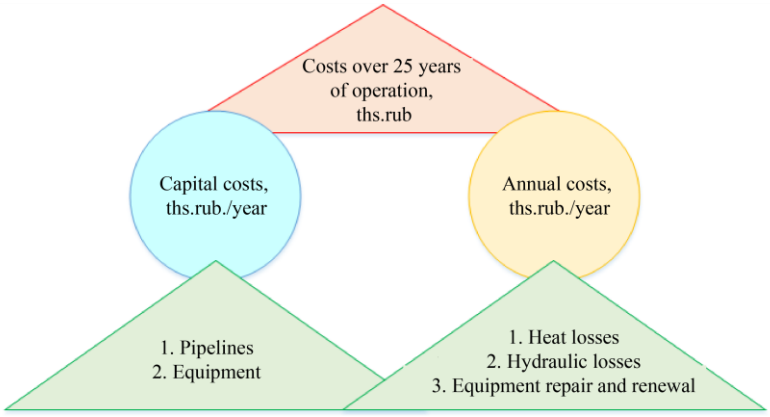

Fig. 4. Pyramid of costs over 25 years of operation

Fig. 4 shows that capital costs include 2 items, while annual costs include 3 items. Figures 5-7 present the interface of the program for choosing the optimal scheme of transition to a closed HWS system with the calculation of weighting factors. Here, a weighting factor equal to 1 approximately corresponds to costs of 100 million rubles.

City		Norilsk	
Heat load, Gcal/h		100	
Heating		80	
HWS		20	
Heat consumption, Gcal/year		500000	
Average network diameter, mm		80	
Analysis of boundary conditions:			
Source	CHPP	Boiler house	
Place for equipment	Yes	No	
Cut	Yes	No	
Scheme	4-pipe	CHSS	IHU
Input of independent variables			
HSDD			6000
Network length for an option with IHP, km			100
Tariff for electrical energy, rub./kWh			4
Tariff for heat energy, rub./Gcal			2000
Soil type (1 for dry, 1.14 for wet)			1

Fig. 5. Initial data input

Cost for network laying					
Dy, mm	Dry soil to spoil	Dry soil with disposal	Wet soil to spoil	Wet soil with disposal	
80	16225.7	17355.48	20801.72	22293.53	
100	19586.28	20833.91	24169.26	25782.91	
125	20981.97	22167.25	25508.4	27116.25	
150	22969.73	24211.56	27553.05	29160.9	
200	26883.82	28418.26	31470.69	33423.71	
250	33121.31	35089.88	37833.5	40132.87	
300	36037.88	37683.05	40680.13	42735.89	
350	42216.64	44354.67	46910.79	49507.08	
400	48161.93	50299.96	52823.73	55454.14	
450	54361.8	56618.46	59029.92	61783.43	
500	59855.17	62111.84	64493.78	67276.8	
			The ratio of wet and dry soils		1.14

Fig. 6. Intermediate calculations

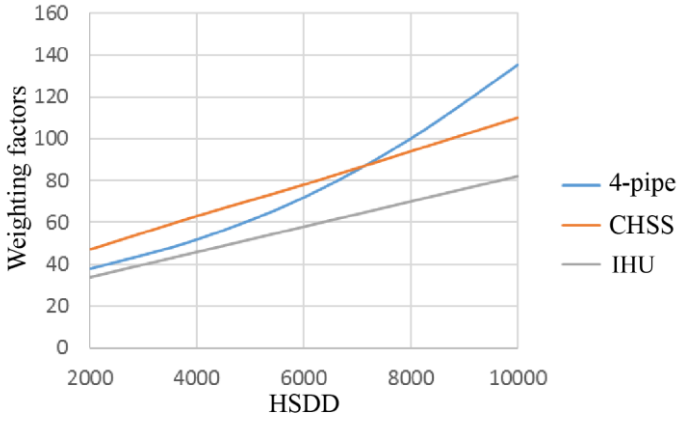

Fig. 7. Calculation results presented in the graphical form

Conclusions

Based on the results of the analysis, the following conclusions can be drawn:

• The final indicator for choosing the option of switching to a closed system is the cash cost over 25 years of operation of the newly introduced or reconstructed heat supply system. However, due to inflation, changes in market prices for equipment and other indicators that affect the final cost of the project, it is difficult to use accurate quantitative indicators to select the optimal solution.

• It has been established that when implementing a closed HWS system, the material characteristic of networks increases as follows: for 100% for a four-pipe network (when switching to a closed HWS system using a four-pipe scheme, it is required to lay 100% of the material characteristic of the pipelines of HWS networks from source to consumers); for 70% for a network with a central heat supply station (when switching to a closed HWS circuit via a CHSS, it is required to lay about 70% of the material characteristics of the pipelines of HWS networks from the central heating system to consumers); 0% for a network with IHU (main networks for HWS are not laid).

• The sharpest increase in heat losses is observed for the variant with a four-pipe system. So for HSDD equal to 9000, the equality of heat losses for the four-pipe heat network and the system with IHU is noticeable.

• About 55% of all costs are heat losses, which means that the HSDD indicator will be one of the most important when choosing a reconstruction option.

• The developed methodology proved its applicability when compared to a detailed feasibility study.

References

1. Kolesnikov AN, Mitin MA. Analysis of execution of the Federal law 416-FZ on transition to closed HWS systems. *New equipment and technologies. Bulletin of DITI* 2017; 2: 84 – 92.
2. Puzakov VS. Analiz razrabotki skhem teplosnabzheniya v RF. *Vodosnabzhenie i sanitarnaya tekhnika*. 2015; 7: 4 - 13. (In Russ).
3. Akhmetova IG, Mukhametova LR. Topical issues of energy efficiency of heat supply organizations. *Power engineering: research, equipment, technology*.. 2015; (11-12):108-113.(InRuss.) https://doi.org/10.30724/1998-9903-2015-0-11-12-108-113.
4. Savina NV., Artjushevskaja EJ. Actual problems of realization of the federal law № 261 from 23.11.2009 in the Russian Federation in the part of heat supply. *Power engineering: research, equipment, technology*..2017; 19(3-4):31-40. (In Russ.) https://doi.org/10.30724/1998-9903-2017-19-3-4-31-40.
5. Strenadko IM, Rozhkov RYu, Kiyski AV. On problems of open thermal supply networks. *Thermal supply news.* 2013; 1:34 -38.
6. Edeleva OA. The choice of an approach to study the problems of energy sources optimum development in the urban heat supply systems. *Power engineering: research, equipment, technology*. 2017; 19(5-6):58-68. (In Russ.) https://doi.org/10.30724/1998-9903-2017-19-5-6-58-68.
7. Zhukov DV, Chicherin SV. Some outcome of Omsk heat transmission pressure tests. *Power engineering: research, equipment, technology*. 2017; 19(1-2):15-22. (In Russ). https://doi.org/10.30724/1998-9903-2017-19-1-2-15-22.
8. Tikhomirov SA, Vasilenko AI. Problems of transition to closed thermal supply networks // *Don engineering bulletin*. 2013; 4(27).
9. Postnikov IV, Stennikov VA. Ensuring of parametric reliability of heat supply systems. *Power engineering: research, equipment, technology*. 2017; 19(3-4):20-30. (In Russ.) https://doi.org/10.30724/1998-9903-2017-19-3-4-20-30.
10. Mukhametova LR, Akhmetova IG, Akhmetov TR. Evaluating the effectiveness of energy efficiency programs. Problems of energy saving in heating. *Power engineering: research, equipment, technology*. 2015;(9-10):12-21.(InRuss). https://doi.org/10.30724/1998-9903-2015-0-9-10-12-21.

Литература

1. Колесников А.Н., Митин М.А. Анализ исполнения федерального закона 416-ФЗ о переходе к закрытым системам ГВС // *Новая техника и технологии. Вестник ДИТИ*. 2017. № 2. С. 84 – 92.
2. Пузаков В.С. Анализ разработки схем теплоснабжения в РФ // Водоснабжение и санитарная техника. 2015. №7. С. 4 –13.
3. Ахметова И.Г., Мухаметова Л.Р. Актуальные вопросы повышения энергоэффективности теплоснабжающих организаций // Известия высших учебных заведений. ПРОБЛЕМЫ ЭНЕРГЕТИКИ. 2015;№ 11-12. С. 108-113.
4. Савина Н.В., Артюшевская Е.Ю. Актуальные проблемы реализации федерального закона № 261 от 23.11.2009 г. в Российской Федерации в части теплоснабжения. Известия высших учебных заведений. ПРОБЛЕМЫ ЭНЕРГЕТИКИ. 2017; Т.19. № 3-4. С. 31-40.
5. Стренадко И. М., Рожков Р. Ю., Кийски А. В. О проблемах открытых систем теплоснабжения // Новости теплоснабжения. 2013. №. 1. С. 34 – 38.
6. Еделева О.А. Выбор методического подхода для решения задачи оптимального развития энергоисточников в теплоснабжающих системах городских территорий. Известия высших учебных заведений. ПРОБЛЕМЫ ЭНЕРГЕТИКИ. 2017; Т.19. №5-6. С. 58-68.
7. Жуков Д.В., Чичерин С.В. Некоторые результаты проведения гидравлических испытаний на магистральных тепловых сетях города Омска // Известия высших учебных заведений. ПРОБЛЕМЫ ЭНЕРГЕТИКИ. 2017. Т. 19. №1-2. С. 15-22.
8. Тихомиров С.А., Василенко А.И. Проблемы перехода на закрытые системы теплоснабжения // Инженерный вестник Дона. 2013. Т. 27. №. 4.
9. Постников И.В, Стенников В.А. Обеспечение параметрической надежности теплоснабжающих систем // Известия высших учебных заведений. ПРОБЛЕМЫ ЭНЕРГЕТИКИ. 2017. Т. 19№ 3-4. С. 20-30.
10. Мухаметова Л.Р., Ахметова И.Г., Ахметов Т.Р. Оценка эффективности реализации программ энергосбережения. Проблемы энергосбережения в теплоснабжении // Известия высших учебных заведений. ПРОБЛЕМЫ ЭНЕРГЕТИКИ. 2015. № 9-10. С. 12-21.
11. Еремин А.В., Колесников С.В., Кудинов И.В., Бранфилева А.Н., Абишева Л.С. Математическая

11. Eremin AV., Kolesnikov SV, Kudinov IV, Branfileva AN, Abisheva LS. Mathematical and computer model of heating network based on the electronic-hydraulic analogy. *Power engineering: research, equipment, technology.* 2017; 19(1-2):3-14. (In Russ). https://doi.org/10.30724/1998-9903-2017-19-1-2-3-14.
12. Varinov AA, Yakimov ND, Erashova YN. Engineering model of the thermal regime in detached house. *Power engineering: research, equipment, technology.*2016;(3-4):22-28.(InRuss). https://doi.org/10.30724/1998-9903-2016-0-3-4-22-28.
13. Golub II, Voitov ON, Boloev EV, Semenova LV. Choice of short-term constant configuration of the distribution network. *Power engineering: research, equipment, technology.* 2018;20(9-10):39-51. (In Russ). https://doi.org/10.30724/1998-9903-2018-20-9-10-39-51.
14. Zvonareva JN, Van'kov JV. Work of system of heat supply at stage-by-stage introduction of the automated individual thermal points. *Power engineering: research, equipment, technology.* 2017; 19(1-2):31-40.(InRuss). https://doi.org/10.30724/1998-9903-2017-19-1-2-31-40.
15. Polovnikov VY. Numerical analysis of the influence of the design type of the channel of heat network on its thermal conditions and heat loss. *Power engineering: research, equipment, technology.* 2017; 19(5-6):79-88.(In Russ). https://doi.org/10.30724/1998-9903-2017-19-5-6-79-88.
16. Gazizov FN, Amosov NT. Prospective and problems of broad introduction of the closed scheme of HWS preparation in settlements of Russian Federation. *9 International school – seminar of young scientists and specialists "Energy saving – theory and practice"*; 2018; *Moscow, Russia*. Moscow: MPEI Publishing House, 2018. (In Russ).

и компьютерная модель объединенной теплосети централизованного теплоснабжения // Известия высших учебных заведений. ПРОБЛЕМЫ ЭНЕРГЕТИКИ. 2017. Т.19. №1-2. С.3-14.
12. Варенов А.А., Якимов Н.Д., Ерашова Ю.Н. Инженерная модель теплового режима в индивидуальном доме // Известия высших учебных заведений. ПРОБЛЕМЫ ЭНЕРГЕТИКИ. 2016. №3-4. С.22-28.
13. Голуб И.И., Войтов О.Н., Болоев Е.В., Семенова Л.В. Выбор краткосрочной фиксированной конфигурации распределительной сети // Известия высших учебных заведений. ПРОБЛЕМЫ ЭНЕРГЕТИКИ. 2018. Т. 20. № 9-10. С.39-51.
14. Звонарева Ю.Н., Ваньков Ю.В. Работа системы теплоснабжения при поэтапном внедрении автоматизированных индивидуальных тепловых пунктов // Известия высших учебных заведений. ПРОБЛЕМЫ ЭНЕРГЕТИКИ. 2017. Т. 19. №1-2. С.31-40.
15. Половников В.Ю. Численный анализ влияния вида конструкций канальной тепловой сети на ее тепловые режимы и тепловые потери // Известия высших учебных заведений. ПРОБЛЕМЫ ЭНЕРГЕТИКИ. 2017. Т.19. №5-6. С.79-88.
16. Газизов Ф.Н., Амосов Н.Т. Перспективы и проблематика широкого внедрения закрытой схемы приготовления ГВС в населенных пунктах Российской Федерации // труды 9 Международной школы – семинара молодых ученых и специалистов «Энергосбережение – теория и практика»; 2018 г., Москва. М.: Издательский дом МЭИ, 2018.

Authors of the publication:

Farit N. Gazizov – technical director of LLC "Neva Energy".

Irina G. Akhmetova – professor at Kazan State Power Engineering University.

Received ***March 05, 2019***

ELECTRICAL ENGINEERING

UDC 621.314 **DOI:10.30724/1998-9903-2019-21-3-135-145**

METHOD FOR CONTROL OF THE START-UP REGULATING DEVICE FOR POWER TRANSFORMERS OF THE POWER SUPPLY SYSTEM

V.S. Klimash, B.D. Tabarov

Komsomolsk-na-Amure State University, Komsomolsk-on-Amur, Russia

Abstract: *Three-phase thyristor switches are designed for pulsed formation of inrush currents of electrical equipment with their subsequent shunting in steady state operation. In transformer substations, they perform a bumpless turning on of a power transformer by connecting its primary winding first to two phases of the network at the moment of zero crossing by the phase voltage of the network third phase, and then to the network third phase at the moment of zero crossing by the line voltage of the other two network phases. In this case, the starting currents of the transformer almost immediately enter the steady state without the appearance of constant components in the magnetization currents and voltage drop. To expand the functionality of thyristor switches, it is proposed, in addition to bumpless turning on of a power transformer, to disconnect it without arcing between the contacts of electrical equipment, as well as to carry out continuous voltage regulation for consumers when voltage in the network changes. The proposed method and structure for its implementation on the basis of two three-phase thyristor reactor keys and a capacitor bank make it possible while changing the network voltage to stabilize the generated reactive power at the input of the substation without creating the current distortions in the power transformer and power transmission simultaneously with stabilizing the substation output voltage. Modeling and research of the start-regulating device as part of a transformer substation was carried out in the MatLab environment. The results of numerical experiments in stationary and dynamic modes of the substation operation showed the feasibility of using the developed technical solutions for the industrial power supply system.*

Keywords: *three-phase network, transformer substation, dual-band regulation, thyristor-reactor regulator, capacitor bank, control method, control operations, consumer voltage stabilization, reactive power compensation of the network, mathematical model.*

For citation: Klimash VS, Tabarov BD. Method for control of the start-up regulating devicefor power transformers of the power supply system. *Power engineering: research, equipment, technology.*2019; 21(3):135-145. (In Russ). doi:10.30724/1998-9903-2019-21-3-135-145.

СПОСОБ УПРАВЛЕНИЯ ПУСКОРЕГУЛИРУЮЩИМ УСТРОЙСТВОМ ДЛЯ СИЛОВЫХ ТРАНСФОРМАТОРОВ СИСТЕМЫ ЭЛЕКТРОСНАБЖЕНИЯ

В.С. Климаш, Б.Д. Табаров

Комсомольский-на-Амуре государственный университет, г. Комсомольск-на-Амуре, Россия

Резюме: *Трехфазные тиристорные ключи предназначены для импульсного формирования пусковых токов электрооборудования с последующим их шунтированием в установившемся режиме работы. Применительно к трансформаторным подстанциям они выполняют безударное включения силового трансформатора за счет подключения его первичной обмотки сначала к двум фазам сети в моменте перехода фазного напряжения третьей фаза сети через ноль, а затем к третьей фазе сети в момент перехода линейного напряжения двух других фаз сети через ноль. При этом пусковые токи трансформатора практически сразу входит в установившиеся режим без возникновения постоянных составляющих в токах намагничивания и спада напряжения. Для расширения функциональных возможностей тиристорных ключей предлагается, кроме безударного подключения силового трансформатора, осуществлять его отключение без образования дуги между контактами электроаппаратуры, а также осуществлять непрерывное регулирование напряжения у потребителей при изменении напряжения в сети. Предложенный способ и структура его реализации на основе двух трехфазных реакторно-тиристорных ключей и конденсаторной батареи позволяют при изменении напряжения сети одновременно со стабилизацией выходного напряжения подстанции стабилизировать генерируемую реактивную мощность на входе подстанции без создания искажений тока в силовом трансформаторе и электропередаче. Моделирование и исследование пускорегулирующего устройства в составе трансформаторной подстанции проводилось в среде MatLab. Результаты численных экспериментов в стационарных и динамических режимах работы подстанции показали целесообразность применения разработанных технических решений для системы промышленного электроснабжения.*

Ключевые слова: *трёхфазная сеть**,** трансформаторная подстанция, двухподдиапазонное регулирование, реакторно-тиристорный регулятор, конденсаторная батарея, способ управление, операции управления, стабилизация напряжения потребителей, компенсация реактивной мощности сети, математическая модель.*

Introduction

The commercially available thyristor AC voltage regulators with natural switching (TRVN) have relatively small overall dimensions, high speed and operational reliability. They are used to start asynchronous motor, at the input of diode rectifiers, in heating installations, lighting systems and in other electrical technologies. According to individual projects, they are manufactured for a voltage of 35 kV and a current of 2 kA for static compensators of reactive power of electric steelmaking plants [1].

At the same time, experimental studies on the use of TRVN as start-regulating devices for power transformers (PT) of substations 6 (10)/0.4 kV did not find practical application. This is due to the fact that with an increase in the control angle of the thyristors, TRVN consumes additional reactive power and introduces distortions in the output voltage and input current of the substation [2-11].

Analytical study of appropriate literature, patents study, and survey of testing experience in industrial operation allowed creating new technical solutions for transformer substations (TS). This is a reactor-thyristor AC voltage regulator with natural switching (R-TRVN) [12, 13] specially designed for PT and its control method [14].

The proposed R-TRVN device is installed on the high side of the PT in the same manner as the mechanical on-load tap-changer, and under continuous regulation it provides stable voltage for consumers with voltage deviations from the nominal by ± 10%. At the same time, it provides a sinusoidal voltage at the input and output of PT for three values of voltage in the network (nominal value, increased and decreased relative to the nominal value by 10%). Between these sinusoidal levels, a continuous narrow-range regulation is carried out in two sub-bands: in the upper one it is

with lowered network voltage, and in the lower one with increased network voltage. Regulation is performed with a harmonic composition of voltage, meeting the Russian State Standard requirements, and without distorting the shape and phase shift of the current network.

The R-TRVN control method, in addition to dual-band regulation, provides bumpless turning on PT under load, in which there are no shock electrodynamic forces on the transformer windings and voltage reduction, and shutdown is performed without arcing on the mechanical contacts of the high voltage switch [15].

The purpose and objectives of research

The purpose of this work is to study the adjusting properties and energy parameters of the substation according to the P-TRVN - PT scheme using a mathematical model.

To achieve this purpose, the following tasks were set and solved in the work.

1. Development of a software package for substation research according to the P-TRVN - PT scheme.

2. Study of voltage at the PT input and at consumers when the voltage deviation in the network is ± 10% of the nominal.

3. Study of current shape in the network, reactor, thyristor switches and at the PT input during the process of voltage stabilization at consumers.

4. Study of the current network phase when voltage deviates from the input of the substation, which includes P-TRVN and a block of capacitors.

Development of a specialized device for a transformer substation

Two schemes are proposed for connecting the P-TRVN device to the primary circuit of the PT substation. They are shown in fig. 1. In the first circuit (Fig. 1, a), the device is connected between the network and the primary PT winding connected in a star, and its pulse-phase control system (PPCS) is synchronized with the voltage of the secondary PT winding. In the second scheme (Fig. 1, b), the device is included in the cut of the star of the primary PT winding, and its pulse-phase control system is synchronized with the network. Both circuits perform regulation with identical physical processes and have their own advantages and disadvantages in the reconstruction of existing and newly designed TSs, taking into account the use of dry or oil PTs in them. At the same time, the advantage of the second circuit is that when a three-phase short circuit occurs in the primary winding of the PT, the thyristors are not exposed to emergency current.

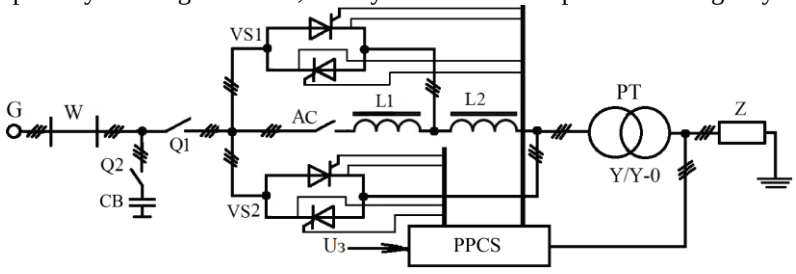

a)

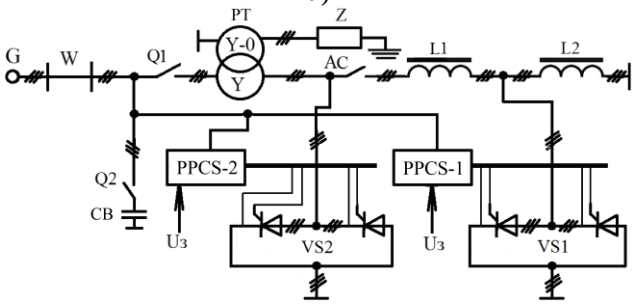

b)

Fig. 1. Schemes of a transformer substation with a reactor-thyristor voltage regulator

The circuits (Fig. 1) contain a three-phase network G, a power line W, an input high-voltage switch Q1, a high-voltage switch Q2 in the CB capacitor bank circuit, modules of the main VS-1 and additional VS-2 thyristor switches with a pulse-phase control system PPCS-1 and PPCS-2, AC contactor, main L1 and additional L2 reactors, power transformer PT and active-inductive load Z.

The device operates as follows.

The power transformer PT is turned on when the additional thyristor switches *VS-2* are completely turned off. In this case, firstly two main thyristor switches *VS-1* using an additional reactor *L2* connect two phases of its primary winding to the corresponding phases of the network *G* at the moment of zero crossing by the phase voltage of the network third phase G, then the third main thyristor switch *VS-1* connects the third phase of the primary winding of the power transformer PT to the network third phase at the moment the line voltage of the other two phases of the network is crossing zero. At the end of the process of turning on the PT power transformer while preparing the substation for voltage regulation, parallel to the fully open main thyristor switches *VS-1*, the main reactor *L1* is connected via a three-phase contactor *AC*. Further, when the conductive state of the thyristors changes, the process of voltage regulation starts both up and down as relating to the network voltage. The upper limit is set by the transformation ratio of the power transformer, and the lower limit is set by the resistance of the reactor.

The proposed R-TRVN control method provides voltage regulation at the input of the power transformer relative to the network voltage and among consumers between the specified regulation limits: the maximum and minimum divided by the nominal level.

The maximum limit of voltage regulation at the power transformer load is set by the transformation coefficient of the power transformer PT with the main switches *VS-1* completely turned off and the additional thyristor switches *VS-2* fully turned on at a reduced voltage in the network *G*. The additional thyristor switches *VS-2* at this moment bypass the main L1 and additional L2 reactors in the circuit primary winding of a power transformer PT.

The rated voltage level at the load is ensured when the main switches *VS-1*, which bypass the main reactor L1, are fully turned on, and the additional thyristor switches *VS-2* are completely turned off at the rated mains voltage *G* and the rated load *Z*.

The minimum regulation limit on the load is set by the total resistance of the main L1 and additional L2 reactor with completely closed main *VS-1* and additional *VS-2* thyristor switches with increased voltage in the network G and rated load Z.

A change in the network voltage affects the voltage of consumers and leads to a change in the reactive power of the capacitor bank and in the network.

The inductance and voltage drop are regulated using R-TRVN at the TS input. Depending on the positive and negative voltage deviations at the substation input, it is necessary to individually select the resistance of the primary and secondary reactors. This contributes to the achievement of high quality load voltage.

It should be noted that the reactive power of capacitors depends on the change in the supply voltage and that during the process of voltage stabilization for consumers, the conductive state of thyristors and inductance of R-TRVN in the PT primary circuit are regulated using a thyristor switch. An increase in inductance simultaneously with an increase in the generated reactive power of capacitors eliminates the deviation of the reactive power (deviation of the current phase) of the network according to the principle of indirect compensation.

The known devices built on the principle of indirect compensation of reactive power with parallel connection to the network and capacitors and a thyristor-reactor device [19] create current distortions in the network and can operate either in the mode of reactive power compensation, or in the mode of voltage maintenance.

For the proposed method and device [13, 14], the distinctive feature of the principle of indirect compensation of network reactive power with simultaneous compensation of voltage deviations at consumers without distorting the PT and network current is that the capacitor is

connected to the network in parallel, and the reactor is connected in series between the network and TS .

An increase in the inductance in the PT circuit during the pulse-phase control of the alternating voltage at the reactors neutralizes the additional reactive power generated by the capacitors, providing a slight deviation of the network phase current from voltage and maintaining the maximum cosφ value. This is one of the great features of the proposed device.

Turning off the substation power transformer PT without the occurrence of an electric arc and switching overvoltages is conducted as follows.

Before turning off the power transformer, pulses are first removed from the additional thyristor switches *VS-2*. Then, the main thyristor switches *VS-1* are transferred to the fully open state and the current through the contacts of the three-phase contactor *AC* and the main reactor L1 is set to zero. After this, the three-phase contactor *AC* is used to disconnect the de-energized main reactor *L1* without arcing and overvoltage. At the final operation of the method, control pulses are removed from the main thyristor switches *VS-1* with natural switching and they are turned off without switching losses when phase currents are crossing zero.

Mathematical modeling of the reactor thyristor device

To study the regulatory properties and energy parameters of the substation according to the R-TRVN - PT scheme and physical processes in static and dynamic modes, a software package was developed in the Matlab environment [16]. The substation model is built for the circuit of Fig. 1b, and is shown in Fig. 2. It contains the following elements and modules: three single-phase sources forming a three-phase network (*Ua, Ub, Uc*); power line *W*; input high-voltage switch *Q1*; high-voltage switch *Q2* in the battery circuit of the capacitor bank CB; contactor *AC*; modules of the main *VS-1* and additional *VS-2* thyristor switches with a pulse-phase control system PPCS-1 and PPCS-2; main *L1* and additional *L2* reactors; power transformer PT; active-inductive load Z and other auxiliary elements.

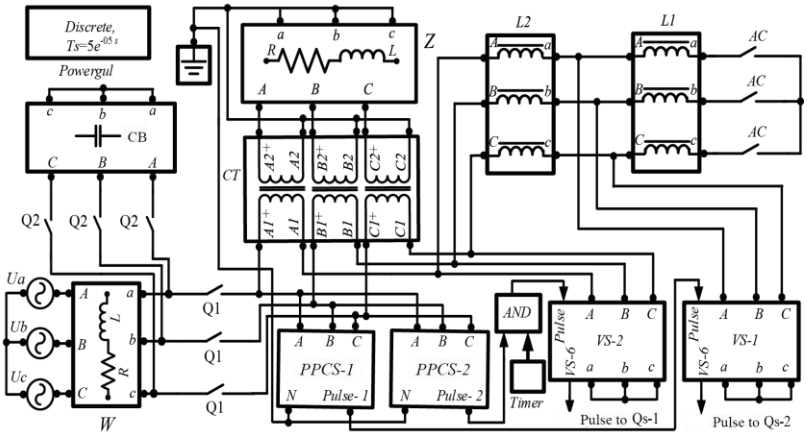

Fig. 2. Block-modular mathematical model of a transformer substation with a dual-band control device

Figure 3 shows detailed schemes of modules that have particular differential equations and, when joint, form a common system of differential equations of the object under study.

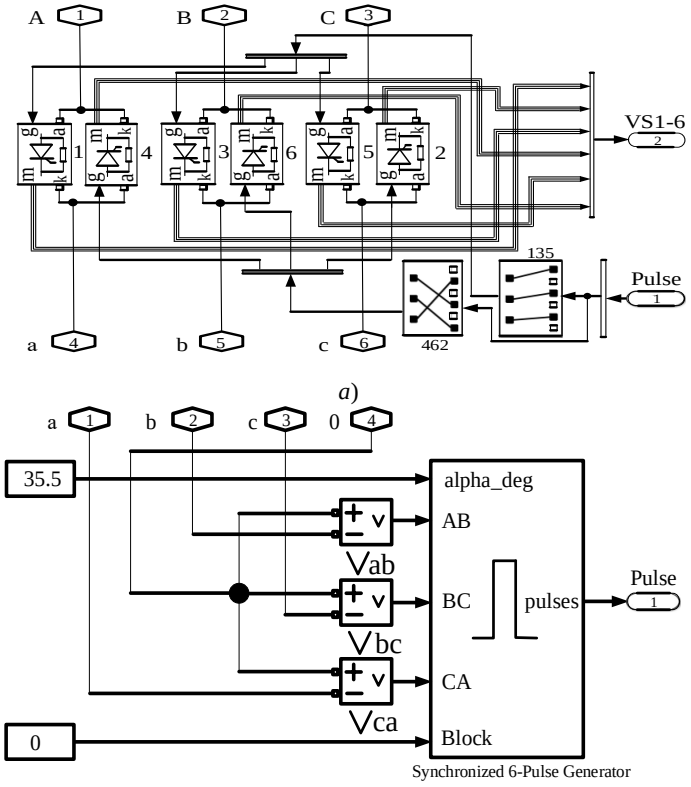

a)

b)

Fig. 3. Detailed schemes of models of the software package:
a) - thyristor key; b) - control systems

Research results of a transformer substation with a start-regulating reactor-thyristor device

When modeling, the following physical processes of substation according to the *R-TRVN - PT* scheme were studied.

1. Study of voltages at the PT input and consumers with voltage deviations in the upper and lower sub-bands of regulation.

2. Study of voltages at *R-TRVN* at the PT input with respect to the network. The obtained oscillograms are shown in Fig. 4.

3. Study of the network current shape at that at the input of PT in the reactor and through the thyristors during voltage stabilization at the consumer when working from dual-band *R-TRVN.*

Further we analyze the results of TS numerical studies in *MatLab* using *the R-TRVN* scheme. Figure 4 shows voltage oscillograms at the TS elements using the R-TRVN scheme. They are obtained at rated load and network voltage deviations of ± 5% of the nominal level and are shown for one phase. It should be noted that when the regulation is shifted from the middle in one direction or another, the voltage shape improves and tends to be sinusoidal.

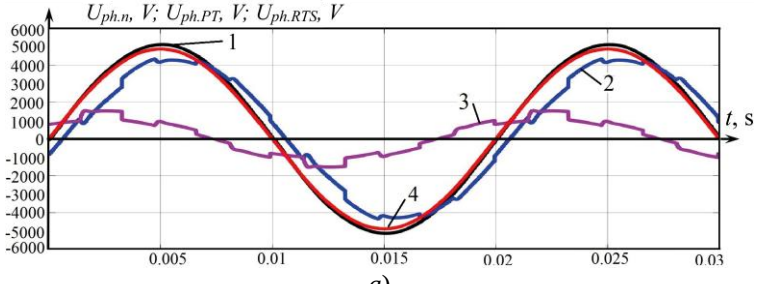

a)

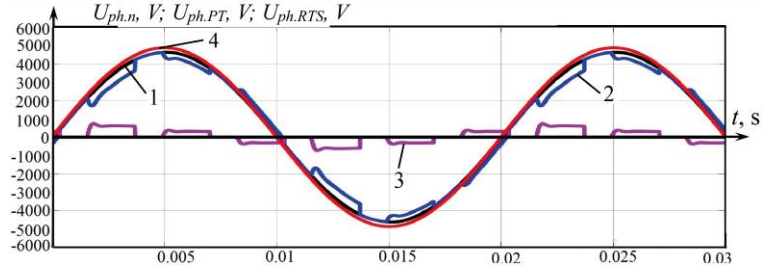

b)

Fig. 4. Oscillograms of voltage drop in the network, transformer and device at the upper (a) and lower (b) voltage control sub-bands:
1, 2, 3 and 4 are the phase voltages in the network, at the PT input, at R-TRVN and phase voltage at the PT input at the network rated voltage

The device employs a narrow-range pulse-phase regulation of alternating voltage with a parallel connection of reactor and thyristor switch [17]. This three-phase device is included in the primary circuit of the PT connected to a star without a neutral wire. Such an inclusion creates an interphase voltage interaction [18], as a result of which the voltage modulation frequency increases three times with respect to the switching frequency of the phase thyristor switches (Fig. 4).

When the network voltage is increased by the deviation $+\Delta U$, the device, increasing the control angle α, reduces the conductive state of the thyristors and, increasing the inductance on the high side of TS, creates a voltage drop $-\Delta U$ on it, while maintaining the required voltage at consumers. With a decrease $-\Delta U$, the device reduces the control angle α, increases the thyristors conductive state and, reducing the inductive resistance on the high side of TS, creates a voltage drop of $+\Delta U$ on it.

Thus, during stabilisation of load voltage, the X_L of reactor thyristor device is regulated, providing the principle of indirect compensation of reactive power [19].

The oscillograms in Fig. 5 illustrate voltage regulation in the upper and lower sub-bands.

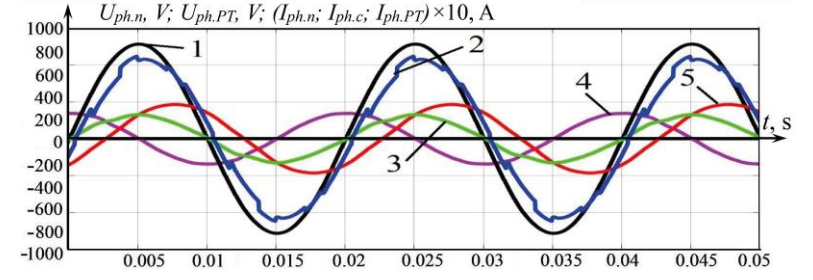

a)

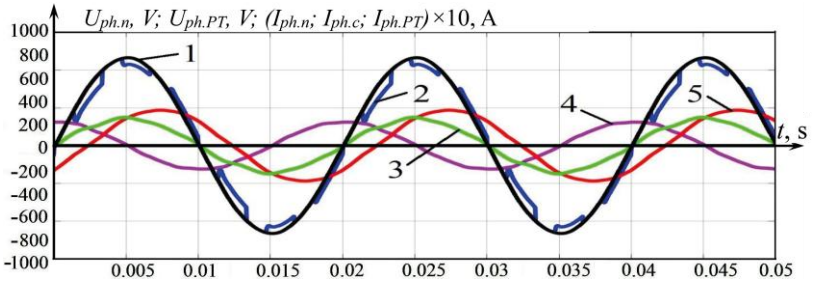

b)

Fig. 5. Oscillograms of currents and voltages in the upper (a) and lower (b) sub-bands of voltage regulation: 1 and 2 - phase voltages of the network and PT input;
3, 4 and 5 - phase currents of the network, capacitor and *PT* input

Analysis of these oscillograms shows that the shape of the network current is distorted slightly, and its phase coincides with the network voltage, which determines high efficiency of electricity consumption of the transformer substation.

R-TRVN studies have revealed that voltage regulation on the TS high side does not adversely affect the shape of the network current. The results of this study are illustrated by the following figures.

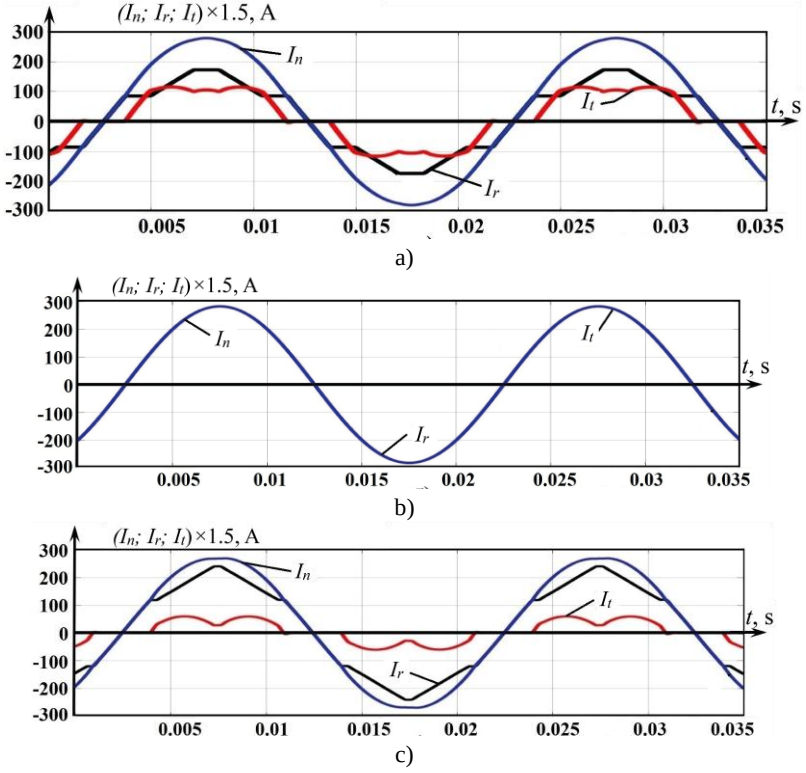

Fig. 6. Oscillograms of currents at different angles of thyristor control:
Ic and *Ip* are the phase currents of the network and additional reactor; *It* is the phase current of the main thyristor switch

Oscillogram in Fig. 6b, illustrates the PT operation at its rated mode and characterizes that, at rated PT operation, the currents of network, additional reactor, and main thyristor switch are equal. It can be seen from the oscillogram (Fig. 6, a and c) that the thyristor and reactor currents are distorted, and their sum, being the network current and the current of the power transformer, retains a sinusoidal shape at any control angles. This is another remarkable property of the device, which does not create additional losses in the power transformer and in the network during regulation [20].

Conclusions

Studies of a mathematical model of dynamic and quasi-stationary processes of a dual-band reactor-thyristor AC voltage regulator with natural switching as part of a transformer substation allowed us to draw the following conclusions:

1. The use of a reactor-thyristor device of continuous operation allows one to release a mechanical switching device with a current-limiting reactor of on-load tap changing type, to simplify the PT design and the technology for production of complete transformer substations.

2. When the voltage deviation in the network is ± 10% of the nominal value, the device maintains the voltage at consumers at a given level with an accuracy of not more than ± 1%.

3. The device, together with a capacitor bank, simultaneously with voltage stabilization at the transformer substation output provides stabilization of the generated reactive power at the substation input.

4. During the process of continuous regulation of voltage at the input of substation under load, the reactor-thyristor AC voltage regulator with natural switching does not create current distortions in the power transformer and in the network.

5. When applying a special control that takes into account electromagnetic processes, the device produces bumpless turning on the power transformer under load without phase currents exceeding their established values and turning it off without arcing at the contacts of high-voltage switching devices.

References

1. Klimash VS., Tabarov BD. Principy postroeniya puskoreguliruyushchego ustrojstva dlya transformatornyh podstancij. *Omsk scientific Bulletin. Ser. Electrical engineering*. 2017; 155(5): 55-60. (In Russ).

2. Panfilov DI, ELGebaly AE. and Astashev MG. Topologies of thyristor controlled reactor with reduced current harmonic content for static VAR compensators.17th EEEIC conference, Milan, Italy, 6–9 June. 2017.

3. Panfilov DI, Gebaly EL AE and Astashev MG Design and Optimization of New Thyristors Controlled Reactors with Zero Harmonic Content. 18th International Conference of Young Specialists on Micro. Nanotechnologies and Electron Devices, June 29–July 3, 2017.

4. DI. Panfilov, AE. ELGebaly and MG. Astashev, “Thyristors Controlled Reactors for Reactive Power Control with Zero Harmonics Content”, 17th IEEE International Conference on Smart Technologies IEEE EUROCON 2017, Ohrid, Macedonia, 6 - 8 July 2017.

5. Yakimov IA, Nikolaev AA., Barabash RO., Anohin VV Issledovanie raboty tiristornogo regulyatora napryazheniya pechnogo transformatora v rezhime stabilizacii pervichnogo toka dugovoj staleplavil'noj pechi // *Elektrotekhnika: setevoj elektronnyj nauchnyj zhurnal Russian Internet Journal of Electrical Engineering*. 2016; 3(4): 3-10. (In Russ).

6. Dionise TJ., Morello S. “Comprehensive Analysis to Specify a Static Var Compensator for an Electric Arc Furnace Upgrade”, *IEEE IAS Annual Meeting Conference Record*, Oct 2014.

7. Dionise TJ., “Assessing the Performance of a Static Var Compensator for an Electric Arc Furnace“, IEEE Industry Applications Society Annual Meeting, Las Vegas, NV, October 2012.

8. Kawamura A. “An Optimal Control Method Applied for the Compensation of the Fundamental

Литература

1. Климаш В.С., Табаров Б.Д. Принципы построения пускорегулирующего устройства для трансформаторных подстанций // Омский научный вестник. Серия «Электротехника». 2017. № 5 (155). С. 55–60.

2.Panfilov D.I., ELGebaly A.E. and Astashev M.G. Topologies of thyristor controlled reactor with reduced current harmonic content for static VAR compensators.17th EEEIC conference, Milan, Italy, 6-9 June 2017.

3. Panfilov DI, ELGebaly AE and Astashev MG Design and Optimization of New Thyristors Controlled Reactors with Zero Harmonic Content. 18th International Conference of Young Specialists on Micro / Nanotechnologies and Electron Devices, June 29–July 3, 2017.

4. Panfilov D.I., ELGebaly A.E. and Astashev M.G. “Thyristors Controlled Reactors for Reactive Power Control with Zero Harmonics Content”, 17th IEEE International Conference on Smart Technologies IEEE EUROCON 2017, Ohrid, Macedonia, 6 - 8 July 2017.

5. Якимов И.А., Николаев А.А., Барабаш Р.О., Анохин В.В. Исследование работы тиристорного регулятора напряжения печного трансформатора в режиме стабилизации первичного тока дуговой сталеплавильной печи // Электротехника: сетевой электронный научный журнал. 2016. Т.3, №4 (3). С. 3–10.

6. T.J. Dionise, S. Morello, “Comprehensive Analysis to Specify a Static Var Compensator for an Electric Arc Furnace Upgrade”, IEEE IAS Annual Meeting Conference Record ;Oct 2014.

7. T.J. Dionise, “Assessing the Performance of a Static Var Compensator for an Electric Arc Furnace“, IEEE Industry Applications Society Annual Meeting, Las Vegas, NV, October 2012.

8. Kawamura A. IEEE Transactions of Industry Applications. 1983. Vol. 1A-19, iss. 3. pp. 414-423.

9. Якимов И.А. Обоснование тиристорного

VAR Fluctuations in the Arc Furnace," IEEE Transactions of Industry Applications. 1983. Vol. 1A-19, iss. 3. pp. 414-423. doi: 10.1109/TIA.1983.4504217.

9. Yakimov IA. Obosnovanie tiristornogo regulirovaniya napryazheniya transformatora dugovoj staleplavil'noj pechi . *Elektrotekhnicheskie sistemy i kompleksy*. 2017; 2 (35): 41-48. (In Russ).

10 Panfilov DI., Elgebaly AE., Astashev MG. Design and Assessment of Static VAR Compensator on Railways Power Grid Operation under Normal and Contingencies Conditions2016, 16th EEEIC conference, Florence7-10 June;Italy.

11. Panfilov DI., ELGebaly AE., "Modified Thyristor Controlled Reactors for Static VAR Compensators" 2016 IEEE 6th International Conference on Power and Energy (PECON 2016), Melaka, Malaysia, November 2016.

12. Getopanov AYu, Tabarov BD, Klimash V.S. Issledovanie regulirovochnyh svojstv i vliyaniya na set' reaktorno-tiristornogo ustrojstva na vysokoj storone pechnogo transformatora // *Elektrotekhnicheskie sistemy i kompleksy* 2018; 39(2):49-56. (In Russ).

13. Klimash VS, Tabarov BD .Ustrojstvo dlya vklyucheniya, vyklyucheniya i regulirovaniya napryazheniya transformatornoj podstancii. Patent RUS 2667481 №2667481 RF. H02P 13/00 (2006.01). №2017143967; Appl. 14.12.2017;, Byul. №26.Accesed :20 Sep 2018.

14. Klimash S, Tabarov BD. Sposob vklyucheniya, viyklyucheniya i regulirovaniya napryaweniya transformatornoy podstansii [A method for switching on and off and regulate voltage transformer substation]. Patent RUS №2667095 RF. H02M 5/25 (2006.01); G05F 1/30 (2006.01). №2017147194; Appl. 29.12.2017; publ. 14.09.2018, Byul. №26

15. Klimash VS, Tabarov BD. *Issledovaniya transformatornoj podstancii s puskoreguliruyushchim ustrojstvom v avarijnyh rezhimah raboty* // 3 Povolzhskaya nauchno-prakticheskaya konferenciya. «Priborostroenie i avtomatizirovannyj elektroprivod v toplivno-energeticheskom komplekse i zhilishchno-kommunal'nom hozyajstve., 7–8 dec Kazan, 2017. pp. 118-123. (In Russ).

16 Klimash VS., Tabarov BD. Programmnyj kompleks matematicheskih modelej magnitno-tiristornogo puskoreguliruyushchego ustrojstva dlya silovogo transformatora v srede MatLab. Patent RUS .Svidetel'stvo o gosudarstvennyj registracii регулирования напряжения трансформатора дуговой сталеплавильной печи // ЭЛЕКТРОТЕХНИЧЕСКИЕ СИСТЕМЫ И КОМПЛЕКСЫ. 2017.Т 35. № 2. С. 41–48.

10. Panfilov D.I., Elgebaly A.E. and Astashev M.G., Design and Assessment of Static VAR Compensator on Railways Power Grid Operation under Normal and Contingencies Conditions2016, 16th EEEIC conference, Florence7-10 June;Italy.

11. Panfilov D.I., ELGebaly A.E. Modified Thyristor Controlled Reactors for Static VAR Compensators 2016 IEEE 6th International Conference on Power and Energy (PECON 2016), Melaka, Malaysia, November 2016.

12. Гетопанов А.Ю., Табаров Б.Д., Климаш В.С. Исследование регулировочных свойств и влияния на сеть реакторно-тиристорного устройства на высокой стороне печного трансформатора // Электротехнические системы и комплексы. Серия «Электротехника». 2018. №2 (39). С. 49–56.

13 Климаш В.С., Табаров Б.Д. Пат. 2667481 Российская Федерация, МПК H02P 13/00 (2006.01). Устройство для включения, выключения и регулирования напряжения трансформаторной подстанции. № 2017143967; 14.12.2017; Бюл. № 26.Ссылка активна на. 20сентября.2018,

14.Климаш В.С., Табаров Б.Д. Пат. 2667095 Российская Федерация, МПК H02M 5/25 (2006.01); G05F 1/30 (2006.01). Способ управления пускорегулирующим устройством силового трансформатора № 2017147194; 29.12.2017. Бюл. № 26. Ссылка активна на: 14.09.2018

15. Климаш В.С., Табаров Б.Д. Исследования трансформаторной подстанции с пускорегулирующим устройством в аварийных режимах работы // 3 Поволжская научно-практическая конференция. «Приборостроение и автоматизированный электропривод в топливно-энергетическом комплексе и жилищно-коммунальном хозяйстве». 7–8 декабря 2017. С. 118–123.

16. Климаш В.С., Табаров Б.Д. Программный комплекс математических моделей магнитно-тиристорного пускорегулирующего устройства для силового трансформатора в среде MatLab. Патент РФ.Свидетельство о государственный регистрации программы для ЭВМ № 2017613852,. Бюл№4.Ссылка активна на:03

programmy dlya EVM № 2017613852 Byul№4 Accessed:03 apr 2017.
17.Zharsky BK, Golubev VV. *Impul'snoe regulirovanie peremennogo napryazheniya.* Kiev: Institut elektromekhaniki AN USSR 1975. (In Russ).
18. Klimash V.S. *Vol'todobavochnye ustrojstva dlya kompensacii otklonenij napryazheniya i reaktivnoj energii s amplitudnym, impul'snym i fazovym regulirovaniem:* Vladivostok, 2002. (In Russ).
19. Solodukha YaYu. *Sostoyanie i perspektivy vnedreniya v elektroprivod staticheskih kompensatorov reaktivnoj moshchnosti (obobshchenie otechestvennogo i zarubezhnogo opyta). Reaktivnaya moshchnost' v setyah s nesinusoidal'nymi tokami i staticheskie ustrojstva dlya eyo kompensacii*. Moskva: Informelektro, 1981. (In Russ).
20. Klimash VS, Tabarov BD. Issledovanie vhodnogo toka transformatornoj podstancii pri rabote ot magnitno-tiristornogo puskoreguliruyushchego ustrojstva. // *Mezhdunarodnyj centr nauchnogo sotrudnichestva «Nauka i prosveshchenie». 9 Mezhdunarodnoj nauchno - prakticheskoj konferencii "World Science: Problems and Innovations"*, Penza, April 30, 2017. P. 167-170. (In Russ).

апреля 2017
17. Жарский Б.К., Голубев В.В. Импульсное регулирование переменного напряжения. Киев: Институт электромеханики АН УССР, 1975.
18. Климаш В.С. Вольтодобавочные устройства для компенсации отклонений напряжения и реактивной энергии с амплитудным, импульсным и фазовым регулированием: Владивосток, 2002. 141 с.
19. Солодуха Я.Ю. Состояние и перспективы внедрения в электропривод статических компенсаторов реактивной мощности Реактивная мощность в сетях с несинусоидальными токами и статические устройства для её компенсации. Москва: Информэлектро, 1981.
20. Климаш В.С., Табаров Б.Д. Исследование входного тока трансформаторной подстанции при работе от магнитно-тиристорного пускорегулирующего устройства. // Международный центр научного сотрудничества «Наука и просвещение». 9 Международной научно - практической конференции «World Science: Problems and Innovations». Пенза, 30 апреля 2017. С. 167–170.

Authors of the publication

Vladimir S. Klimash - doctor of technical Sciences, Professor, Professor of the Department of "Industrial electronics". E-mail: klimash@yandex.ru.

Bekhruz D. Tabarov – post-graduate student of the Department "Industrial electronics", E-mail: behruz.tabarov@mail.ru.

Received ***April 02, 2019***

UDC 621.315.1 **DOI:10.30724/1998-9903-2019-21-3-146-159**

DISTORTION OF LOCATION PULSES IN HIGH-FREQUENCY PATHS OF OVERHEAD POWER LINES

V.A. Kasimov

Kazan State Power Engineering University, Kazan, Russia
ORCID: https://orcid.org/0000-0002-2316-2278, *VasilKasimov@yandex.ru*

Abstract: *The work is devoted to the features of propagation of electromagnetic signals (20–1000 kHz) along multi-wire overhead transmission lines. For monitoring the status of overhead power lines, a location method can be used. For connection to power lines, the connection equipment is used, which forms the high-frequency path of the power line, which has a limited frequency bandwidth. To select the optimal signals of location probing, it is necessary to investigate the impact of high-frequency path on the pulsed signals. This paper investigates the distortion of pulsed location signals in high-frequency paths. The influence of elements of the high-frequency path is studied using a simulation model of the high-frequency path of an overhead transmission line developed in the PSCAD software environment with subsequent experimental verification. Elements of high-frequency path of the developed simulation model are described. The influence of duration of the probe pulses on the shape and spectrum of the reflected signals is analyzed. It was established that during the passage of microsecond pulses, their differentiation occurs, the reflected signal is a combination of responses from the rising and falling edges of the probe pulse. With this in mind, criteria are proposed for optimizing the duration of the location pulses. During formation of ice deposits on the overhead lines wires, additional distortion of the pulse signals' shape occurs. Using the experimental data, the distortions of the reflected pulsed signals and their spectra are analyzed as ice deposits grow on the wires of overhead power lines. The established patterns of pulse shape distortion and the developed criteria for optimizing the pulse duration are used for location probing of overhead power lines to control ice deposits on the wires and to detect damage.*

Keywords: *overhead power line; high-frequency paths; location probing; pulse signal; shape; spectrum; duration; distortion; simulation model; ice deposits.*

Acknowledgments: *The work was performed with financial support from the Ministry of Science and Higher Education of the Russian Federation under Agreement No. 14.574.21.0141 dated September 26, 2017, the unique project identifier RFMEFI57417X041.*

For citation: Kasimov VA. Distortion of location pulses in high-frequency paths of overhead power lines. *Power engineering: research, equipment, technology.* 2019; 21(3):146-159. (In Russ). doi:10.30724/1998-9903-2019-21-3-146-159.

ИСКАЖЕНИЯ ЛОКАЦИОННЫХ ИМПУЛЬСОВ В ВЫСОКОЧАСТОТНОМ ТРАКТЕ ВОЗДУШНОЙ ЛИНИИ ЭЛЕКТРОПЕРЕДАЧИ

В.А. Касимов

Казанский государственный энергетический университет, г. Казань, Россия
ORCID: https://orcid.org/0000-0002-2316-2278, VasilKasimov@yandex.ru

Резюме: *Работа посвящена особенностям распространения электромагнитных сигналов (20–1000 кГц) по многопроводным воздушным линиям электропередачи. Для мониторинга состояния воздушных линий электропередачи может использоваться локационный метод. Для подключения к линиям электропередачи используется аппаратура присоединения, образующую высокочастотный тракт линии электропередачи, который имеет ограниченную частотную полосу пропускания. Для выбора оптимальных сигналов локационного зондирования необходимо исследовать влияние высокочастотного тракта на импульсные сигналы. В работе исследуются искажения импульсных локационныхсигналов в высокочастотных трактах. Влияние элементов высокочастотного тракта исследуется с помощью разработанной в программной среде PSCAD имитационной модели высокочастотного тракта воздушной линии электропередачи с последующей экспериментальной проверкой.Описываются элементы высокочастотного тракта разработанной имитационной модели. Анализируется влияние длительности зондирующих импульсов на форму и спектр отраженных сигналов.Установлено, что при прохождении микросекундных импульсов происходит их дифференцирование, отраженный сигнал является комбинацией откликов от переднего и заднего фронтов зондирующего импульса. С учетом этого предлагаются критерии оптимизации длительности локационных импульсов. При образовании гололедных отложений на проводах воздушных линий происходит дополнительное искажение формы импульсных сигналов. По экспериментальным данным анализируются искажения отраженных импульсных сигналов и их спектров при нарастании гололедных отложений на проводах воздушных линий электропередачи. Установленные закономерности искажения формы импульсов и разработанные критерии оптимизации длительности импульсов используются при локационном зондировании воздушных линий электропередачи для контроля гололедных отложений на проводах и обнаружения повреждений.*

Ключевые слова: *воздушная линия электропередачи; высокочастотный тракт; локационное зондирование; импульс; форма; спектр; длительность; искажения; имитационная модель; гололедные отложения.*

Благодарности: *Материалы для публикации подготовлены при финансовой поддержке Министерства науки и высшего образования РФ по Соглашению № 14.574.21.0141 от 26 сентября 2017 года, уникальный идентификатор проекта RFMEF157417X0141.*

Introduction

Overhead power lines (OHPL) are the least reliable elements of a power system, as they are long, and are exposed to atmospheric and human impacts. During their operation, dangerous impacts on their elements can appear that are not provided by the conditions of normal operation and lead to damage and, consequently, to serious accidents. In addition, in some cases the reliability of the overhead line operation is reduced due to the existing deterioration of electrical equipment. Therefore, the issues of OHPL monitoring, timely preventive control of wires condition, rapid detection and elimination of accidents consequences are urgent tasks for power engineers around the world.

According to the high voltage classes, the most massive and extended class of 110 kV brings the largest number of technological violations. A significant contribution to the accident statistics of overhead lines is made by glacial accidents occurring due to the formation of glaze deposits of excess size. For example, in the autumn-winter period of 2017-2018, the share of accidents caused by ice was about 15% of the total number of accidents[1].

Location monitoring of overhead lines

[1] All-Russian meeting "*Results of the autumn-winter period of 2017-2018*" Ministry of Energy of the Russian Federation 2018. Available at: https://minenergo.gov.ru/node/7822 Accessed: 14 Apr 2019.

One of the promising methods for remote monitoring of the overhead power lines state is the method of location probing [1-5]. This method provides early detection of the beginning of the icing process on the wires, followed by monitoring the dynamics of the growth of ice deposits, determining the moments of the beginning and end of ice melting. In case of an accident, this method determines the distance to the place of damage.

Figure 1 shows a diagram of connection of location equipment to an overhead power line at the Kutlu-Bukash substation (SS) using a coupling capacitor (CC) and a connection filter (CF). To prevent shunting of substation buses, a high-frequency stopper (HFS) is used, which together with the overhead lines form a high-frequency (HF) overhead line path. A connection filter FPM-6400 (passband of 51–1000 kHz) with a coupling capacitor SMP-110√3-6400 and a supression filter VZ-630-0.5 (suppression band is 160–1000 kHz) are installed on this overhead line.

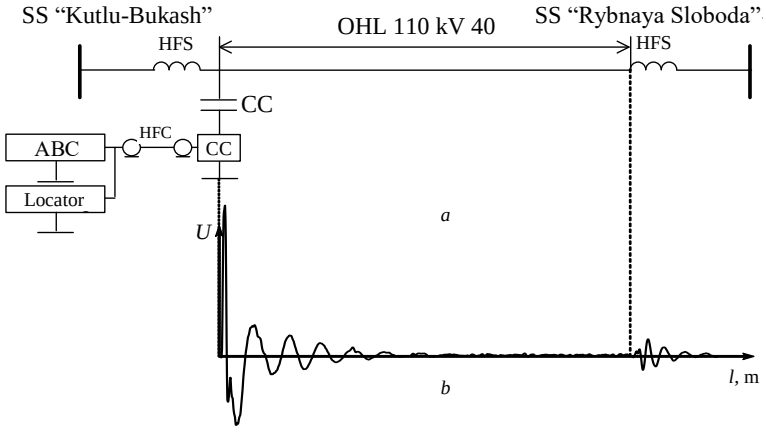

Fig. 1. Connection diagram of the location device to the wires of the 110 kV “Kutlu-Bukash – Rybnaya Sloboda” OHPL (a), reference reflectogram (b)

The transmitter of the location device emits a probe pulse to the overhead power line, which after reflection from the inhomogeneities of the wave resistance of the overhead line (for example, the line end, branch, damage) is received by the receiver of the location device. In this case, the propagation time and amplitude of the reflected pulse characterize this inhomogeneity and the propagation conditions of pulse in the line.

Most commonly, a location device works in parallel with technological high-frequency communication equipment, which imposes a number of requirements on the mutual compatibility of equipment [6], and on the methods used to extract location signals among technological RF communication signals [7]. The existing simulation models of overhead power lines either do not take into account the influence of the connection equipment [8, 9], or describe the line wires using a phase-independent frequency model [10], and this is a reason why there is a discrepancy between the model and experimental results.

Simulation model of an overhead power line

To study the features of distribution of location signals along the HF paths of the overhead lines, a simulation model was developed in the PSCAD software environment. The model of the HF path of the overhead line includes: multi-wire lines near the earth surface (phase wires and ground wearers of the overhead line); connection devices consisting of connection filters with coupling capacitors, HF cables; processing devices, consisting of high-frequency stoppers - separation circuits, which are a particular case of separation filters; high-voltage equipment of substations, located behind the high-frequency stopper (it is presented by an equivalent active resistance and capacity).

The RF path circuit starts with a pulse generator and ends with a “connection device”, simulated by a 75 Ohm load. Consider the process of setting the parameters of the elements of the RF path.

1. The pulse generator is a standard component from the PSCAD component library and allows one to get a pulse of a given duration and amplitude. The following basic parameters are set for the generator: the start time of the pulse generation, duration, pulse amplitude and output resistance. The probe pulse duration of location probing can be set in the range from 1 to 200 μs, the pulse repetition period is from 0.1 to 100 ms. The pulse generator is connected directly to the HF cable. An oscilloscope is connected to the same point, which enables recording probe and reflected signals with a given time step, and this is a way to measure the reflectogram.

2. The connection device consists of a high-frequency cable (HFC), a connection filter and a coupling capacitor. The RC-75 high-frequency coaxial cable is a standard component from the cable library. The main parameters specified for this component are: cable length, radius of the current-carrying core, radius of the insulating layer, radius of the protective coat, specific resistance of the core, specific resistance of the ground, frequency range. The high-frequency cable is connected to the connection filter (Fig. 2).

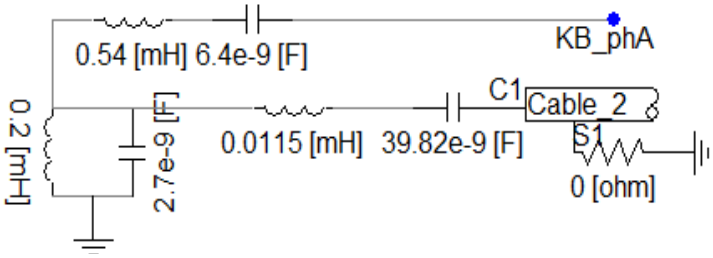

Fig. 2. Wiring diagram of the RF cable to the connection filter

The connection filter performs the following functions: compensates the reactance of the coupling capacitor at operating frequencies; grounds the lower lining of the coupling capacitor at a frequency of 50 Hz; serves as a matching element between the RF cable and the linear path. FPM-6400 connection filter is installed at the 110 kV overhead line “Kutlu-Bukash – Rybnaya Sloboda”. The coupling capacitor SMP-110 is represented by a capacity of 6400 pF.

3. The processing device consists of VZ-630 high-frequency stopper. The stopper is cut into the line working wire between the connection point of the coupling capacitor and the substation buses. In this range, it is possible to form the following tuner configurations: single-frequency, double-frequency, single-frequency blunt, double-frequency blunt, broadband. The diagram of VZ-630 stopper is shown in Fig. 3.

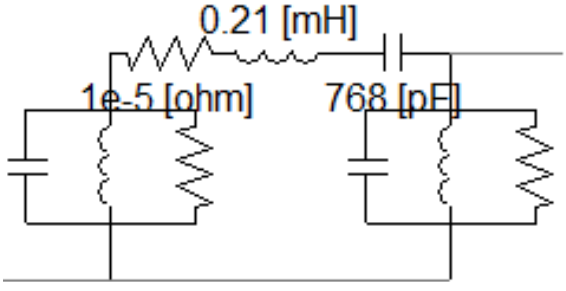

Fig. 3. Electrical circuit of the high-frequency stopper.

4. The linear RF path is formed by the OHPL phase wires and ground wearers, if the overhead line is double-circuit, then the phase wires of the second circuit are also taken into account. Power line wires are presented in the form of a coaxial cable with a zero thickness of the insulating layer and a protective coat, although the PSCAD software environment has standard libraries for Tline overhead lines. This choice of model is due to the fact that in this model it is possible to set the core cross section of the steel-aluminum wire. The 110 kV overhead line "Kutlu-Bukash – Rybnaya Sloboda" in the model is represented by the Line09 element (Figs. 4, 5). The terminal ends of the three phase wires and ground wearers at the substations "Kutlu-Bukash" and "Rybnaya Sloboda" are designated as C1, C2, C3 and C4. The ends of the ground wearers C4 are low-resistance grounded.

The main parameters specified for this component are: the overhead line length, the location of the wires in vertical and horizontal directions relative to the ground, the steel core radius, the aluminum coil radius, the insulating layer radius, the wire resistivity, the ground resistivity, the frequency range.

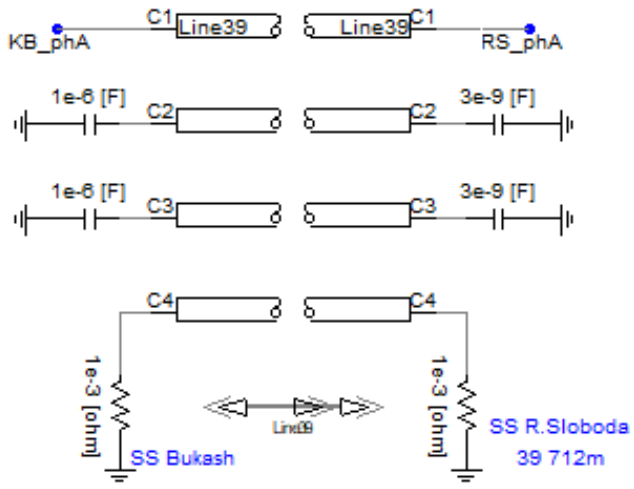

Fig. 4. Elements of the model of the 110 kV overhead power line.

5. The input resistance of the substation at the ends of the HF path, at the places of HF bypass and at the taps is set by the equivalent capacitance, the value of which is determined in accordance with the recommendations set out in the Methodological guidelines for calculating the parameters and choosing high-frequency path circuits for 35-750 kV AC power lines (Standard of PJSC FGC UES STO 56947007-33.060.40.052-2010. - Access mode: http://www.fskees.ru/upload/docs/sto_56947007-33.060.40.05.05-2010_red.pdf. (Access date 12/20/2018).).

Simulation procedure

In the developed model of the 110 kV "Kutlu-Bukash – Rybnaya Sloboda" overhead line, the optimal parameters of the probe pulse were determined by simulation. The expected shape of the received reflected pulses was obtained upon reflection from the end of HF path to supply the highest amount of probe pulse energy to the HF path and optimization the measurement results processing. In addition, this model allows one to simulate the detection of damage on the overhead power lines wires using the location method [11].

The results of calculating the pulse shapes and the corresponding frequency spectra during the passage of a rectangular pulse of 2 μs duration through the HF elements of the "Kutlu-Bukash-Rybnaya Sloboda" overhead line are shown in Fig. 6.

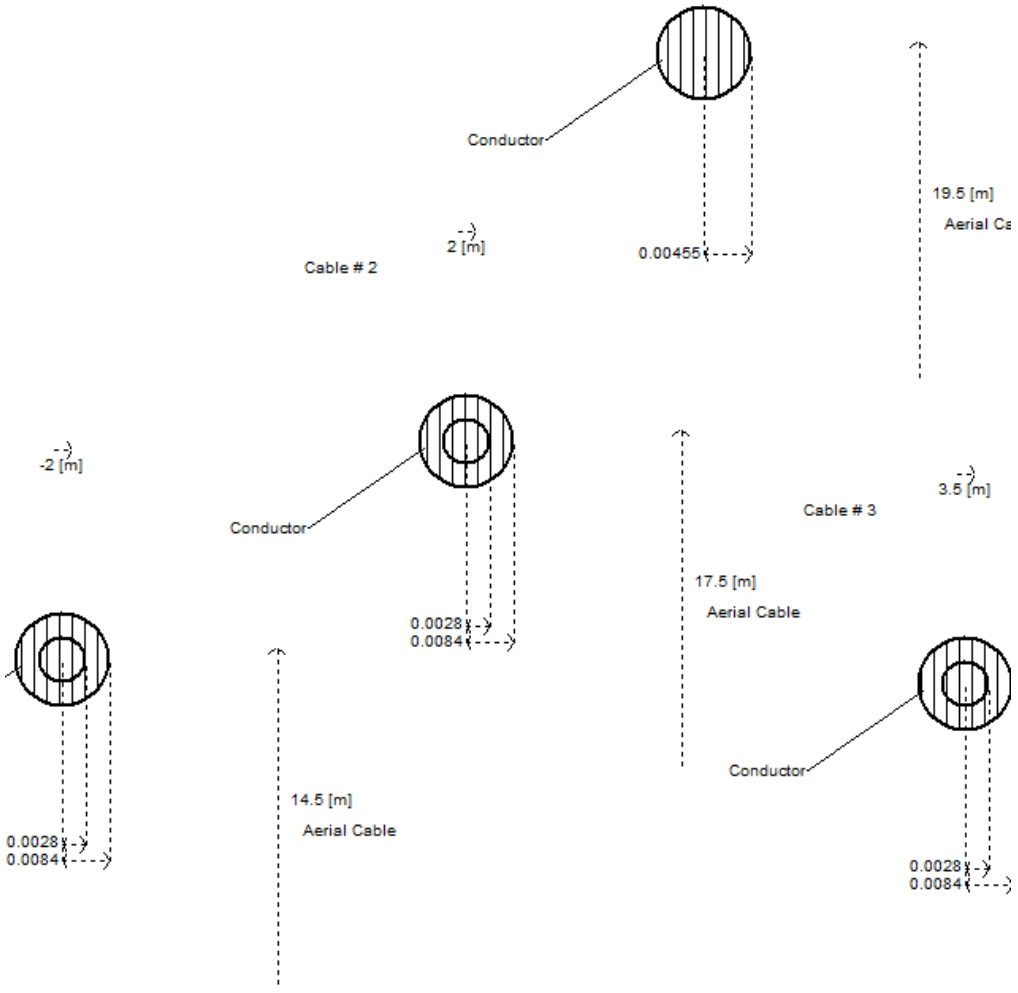

Fig. 5 The layout of the 110 kV overhead power line wires relative to the earth

The rectangular pulse (Fig. 6, a) after passing through the high-frequency cable remains practically unchanged: there is a slight increase in the duration of the fronts (Fig. 6, b). After passing through the connection filter, the pulse turns into a response (Fig. 6, c), which is approximately similar to one and a half period of a sinusoidal signal of approximately 15 μs. In this case, the constant component disappears, since the signal passes through the coupling capacitor, and the amplitudes of the low-frequency components (harmonics) sharply decrease, the maximum of the spectrum is in the region of 120 kHz.

After the pulse signal passes through the connection filter, damped oscillations appear (Fig. 6, c), as was indicated above. The HF stopper partially shunts these oscillations (Fig. 6d) and their amplitude decreases. Under the influence of HF trap, a maximum of the spectrum appears in the region of 60 kHz, due to the occurrence of “ringing effect” of the HF stopper. After the signal passes through the line wires, the maximum of the spectrum appears in the region of 140 kHz, and a pulse delay of 135 μs appears, which is determined by the covered distance of 40 km. When the pulse passes back and forth twice (Fig. 6, f), a delay of 270 μs appears, and the signal amplitude decreases by about 10 times. The amplitude of the reflected signal (marked by a solid oval in Fig. 6, f) becomes comparable with the amplitude of the “ringing" (marked by a dashed oval in Fig. 6, f) of the stopper.

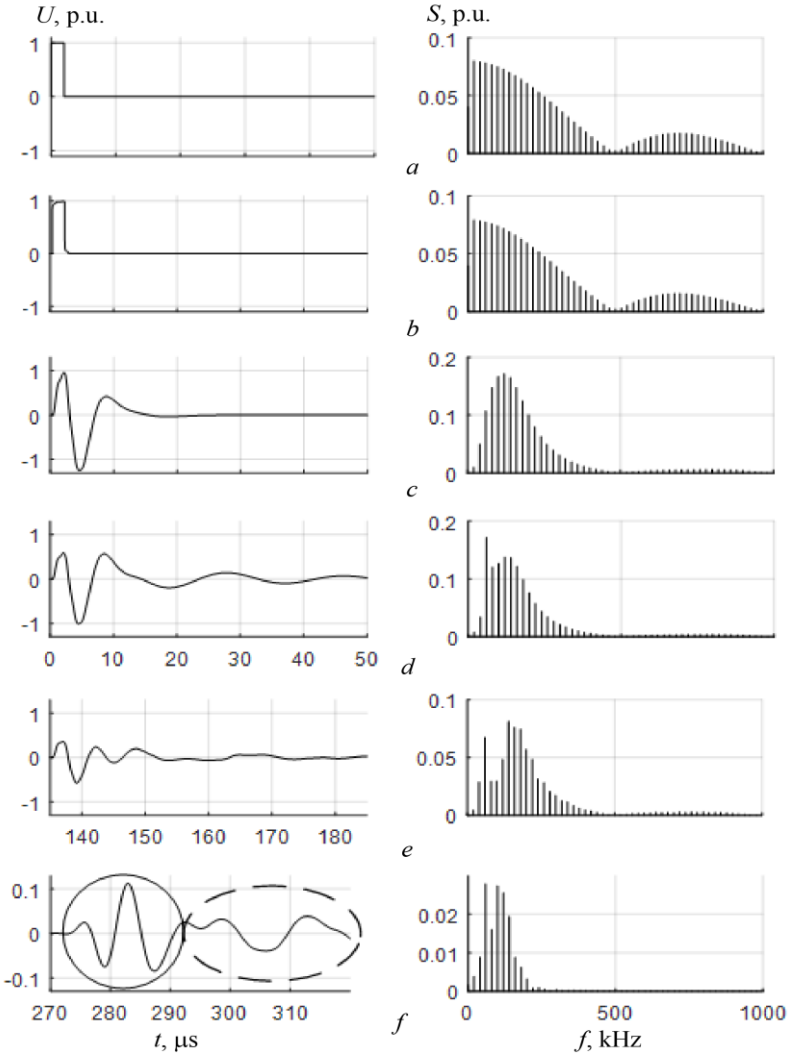

Fig. 6. Changes in the shape of the location signal (a) of a 2 μs duration (left column) and its spectrum (right column) after passing through the elements of the HF path: b - HFC; c - HFC and CF; g - HFC, CF and HFS; d - after passing the HF path (HFC, CF, HFS and line wires) in one direction; e - after two-fold passing the HF path back and forth; the solid oval marks the reflected signal, and the dashed line indicates the "ringing" of the HFS

Distortion of various-duration pulses

The pulse energy is determined by its amplitude and duration. In the simulation model, studies were conducted of the passage of rectangular pulses with a duration of 2–12 μs through the 40 km long HF path of the "Kutlu-Bukash – Rybnaya Sloboda" overhead line (Fig. 7).

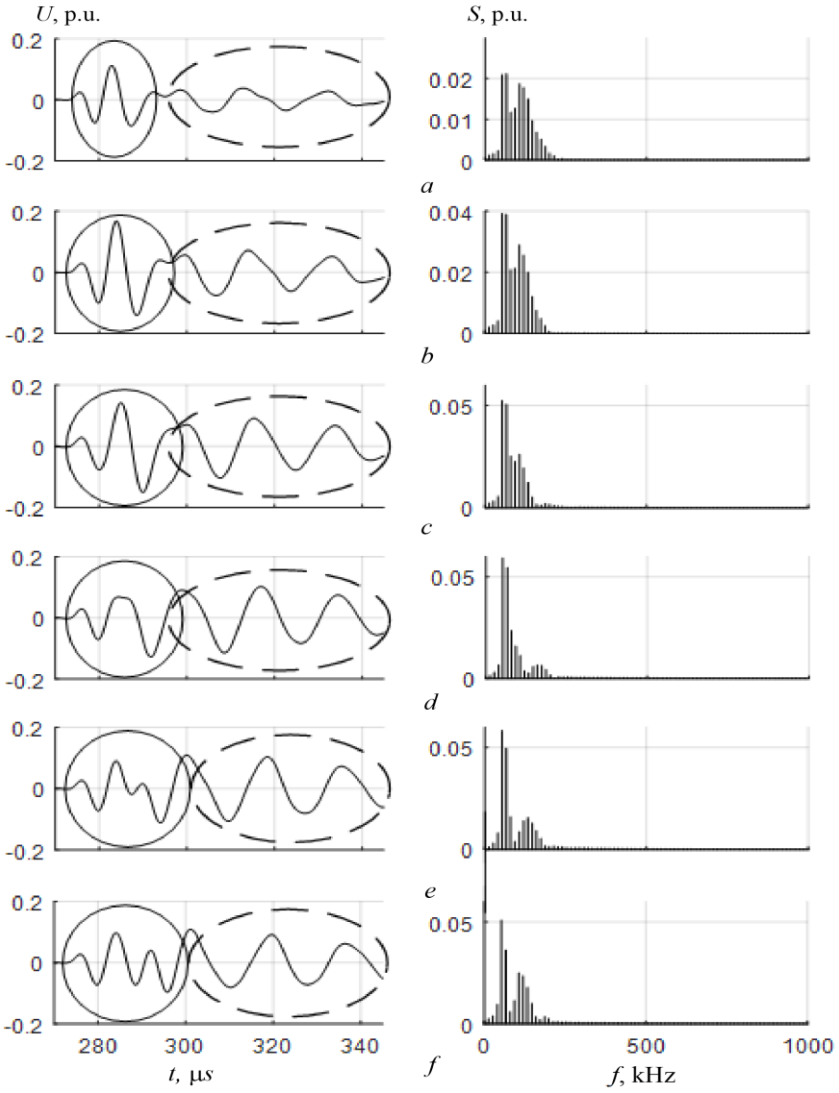

Fig. 7. Changes in the shape of location signals (left column) with durations of 2 (a), 4 (b), 6 (c), 8 (d), 10 (d), 12 μs (f) in the HF path of the 110 kV "Kutlu-Bukash – Rybnaya Sloboda" OHPL and their spectra (right column); the solid oval marks the reflected signal, and the dashed line indicates the "ringing" of the HFS

When changing the duration of the probe pulse, the shape of the reflected pulses changes. At the minimum studied pulse duration τ = 2 μs, the amplitude of the reflected pulse does not have time to reach its possible maximum (Fig. 7, a), in contrast to pulses with long durations (Fig. 7, b-c).

According to fig. 7, the probe pulse, when passing through the HF tract, "differentiates", as shown in Fig. 6. In this case, the pulses turn into responses in the form of several periods of sinusoidal oscillation. In addition, damped oscillations ("ringing") are superimposed on the reflected signals, marked by dashed ovals in Fig. 7(a–e), which are caused by a high-frequency stopper, as was shown in Fig. 6.

With an increase in the pulse duration of more than 6 μs, the amplitude of the reflected signals decreases (marked by solid ovals in Fig. 7), which is caused by the fact that the responses

from the falling and rising edges of the probe pulse begin to diverge in time, turning into separate responses.

Thus, pulses with τ = 2–6 μs, having the largest amplitude of the negative burst, are optimal for high-voltage lines with a length of 40 km, which makes it easier to separate them from the noise constantly present in the high-frequency path of power lines. An increase in the pulse duration from 2 μs to 8 μs causes an increase in the amplitude of the "ringing" of the airspace, with a further increase in the pulse duration, the amplitude of the "ringing" practically does not change.

Moreover, the correlation coefficients of the reflected signals obtained experimentally and during simulation for the durations of the probe pulses of 2-12 μs are at least 0.9, which confirms the adequacy of the developed simulation model.

To study the responses from the falling and rising edges of the pulse, model studies of passage of pulses with a duration of more than 200 μs were performed (Fig. 8). For such duration of the probe pulse, the response from the falling edge comes after the oscillatory processes caused by the leading edge of the pulse have completely decayed.

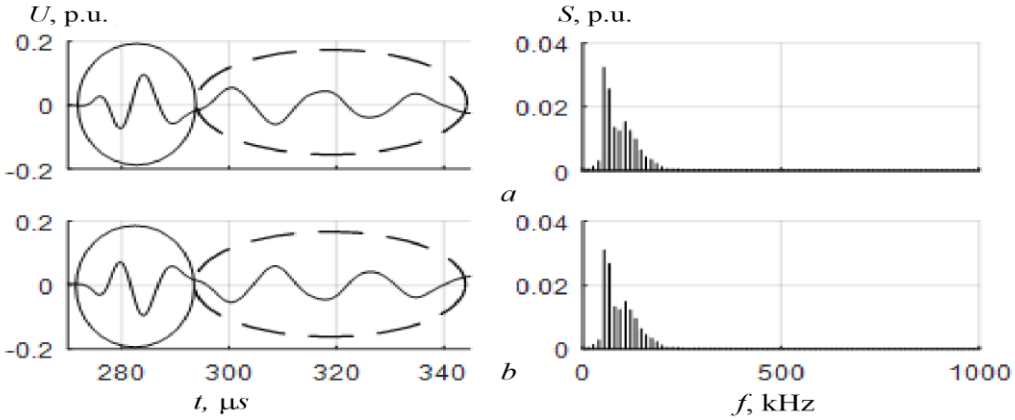

Fig. 8. Responses to the rising (a) and falling (b) edges of the probe pulse with a duration of 200 μs in the HF path of the 110 kV "Kutlu-Bukash – Rybnaya Sloboda" OHPL (left column) and their spectra (right column); the solid oval marks the reflected signal, and the dashed line indicates the "ringing" of the HFS

As it is seen from fig. 8, the reflections of the rising and falling edges of the probe pulse differ only in polarity, while their spectra also completely coincide. In this regard, by varying the pulse duration, it becomes possible to suppress the HFS "ringing" or to increase the amplitude of the reflected signal to a maximum.

Figure 9 shows the reflected signals for pulse durations of 4.8 μs and 17.6 μs. In the first case, due to the superposition of the reflection from the rising and falling edges, an almost twofold increase in the reflected signal amplitude is achieved (see Fig. 8). In the second case due to the mixing of reflections from the fronts for the period of "ringing" oscillations (17.6 μs) the "ringing" from the rising edge is compensated by "ringing" from the falling edge, while the reflected signal separates the reflections from the rising and falling edges of the probe pulse.

Investigations were carried out on the existing 110 kV "Kutlu-Bukash – Rybnaya Sloboda" OHPL of 40 km length. A comparison of the results of model calculations with experimental data shows that the main patterns of transformation of the reflected pulses' shape with a change in its duration coincide. The response from the rising edge of the signal pulse stably maintains its position on the time axis of the reflectorgam. Moreover, it is practically independent of the duration of the probe pulse. The reflected pulse with its short duration is the sum of two responses from the rising and falling edges. With increased pulse duration, these responses diverge in time and are not summed. Therefore, a subsequent increase in the pulse duration does not lead to an increase in the amplitude of the reflected signal, but can be used to suppress the "ringing" of the HF line path.

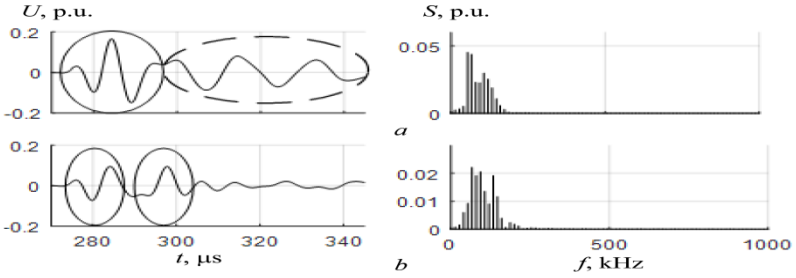

Fig. 9. Reflected signals (left column) at optimal probe pulse durations of 4.8 μs (a) and 17.6 μs (b) in the HF path of the 110 kV "Kutlu-Bukash – Rybnaya Sloboda" OHPL and their spectra (right column); the solid oval marks the reflected signal, and the dashed line indicates the "ringing" of the HFS

Distortion of reflected signals when ice deposits appear

When ice deposits appear on the wires, the conditions of signal propagation along the HF paths of the overhead lines change: the propagation speed of electromagnetic waves decreases, causing a delay $\Delta\tau$ of the location signals, and additional attenuation $\Delta\alpha$ appears due to dielectric losses in ice.

Figure 10 shows the change dynamics of delay $\Delta\tau$ and attenuation $\Delta\alpha$ of the reflected location signals in the HF path of the 110 kV "Kutlu-Bukash – Rybnaya Sloboda" OHPL for December 23-24, 2016. During this period, intense icing occurred on the wires of overhead power transmission lines. The growth of icy deposits continued around 30 hours; by 1 p.m. on December 24, the maximum thickness of ice deposits was about 8 mm. Deposits remained on the wires until 9 a.m. on December 25, after which their sizes began to decrease naturally, and in a week, the wire line was completely cleared of ice.

Sections of seven reflectograms for the period of December 23-24, 2016 were analyzed to study changes in the shape of location pulses during icing. The reflectogram measuring times are marked with bold dots I – VII in Fig. 10.

Fig. 11 shows sections of reflectograms of HF path of the 110 kV "Kutlu-Bukash – Rybnaya Sloboda" OHPL. To illustrate the changes in the reflected pulses, the intervals Δt_i indicate the positions of the reflected signals peaks relative to 260 μs (the beginning of the time window for searching of the reflected signal in the reflectogram of this overhead line). In this case, the signal delay $\Delta\tau_i$ is connected with the interval Δti via relation $\Delta\tau_i = \Delta t_i - \Delta t_1$.

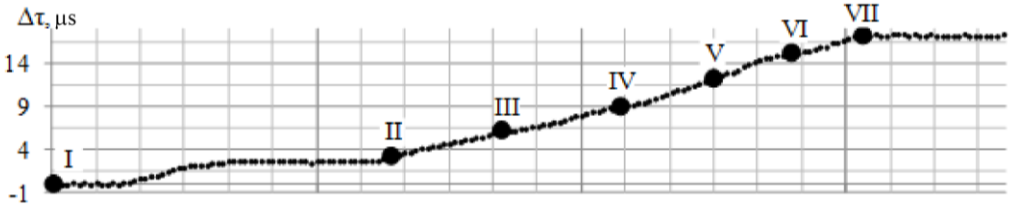

a)

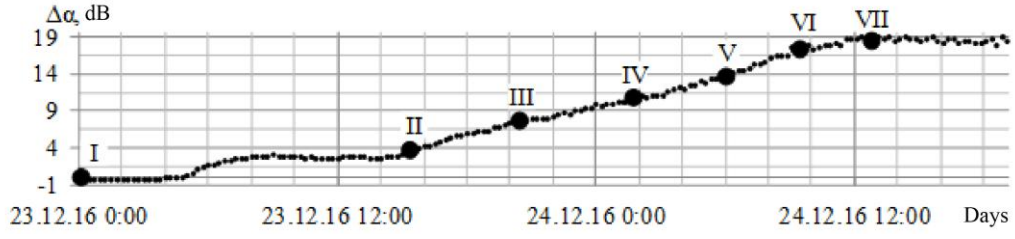

b

Fig. 10. Dynamics of changes in delay Δτ (a) and attenuation Δα (b) of the reflected location signals in the HF path of the 110 kV "Kutlu-Bukash – Rybnaya Sloboda" OHPL for December 23–24, 2016

Fig. 11 shows a decrease in the amplitude of the reflected signal both on reflectograms and on their spectra. Initially, the spectrum of the reflected signal is concentrated in the frequency range 50–150 kHz with a maximum at a frequency of 90 kHz. With the formation of ice deposits, the duration of the reflected signals increases and the maximum of the spectrum of the reflected signal shifts to lower frequencies by 70–80 kHz, this is due to the fact that the components of the signal at higher frequencies decay faster than the signal components at low frequencies [12].

Also, a tendency toward an increase in the reflected signals delay as ice builds up on the wires is observed in Fig. 11. In the absence of ice deposits on the wires, the time of location pulse propagation (Fig. 11, a) is approximately 270 μs, and it gradually increases as ice builds up, and reaches 287 μs (Fig. 11, g).

The maximum changes in delay and attenuation for Fig. 11, g were 17 μs and 19 dB. In this case, the amplitude of the reflected signals decreased from approximately 2 V to 0.15 V. Table 1 shows the attenuation and delay of signals for these seven reflectograms.

Table 1

Changes in attenuation and delay of location signals with ice growing

Measurement No.	I	II	III	IV	V	VI	VII
Date, time	23.12.2016			24.12.2016			
	00:30	15:30	20:45	01:50	06:00	9:50	13:00
Delay Δτ, μs	0	3	6	9	12	15	17
Attenuation Δα, dB	0	4	8	11	14	17	19

The maximum dimensions (wall thickness) of the ice clutch, according to calculations, amounted to about 8 mm, such deposits are not able to cause wire breakage. Therefore, the removal of ice deposits in this case was not performed, and they disappeared naturally in the next 6-7 days.

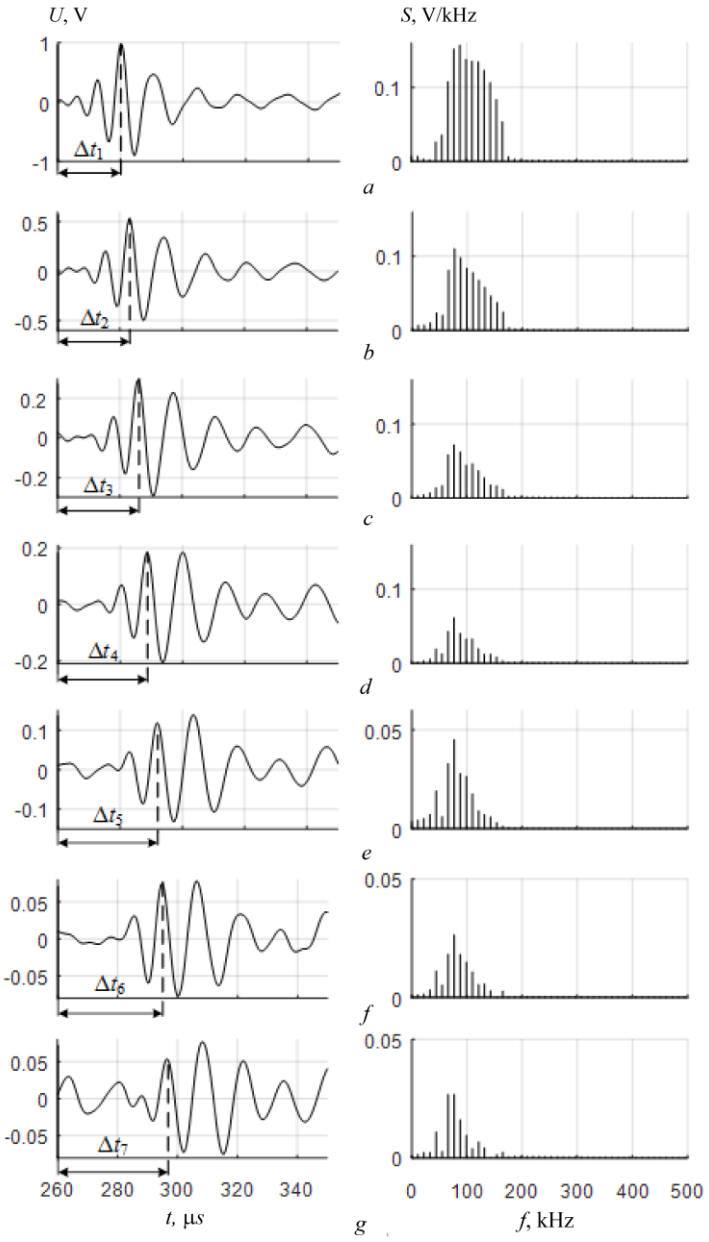

Fig. 11. Changes in reflected location signals in the HF path of the 110 kV "Kutlu-Bukash – Rybnaya Sloboda" OHPL (left column) and their spectra (right column) for the period from December 23–24, 2016 when ice is formed on the wires (moments of reflectogram measurement a-g are marked with points I – VII in Fig. 10)

Conclusions

The changes of location signal shapes during the passage of the elements of the high-frequency path were studied using a simulation model. The developed simulation model for the propagation of broadband probe pulses through narrow-band HF paths of OHPL makes it possible to determine the distortion of location pulses depending on their shape and duration. Elements of high-frequency path make a filtering impact on the broadband location signal. As a result, in this example the spectrum width of the reflected location signal is narrowed significantly from 1000 kHz to 200 kHz.

Analysis of the passage of pulses of different durations showed that the optimal pulse duration can be selected based on two criteria: minimizing the oscillatory processes caused by the high-frequency stopper, or maximizing the amplitude of the reflected location signal. The probe pulses durations will be determined either by the period of the oscillatory process caused by high-frequency stopper or by the half-period of the center frequency of the reflected location signal.

Analysis of changes in the parameters of reflected location pulses during ice formation showed that ice deposits cause a decrease in the propagation speed of location signals, which leads to a delay in reflected signals, in addition, ice causes significant attenuation of location signals, while the high-frequency components decay faster, which leads to a gradual shift of central frequency of the reflected location signals spectrum to the low-frequency region.

The research results are used to optimize the parameters of the probe pulse signals of the location software and hardware complex.

The author is grateful to R.G. Minullin, Yu.V. Piskovatsky, M.R. Yarullin, as well as to the staff of the Volga electric networks (JSC "Grid Company", Tatarstan) for their help in conducting experiments and analyzing the results.

References

1. Minullin RG. *Lokacionnyj monitoring gololedno-izmorozevyh otlozhenij i povrezhdenij na provodah vozdushnyh linij elektroperedachi*. Moscow: NTF "Energoprogress": Energetik; 2017. (In Russ).
2. Minullin RG. *Lokacionnyj monitoring gololedno-izmorozevyh otlozhenij i povrezhdenij na provodah vozdushnyh linij elektroperedachi*. Moscow: NTF "Energoprogress": Energetik; 2017. Pt 2. (In Russ).
3. Minullin RG. *Lokacionnyj monitoring gololedno-izmorozevyh otlozhenij i povrezhdenij na provodah vozdushnyh linij elektroperedachi*. Moscow: NTF "Energoprogress": Energetik; 2017. Pt 3. (In Russ).
4. Dogadkin D, Marin R, Shirshova E, Ismukov G, Kulikov A, Lint M, Podshivalin A. Ustrojstvo avtomaticheskogo povtornogo vklyucheniya kabel'no-vozdushnyh linij elektroperedachi megapolisov. *Elektroenergiya. Peredacha i raspredelenie*. 2016; 38(5):98-103. (In Russ).
5. Shilin AN, Shilin AA, Artyushenko NS, Avdeyuk DN. Reflektometr dlya linij elektroperedachi s avtomaticheskoj korrekciej metodicheskoj pogreshnosti. *Kontrol'. Diagnostika*. 2018; 4:52-57. doi: 10.14489/td.2018.04.pp.052-057.(In Russ).
6. Minullin RG. Elektromagnitnaya sovmestimost' apparatury lokacionnogo monitoringa linij elektroperedachi s vysokochastotnoj apparaturoj tekhnologicheskoj svyazi. *Elektricheskie stancii*. 2019; 1(1050):16-27. (In Russ).
7. Kasimov VA, Minullin RG. Obrabotka reflektogramm zondirovaniya vozdushnyh linij elektroperedachi. *Materialy 7 Mezhdunarodnoj nauchno-tekhnicheskoj konferencii "Elektroenergetika glazami molodezhi"*. Kazan,

Литература

1. Минуллин Р.Г. Локационный мониторинг гололедно-изморозевых отложений и повреждений на проводах воздушных линий электропередачи. М.: НТФ "Энергопрогресс": Энергетик, 2017. 88 с.
2. Минуллин Р.Г. Локационный мониторинг гололедно-изморозевых отложений и повреждений на проводах воздушных линий электропередачи. М.: НТФ "Энергопрогресс": Энергетик, 2017. Ч.2. 76 с.
3. Минуллин Р.Г. Локационный мониторинг гололедно-изморозевых отложений и повреждений на проводах воздушных линий электропередачи. М.: НТФ "Энергопрогресс": Энергетик, 2017. Ч.3. 60 с.
4. Догадкин Д., Марин Р., Ширшова Е., Исмуков Г., Куликов А., Линт М., Подшивалин А. Устройство автоматического повторного включения кабельно-воздушных линий электропередачи мегаполисов // Электроэнергия. Передача и распределение. 2016. № 5 (38). С. 98-103.
5. Шилин А.Н., Шилин А.А., Артюшенко Н.С., Авдеюк Д.Н. Рефлектометр для линий электропередачи с автоматической коррекцией методической погрешности // Контроль. Диагностика. 2018. № 4. С. 52-57.
6. Минуллин Р.Г. Электромагнитная совместимость аппаратуры локационного мониторинга линий электропередачи с высокочастотной аппаратурой технологической связи // Электрические станции. 2019. № 1 (1050). С. 16-27.
7. Касимов В.А., Минуллин Р.Г. Обработка рефлектограмм зондирования воздушных линий

Russia. Kazan: KGEU.2016. pp. 65-68.
8. Shagiev RI. Imitacionnaya model' lokacionnogo metoda diagnostiki elektrolinij s drevovidnoj topologiej. *Zhurnal radioelektroniki*. 2016; 10:1–18 (In Russ).
9. Shagiev RI, Karpov AV, Kalabanov SA. Model' metoda opredeleniya mesta povrezhdeniya LEP s ispol'zovaniem reflektometrii vo vremennoj oblasti. *Fizicheskij zhurnal*. 2017; 803:1–7. (In Russ).
10. Yarullin MR, Minullin RG. Optimizaciya formy impul'snyh signalov pri lokacionnom zondirovanii linij elektroperedachi. *Energetika Tatarstana*. 2014; 2(34):62–65. (In Russ).
11. Kasimov VA, Minullin RG, Piskovatsky YuV, Abdullazyanov EYu. Model-experimental detection of damage on the overhead transmission lines wires by location method. *Electrosvyaz.* 2019; 4:102–108. (In Russ).
12. Kasimov VA, Minullin RG. Detection of icing and freezing deposits on the wires of overhead power lines by the location method. *Power Stations.* 2018; 10:38–48. (In Russ).

электропередачи // Материалы 7 Международной научно-технической конференции «Электроэнергетика глазами молодежи»; Казань. КГЭУ, 2016. С. 65–68.
8. Шагиев Р.И. Имитационная модель локационного метода диагностики электролиний с древовидной топологией // Журнал радиоэлектроники. 2016. №10. С. 1–18.
9. Шагиев Р.И, Карпов А.В., Калабанов С.А. Модель метода определения места повреждения ЛЭП с использованием рефлектометрии во временной области // *Физический журнал: Серии конференций.* 2017. №803. С. 1–7.
10. Яруллин М.Р., Минуллин Р.Г. Оптимизация формы импульсных сигналов при локационном зондировании линий электропередачи. // Энергетика Татарстана. 2014. № 2 (34). С. 62–65.
11. Касимов В.А., Минуллин Р.Г., Писковацкий Ю.В., Абдуллазянов Э.Ю. Модельно-экспериментальное обнаружение локационным методом повреждений на проводах воздушных линий электропередачи // Электросвязь. 2019. № 4. С. 102–108.
12. Касимов В.А., Минуллин Р.Г. Распознавание локационным методом гололедных и изморозевых отложений на проводах воздушных линий электропередачи // Электрические станции. 2018. №10. С. 38–48.

Authors of the publication

Vasil A. Kasimov **–** PhD in Engineering sciences, Associate Professor Kazan State Power Engineering University, Kazan, Russia. E-mail: VasilKasimov@yandex.ru.

Received ***April 29, 2019***

INSTRUMENT MAKING, METROLOGY AND INFORMATION-MEASURING DEVICES AND SYSTEMS

UDC 004.3 **DOI:10.30724/1998-9903-2019-21-3-160-171**

METHOD FOR CONTROL THE MECHANICAL PARAMETERS OF OVERHEAD POWER LINES BASED ON IMPROVED INCLINOMETRY

M.P. Goryachev, M.F. Sadykov, D.A. Yaroslavskiy

Kazan State Power Engineering University, Kazan, Russia
goryachev91@mail.ru

Abstract: *Structural elements of overhead power transmission lines are experiencing both horizontal and vertical loads. Wires and cables are elements of the overhead power line, on which changes in mechanical loads are observed to a greater degree. This occurs due to the change in the tension force of the wire/cable depending on the temperature and the formation of icy-rime deposits on it, as well as fluctuations in wind gusts. The article describes the most common systems and methods for determining the mechanical loads on an overhead power transmission line. A method is proposed for calculating the mechanical loads on an overhead transmission line based on mathematical models of a flexible wire, rope and a model for determining ice deposits on wires, taking into account the rotation of the wire/cable around its axis. A comparison of the improved inclinometry method with the method developed earlier for the case of formation of ice deposits on the S-50 cable has been carried out. A comparison was made on the error in determining the tension of the S-50 ground-wire protection cable using the method developed to control the mechanical parameters of overhead power lines, which takes into account the wire/cable rotation around its axis and the method for determining icy-rime deposits developed earlier. The developed method allows determining the elongation of the wire/cable in the span with one anchor support, as well as the strength of its tension with greater accuracy. However, additional clarification is required due to the influence of the wind, the formation of icy-rime deposits of various shapes, as well as the structural limitations of the wire/cable rotation when attaching it to the support.*

Keywords: *overhead power line, overhead line monitoring, mechanical loads, cable rotation, rotation of ground wire, icy-rime deposits, icing.*

For citation: Goryachev MP, Sadykov MF, Yaroslavskiy DA. Method for control the mechanical parameters of overhead power lines based on improved inclinometry. *Power engineering: research, equipment, technology.* 2019; 21(3):160-171. (In Russ). doi:10.30724/1998-9903-2019-21-3-160-171.

МЕТОДИКА КОНТРОЛЯ МЕХАНИЧЕСКИХ ПАРАМЕТРОВ ВОЗДУШНЫХ ЛИНИЙ ЭЛЕКТРОПЕРЕДАЧИ НА ОСНОВЕ УЛУЧШЕННОГО ИНКЛИНОМЕТРИЧЕСКОГО МЕТОДА

М.П. Горячев, М.Ф.Садыков, Д.А. Ярославский

Казанский государственный энергетический университет, Казань, Россия
goryachev91@mail.ru

Резюме: *Конструктивные элементы воздушных линий электропередачи испытывают как горизонтальные, так и вертикальные нагрузки. Провода и тросы являются элементами воздушной линии, на которых в большей степени наблюдаются изменения механических нагрузок ввиду изменения силы натяжения провода/троса в зависимости от температуры и образования на нём гололёдно-изморозевых отложений, а также колебаний от порывов ветра.В статье описаны наиболее распространенные системы и методики определения механических нагрузок на воздушной линии электропередачи. Предлагается методика расчёта механических нагрузок на воздушной линии электропередачина основе математических моделей гибкой нити, каната и модели определения гололёдных отложений на проводах/тросах, учитывающая вращение провода/троса вокруг своей оси.Проведено сравнение улучшенного инклинометрического метода с методом, разработанным ранее для случая образования гололёдных отложений на тросе С-50. Оценены погрешности при определении силы тяжения грозозащитного троса С-50предлагаемой методикой контроля механических параметров воздушных линий электропередачи, учитывающей вращение провода/троса вокруг своей оси, и методикой определения гололёдно-изморозевых отложений, разработанной ранее. Разработанная методика позволяет определить удлинение провода/троса в пролёте с одной анкерной опорой, а также силу его тяжения с большей точностью, однако требует дополнительного уточнения, связанного с влиянием ветра, образованием гололёдно-изморозевых отложений различной формы, а также конструктивными ограничениями вращения провода/троса при креплении его к опоре.*

Ключевые слова: *воздушная линия электропередачи, мониторинг воздушных линий,механические нагрузки, вращение провода, вращение грозозащитного троса, гололедно-изморозевые отложения, гололед.*

Introduction

Electrical energy is transferred from power plants or substations to the consumer via power lines (mainly overhead), which are part of the electrical system. An overhead power line is a device for transmitting electrical energy through wires located in the open air and secured with insulators and linear fittings to the supports. In addition, lightning protection cables are also used on overhead lines.

The length of overhead power lines in the Russian Federation is over 2.8 million km. The power grid is rapidly becoming obsolete. The level of equipment wear reaches 70% [1]. At the same time, due to the increase in electricity consumption and the commissioning of new sections of overhead power lines, the need for a full-fledged survey to prevent emergency situations increases.

All elements of overhead power lines experience mechanical stress and can be damaged if their mechanical strength limit is exceeded.

Structural elements of overhead power lines experience both horizontal (for example, mechanical stresses in a stretched wire/cable) and vertical loads (for example, from its own weight

or the weight of the wire/cable). Wires and cables are elements of the overhead line on which changes in mechanical loads are observed to a greater degree due to changes in the tension of the wire/cable depending on temperature and the formation of icy-rime deposits on it [2], as well as fluctuations from wind gusts. The main mechanical stresses in the wire/cable of the overhead line are associated with its extension. With an increase in the tensile strength of the wire or rods (cores) of which it is made, its tension also increases.

Exceeding the tensile strength of an overhead power line element can lead to its damage: wire/cable breakage, failure or breakdown of the insulator, interphase short circuit due to wire "dancing" and others.

Mechanical overload of a power line structural element can occur due to the appearance of icy-rime deposits (IRD), the development of fatigue of the air power transmission line structural element, errors in the construction of the line, as well as repair and restoration work. Among the listed reasons, the appearance of IRD is accompanied by the most serious consequences. Therefore, in the future, this problem will catch special attention.

According to the map of ice loads, the Republic of Tatarstan belongs mainly to the second risk group (the normative ice wall thickness on a wire/cable is at least 15 mm). However, the Bugulminsky district, for example, belongs to the fourth, most dangerous group (the normative ice wall thickness on the wire/cable is at least 25 mm). Problems with ice formation were also detected in Leninogorsk, Nurlat and Almetyevsk regions. The number of temperature transitions through 0 °C increased, which led to an increase in the probability of ice formation, since icy-rime deposits on the wires/cables of power lines are formed when supercooled drops of rain, drizzle or fog freeze at temperatures from 0 °C and below [3]. During a relatively mild winter, with a sharp difference in ambient temperature from positive to negative, drops of water settle on the wires/cables and an avalanche-like process of formation of a thick ice crust begins, reaching a thickness of several tens of millimeters, which significantly increase weights of wires/cables.

Deposits of ice, rime and wet snow pose a great danger to the normal operation of overhead transmission lines (OTL). They can cause: a) misalignment of wires and cables and their reprochement with each other; b) reprochement of wires and cables during a jump due to non-simultaneous discharge of ice; c) intense dancing, causing short circuits between wires and between wires and cables, burns of wires and cables, and in some cases damage to linear fittings and fixtures; d) a significant overload of wires and cables and their breaks; e) destruction of supports as a result of breakage of wires and cables during overloading from ice, when unbalanced loads on supports from remaining whole wires and cables significantly exceed the calculated ones, as well as when ice is combined with strong wind; f) overlap of the linear insulation of overhead lines during ice melting, due to a significant decrease in the ice discharge characteristics of insulators as compared to moisture discharge characteristics, which usually select the required level of linear insulation [2].

Thus, it is necessary to accurately localize a site or defect that is problematic with ice, since it is often difficult to travel along overhead lines (deep snowdrifts; natural barriers, i.e. marshy terrain; relief, etc.), and the speed of preventing/eliminating an emergency directly related to the losses incurred.

1. Overview of existing methods and means of determining mechanical loads on an overhead power line

Wires and cables suspended to the supports of an overhead power line are constantly exposed to a vertical load from its own weight, evenly distributed along the length of the line. In addition, other loads can affect them: vertical from ice and horizontal from wind. Therefore, the task of determining mechanical loads on an overhead power line from a practical point of view is inextricably linked with the determination of ice-wind loads. Therefore, it is necessary to consider the methods for identifying and monitoring these types of loads.

The following systems based on stationary devices are used to monitor the state of overhead lines: *CAT-1* (USA) [4], *DiLin* (RF) [5], *Astrose* (Germany) [6], *LINDSEY* (USA) [7], etc.

The *CAT-1* system monitors weather conditions and mechanical loads at the points of wire suspension to the support. The system is quite simple, but due to the patented analysis algorithms it is possible to determine such OTL parameters as: sag arrow, presence of IRD. The main disadvantage of this system is the use of strain gauges mounted on the traverse of the supports, which complicates the installation of the *CAT-1* system [8].

The operation of the *DiLin* system (RF) [9] is based on the frequency method [10,11] for controlling ice formation on overhead lines. Monitoring the presence of icy-rime deposits on overhead line wires is determined by the change in the speed of the electromagnetic field wave along the power line wire. The appearance of ice on the wires is equivalent to the appearance of a large number of short-circuited circuits covering the linear wire in the icing zone. With an increase in the icing zone of wires and the thickness of the ice layer, the influence of these "active - inductive" circuits also increases. This, in turn, leads to an increase in the wave impedance of the overhead line. The active component of the resistance of icy contours leads to an increase in the attenuation of the amplitude of high-frequency signals moving along the line. The reactive resistance of the ice contours slows down the speed of the electromagnetic field wave along the line wires. However, this method has several disadvantages: a high error in the localization of defect sites (up to kilometers); increased influence of connections to the overhead line and environmental factors (the internal resistance of the line changes, which affects the reflected signals) [10].

The *LINDSEY* (USA) [7] and *Astrose* (Germany) [6] systems have proven themselves best of the systems for monitoring the state of overhead lines by indirect methods. They include a tilt angle sensor, a temperature sensor and a current sensor, which allows determining the mechanical loads and parameters of the overhead line [11]. *LINDSEY* and *Astrose* are very informative and form a self-organizing wireless data network. However, these systems have a number of drawbacks: the mathematical model does not allow tracking the icing process, does not take into account the hauling of the wire between adjacent spans, as well as the change in the overhead line geometry depending on the wire temperature [8].

Thus, two methods are mainly used to calculate the mechanical loads of overhead power lines: direct determination (using tensometric sensors) or indirect (inclinometry methods, which are based on the angle of the wire).

2. Improved inclinometry method for determining mechanical loads on an overhead power line

The most promising method for determining mechanical loads on a wire/cable is the inclinometry method based on measuring the angle of inclination of various objects relative to the gravitational field of the earth. As a verification method, a technique is being developed to determine the mechanical loads on a wire/cable depending on the angle of its rotation around its axis. In this case, the monitoring device should be installed in close proximity to the point of suspension of the wire/cable to the string of insulators on the anchor support (for example, 1 meter from the point of suspension of the wire/cable). This is possible due to the fact that when the wire/cable is stretched, its rotation around its axis is observed, which allows obtaining additional information, and therefore to improve the existing inclinometry method for determining the tension of the wire/cable from its angle of inclination.

The spiral shape that is attached to the wire when twisting a high-voltage wire/cable is subsequently maintained due to residual strains obtained by twisting. Stresses that occur in the wire during twisting are mainly driven by bending and torsion. If the stresses are within the elastic range, then the wire after the termination of the impact from external forces will restore its original direct shape. In fact, when twisting a wire/cable, its rods always get residual deformations [12].

Due to the presence of mechanical deformations during tension of the wire/cable, its rotation around its axis is observed, which allows obtaining additional information about the behavior of the wire/cable on the overhead power line and consider it not within a single span, but as a whole interconnected section with the redistribution of mechanical loads between spans.

The methodology for calculating mechanical loads on an overhead power line using the improved inclinometry method includes two stages: 1) the calibration stage; 2) the IRD calculation stage.

2.1. The calibration stage

In the absence of IRD, when calculating the length of an unstretched wire/cable, we use the theory of ideal cable (thread) to determine the unknown parameters [14].

The system of equations for fiber balance:

$$\begin{cases} u = \frac{1}{2}\left(\frac{l}{a} - \alpha^* q_0 L_0\right) \\ \mathrm{sh}(u) = \frac{L_0}{2a} \end{cases} \quad (1)$$

where l is the span length, m; q_0 is the gravity force referred to a unit of length of an unstretched wire/cable, N/m; $a = \frac{H}{q_0}$ is the ratio between the horizontal gravity force to the gravity force referred to a unit of length of an unstretched wire/cable; α^* is the specific relative elongation of cable/wire, N^{-1}; L_0 is the length of the unstretched wire/cable, m.

To simplify further calculations, a variable u is introduced [14]:

$$u = \ln \mathrm{tg}\left(\frac{\pi}{4} + \frac{\alpha}{2}\right) \quad (2)$$

where α is the wire/cable tilt angle at the suspension point.

Based on the system of equations of balance of the fiber balance, by means of exclusion of a and expression, L_0 we obtain the following expression for determining the length of an unstretched wire/cable at the current temperature:

$$L_0 = \frac{-u + \sqrt{2\alpha^* l \times q_0 \times \mathrm{sh}(u) + u^2}}{\alpha^* q_0} \quad (3)$$

Based on the fact that the length of the unstretched wire/cable is calculated according to its physicochemical characteristics at a temperature of 20 °C, it is necessary to take into account the change in the length of the unstretched wire/cable depending on the ambient temperature. In the formula listed above, the temperature dependence is observed for the parameter q_0 since when the length of the wire/cable changes, its linear mass also changes. Therefore, the gravity referred to the unit length of the unstretched wire/cable will be equal to:

$$q_0 = \frac{q_{0t}}{1 + \beta(t_1 - t_0)} \quad (4)$$

where q_{0t} is the gravity force referred to the unit of length of the unstretched wire/cable (obtained by multiplying the gravity acceleration by the linear mass of the wire/cable taken from the handbook) [15]; t_0 is the temperature of wire/cable fabrication, °C; t_1 is the current temperature of wire/cable, °C; β is the temperature coefficient of linear elongation, $°C^{-1}$.

A wire/cable has the lowest intrinsic stress in the absence of external forces acting on it at the temperature of its fabrication. Therefore, it is necessary to divide the current length of the unstretched wire/cable to the length of the unstretched wire/cable at the temperature of its fabrication:

$$L_{0t} = \frac{L_0}{1 + \beta(t_1 - t_0)} \quad (5)$$

where L_0 is the length of the unstretched wire/cable at current temperature, m; L_{0t} is the length of the unstretched wire/cable at the temperature of its fabrication, m.

To reduce the possible error, the parameter L_{0t} should be averaged over the entire calibration period (overhead line operation time without IRD).

To describe the rotation of the wire/cable, a rope model should be considered [16].

At the ends of the rod span, the wires/cable are rigidly connected to each other and therefore receive the same end displacements, which means that in any section of the wire/cable along the length, all wires receive the same displacements. This means that due to the compatibility of the elastic displacements of the wire layers, despite the contact pressure between them, the internal friction forces can be neglected.

Thus, we obtain a generalized equation of static wire/cable:

$$\begin{cases} T = A \times \varepsilon + C \times \theta \\ M = C \times \varepsilon + B \times \theta \end{cases} \tag{6}$$

where T is the gravity of wire/cable; M is the cross-section torque of wire/cable; A, B, C, are the generalized wire/cable stiffness factors;

$\varepsilon = \dfrac{ds - ds_0}{ds_0}$ where s ds is the longitudinal displacement of rods when the length of the wire/cable ds_0 changes; ε is the longitudinal deformation in the rod of wire/cable; θ is the angular deformation in the rod of wire/cable, $\theta = \dfrac{d\varphi}{ds_0}$, where $d\varphi$ is the angular displacement in rods w when the length of the wire/cable s_0 changes.

The generalized equation of wire/cable statics gives a complete description of its aggregate mechanical properties during tension and torsion. For a mechanical system, the number of degrees of freedom is equal to the number of joint equations describing its displacements under the influence of an external load. For a wire/cable, we have a system of two equations. Therefore, it acts as a system with two degrees of freedom, that is, all its mechanical properties are similar to that for an elastic system with two degrees of freedom.

To do this, we consider the main special cases of load on the wire/cable: pure tension and free tension.

Pure tension is observed when the wire/cable is stretched by force T when its ends are fixed from rotation ($\theta = 0$).This mode of mechanical loads is characteristic for the operation of the wire/cable in the spans with bushings. In this case, the following relations are obtained:

$$\begin{cases} T = A \times \varepsilon \\ M = C \times \varepsilon \end{cases} \tag{7}$$

From the first equation it follows that the coefficient A is the elastic modulus of the wire/cable.

If in case of pure tension, one removes the securing of the second end of the wire/cable from rotation, then the wire/cable under the action of internal torque will unwind. This mode of mechanical loads is characteristic for the operation of the wire/cable in the spans with one passage and one anchor support. The external moment is zero ($M = 0$) This type of load is called free stretching.

Moreover, we obtain the following equalities:

$$T = (A - \frac{C^2}{B}) \times \varepsilon = (\frac{A \times B}{C} - C) \times \theta. \tag{8}$$

The factor before ε characterizes the longitudinal displacement of the rods, and the factor before θ characterizes the angular displacement of the wires in the wire/cable. Based on this, we obtain the following equation for the dependence of the extension of the wire/cable on the angle of rotation around its axis, which is then simplified by dividing both parts by ds_0 and independently integrating both parts of the expression:

$$\int(A-\frac{C^2}{B})\times ds=\int(\frac{A\times B}{C}-C)\times d\varphi\Rightarrow\Delta L=\frac{B}{C}\Delta\varphi \quad (9)$$

where ΔL is the change in length of wire/cable; $\Delta\varphi$ is the change in the rotation angle of the wire/cable around its axis.

To calculate the elongation of the wire/cable, we use the formula from the hyperbolic model of wire calculation [17]

.

$$\Delta L=\frac{\alpha^*}{2}a\times q_0\left[1+L_0(\mathrm{ch}(u)-\alpha^*\times a\times q_0)\right]. \quad (10)$$

Thus, the identity in formula (9) takes the following form:

$$\frac{B}{C}(\varphi_1-\varphi_0)=\frac{\alpha^* a\times q_0\left[1+L_{0t}(\mathrm{ch}(u)-\alpha^*\times a\times q_0)\right]}{2} \quad (11)$$

where φ_1 is the angle of rotation of the wire/cable around its axis at current mechanical loads on the wire/cable and the ambient temperature before IRD appearance; φ_0 is the initial angle of rotation of the wire/cable around its axis until the appearance of the IRD.

In expression (11), the coefficient of the ratio of horizontal gravity to gravity, referred to the unit length of the unstretched wire/cable, is determined as follows:

$$a=\frac{L_0}{2\mathrm{sh}(u)} \quad (12)$$

From formula (11) we take φ_0 and calculate it at the current temperature. At the same time, one should not forget to correct the gravity referred to the unit length of the unstretched wire/cable to its current temperature in accordance with formula (4).

To reduce the possible error in determining the initial angle of rotation of the wire/cable around its axis, the parameter φ_0 should be averaged over the entire calibration period (the period of overhead line operation without IRD).

Thus, the calibration step ends when determining the initial angle of rotation of the wire/cable around its axis, as well as the length of the unstretched wire/cable at its temperature of fabrication.

The stage of determining mechanical loads on an overhead power line by the improved inclinometry method

When the preconditions for the IRD formation (humidity above 80%, the temperature of the wire/cable is in the range from 0 to -5 °C) appear, the system for determining mechanical loads switches to control mode.

The simplification variable u is calculated by the formula (2) at the inclination angles of the wire/cable for cases of rapid increase in mechanical loads on the wire/cable (for example, the formation of IRD).

Next, the length of the unstretched wire/cable is calculated at the current temperature in relation to the length of the unstretched wire/cable at the temperature of its fabrication in accordance with formula (5):

$$L_{0g}=L_{0t}(1+\beta(t_1-t_0)) \quad (13)$$

In formula (11), we replace $a\times q_0$ with H and express the horizontal tension force of the wire/cable:

$$H=\frac{\alpha^*(1+L_{0g}\times\mathrm{ch}(u))-\sqrt{(\alpha^*)^2(1+L_{0g}\times\mathrm{ch}(u))^2-8(\alpha^*)^2L_{0g}(\varphi_1-\varphi_0)\frac{B}{C}}}{2\alpha^*L_{0g}} \quad (14)$$

As a result, we find the gravity of the wire/cable:

$$T = H \times \mathrm{ch}(u) \quad (15)$$

For an overhead power line, it is the wire/cable tension parameter that is critical in terms of mechanical stress. Therefore, the process of determining mechanical loads on an overhead power line can be completed at this stage.

Results and discussion

The data obtained from monitoring systems include the error of the measuring sensors. Thus, the developed system for monitoring mechanical loads on a wire/cable has instrumental and methodological errors.

Instrumental errors include deviations of sensor readings. For this model, the following data is required: the angle of rotation of the wire/cable around its axis, the angle of inclination of the wire/cable and the temperature of the wire/cable. The maximum deviations in the readings of the sensors in the range of formation of ice deposits (from -20 to 0 °C, from 70 to 100% of relative humidity) are: ± 0.2 ° C for temperature; 0.0039 rad along the axes *X* and *Y*.

To test the method for determining the mechanical loads on the wires/cables of overhead lines, we calculated the steel lightning protection cable S-50 for an anchor span of 50 meters in length, where conditions for free rotation of the lightning cable under consideration appear. The length of the unstretched cable L_{0t} was taken equal to 50.1 m. The stiffness factors A=9.196·10^6 N, B=6.521 N·m^2 and C=5.994·10^3 N·m for the S-50 cable were taken from the table of the book "Steel hoisting ropes "[16] for the type of strand 1+6+12. In addition, the following S-50 cable parameters were used: $\beta = 12 \cdot 10^{-6}$ °C^{-1}, q_0 =4.094 N/m; φ_0 =0º.

As parameters for calculation mechanical loads on overhead power lines, the conditions for operating the overhead line at a temperature of -5 °C without IRD on the cable, as well as in the presence of an IRD with a diameter of up to 40 mm, were selected[1] [18].

The load from ice formations on the cable was calculated by the following formula

$$T_g = q_{0g} \times 9{,}8 \times \pi \times c \times (d_{\mathrm{cab}} + c) \times L_{0g} \quad (16)$$

where q_{0g} is the IRD density (900 kg/m^3); c is the thickness of the icy socket, m (c =0.01545 m); d_{cab} is the wire diameter, m (for S-50 d_{cab} = 0.0091 m).

Thus, the load from an IRD with a diameter of 40 mm on the S-50 cable at a temperature of -5 °C is 526.6 N.

In the absence of IRD on the cable, the angle of rotation of the cable around its axis is 3.452 rad, and the angle of inclination of the cable is 0.103 rad. When an icy socket with a diameter of 40 mm appears on the cable, the rotation angle of the cable around its axis is 101.984 rad, and the angle of inclination of the cable is 0.153 rad.

Based on formulas (14) and (15), we find the value of the tension force of the wire/cable:

$$T = \frac{(1 + L_{0g} \times \mathrm{ch}(u)) - \sqrt{(1 + L_{0g} \times \mathrm{ch}(u))^2 - 8 L_{0g} (\varphi_1 - \varphi_0) \frac{B}{C}}}{2\alpha^* L_{0g} \times \cos(\alpha)} \quad (17)$$

The resulting dependence of the obtained tension force of the cable on the angle of its rotation shown in the figure.

The tension strength of the wire/cable depends on 3 parameters: the angle of rotation of the wire/cable around its axis, the angle of inclination of the wire/cable and the temperature of the wire/cable. Therefore, when calculating the error, it is necessary to take into account the influence

[1] PUE. 7-nd. Pt. 2.5. Vozdushnye linii elektroperedachi napryazheniem vyshe 1 kV. M.: OAO «VNIIE», 2003. Available at: https://www.ruscable.ru/info/pue/2-5.html.

of these parameters on the result of calculating the tensile strength of the wire/cable:

$$\Delta T = \frac{dT}{df}\Delta\varphi + \frac{dT}{d\alpha}\Delta\alpha + \frac{dT}{dt}\Delta t \qquad (18)$$

where Δt Is the deviations in the readings of the temperature sensor in the range of ice formation.

The error of the developed method [18] was analyzed by comparing it with the previously developed method for monitoring ice on the wires of an overhead power line. The algorithm for calculating the error of the previously developed methodology is described in detail in the dissertation “System for the automated monitoring of ice deposits of overhead power lines based on the inclinometry-meteorological method” [19].

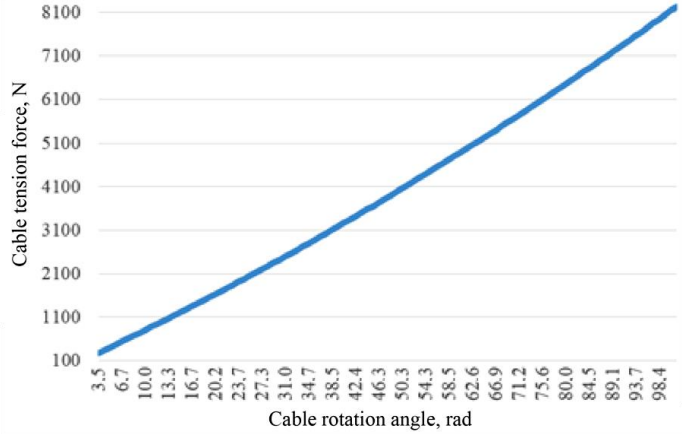

Fig. Relationship between the tension force of the cable and the rotation angle

For the conditions described earlier in this article when calculating the mechanical loads on the S-50 cable, the error of the developed method (taking into account the angle of rotation of the wire/cable around its axis) and the method developed earlier (excluding the rotation of the wire/cable around its axis), amounted to 0.46% (1.27 N) against 42.6% (118 N) with a minimum load and 0.04% (3.55 N) against 2.2% (183.94 N) when an icy socket with a 40 mm diameter appeared on the cable, respectively.

A comparison of the classical inclinometry and the developed methodology, taking into account the rotation of the wire/cable, is used as an example for calculating the S-50 by such characteristics as sensitivity and errors, in the range of operation from the minimum load to the load when an ice- socket with a diameter of 40 mm is formed on the cable is presented in the table.

Table

Comparison of the classic and developed methods that take into account the rotation of the cable

Characteristics	Classic	Developed
Temperature sensitivity, N/ºC	45	0. 05
Inclination angle sensitivity, N/deg	2230 ÷ 3375	4 ÷ 17
Rotation angle sensitivity, N/deg	No	1. 4
Error of the method, %	2. 2 ÷ 42.6	0. 04 ÷ 0. 46

Thus, the developed method for control the mechanical parameters of overhead power lines, taking into account the rotation of the wire/cable around its axis, is more accurate than the IRD determination method developed previously [21]. However, in practice, it is possible to use this technique based on the improved inclinometry method for the rotation angles of the wire/cable up to 180 º, which is due to structural limitations of the rotation of the wire/cable when attaching it to the support. In this case, the initial angle of rotation of the wire/cable is taken equal to 0º

degrees when the tension force of the wire/cable is close to the mounting one and at the temperature of this wire/cable fabrication. Thus, the diameter of the ice-clutch for calculating the S-50 ground wire in this article should not exceed 12.5 mm and is made only for flights with one anchor support.

Conclusions

A method has been developed for determining mechanical loads on wires/cables of overhead lines based on mathematical models of ideal cable, rope and a model for determining ice deposits on wires [15–17,20], taking into account the rotation of the wire/cable around its axis. This method allows more accurate determining the elongation of the wire/cable in the span with one anchor support, as well as the its tension force, however, it requires additional refinement related to the influence of the wind, the formation of IRD of various shapes, as well as structural limitations of the rotation of the wire/cable when attaching it to the support. The implementation of this technique will allow monitoring the mechanical parameters of wires/cables, as well as identifying areas with the formation of IRD in the early stages in order to prevent related emergencies.

The methodology for monitoring the mechanical parameters of overhead power lines based on the improved inclinometry method is the result of studies described in [17, 20]. For the practical implementation of the method, a technical solution was developed in the form of a measuring device for monitoring the mechanical parameters of an overhead power line [21].

The developed methodology for determining the mechanical loads on the wires/cables of overhead lines and the mathematical model are tested on the SMG-16 system, which was put into trial operation at PJSC Tatneft.

References

1 Bokov G. Tekhnicheskoe perevooruzhenie rossijskih elektricheskih setej. Skol'ko eto mozhet stoit'?.Novosti Elektrotekhniki 2002;24(2).(In Russ).

2. Sacuk EI. Programmno-tekhnicheskie sredstva monitoringa vozdushnyh linij elektroperedachi i upravleniya energosistemoj v ekstremal'nyh pogodnyh usloviyah. [dissertation]. Novocherkassk, 2011.Available at:https://www.dissercat.com/content/programmno-tekhnicheskie-sredstva-monitoringa-vozdushnykh-linii-elektroperedachi-i-upravleni.Accessed: 26 May 2011. (In Russ).

3.Titov DE., Soshinov AG., Shewchenko NJ. Thermodynamic method of glaze ice monitoring on air lines wires. *Applied Mechanics and Materials. Trans Tech Publications*. 2015; (698):803-807. (In Russ).

4. Kostikov I. Sistema monitoringa «SAT-1» – effektivnaya zashchita VLEP ot gololyoda. Available at: http://www.ruscable.ru/article/sistema_monitoringa_sat_1_effektivnaya_zashhita. Accessed: 25 Jan 2018. (In Russ).

5 Panasenko MV. Analiticheskij obzor sposobov i ustrojstv monitoringa promezhutochnogo proleta vozdushnoj linii elektroperedachi. *Mezhdunarodnyj zhurnal prikladnyh i fundamental'nyh issledovanij*.

Литература

1. Боков Г. Техническое перевооружение российских электрических сетей. Сколько это может стоить? // Новости Электротехники. 2002. №2(14).

2.Сацук Е.И. Программно-технические средства мониторинга воздушных линий электропередачи и управления энергосистемой в экстремальных погодных условиях.: Дис. … д-ра техн. наук. Новочеркасск,2011.Доступно по: https://www.dissercat.com/content/programmno-tekhnicheskie-sredstva-monitoringa-vozdushnykh-linii-elektroperedachi-i-upravleni. Ссылка активна на:26 мая 2011.

3.Titov D. E., Soshinov . G., Shewchenko N. J. Thermodynamic method of glaze ice monitoring on air lines wires //Applied Mechanics and Materials. – Trans Tech Publications, 2015; (698):803-807.

4. Костиков И. Система мониторинга «САТ-1» – эффективная защита ВЛЭП от гололёда. Доступно по:URL:http://www.ruscable.ru/article/sistema_monitoringa_sat_1_effektivnaya_zashhita/.Ссылка активна на:25 янв. 2018.

5.Панасенко М.В. Аналитический обзор способов и устройств мониторинга промежуточного пролета воздушной линии электропередачи // Международный журнал прикладных и

2014; 11. Pt. 4. pp 572 - 576. (In Russ).
6. Otto T. et al. Integrated Microsystems for Smart Applications. Sensors and Materials. 2018; 30(4):767-778.
7. Lindsey KE, Spillane PE, An-Chyun W. Dynamic real time transmission line monitor and method of monitoring a transmission line using the same .PATENT USA. №15725207.2018.Available at:http://lindsey-usa.com/wp-content/uploads/2015/10/11F-001-TLM-8-2014.
8. Yaroslavsky DA., Sadykov MF. Razrabotka ustrojstva dlya sistemy monitoringa i kolichestvennogo kontrolya gololyodoobrazovaniya na vozdushnyh liniyah elektroperedachi *Proceeding of the higher educational institutions*. ENERGY SECTOR PROBLEMS. 2017; 19(3-4): 69–79. (In Russ). doi.org/10.30724/1998-9903-2017-19-3-4-69-79.
9. DiLin - a system for monitoring the presence of ice on the wires of overhead lines. Available at: URL: https://dimrus.ru/dilin.html / Accessed: 25 Jan. 2018. (In Russ).
10. Rui X, Ji K. and McClure G. Dynamic response of overhead transmission lines with eccentric ice deposits following shock loads *IEEE Transactions on Power Delivery*. 2017; 32(3):1287-1294. doi:10.1109/tpwrd.2015.2501029.
11. Minullin RG., Kasimov VA, Filimonova TK, et al. Lokacionnoe obnaruzhenie gololyoda na vozdushnyh liniyah elektroperedachi.Pt1. Sposoby obnaruzheniya gololyoda. *Nauchno-tekhnicheskie vedomosti SPbGPU*. Informatika. Telekommunikacii. Upravlenie .2014; 2(193):61 - 73. (In Russ).
12. Minullin RG., Kasimov VA, Yarullin MR. Opredelenie tolshchiny ledyanyh otlozhenij na provodnikah vozdushnyh linij elektroperedachi metodom opredeleniya mestopolozheniya .*Trudy Mezhdunarodnogo seminara po atmosfernomu obledeneniyu konstrukcii* . Kazan , Russia. 2015. P. 101. (In Russ).
13Boshnyakovich AD. Mekhanicheskij raschet provodov i trosov linij elektroperedachi. M.-L.: Gosenergoizdat 1962. (In Russ).
14. Merkin DR. *Vvedenie v mekhaniku gibkoj niti*. M.: Nauka. Glavnaya redakciya fiziko-matematicheskoj literatury. 1980. (In Russ).
15. Kesel'man LM. *Osnovy mekhaniki vozdushnyh linij elektroperedachi* .M.: Energoatomizdat, 1992.(In Russ).
16.Glushko MF. Stal'nye pod"emnye kanaty. K.:

фундаментальных исследований. 2014. № 11. Ч.4. С. 572-5766.
6. Otto T. et al. Integrated Microsystems for Smart Applications //Sensors and Materials. 2018. Vol. 30. N 4.pp 767-778.
7.Lindsey K.E., Spillane P.E., An-Chyun W. Dynamic real time transmission line monitor and method of monitoring a transmission line using the same : заяв. пат. 15725207 США. 2018. Доступно по: at:http://lindsey-usa.com/wp-content/uploads/2015/10/11F-001-TLM-8-2014.
8. Ярославский Д.А., Садыков М.Ф. Разработка устройства для системы мониторинга и количественного контроля гололёдообразования на воздушных линиях электропередачи //Известия высших учебных заведений. ПРОБЛЕМЫ ЭНЕРГЕТИКИ. 2017. Т.19. №. 3-4. С 69–79.
9.DiLin – система контроля наличия гололеда на проводах воздушных линий. Доступно по URL: https://dimrus.ru/dilin.html .Ссылка активна на :25 янв. 2018.
10. Rui X., Ji K. and McClure G. Dynamic response of overhead transmission lines with eccentric ice deposits following shock loads //IEEE Transactions on Power Delivery. 2017.Vol. 32,N 3.pp.1287-1294.
11. Минуллин Р.Г., В.А. Касимов., Т.К. Филимонова., и др. Локационное обнаружение гололёда на воздушных линиях электропередачи. Ч.1. Способы обнаружения гололёда // Научно-технические ведомости СПбГПУ. Информатика. Телекоммуникации. Управление.2014. № 2 (193). С. 61 – 73.
12 Минуллин Р.Г, Касимов В.А, Яруллин М.Р. Определение толщины ледяных отложений на проводниках воздушных линий электропередачи методом определения местоположения // Труды Международного семинара по атмосферному обледенению конструкции 2015.С. 101.
13. Бошнякович А.Д.. Механический расчет проводов и тросов линий электропередачи. М.-Л.: Госэнергоиздат, 1962. 254 с.
14.Меркин Д.Р. Введение в механику гибкой нити. М.: Наука. Главная редакция физико-математической литературы, 1980. 240 с.
15.Кесельман Л.М. Основы механики воздушных линий электропередачи //М.: Энергоатомиздат, 1992. 352 с.
16.Глушко М.Ф. Стальные подъемные канаты. К.: Техніка, 1966.
17. Горячев М.П, Ярославский Д.А, Садыков

Tekhnika, 1966. (In Russ).
17. Goryachev MP, Yaroslavsky DA, Sadykov MF,et al. Metodika kontrolya ledyanogo pokrytiya na vozdushnyh liniyah elektroperedachi s uchetom smeshcheniya s ispol'zovaniem datchikov besprovodnyh kanalov svyazi 2017;12(22):6479-6482. (In Russ).
18 Dushin EM. *Osnovy metrologii i elektricheskie izmereniya* 6nd ed. L.: Energoatomizdat. 1987. (InRuss).
19. Yaroslavskij DA. *Sistema avtomatizirovannogo monitoringa gololednyh otlozhenij vozdushnyh linij elektroperedach na osnove inklinometrichesko-meteorologicheskogo metoda*: Kazan;2017.Available at: https://www.dissercat.com/content/povyshenie-nadezhnosti-selskikh-vozdushnykh-linii-elektroperedachi-10-6-kv-v-usloviyakh-vozd [dissertation]. Accessed: 5 Nov 2017. (In Russ).
20 Sadykov MF., Goryachev MP., Yaroslavskij DA., Ivanov DA, Koryshkin IM. *Ustrojstvo operativnogo monitoringa tekhnicheskogo sostoyaniya vysokovol'tnyh linij elektroperedachi* Patent RUS.№185311.30.05.2018. Byul № 2018120028.Available at : Deliverability 2015–2018. Accessed: 29 Nov 2018 (In Russ).

М.Ф, и др. // Методика контроля ледяного покрытия на воздушных линиях электропередачи с учетом смещения с использованием датчиков беспроводных каналов связи 2017. №12.(22). С. 6479-6482.
18. Душин Е.М. Основы метрологии и электрические измерения ./Под общей редакцией. Душина Е. М..6-е изд., перераб. и доп. Л.: Энергоатомиздат, 1987. 51–56 с.
19. Ярославский Д.А. Система автоматизированного мониторинга гололедных отложений воздушных линий электропередач на основе инклинометрическо-метеорологического метода.: Дис. ... канд. техн. наук:. Казань, 2017. Доступно по: https://www.dissercat.com/content/povyshenie-nadezhnosti-selskikh-vozdushnykh-linii-elektroperedachi-10-6-kv-v-usloviyakh-vozd Ссылка активна на 5ноября.2013.
20.Садыков М.Ф., Горячев М.П., Ярославский Д.А., Иванов Д.А, Корышкин И.М. Устройство оперативного мониторинга технического состояния высоковольтных линий электропередачи Патент РФ.№185311. 30.05.2018. Бюл № 2018120028..Доступно по :Deliverability 2015–2018. Ссылка активна на: 29 ноября 2018.

Authors of the publication

Mikhail P. Goryachev –Department “Theoretical basics of Electrotechnics” of Kazan State Power Engineering University. E-mail: goryachev91@mail.ru.

Marat F. Sadykov – Head of Departament “Theoretical basics of Electrotechnics” of Kazan State Power Engineering University. E-mail: s-marik@yandex.ru; sadykov@kgeu.ru.

Danil A. Yaroslavskiy – Department “Theoretical basics of Electrotechnics” of Kazan State Power Engineering University.

Received ***April 25, 2019***